

UNCLASSIFIED

AD NUMBER

ADB014360

LIMITATION CHANGES

TO:

Approved for public release; distribution is unlimited.

FROM:

Distribution authorized to U.S. Gov't. agencies only; Test and Evaluation; OCT 1976. Other requests shall be referred to Air Force Armament Laboratory, Attn: AFATL/ DLJC, Eglin AFB, FL32542.

AUTHORITY

USADTC ltr, 2 Apr 1980

THIS PAGE IS UNCLASSIFIED

AEDC-TR-76-147
AFATL-TR-76-113

ey. 1

**ARCHIVE COPY
DO NOT LOAN**



**AERODYNAMIC LOADS AND SEPARATION
CHARACTERISTICS OF THE BLU-27B/B,
MK-82SE, AND GBU-8 WEAPONS IN THE
F-16 AIRCRAFT FLOW FIELD AT
MACH NUMBERS FROM 0.4 TO 1.2**

**PROPELLION WIND TUNNEL FACILITY
ARNOLD ENGINEERING DEVELOPMENT CENTER
AIR FORCE SYSTEMS COMMAND
ARNOLD AIR FORCE STATION, TENNESSEE 37389**

October 1976

**This document has been approved for public release
and its distribution is unlimited. Per TAB 80-13
Final Report for the Period May 10-14, 1976**

Distribution limited to U.S. Government agencies only; this report contains information on test and evaluation of military hardware; October 1976; other requests for this document must be referred to Air Force Armament Laboratory (AFATL/DLJC), Eglin Air Force Base, Florida 32542.

**Property of U. S. Air Force
AEDC LIBRARY
F40600-75-C-0001**

Prepared for

**AIR FORCE ARMAMENT LABORATORY (AFATL/DLJC)
EGLIN AIR FORCE BASE, FLORIDA 32542**

AEDC TECHNICAL LIBRARY
5 07220 00034 0432

NOTICES

When U. S. Government drawings specifications, or other data are used for any purpose other than a definitely related Government procurement operation, the Government thereby incurs no responsibility nor any obligation whatsoever, and the fact that the Government may have formulated, furnished, or in any way supplied the said drawings, specifications, or other data, is not to be regarded by implication or otherwise, or in any manner licensing the holder or any other person or corporation, or conveying any rights or permission to manufacture, use, or sell any patented invention that may in any way be related thereto.

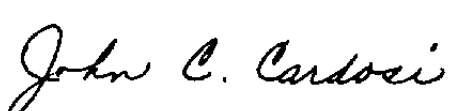
Qualified users may obtain copies of this report from the Defense Documentation Center.

References to named commercial products in this report are not to be considered in any sense as an endorsement of the product by the United States Air Force or the Government.

APPROVAL STATEMENT

This technical report has been reviewed and is approved for publication.

FOR THE COMMANDER



JOHN C. CARDOSI
Lt Colonel, USAF
Chief Air Force Test Director, PWT
Directorate of Test



ALAN L. DEVEREAUX
Colonel, USAF
Director of Test

ERRATA

AEDC-TR-76-147 (AFATL-TR-76-113) October 1976
(UNCLASSIFIED REPORT)

AERODYNAMIC LOADS AND SEPARATION CHARACTERISTICS OF THE BLU-27B/B, MK-82SE, AND GBU-8 WEAPONS IN THE F-16 AIRCRAFT FLOW FIELD AT MACH NUMBERS FROM 0.4 TO 1.2

E. G. Allee, Jr., ARO, Inc.

Arnold Engineering Development Center
Air Force Systems Command
Arnold Air Force Station, Tennessee

The X_{cg} value of 6.608 quoted for the GBU-8 store in Table 1 should have been 5.135.

Please substitute the corrected table in your copy of the report.

Table 1. Metric Model Parameters

	BLU-27 B/B	GBU-8	MK-82SE
b	1.563	1.5	0.896
C_{f_p}	NA	-18.048	-5.0
C_{m_q}	NA	-180.48	-53.0
C_{n_r}	NA	-180.48	-53.0
F_{z_1}	NA	2030.0	1680.0 1113.0*
F_{z_2}	NA	1780.0	1333.3 1900.0*
h	NA	5,000	5,000
I_{xx}	NA	24.7	2.1
I_{yy}	NA	524.2	53.0
I_{zz}	NA	524.2	53.0
M	NA	70.243	17.1
S	1.917	1.767	0.630
X_{cg}	5.358	5.135	3.375
X_{L_1}	NA	0.817	1.000
X_{L_2}	NA	-0.850	-0.667
Z_E	NA	0.343	0.343

*Selected Runs

UNCLASSIFIED

UNCLASSIFIED

20. ABSTRACT (Continued)

0.4 to 1.2 for various weapons loading configurations of the F-16. Other variables included aircraft angles of attack from 0 to 10 deg and wing leading-edge-flap deflection angles of 0, 4, and 15 deg.

PREFACE

The work reported herein was conducted by the Arnold Engineering Development Center (AEDC), Air Force Systems Command (AFSC), at the request of the Air Force Armament Laboratory (AFATL/DLJC), under Program Element 62602F, Project 2567, Task 01. The AFATL project monitor was Mr. Al Marrin. The test results were obtained by ARO, Inc. (a subsidiary of Sverdrup & Parcel and Associates, Inc.), contract operator of the AEDC, AFSC, Arnold Air Force Station, Tennessee, under ARO Project No. P41C-C6A. The author of the report was E. G. Allee, Jr., ARO, Inc. Testing was accomplished during the period May 10 through 14, 1976, and the data reduction was completed on June 10, 1976. The manuscript (ARO Control No. ARO-PWT-TR-76-96) was submitted for publication on August 23, 1976.

CONTENTS

	<u>Page</u>
1.0 INTRODUCTION	7
2.0 APPARATUS	
2.1 Test Facility	7
2.2 Test Articles	8
2.3 Instrumentation	9
3.0 TEST DESCRIPTION	
3.1 Test Conditions	9
3.2 Data Acquisition	10
3.3 Corrections	11
3.4 Precision of Data	12
4.0 RESULTS AND DISCUSSION	
4.1 Trajectory Data	13
4.2 Free-Stream Data	13
4.3 Aerodynamic Loads Surveys	13

ILLUSTRATIONS

Figure

1. Isometric Drawing of a Typical Store Separation Installation and a Block Diagram of the Computer Control Loop	15
2. Schematics of Test Installations	16
3. Dimensional Sketch of the F-16 Parent Model	18
4. Dimensional Sketches of the Store Models	19
5. F-16 Model Pylons and Racks	25
6. Installation Photographs	30
7. Store Orientation	33
8. Configuration Identification	34
9. Trajectories Obtained with the GBU-8	35
10. Trajectories Obtained with the MK-82SE	39

<u>Figure</u>		<u>Page</u>
11.	Free-stream Aerodynamic Coefficients	41
12.	Aerodynamic Characteristics of the BLU-27B/B, Configuration 1	46
13.	BLU-27B/B Coefficient Variation with Aircraft Angle of Attack, Configuration 1	51
14.	Effect of an Adjacent Store on the BLU-27B/B, Configurations 1 and 2	54
15.	Aerodynamic Characteristics of the BLU-27B/B, Configuration 3	59
16.	BLU-27B/B Coefficient Variation with Aircraft Angle of Attack, Configuration 3	64
17.	Effect of an Adjacent Store on the BLU-27B/B, Configurations 3 and 4	68
18.	Aerodynamic Characteristics of the BLU-27B/B, Configuration 5	73
19.	Aerodynamic Characteristics of the BLU-27B/B, Configuration 6	74
20.	Aerodynamic Characteristics of the GBU-8, Configuration 7	75
21.	GBU-8 Coefficient Variation with Aircraft Angle of Attack, Configuration 7	76
22.	Effect of the Addition of an Inboard 370-gal Fuel Tank on the GBU-8, Configurations 7 and 9	77
23.	Aerodynamic Characteristics of the GBU-8, Configuration 8	78
24.	Aerodynamic Characteristics of the MK-82SE, Configuration 10	79
25.	MK-82SE Coefficient Variation with Aircraft Angle of Attack, Configuration 10	80
26.	Aerodynamic Characteristics of the MK-82SE, Configuration 11	82

<u>Figure</u>	<u>Page</u>
27. MK-82SE Coefficient Variation with Aircraft Angle of Attack, Configuration 11	87
28. Effect of an Adjacent Store on the MK-82SE, Configurations 11 and 13	89
29. Aerodynamic Characteristics of the MK-82SE, Configuration 12	94
30. MK-82SE Coefficient Variation with Aircraft Angle of Attack, Configuration 12	99
31. Aerodynamic Characteristics of the MK-82SE, Configuration 14	104
32. MK-82SE Coefficient Variation with Aircraft Angle of Attack, Configuration 14	109
33. Aerodynamic Characteristics of the MK-82SE, Configuration 15	111
34. MK-82SE Coefficient Variation with Aircraft Angle of Attack, Configuration 15	116
35. Aerodynamic Characteristics of the MK-82SE, Configuration 16	119
36. MK-82SE Coefficient Variation with Aircraft Angle of Attack, Configuration 16	120
37. Aerodynamic Characteristics of the MK-82SE, Configuration 17	121
38. MK-82SE Coefficient Variation with Aircraft Angle of Attack, Configuration 17	122
39. Coefficient with Wing Leading-Edge-Flap Deflection, Configuration 10	123
40. Coefficient Variation with Wing Leading-Edge-Flap Deflection, Configuration 11	124
41. Coefficient Variation with Wing Leading-Edge-Flap Deflection, Configuration 12	128
42. Coefficient Variation with Wing Leading-Edge-Flap Deflection, Configuration 13	130

<u>Figure</u>	<u>Page</u>
43. Coefficient Variation with Wing Leading-Edge-Flap Deflection, Configuration 14	133
44. Coefficient Variation with Wing Leading-Edge-Flap Deflection, Configuration 15	136
45. Coefficient Variation with Wing Leading-Edge-Flap Deflection, Configuration 16	140
46. Coefficient Variation with Wing Leading-Edge-Flap Deflection, Configuration 17	141

TABLES

1. Metric Model Parameters	142
2. Run Compendium	143
3. Typical Data Uncertainties	148
NOMENCLATURE	149

1.0 INTRODUCTION

An investigation of the flow-field characteristics in the vicinity of the midwing and inboard weapons stations (wing stations 7 and 6) of the F-16 aircraft was conducted in the Aerodynamic Wind Tunnel (4T) of the Propulsion Wind Tunnel Facility. Aerodynamic loads on the BLU-27B/B, the GBU-8, and the MK-82SE stores positioned at various locations in the aircraft flow field were determined for different combinations of pylons, racks, and weapons. Loads data were also obtained on the MK-82SE with the F-16 wing leading-edge-flaps deflected 0, 4, and 15 deg. A limited number of captive separation trajectories was acquired with the MK-82SE and GBU-8 released from both the midwing and inboard weapons pylons at a simulated altitude of 5,000 ft. Test parameters included Mach numbers from 0.4 to 1.2 and aircraft angles of attack from 0 to 10 deg.

2.0 APPARATUS

2.1 TEST FACILITY

The Aerodynamic Wind Tunnel (4T) is a closed-loop, continuous flow, variable-density tunnel in which the Mach number can be varied from 0.1 to 1.3 and can be set at 1.6 and 2.0 by placing nozzle inserts over the permanent sonic nozzle. At all Mach numbers, the stagnation pressure can be varied from 300 to 3,700 psfa. The test section is 4 ft square and 12.5 ft long with perforated, variable porosity (0.5- to 10-percent open) walls. It is completely enclosed in a plenum chamber from which the air can be evacuated, allowing part of the tunnel airflow to be removed through the perforated walls of the test section.

Two separate and independent support systems were used to support the models. The parent aircraft model was inverted in the test section and supported by an offset sting attached to the main pitch sector. The store model was supported by the captive trajectory support (CTS)

which extends down from the tunnel top wall and provides store movement (six degrees of freedom) independent of the parent-aircraft model. An isometric drawing of a typical installation is shown in Fig. 1.

Also shown in Fig. 1 is a block diagram of the computer control loop used during testing. The analog system and the digital computer work as an integrated unit and, utilizing required input information, control the store movement. Positioning is accomplished by use of six individual d-c electric motors. Maximum translational travel of the CTS is ± 15 in. from the tunnel centerline in the lateral and vertical directions and 36 in. in the axial direction. Maximum angular displacements are ± 45 deg in pitch and yaw and ± 360 deg in roll. A more complete description of the test facility can be found in the Test Facilities Handbook.¹ A schematic showing the test section details and the location of the models in the tunnel is shown in Fig. 2.

2.2 TEST ARTICLES

Models used during this test were 0.0667-scale replicas of the F-16 aircraft and associated pylons, triple (TER) and multiple (MER) ejection racks, the MK-82SE, BLU-27B/B, and GBU-8 munitions, the AIM-9J missile and wingtip launcher rail, the 370-gal fuel tank, and the ALQ-119-12 ECM pod. Details of these models are presented in Figs. 3, 4, and 5. The leading-edge flaps of the F-16 model could be set at angles of 0, 4, and 15 deg. During the test, the horizontal stabilizers of the F-16 model were removed to avoid interference with the store-model sting support.

¹ Test Facilities Handbook (Tenth Edition). "Propulsion Wind Tunnel Facility, Vol. 4." Arnold Engineering Development Center, May 1974.

Store parameters used in the calculation of the aerodynamic loads and trajectories are included in Table 1. Typical tunnel installation photographs showing the aircraft model, stores, and CTS are shown in Fig. 6. Store orientation and station numbering sequence on the MER and TER are included in Fig. 7. A summary of the various configurations tested is presented in Fig. 8.

2.3 INSTRUMENTATION

A six-component internal strain-gage balance was used to obtain store aerodynamic force and moment data. Translational and angular positions of the store were obtained from CTS analog inputs during separation trajectories and from digital computer commands during aerodynamic testing.

A touch-wire system was used to accurately position the store model with respect to the aircraft model. The system was also electrically wired to automatically stop the CTS motion and give visual indication should the store or its sting support make contact with any surface other than the touch wire.

3.0 TEST DESCRIPTION

3.1 TEST CONDITIONS

A complete test summary and the wind tunnel test conditions are given in Table 2. Aerodynamic loads data were obtained at Mach numbers from 0.4 to 1.2. Separation trajectory data were obtained at Mach numbers from 0.6 to 1.2. Tunnel conditions were held constant at the desired Mach number while the data were obtained. The trajectories were terminated when the store or its sting contacted the aircraft model or when a CTS limit was reached.

3.2 DATA ACQUISITION

3.2.1 Aerodynamic Loads Data

Store aerodynamic data in the free stream and in the aircraft model flow field were obtained in the following manner. After tunnel conditions were established and the aircraft model angle of attack was set (when applicable), the store was set at $\alpha_s = 0$ (free-stream data) or at the carriage position ($X_p = Y_p = Z_p = 0$ for aerodynamic loads data). Operational control of the CTS was then switched to the digital computer, which positioned the store at previously selected locations related to its initial position by commands to the CTS (see block diagram, Fig. 1). At each position set, the wind tunnel operating conditions and the store model forces and moments were measured and recorded. The model aerodynamic loads were then reduced to coefficient form and tabulated point by point by the digital computer.

3.2.2 Trajectory Data

To obtain a trajectory, test conditions were established in the tunnel and the aircraft model was positioned at the desired angle of attack. Operational control of the CTS was then switched to the digital computer which automatically oriented the store model at a position corresponding to the carriage location and then controlled the store movement during the trajectory through commands to the CTS analog system (see block diagram, Fig. 1). Data from the wind tunnel, consisting of measured model forces and moments, wind tunnel operating conditions, and CTS rig positions, were input to the digital computer for use in the full-scale trajectory calculations.

The digital computer was programmed to solve the six-degree-of-freedom equations to calculate the angular and linear displacements of the store relative to the aircraft pylon. In general, the program involves using

the last two successively measured values of each static aerodynamic coefficient to predict the magnitude of the coefficients over the next time interval of the trajectory. These predicted values are used to calculate the new position and attitude of the store at the end of the time interval. The CTS is then commanded to move the store model to this new position, and the aerodynamic loads are measured. If these new measurements agree with the predicted values, the process is continued over another time interval of the same magnitude. If the measured and predicted values do not agree within the desired precision, the calculation is repeated over a time interval one-half the previous value. This process is repeated until a complete trajectory has been obtained.

In applying the wind tunnel data to the calculations of the full-scale store trajectories, the measured forces and moments are reduced to coefficient form and then applied with proper full-scale store dimensions and flight dynamic pressure. Dynamic pressure was calculated using a flight velocity equal to the free-stream velocity component plus the components of store velocity relative to the aircraft, and a density corresponding to the simulated altitude.

The initial portion of each launch trajectory incorporated simulated ejector forces in addition to the measured aerodynamic forces acting on the store. The ejector force was considered to act perpendicularly to the pylon or rack mounting surface. The ejector forces and locations, along with other full-scale store parameters used in the trajectory calculations, are included in Table 1.

3.3 CORRECTIONS

Balance, sting, and support deflections caused by the aerodynamic loads on the store models were accounted for in the data reduction program to calculate the true store-model angles. Corrections were also

made for model weight tares to calculate the net aerodynamic forces on the store model. No correction was made to account for angular deflections of the aircraft model.

3.4 PRECISION OF DATA

Data obtained using the CTS are subject to error from several sources including tunnel conditions, balance measurements, extrapolation tolerances allowed in predicting coefficients (for trajectory data), and CTS positioning control. The maximum error in CTS position control was ± 0.05 in. (0.06 ft full scale) in translational settings, ± 0.15 deg for angular displacement settings in pitch and yaw, and ± 1.0 deg in roll. Extrapolation tolerances were ± 0.10 for each of the aerodynamic coefficients. Typical uncertainties in the full-scale position data resulting from balance precision limitations are presented in Table 3. These values are conservative in that they were determined by assuming that balance measurement errors accumulate as a bias uncertainty in the trajectory calculations. Uncertainties in the aerodynamic coefficients obtained during the flow-field surveys are also included in this table. All calculated coefficient uncertainties are based on a 95-percent confidence level. The uncertainty in determining the aircraft model angle of attack is estimated to be no larger than ± 0.10 deg.

4.0 RESULTS AND DISCUSSION

Selected aerodynamic free-stream data, aerodynamic loads (grid) data, and separation trajectory data are included in this report. The data included were chosen to show the basic aerodynamic characteristics of each store in the various configurations or to indicate the effect on the store of changing a particular parameter. The configurations for which data were acquired are shown in Fig. 8. Although only a portion of the total data obtained is presented, a complete summary of the test is included in Table 2. Model parameters used in the data calculations are detailed in Table 1.

4.1 TRAJECTORY DATA

Separation trajectory data were obtained on the GBU-8 and MK-82SE stores only. These data are presented in Figs. 9 and 10 in the flight-axis coordinate system with the origin at the carriage position of the respective store. Upon release, the GBU-8 exhibited slight pitch and yaw oscillations, the magnitude of which varied with Mach number. The MK-82SE exhibited a much larger initial pitch rate. At Mach numbers of 0.9 and 0.95, the initial pitch motion was so rapid that CTS travel limits were encountered before the store reached the maximum nose-down pitch attitude.

4.2 FREE-STREAM DATA

Summaries of the aerodynamic coefficients obtained in the free stream with the three store models are included in Fig. 11. The data are presented as store body-axis coefficients and were acquired with the F-16 aircraft model removed from the wind tunnel.

4.3 AERODYNAMIC LOADS SURVEYS

Aerodynamic body-axis coefficients obtained from the surveys made in the influence of the F-16 flow field are presented in Figs. 12 through 19 for the BLU-27B/B, in Figs. 20 through 23 for the GBU-8, and in Figs. 24 through 46 for the MK-82SE. The data are plotted as functions of the pylon-axis spatial coordinates at which the data were acquired. The indicated aircraft configurations are defined in Fig. 8. All surveys were initiated with the store in the carriage position at the pylon and rack location given in the figure heading. Rack stations are numbered as shown in Fig. 7.

In general, flow-field effects on the aerodynamic coefficients of the BLU-27B/B had dissipated at a vertical separation of 16 ft or greater, regardless of the aircraft configuration. The actual distance at which the effects were no longer significant did vary slightly with configuration and with the aerodynamic coefficient under consideration.

Aircraft flow-field effects noted on the GBU-8 were considerably more pronounced than those on the BLU-27B/B and persisted to distances beyond 18 ft (especially at supersonic Mach numbers). The variation in coefficients resulting from the addition of a 370-gal fuel tank to the inboard pylon was most evident at $M_\infty = 1.2$ and also continued beyond 18 ft vertically from the aircraft.

Data acquired with the MK-82SE indicated that the aerodynamic coefficients were approaching free-stream values at separations of 16 ft when the aircraft angle of attack was 6 deg or less. At an angle of attack of 10 deg, the effect of the F-16 flow field was still evident at 18 ft, which was the maximum vertical separation obtained with the MK-82SE.

The change in aerodynamic coefficients caused by deflecting the F-16 wing-leading-edge flaps 4 deg and 15 deg was investigated using the MK-82SE. The variation caused by placing the flaps in the 4-deg position was very small and had dissipated within 1 ft of the carriage position. The effects with the 15-deg flap deflection were of greater magnitude and extended beyond 14 ft separation in some instances. The actual distance at which the flap effects ceased to be significant was configuration dependent.

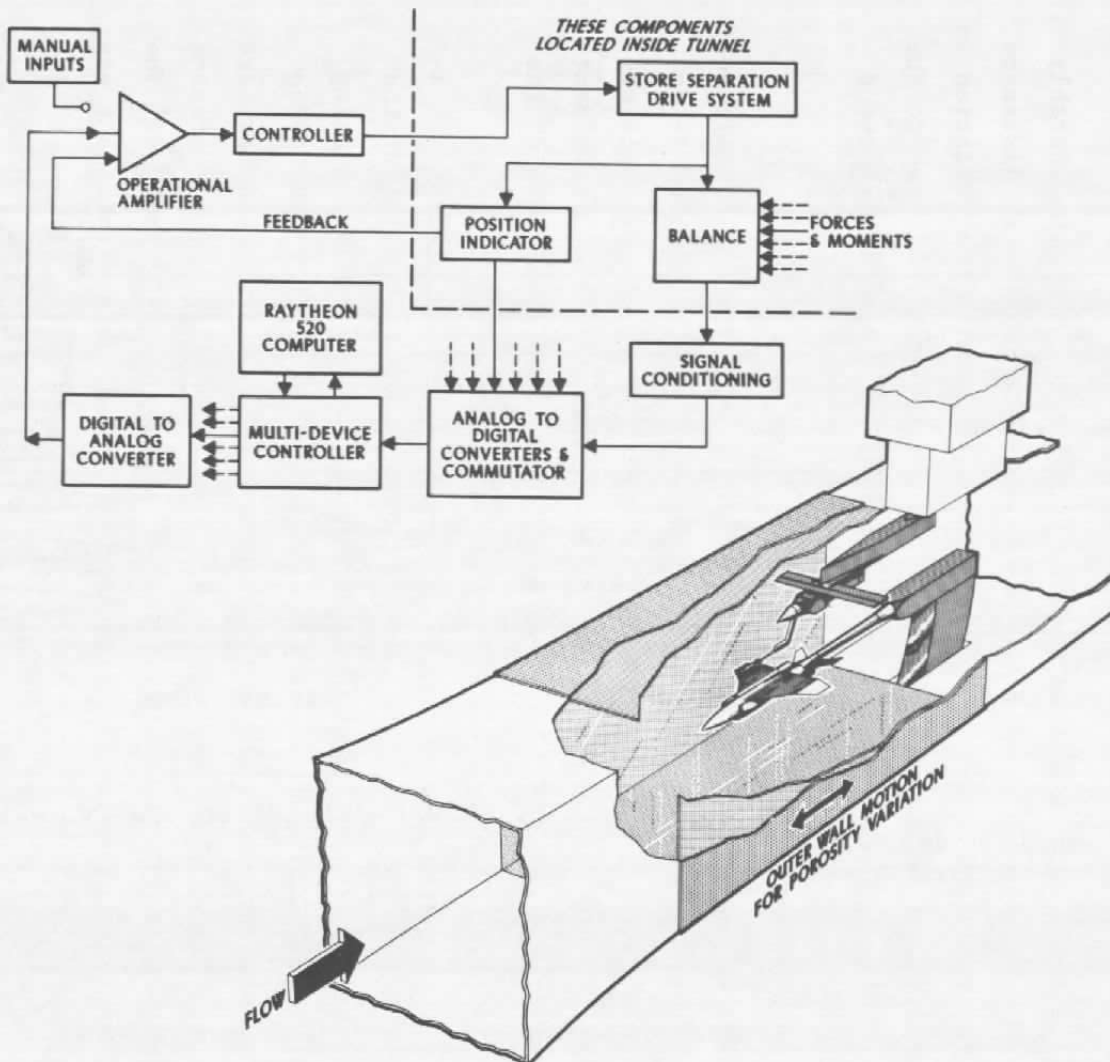
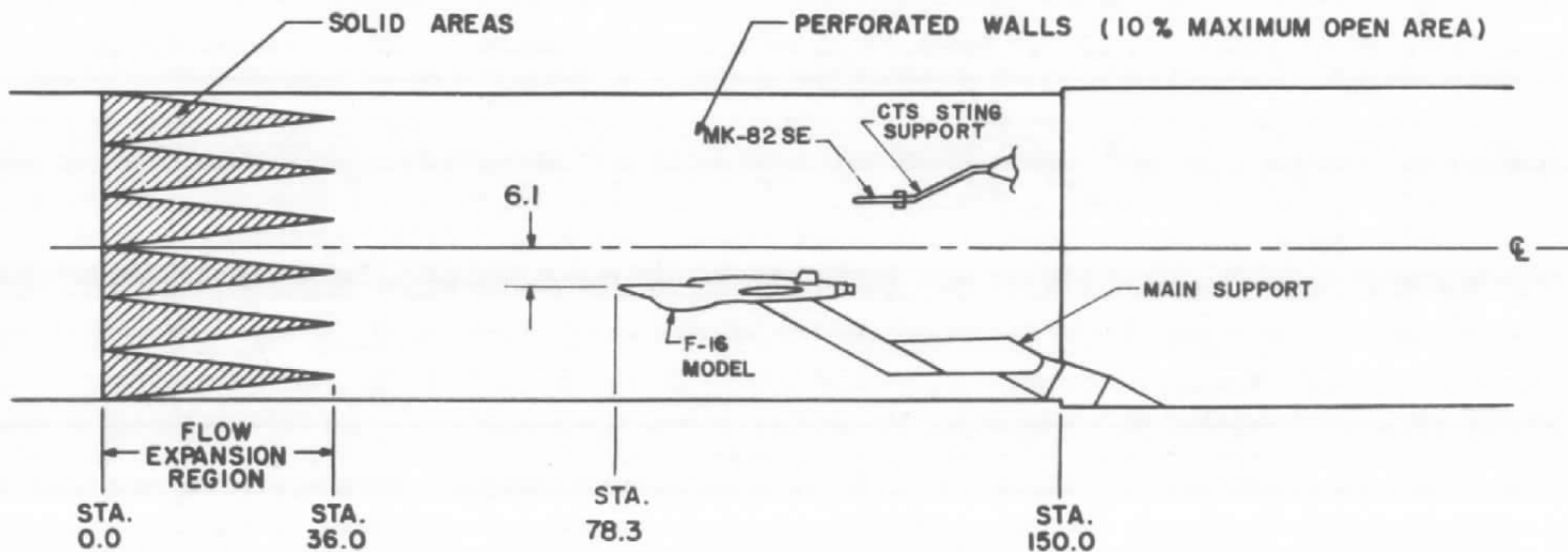
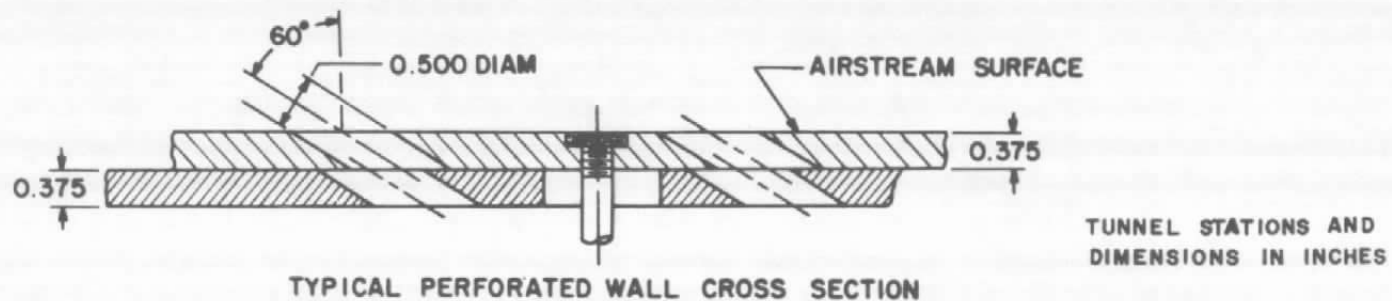
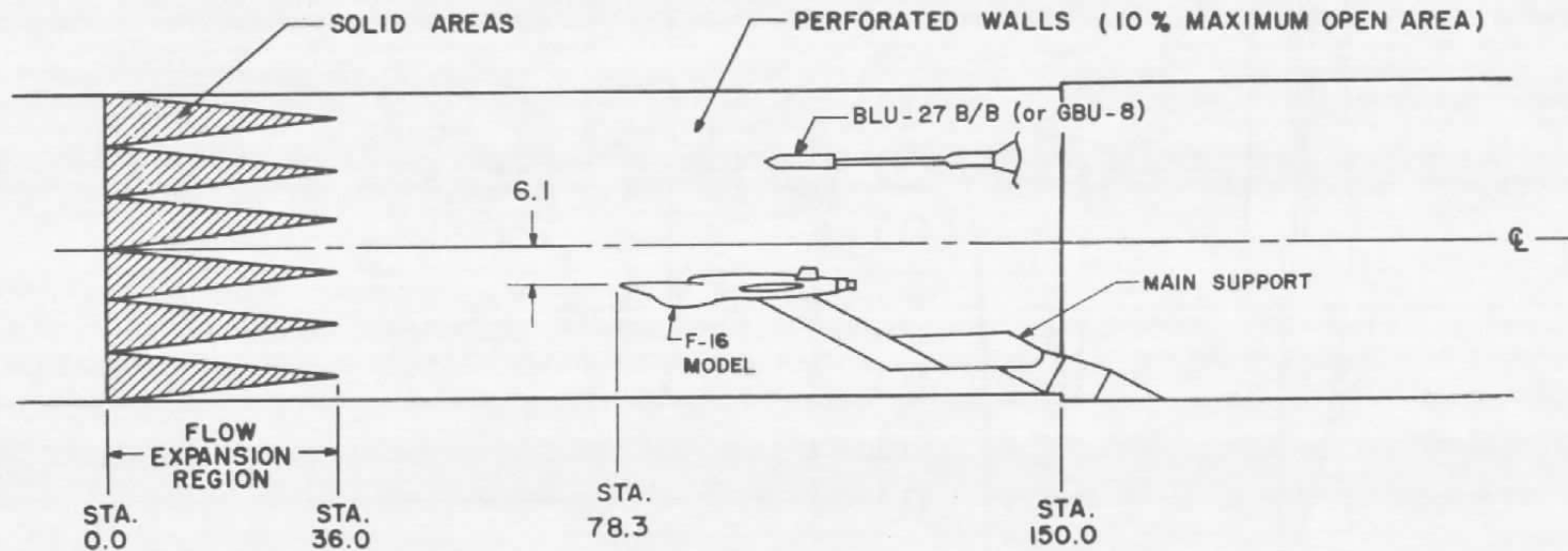
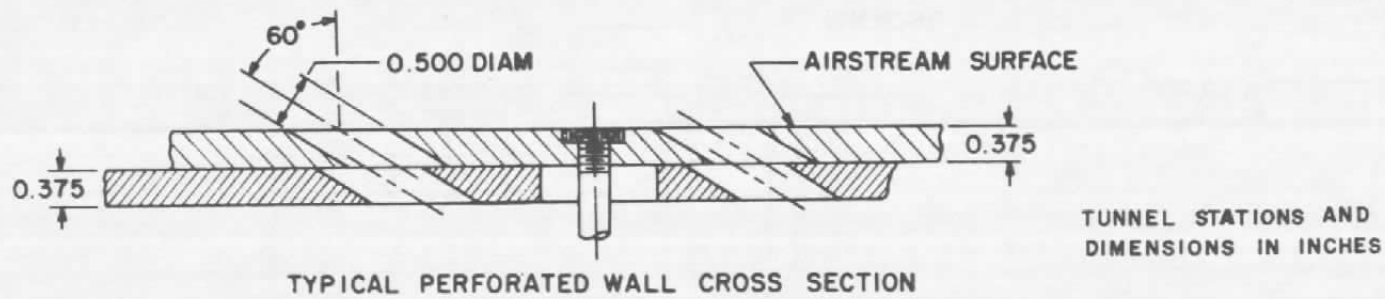


Figure 1. Isometric drawing of a typical store separation installation and a block diagram of the computer control loop.



a. MK-82SE

Figure 2. Schematics of test installations.



b. BLU-27B/B or GBU-8
Figure 2. Concluded.

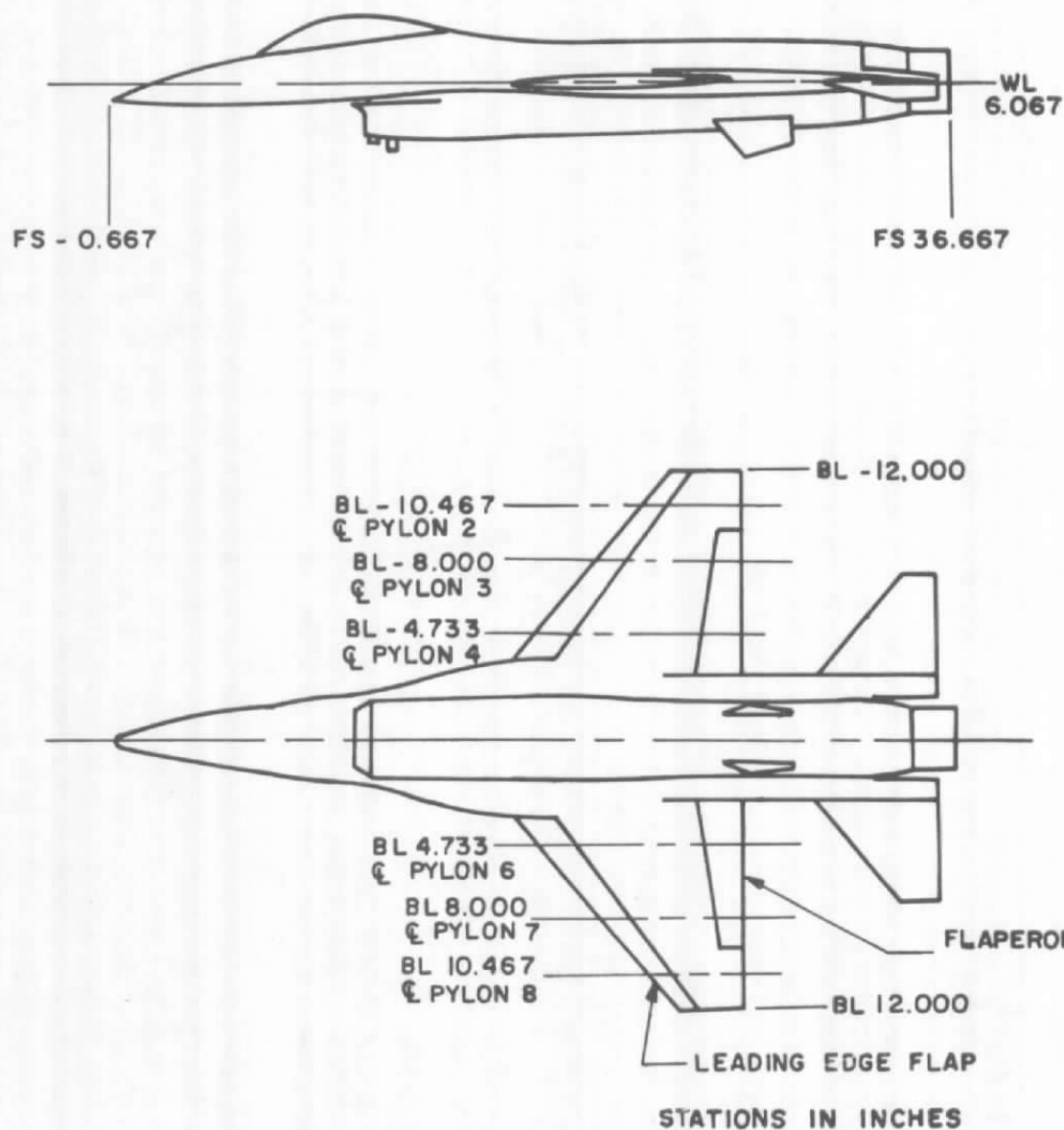
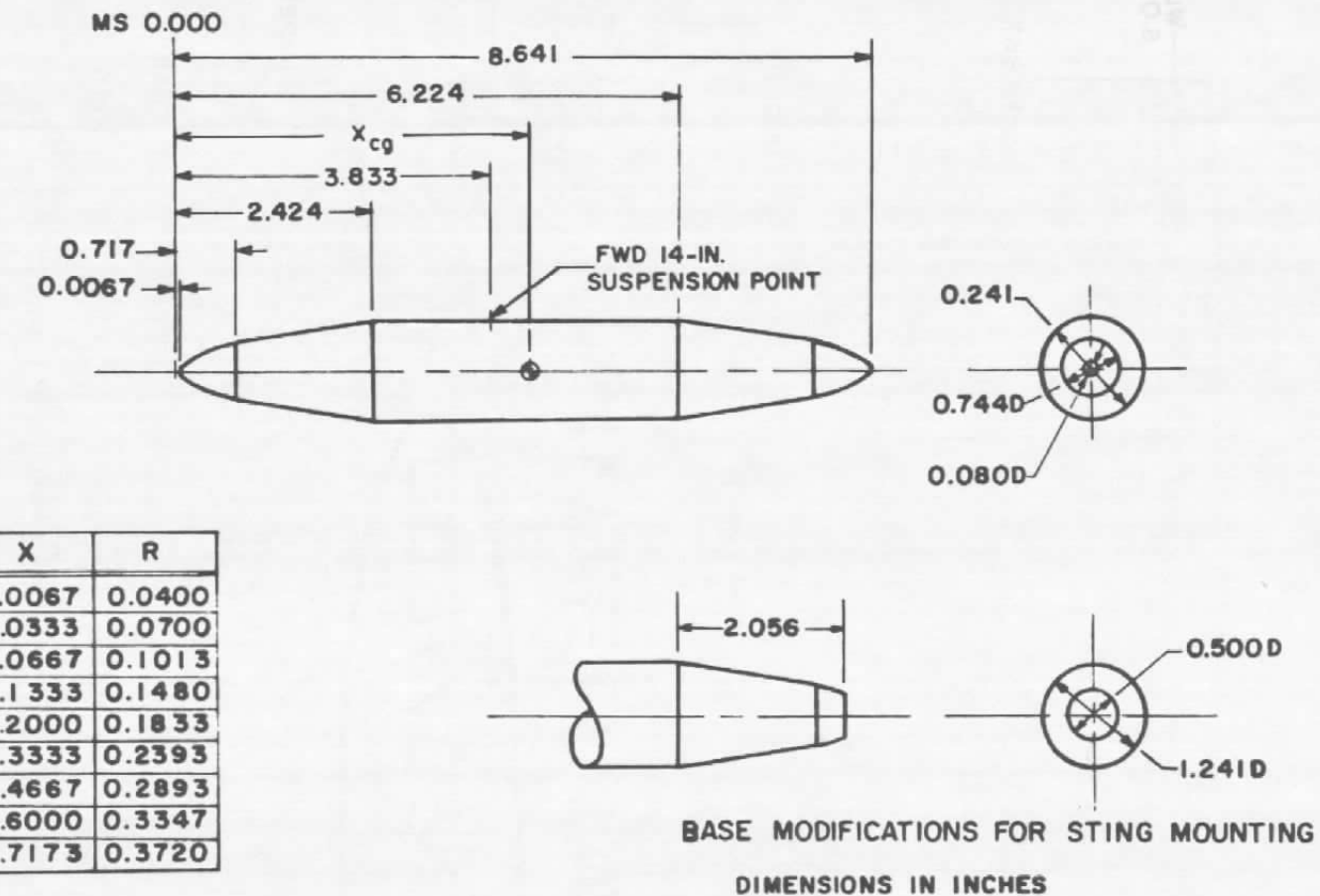
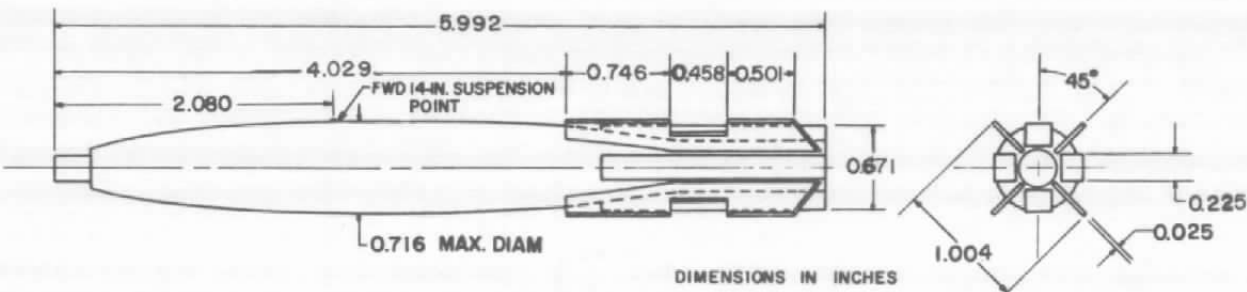


Figure 3. Dimensional sketch of the F-16 parent model.



a. BLU-27B/B
Figure 4. Dimensional sketches of the store models.

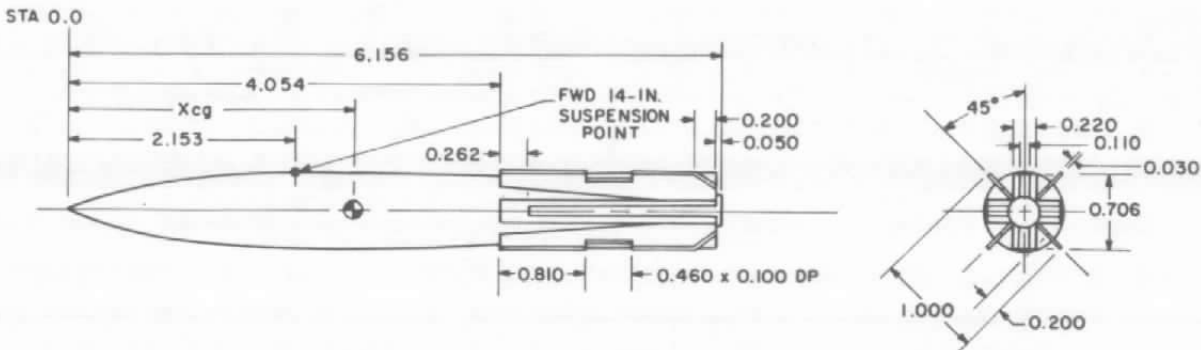


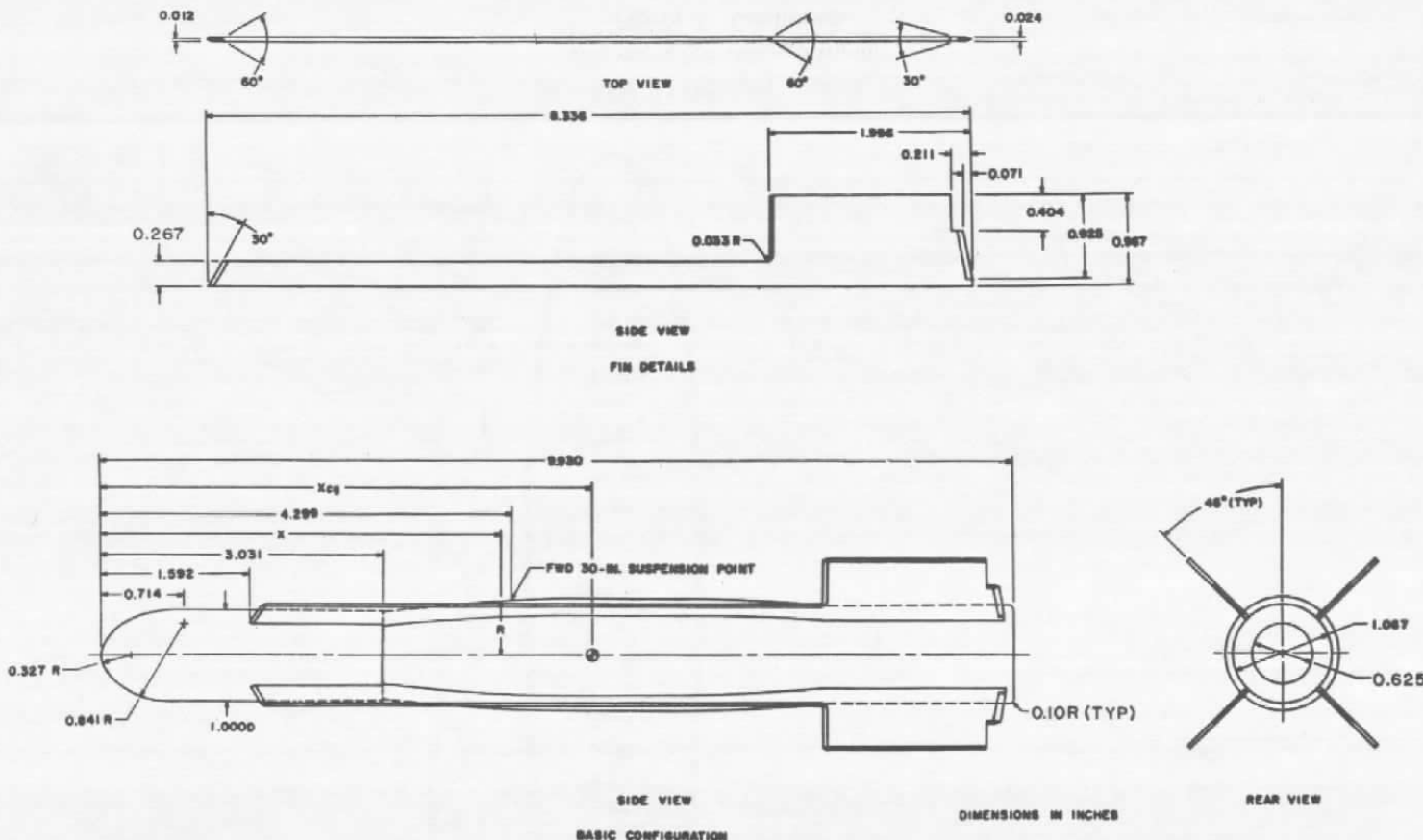
b. MK-82SE metric model

BODY GEOMETRY

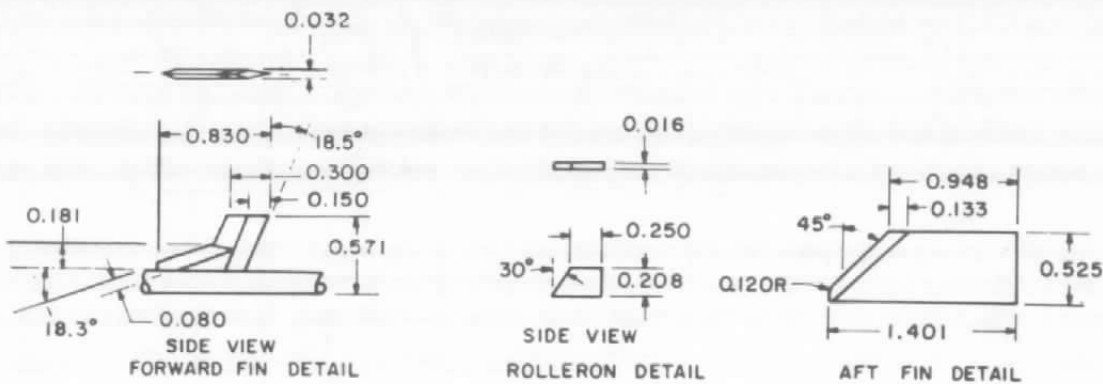
20

STA	DIAM
0	0
0.080	0.096
0.240	0.224
0.587	0.416
1.088	0.566
1.611	0.668
2.157	0.716
CONST DIAM	
3.045	0.716
3.592	0.692
4.054	0.630
CONST SLOPE	
5.501	0.300
CONST DIAM	
6.156	0.300

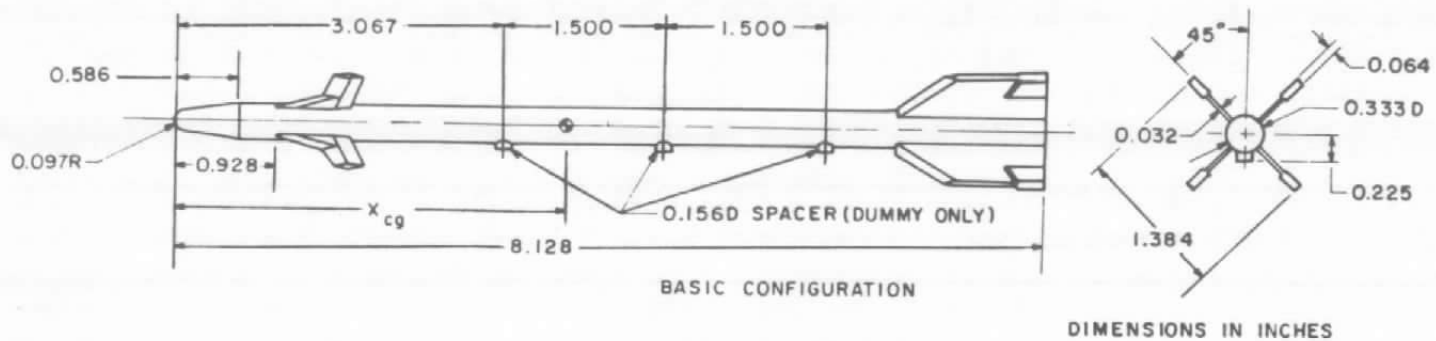
c. MK-82SE dummy model
Figure 4. Continued.



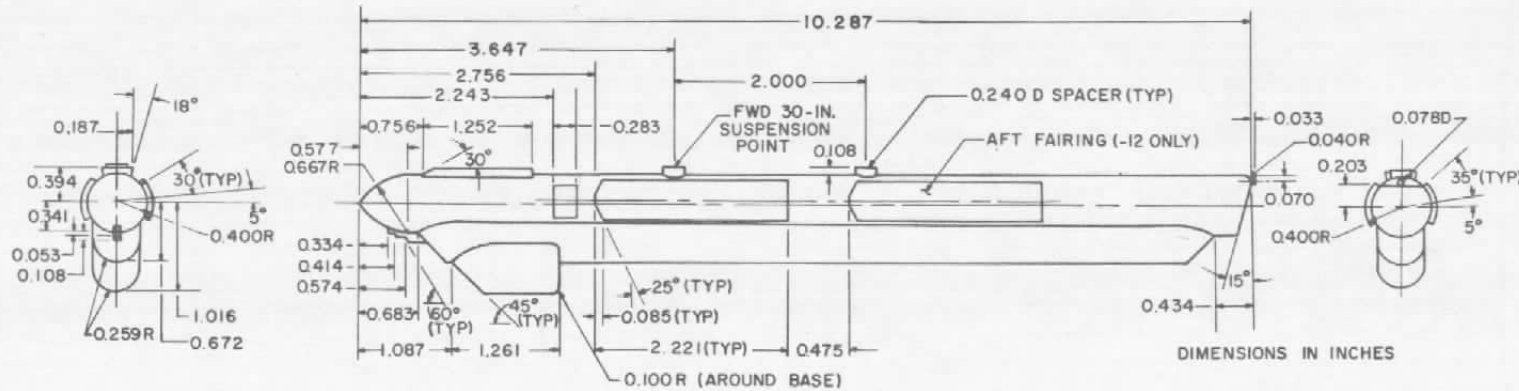
d. GBU-8 metric model
Figure 4. Continued.



22

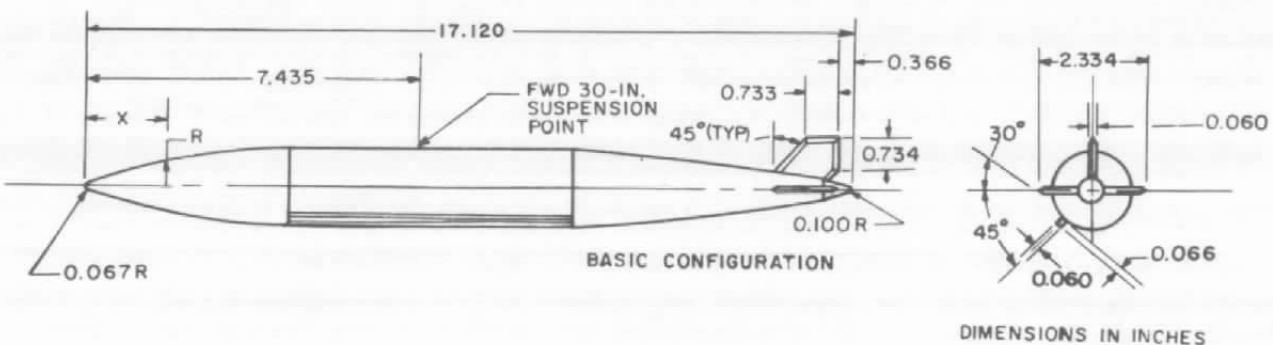


e. AIM-9J dummy model
Figure 4. Continued.

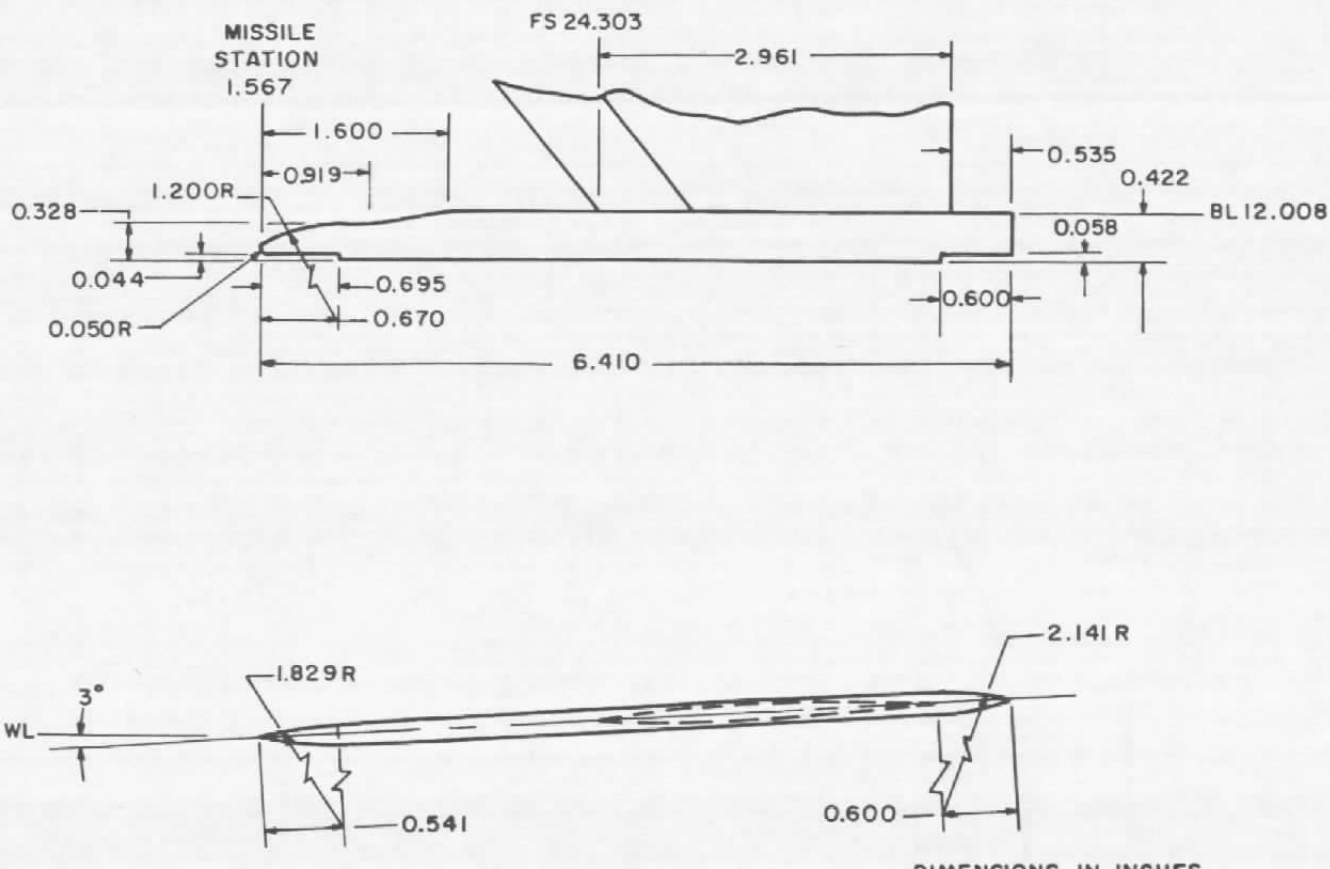


f. ALQ-119-12 ECM pod dummy model
Figure 4. Continued.

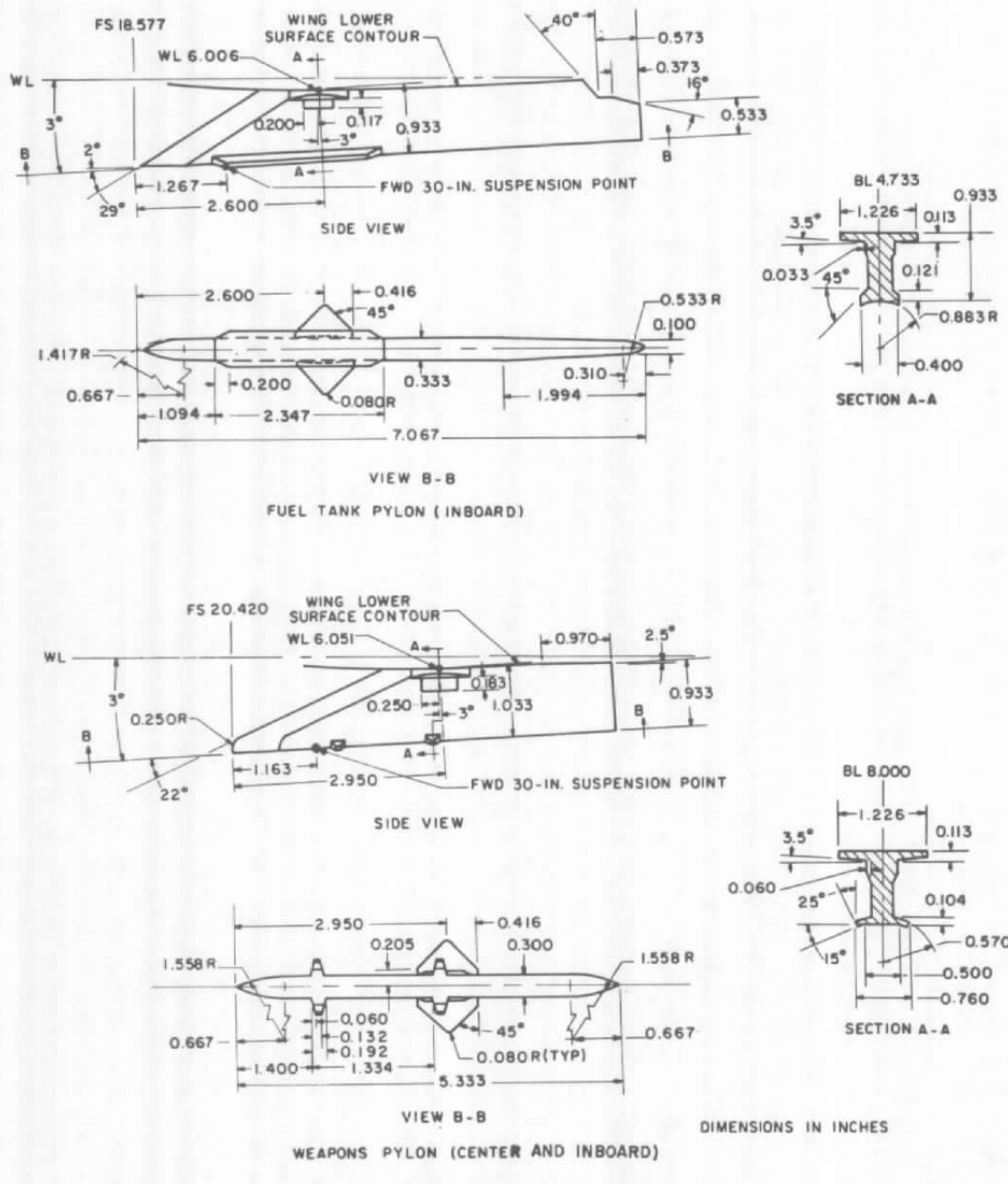
X, in.	R, in.	X, in.	R, in.	X, in.	R, in.	X, in.	R, in.
0	0	1.120	0.451	4.520	0.883 CONST DIAM.	14.003	0.577
0.053	0.068	1.253	0.484	10.836	0.883 CONST SLOPE	14.136	0.561 CONST SLOPE
0.120	0.100	1.587	0.554	12.270	0.757	16.520	0.242
0.186	0.131	1.920	0.611	12.336	0.752	16.587	0.231
0.320	0.188	2.253	0.660	12.670	0.721	16.653	0.220
0.453	0.242	2.586	0.701	13.004	0.688	16.787	0.192
0.587	0.291	2.920	0.737	13.337	0.653	16.920	0.156
0.720	0.336	3.253	0.770	13.670	0.616	17.054	0.097
0.854	0.377	3.587	0.799			17.120	0
0.951	0.416		CONST SLOPE				



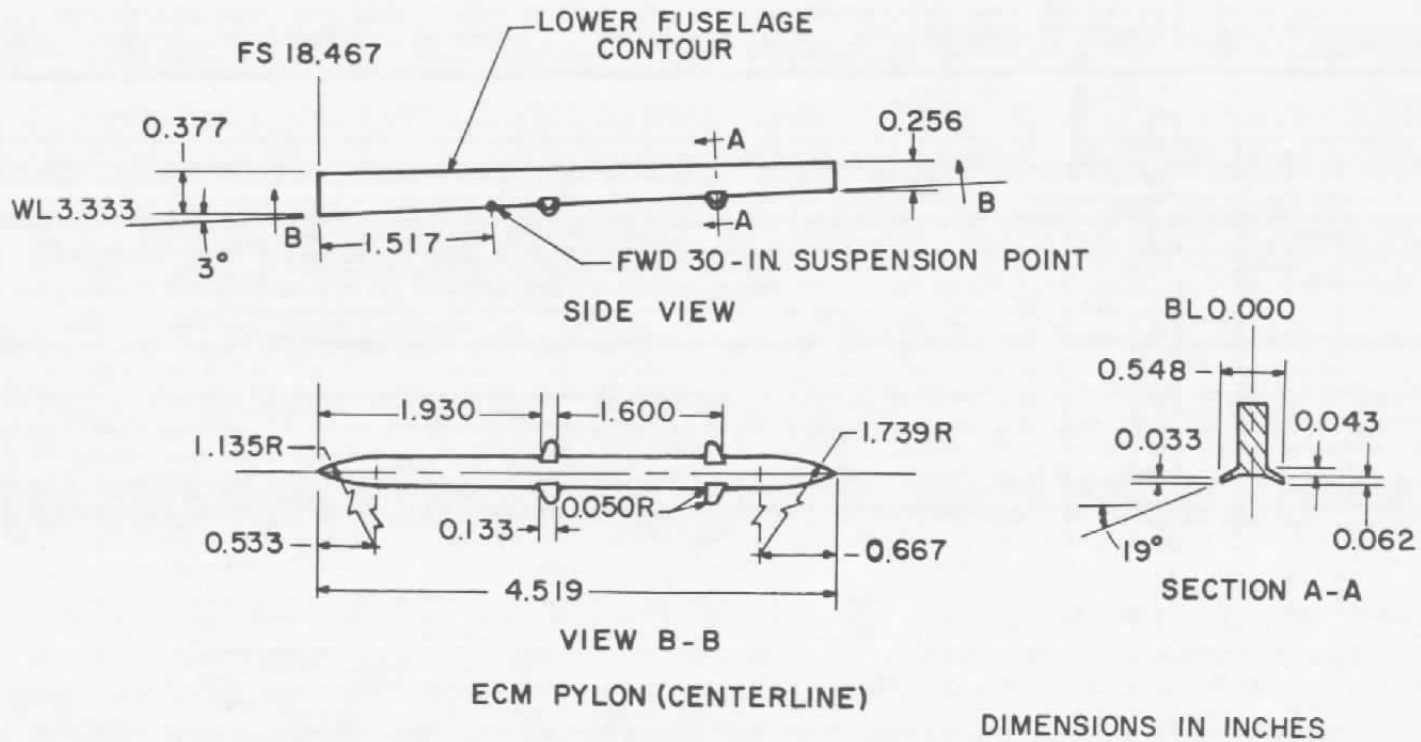
g. 370-gal fuel tank dummy model
Figure 4. Concluded.



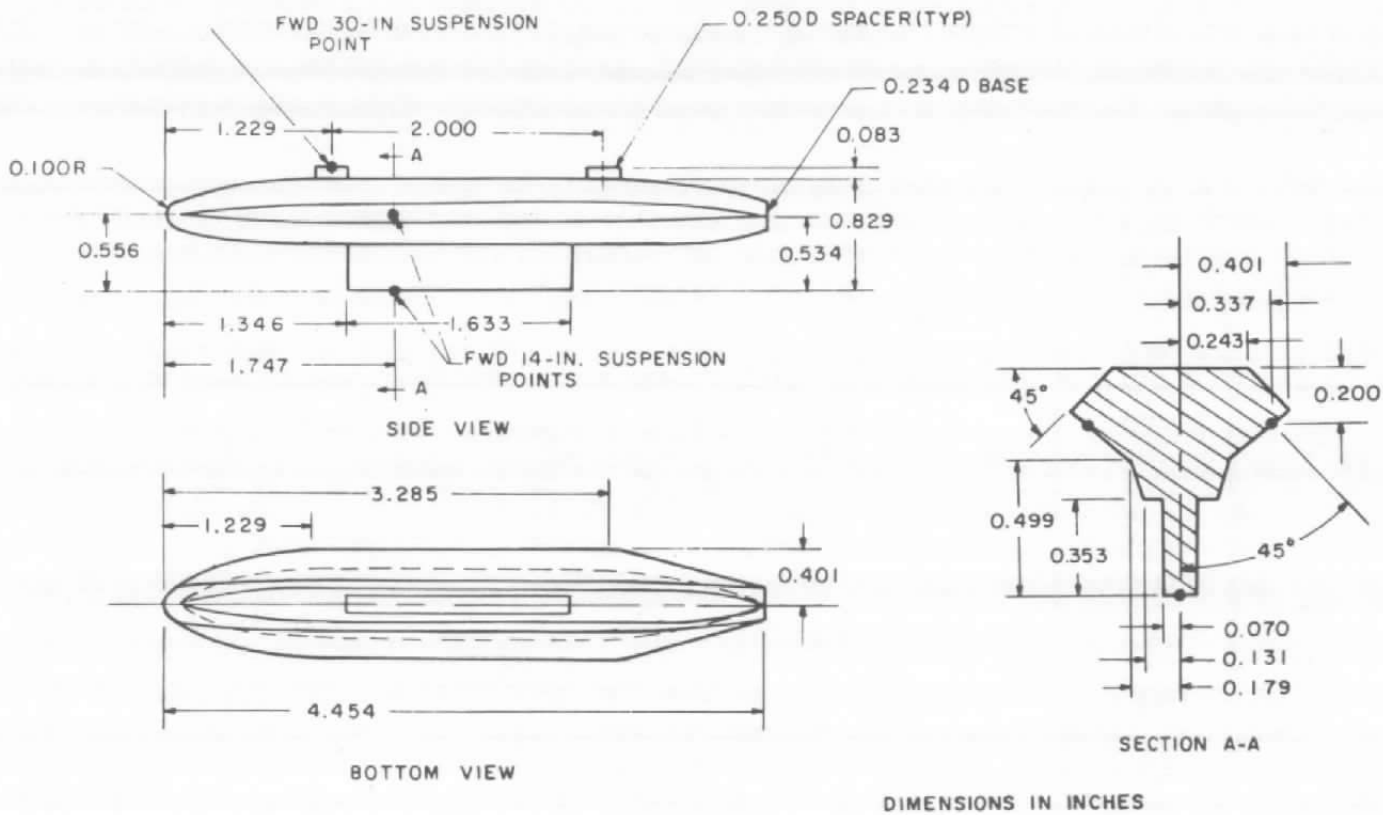
AIM-9J wing tip launcher
Figure 5. F-16 model pylons and racks.



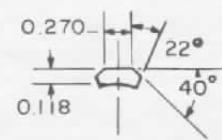
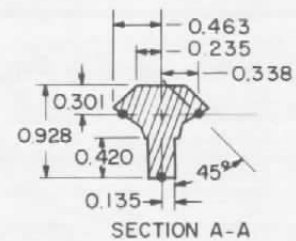
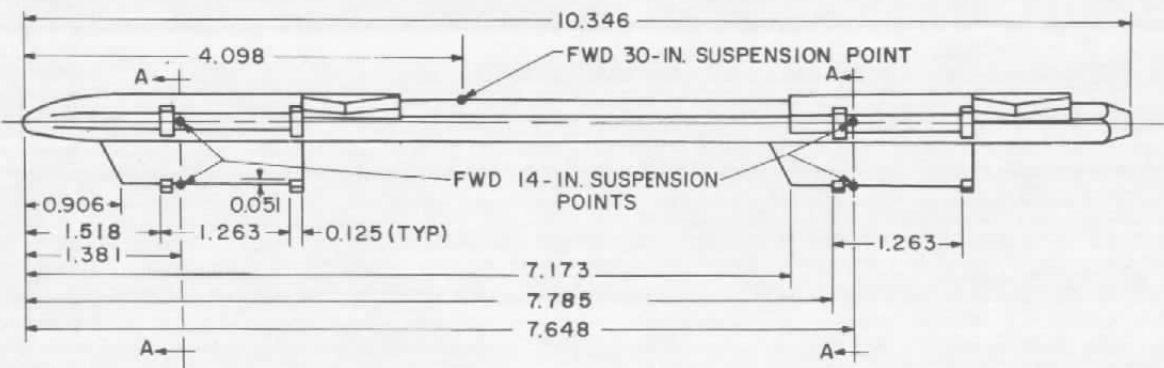
b. Midwing and inboard pylons
Figure 5. Continued.



c. Centerline ECM pylon
Figure 5. Continued.

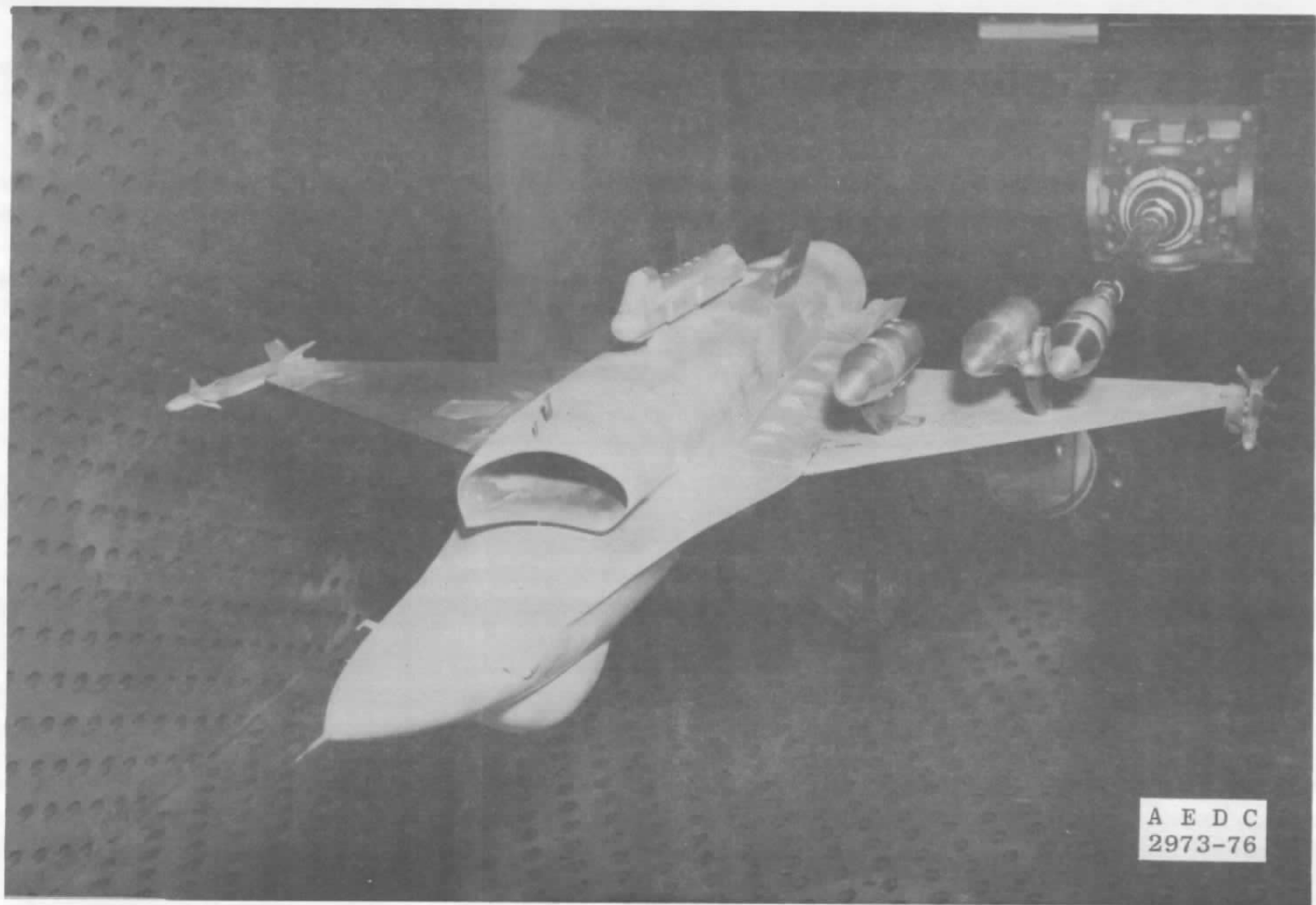


d. Triple ejection rack
Figure 5. Continued.

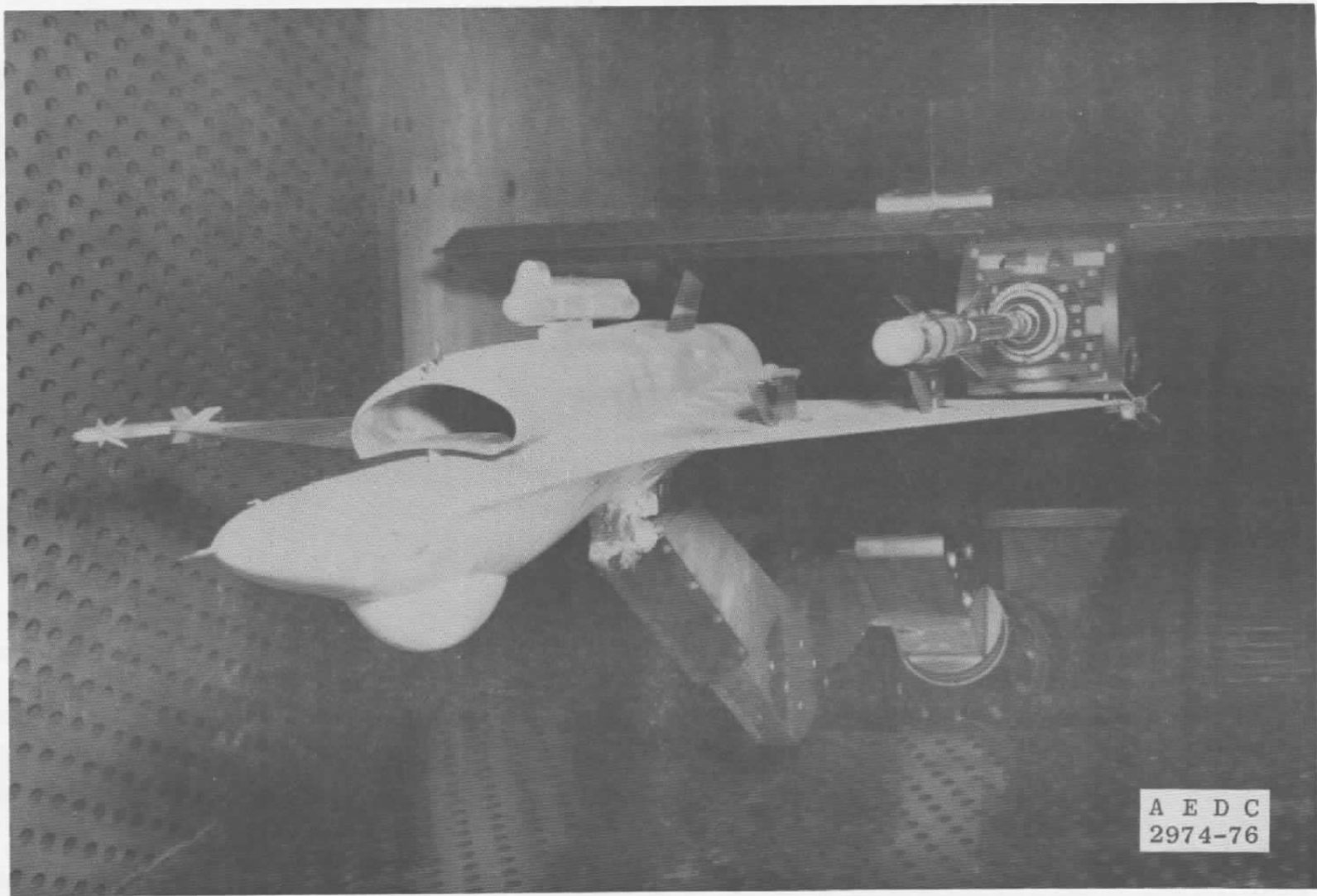


DIMENSIONS IN INCHES

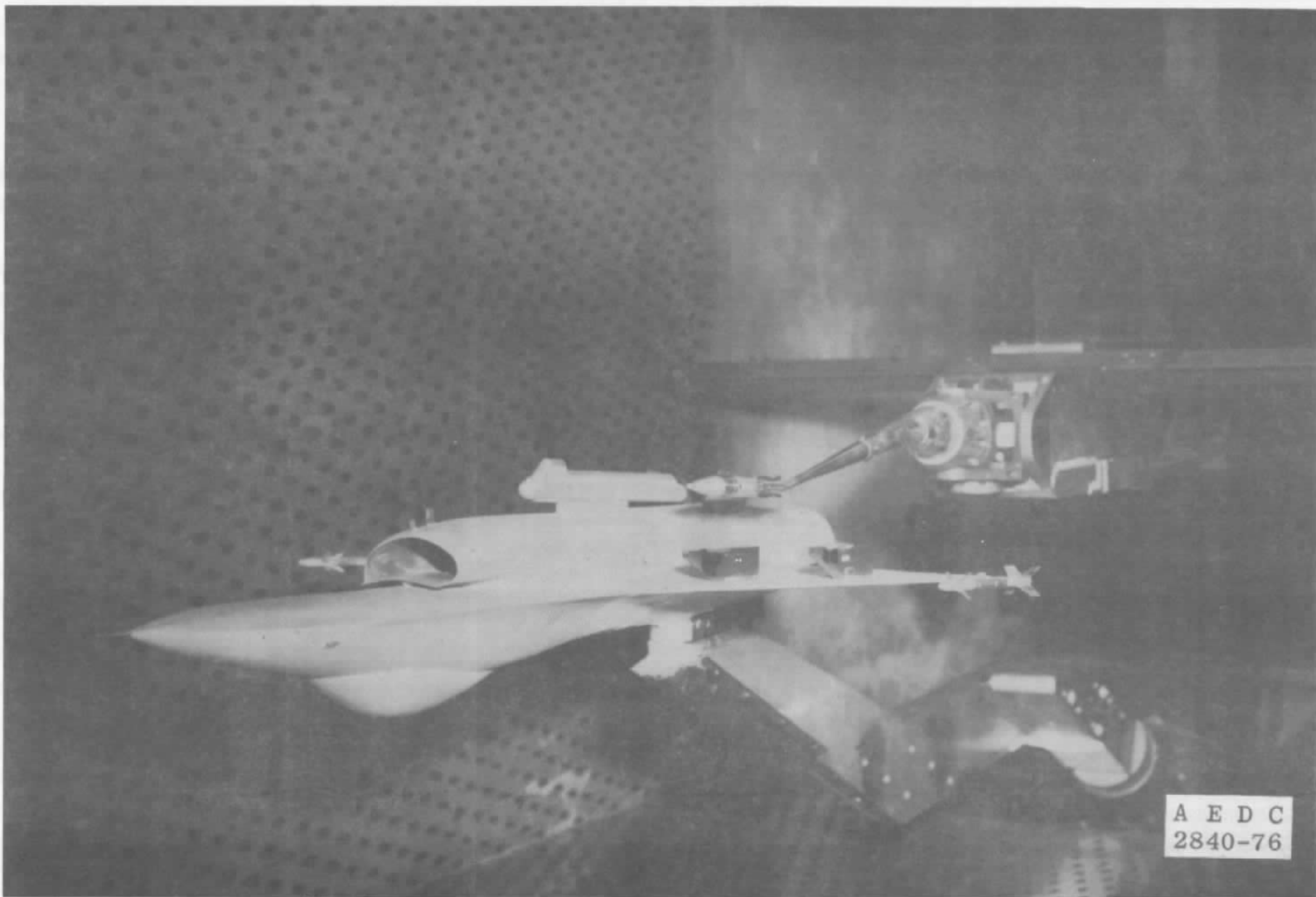
e. Multiple ejection rack
Figure 5. Concluded.



a. BLU-27B/B, configuration 4
Figure 6. Installation photographs.

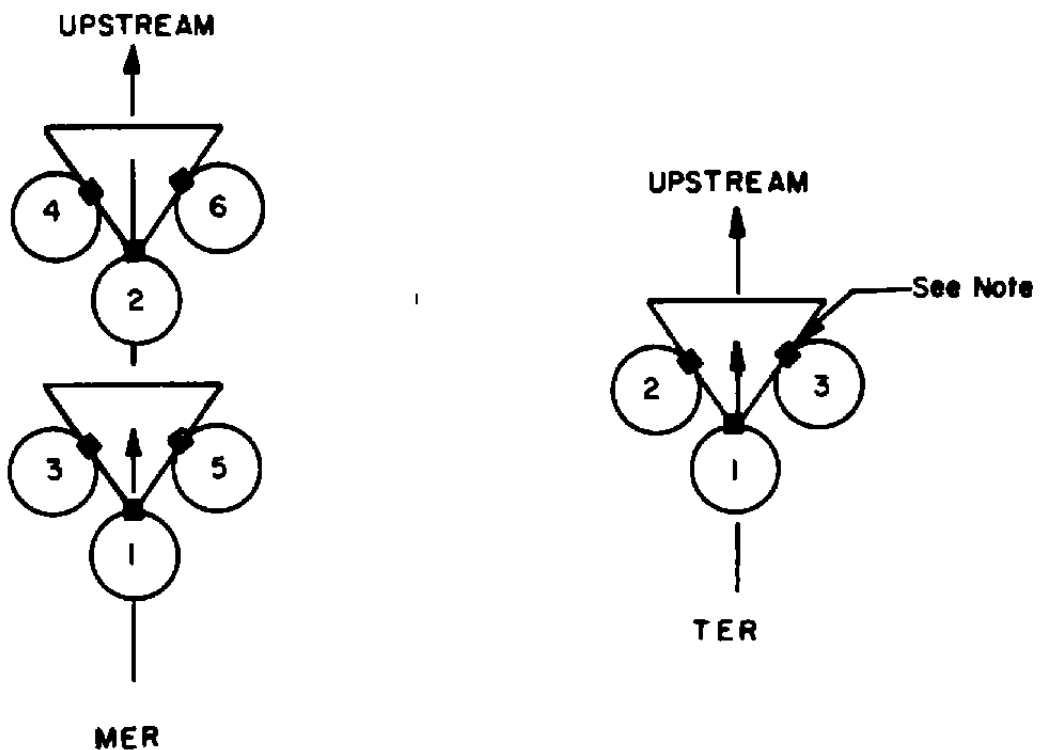


b. GBU-8, configuration 7
Figure 6. Continued.



A E D C
2840-76

c. MK-82SE, configuration 17
Figure 6. Concluded.



NOTE: The square indicates the orientation of the suspension lugs

TYPE RACK	STATION	ROLL ORIENTATION, deg
MER	1	0
	2	0
	3	45
	4	45
	5	-45
	6	-45
TER	1	0
	2	45
	3	-45

Figure 7. Store orientation.

Weapons Stations

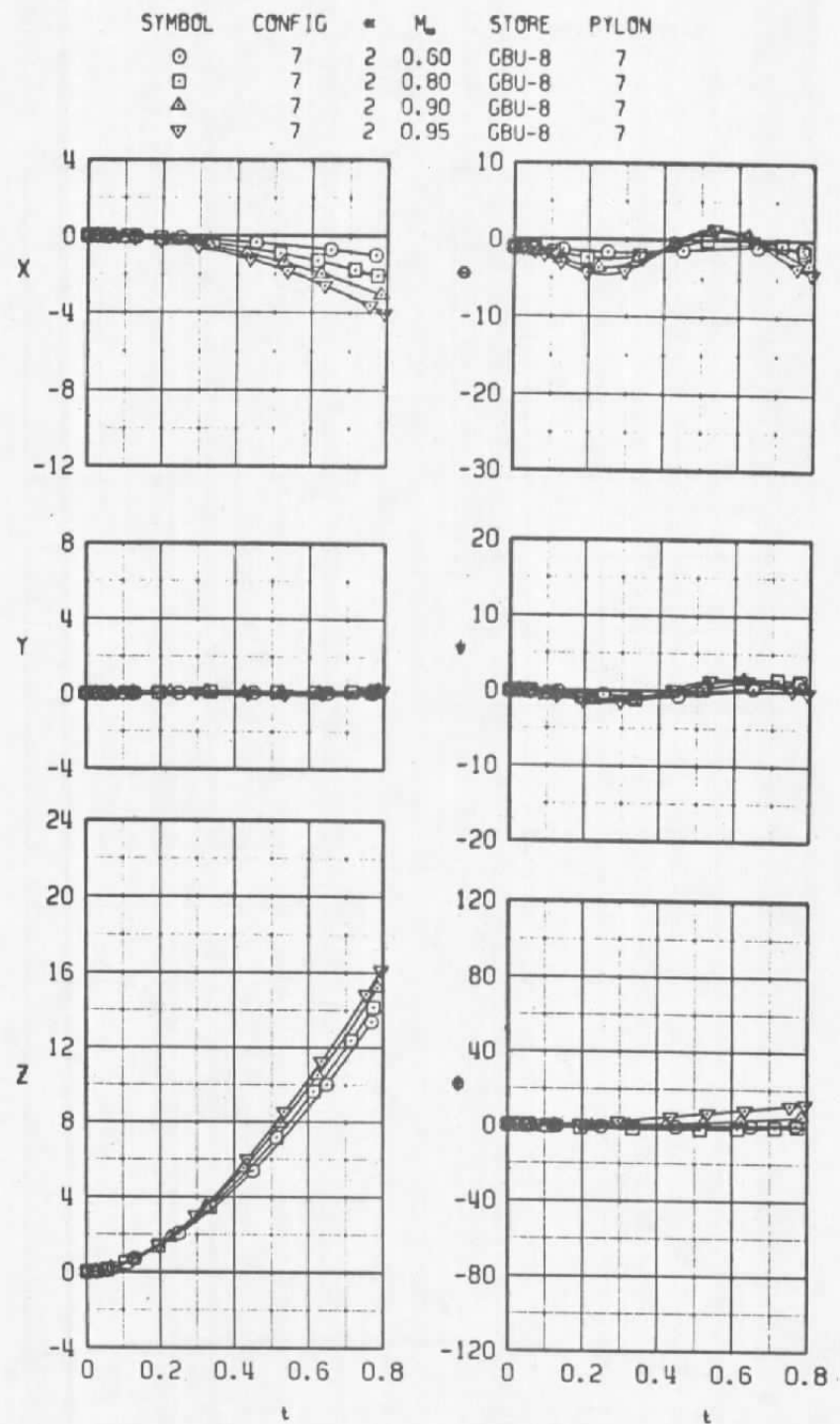
F-16 Looking Upstream

Config.	1	2	3	4	5	6	7	8	9
1	AIM-9J	Clean	Clean	Clean	ALQ 119-12	BLU-27	BLU-27	Clean	AIM-9J
2						BLU-27	BLU-27		
3						BLU-27	BLU-27		
4						BLU-27	BLU-27		
5						Empty	BLU-27		
6						BLU-27	Empty		
7						Empty	GBU-8		
8						GBU-8	Empty		
9						370 gal Tank	GBU-8		
10						MK-82SE	MK-82SE		
11						MK-82SE	MK-82SE		
12						MK-82SE	MK-82SE		
13						MK-82SE	MK-82SE		
14						MK-82SE	Empty		
15						MK-82SE	Empty		
16						Empty	GBU-8		
17						MK-82SE	Empty		

Solid Symbol Denotes Metric Store
Clear Symbol Denotes Dummy Store

Clean Denotes Pylon Removed
Empty Denotes No Store on Pylon

Figure 8. Configuration identification.



a. Configuration 7, $M_\infty = 0.6$ to 0.95
 Figure 9. Trajectories obtained with the GBU-8.

SYMBOL	CONFIG	\in	M_∞	STORE	PYLON
○	7	0	1.05	GBU-8	7
□	7	0	1.20	GBU-8	7

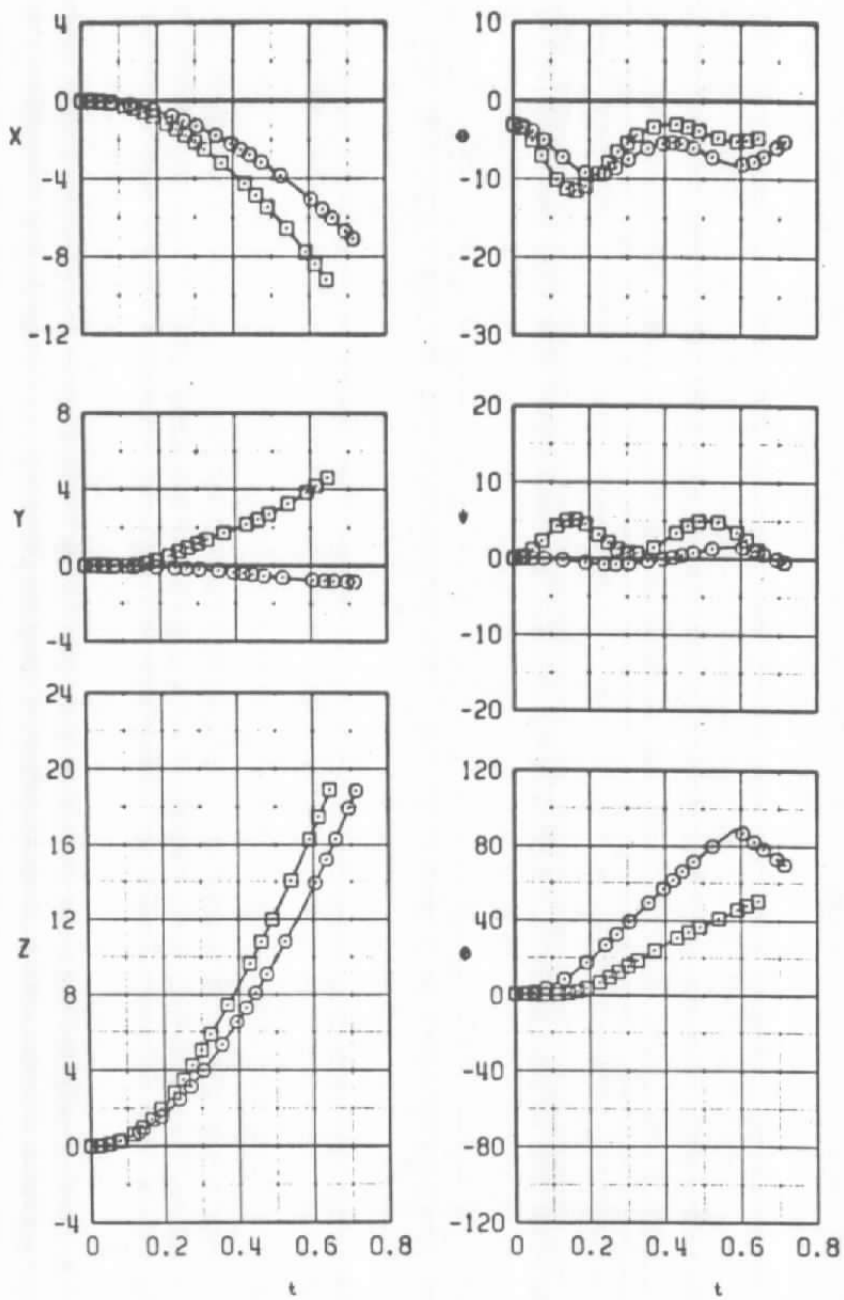
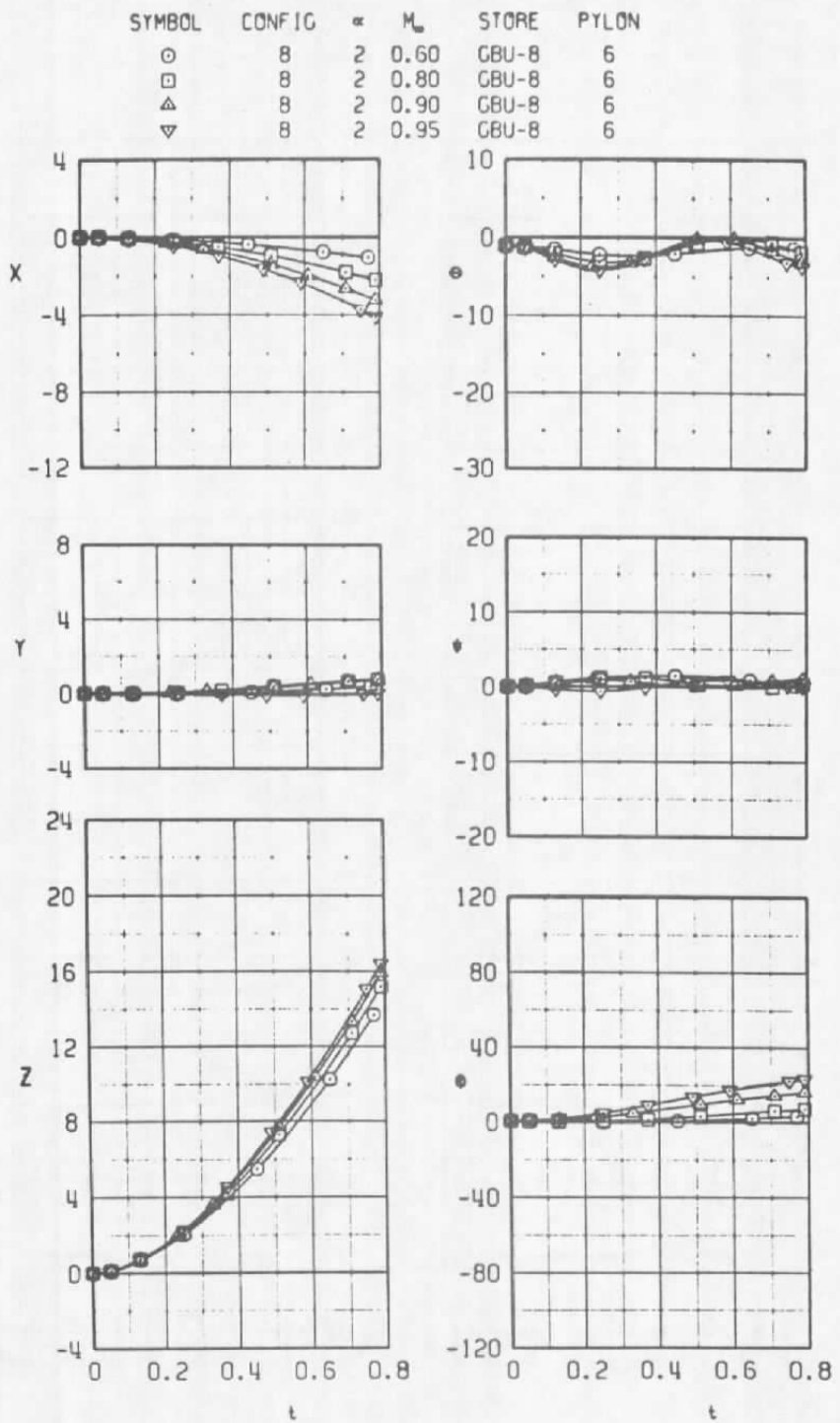
b. Configuration 7, $M_\infty = 1.05$ and 1.20

Figure 9. Continued.



c. Configuration 8, $M_\infty = 0.6$ to 0.95
Figure 9. Continued.

SYMBOL	CONFIG	M_∞	STORE	PYLON	
○	8	0	1.05	GBU-8	6
□	8	0	1.20	GBU-8	6

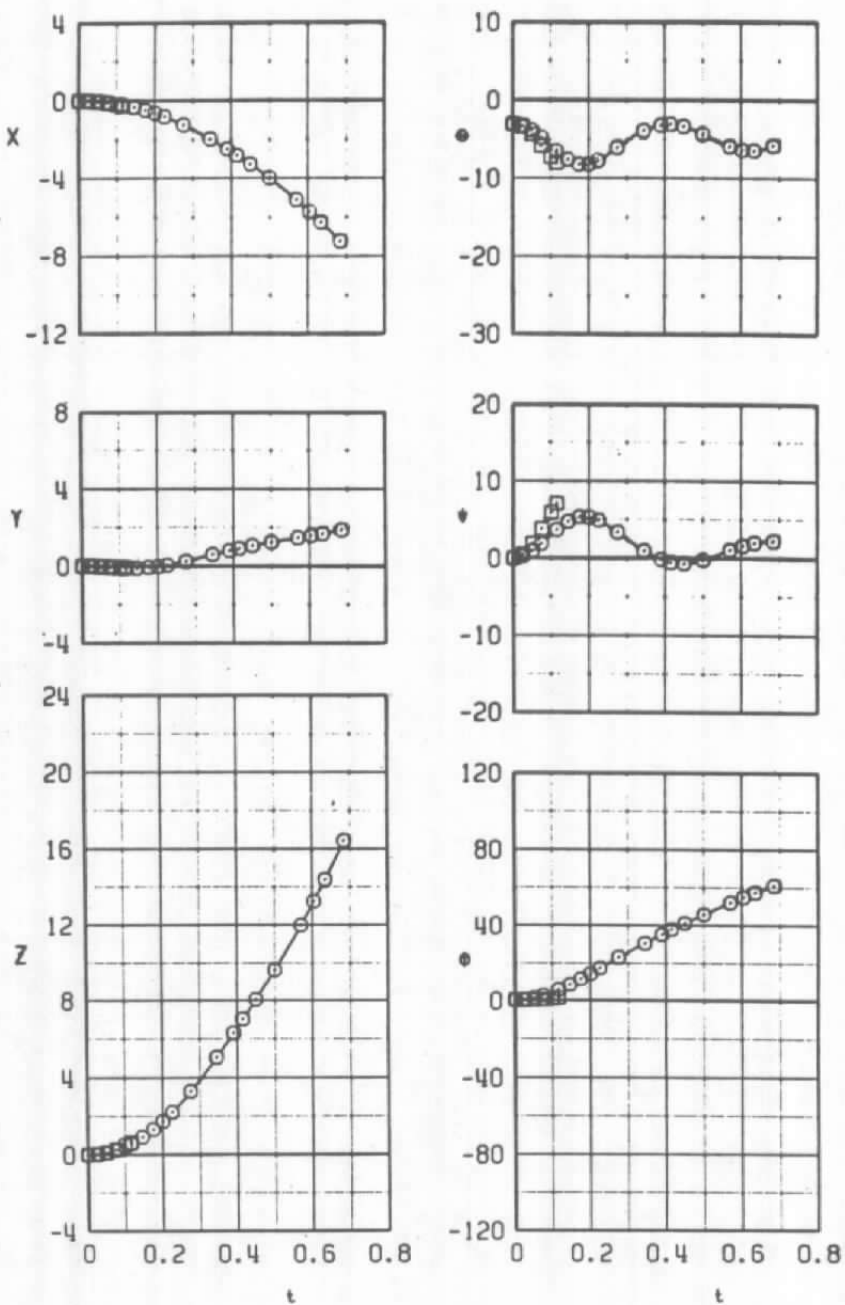
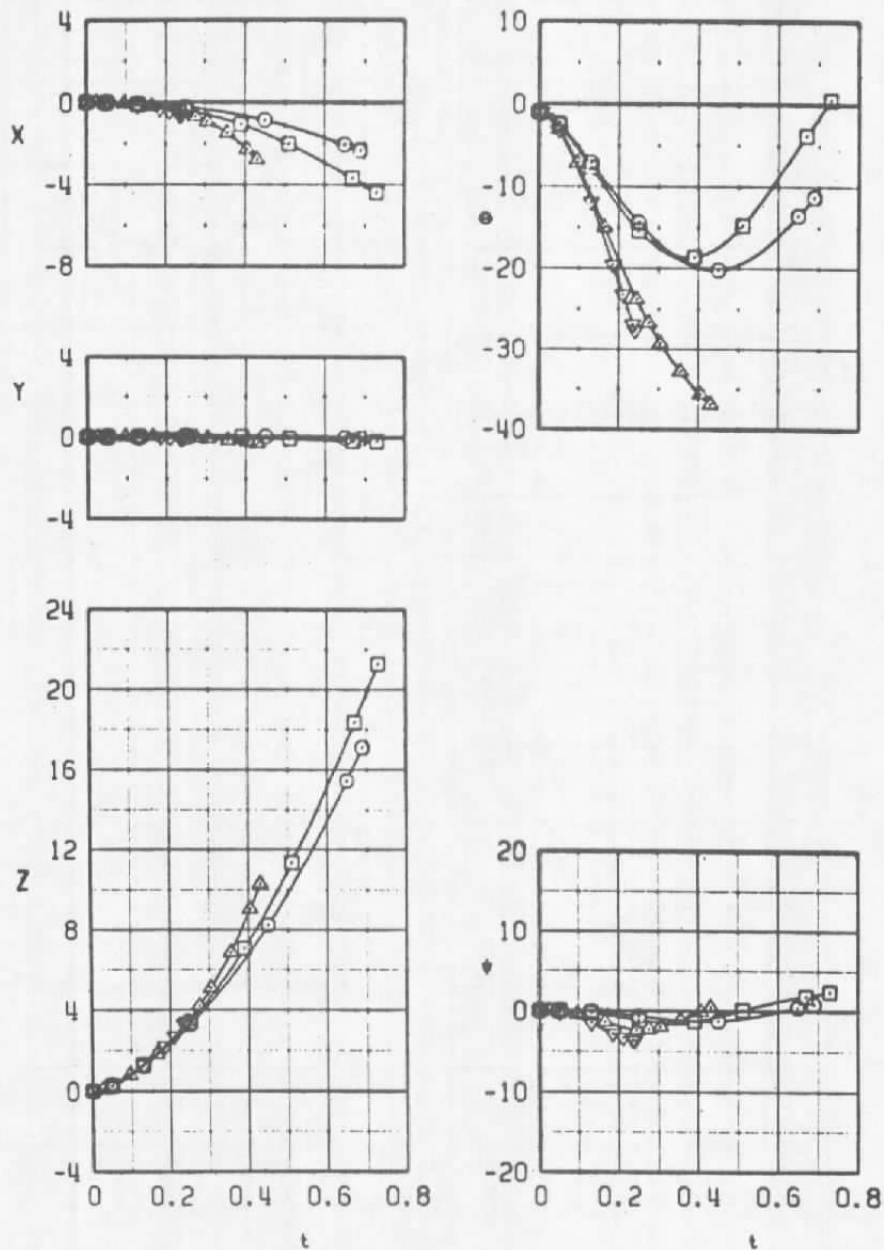
d. Configuration 8, $M_\infty = 1.05$ and 1.20

Figure 9. Concluded.

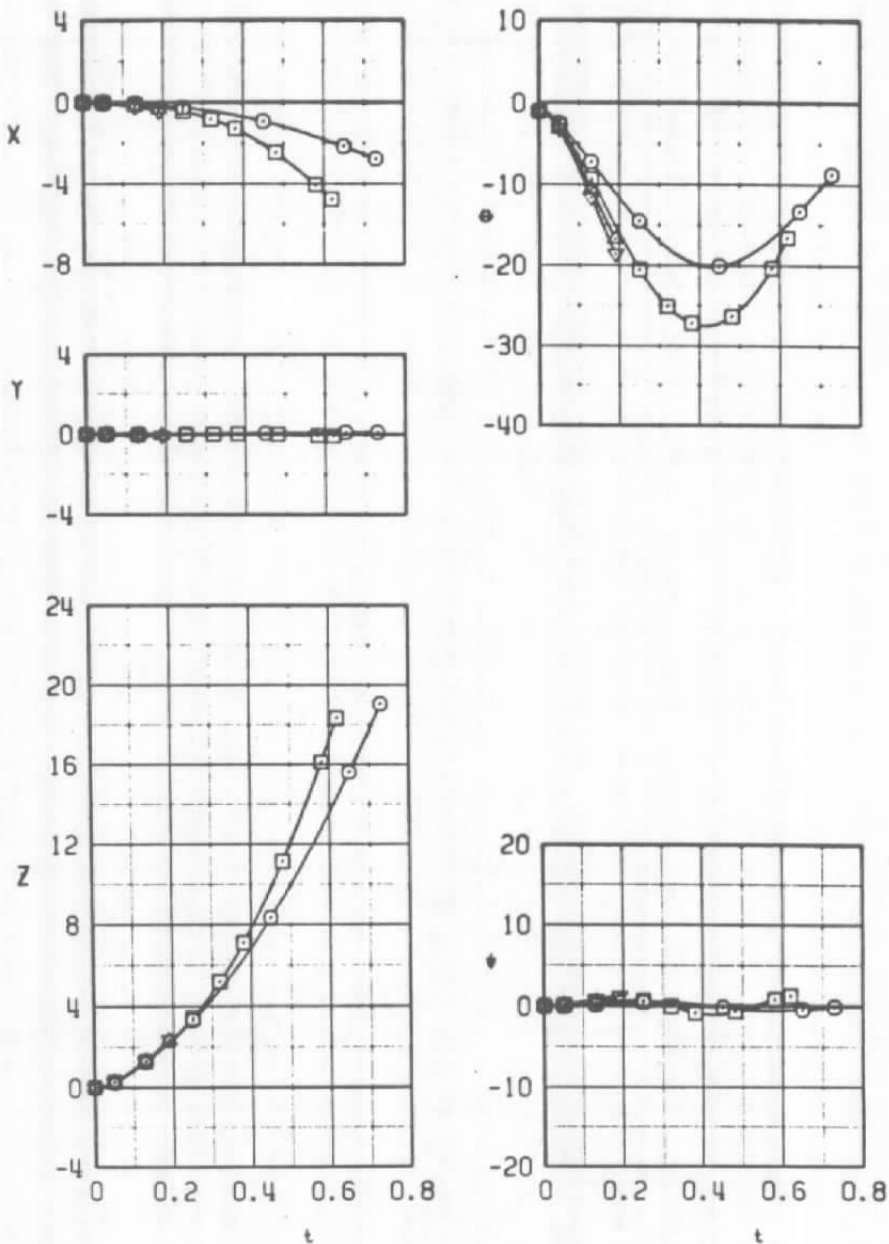
SYMBOL	CONFIG	α	M_∞	STORE	PYLON
○	16	2	0.60	MK-82SE	7
□	16	2	0.80	MK-82SE	7
△	16	2	0.90	MK-82SE	7
▽	16	2	0.95	MK-82SE	7



a. Configuration 16

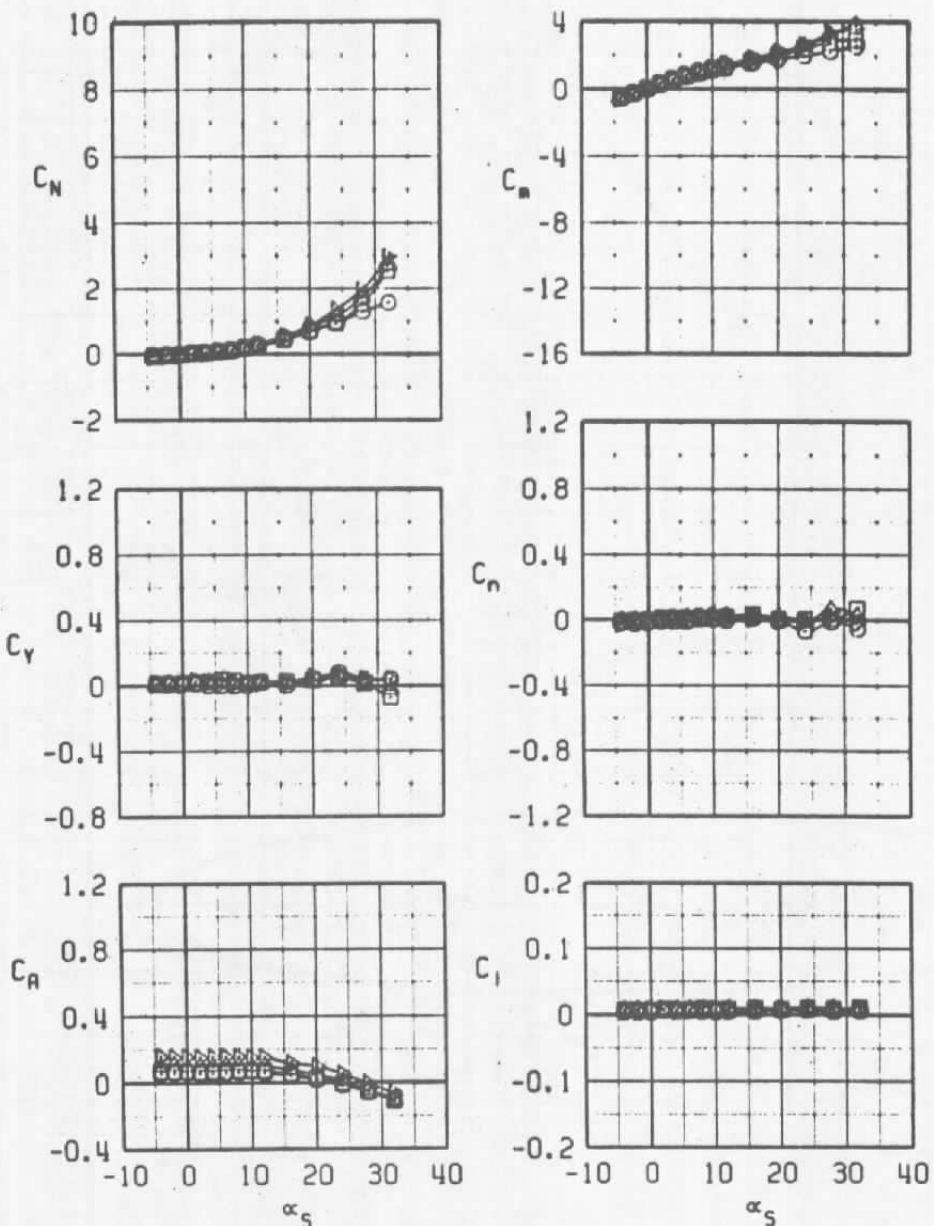
Figure 10. Trajectories obtained with the MK-82SE.

SYMBOL	CONFIG	α	M_∞	STORE	PYLON
○	17	2	0.60	MK-82SE	6
□	17	2	0.80	MK-82SE	6
△	17	2	0.90	MK-82SE	6
▽	17	2	0.95	MK-82SE	6



b. Configuration 17
Figure 10. Concluded.

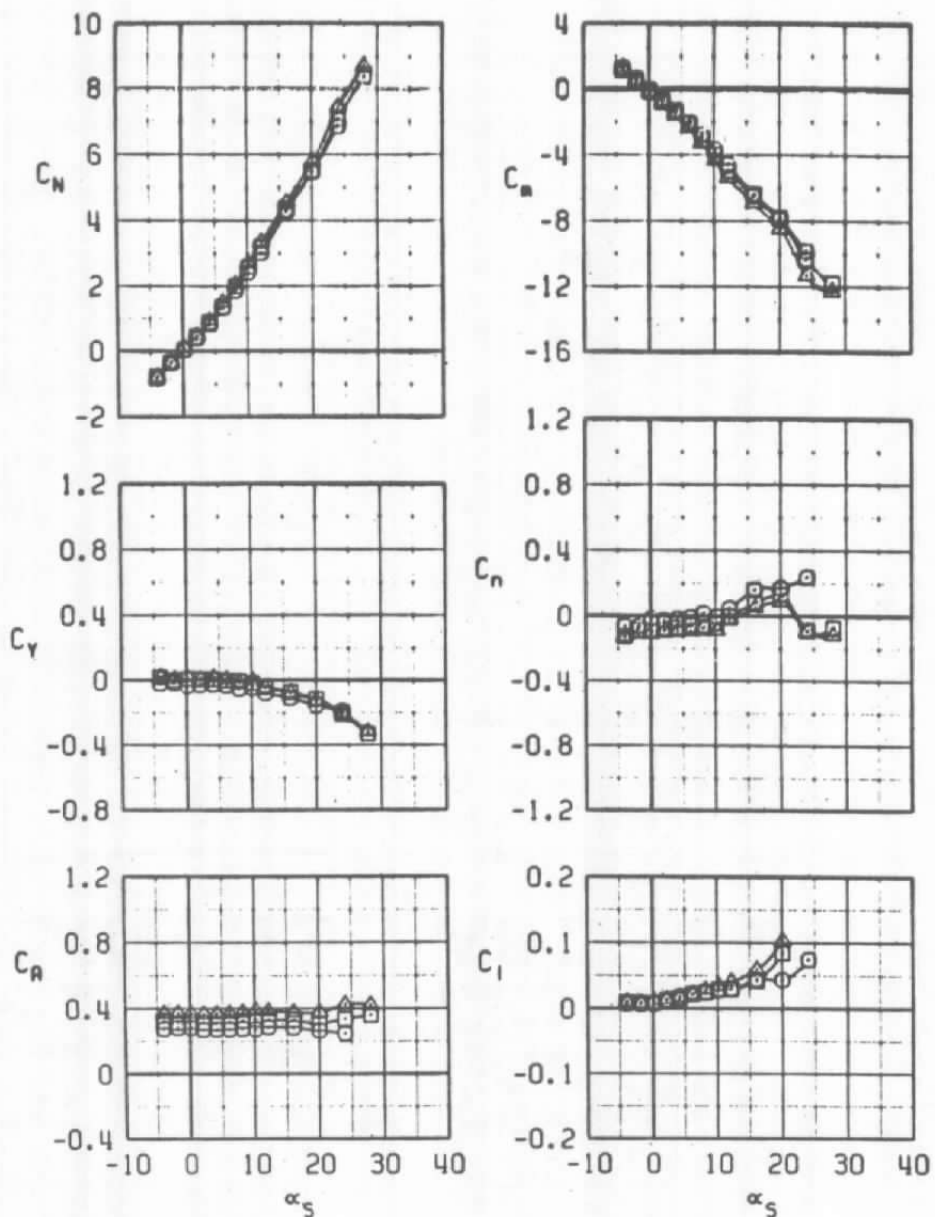
SYMBOL	CONFIG	M_∞	STORE
○	FREESTREAM	0.60	BLU-27B/B
□	FREESTREAM	0.80	BLU-27B/B
△	FREESTREAM	0.90	BLU-27B/B
▷	FREESTREAM	0.95	BLU-27B/B



a. BLU-27B/B

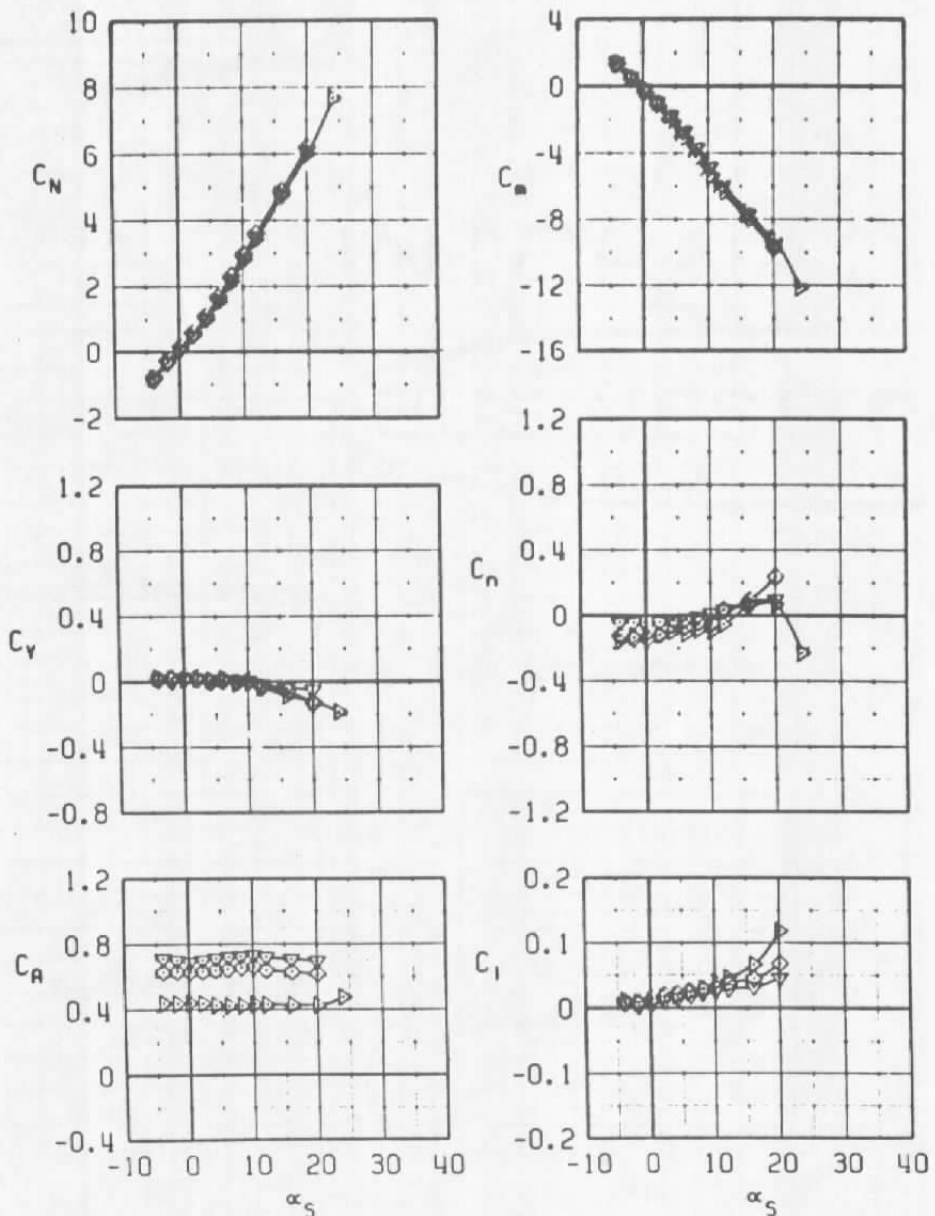
Figure 11. Free-stream aerodynamic coefficients.

SYMBOL	CONFIG	M_∞	STORE
○	FREESTREAM	0.60	GBU-8
□	FREESTREAM	0.80	GBU-8
△	FREESTREAM	0.90	GBU-8



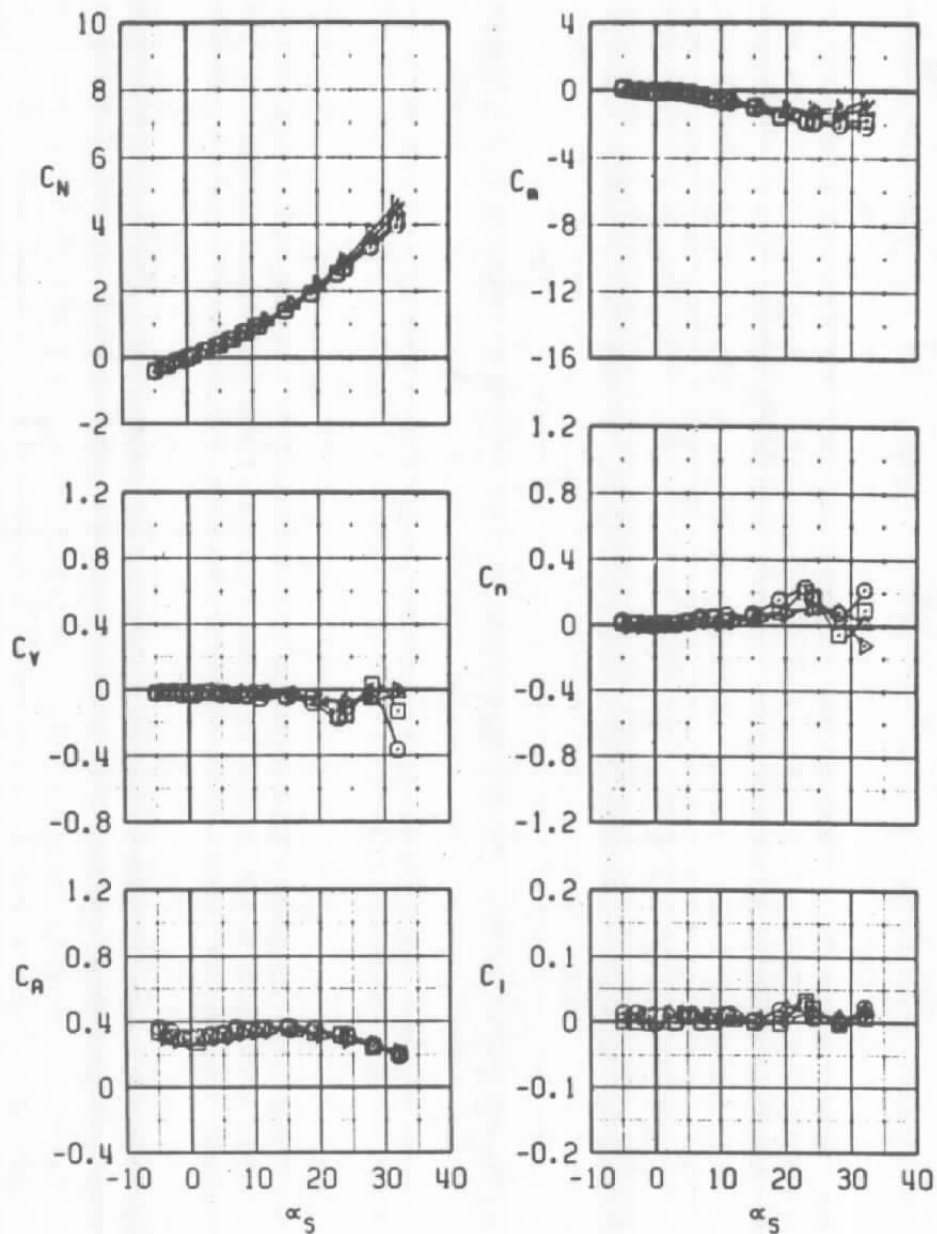
b. GBU-8
Figure 11. Continued.

SYMBOL	CONFIG	M_∞	STORE
▷	FREESTREAM	0.95	GBU-8
○	FREESTREAM	1.05	GBU-8
▽	FREESTREAM	1.20	GBU-8



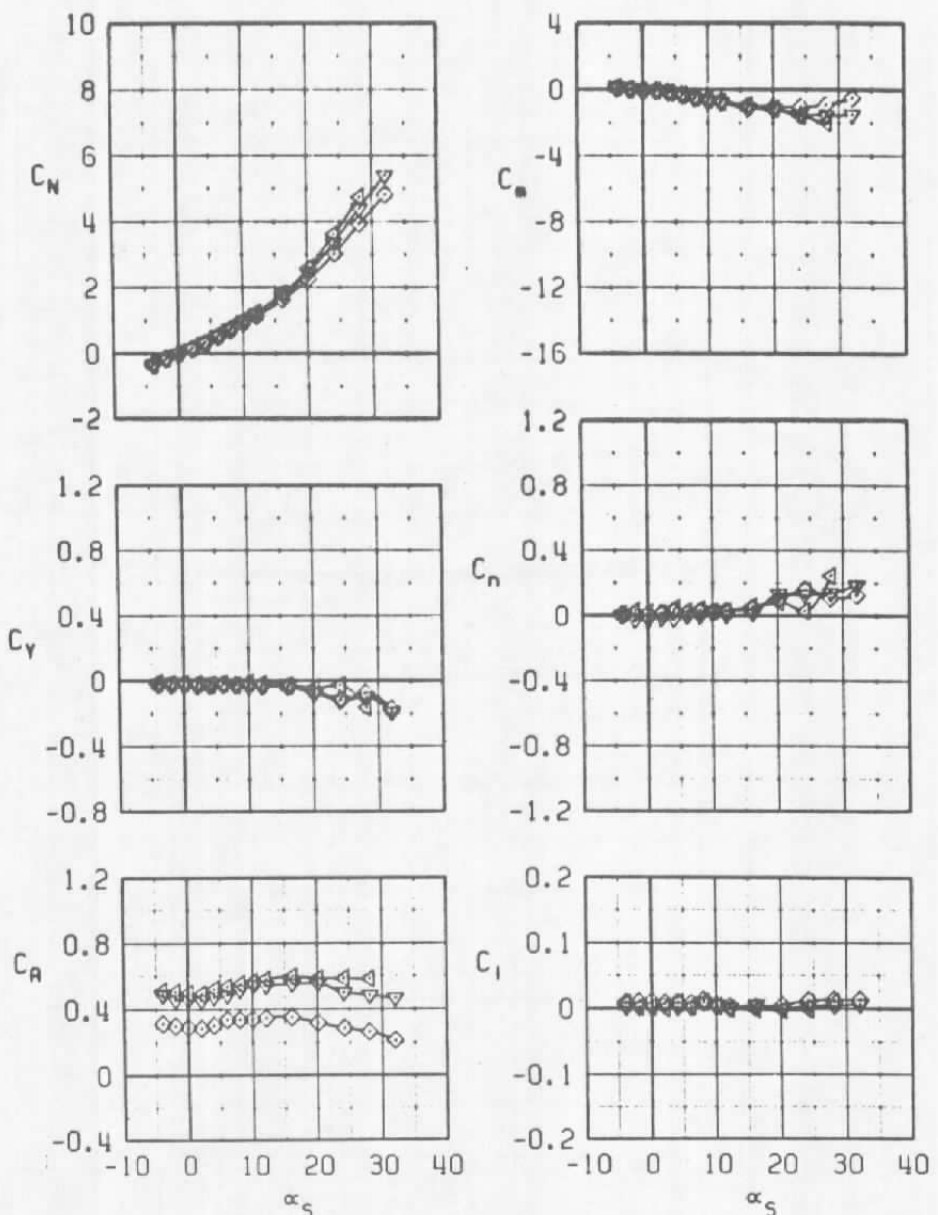
b. Concluded
Figure 11. Continued.

SYMBOL	CONFIG	M_∞	STORE
○	FREESTREAM	0.40	MK-82SE
□	FREESTREAM	0.60	MK-82SE
△	FREESTREAM	0.80	MK-82SE
▷	FREESTREAM	0.90	MK-82SE



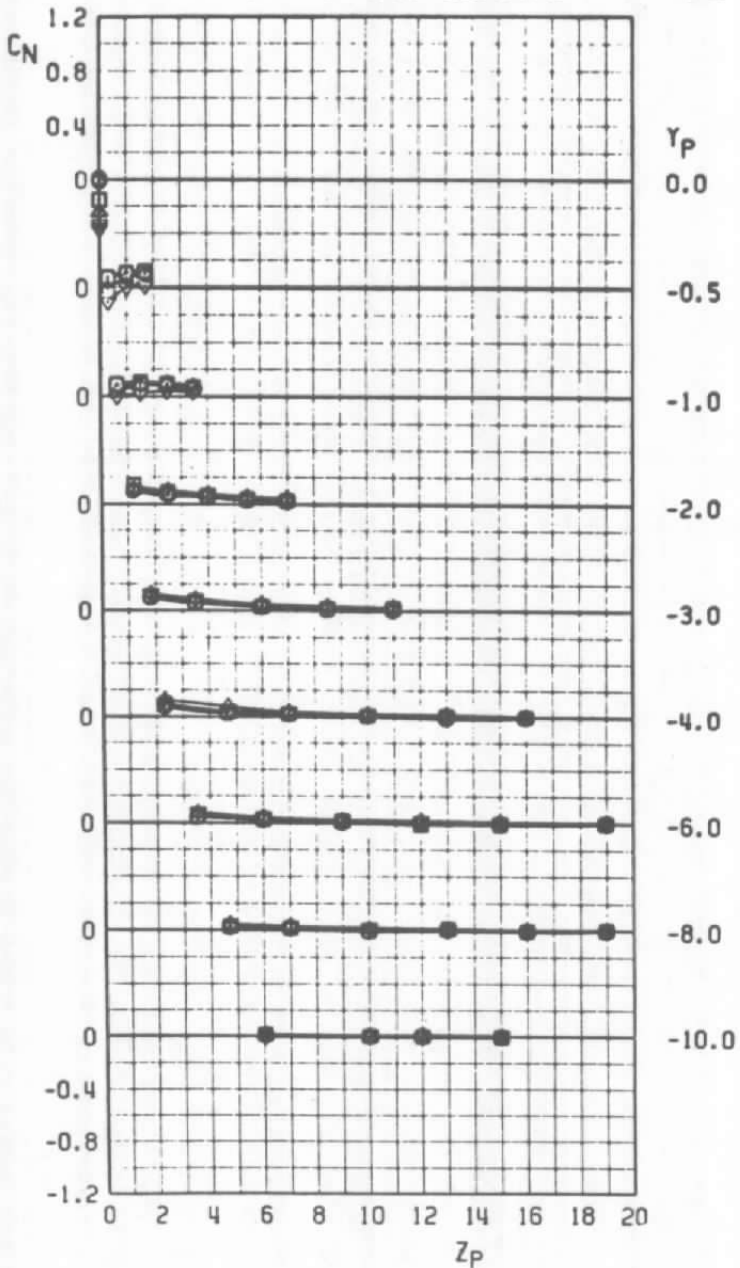
c. MK-82SE
Figure 11. Continued.

SYMBOL	CONFIG	M_∞	STORE
◊	FREESTREAM	0.95	MK-82SE
▽	FREESTREAM	1.05	MK-82SE
△	FREESTREAM	1.20	MK-82SE



c. Concluded
Figure 11. Concluded.

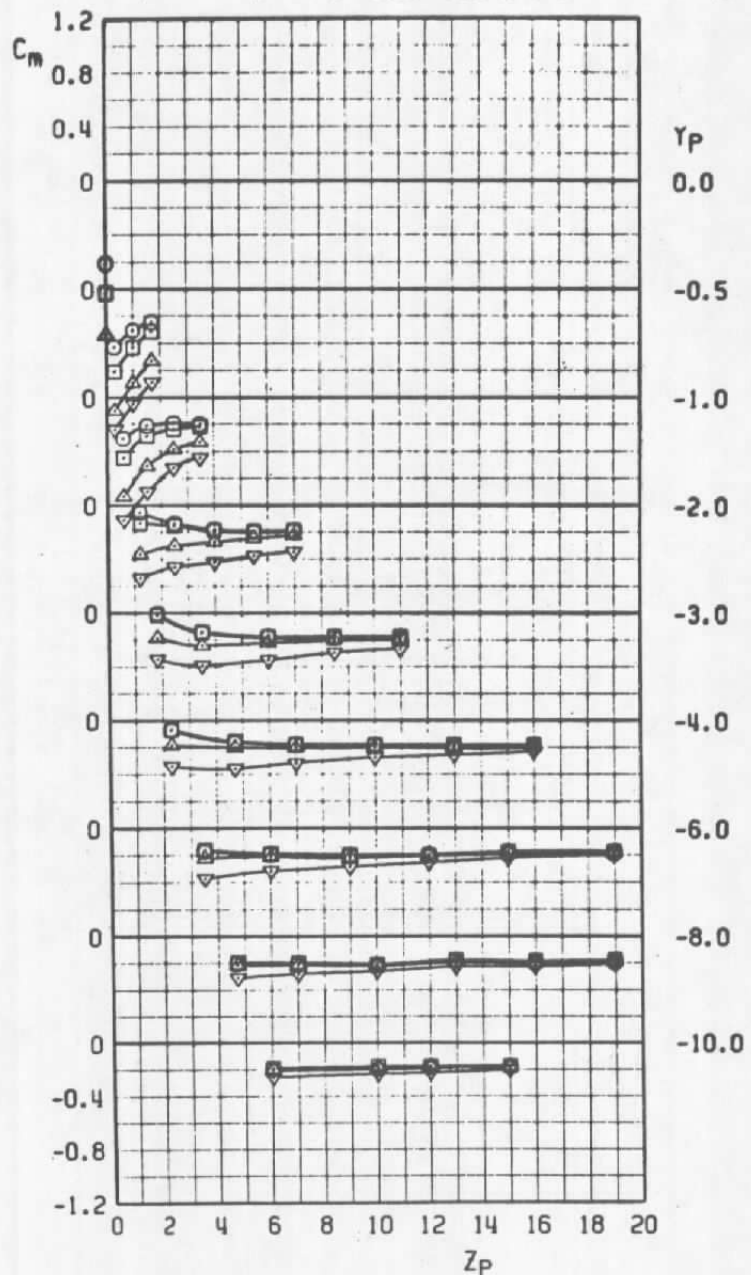
SYMBOL	CONFIG	α	M_∞	STORE	PYLON	RACK
○	1	2	0.60	BLU-27B/B	7	T-2
□	1	2	0.80	BLU-27B/B	7	T-2
△	1	2	0.90	BLU-27B/B	7	T-2
▽	1	2	0.95	BLU-27B/B	7	T-2



a. Normal-force coefficient

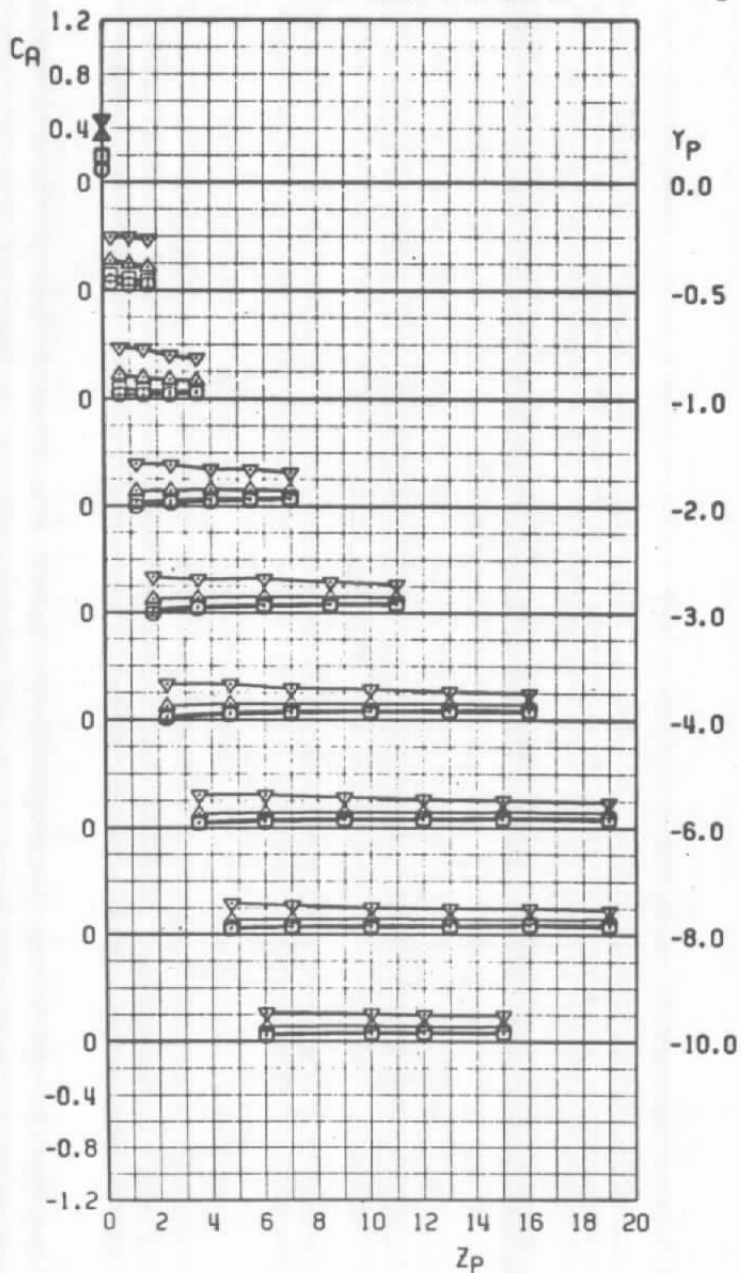
Figure 12. Aerodynamic characteristics of the BLU-27B/B, configuration 1.

SYMBOL	CONFIG	α	M_∞	STORE	PYLON	RACK
○	I	2	0.60	BLU-27B/B	7	T-2
□	I	2	0.80	BLU-27B/B	7	T-2
△	I	2	0.90	BLU-27B/B	7	T-2
▽	I	2	0.95	BLU-27B/B	7	T-2



b. Pitching-moment coefficient
Figure 12. Continued.

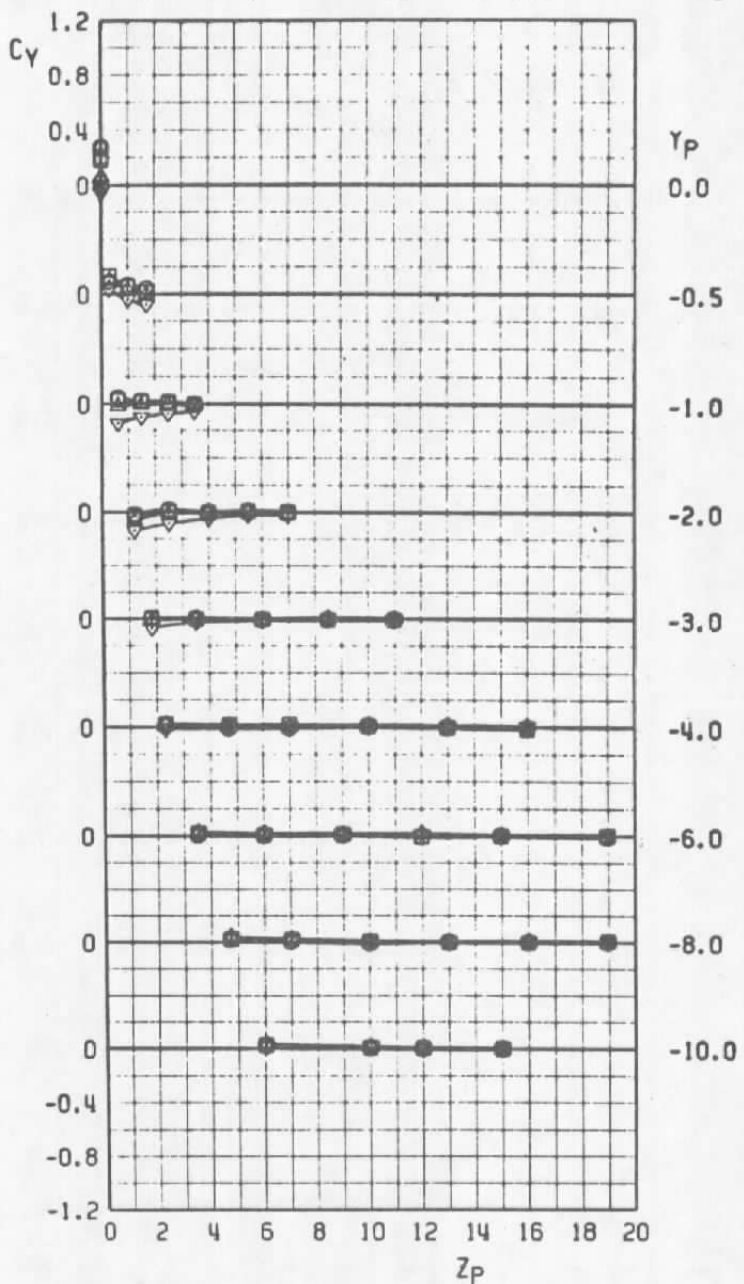
SYMBOL	CONFIG	α	M_∞	STORE	PYLON	RACK
○	1	2	0.60	BLU-27B/B	7	T-2
□	1	2	0.80	BLU-27B/B	7	T-2
△	1	2	0.90	BLU-27B/B	7	T-2
▽	1	2	0.95	BLU-27B/B	7	T-2



c. Axial-force coefficient

Figure 12. Continued.

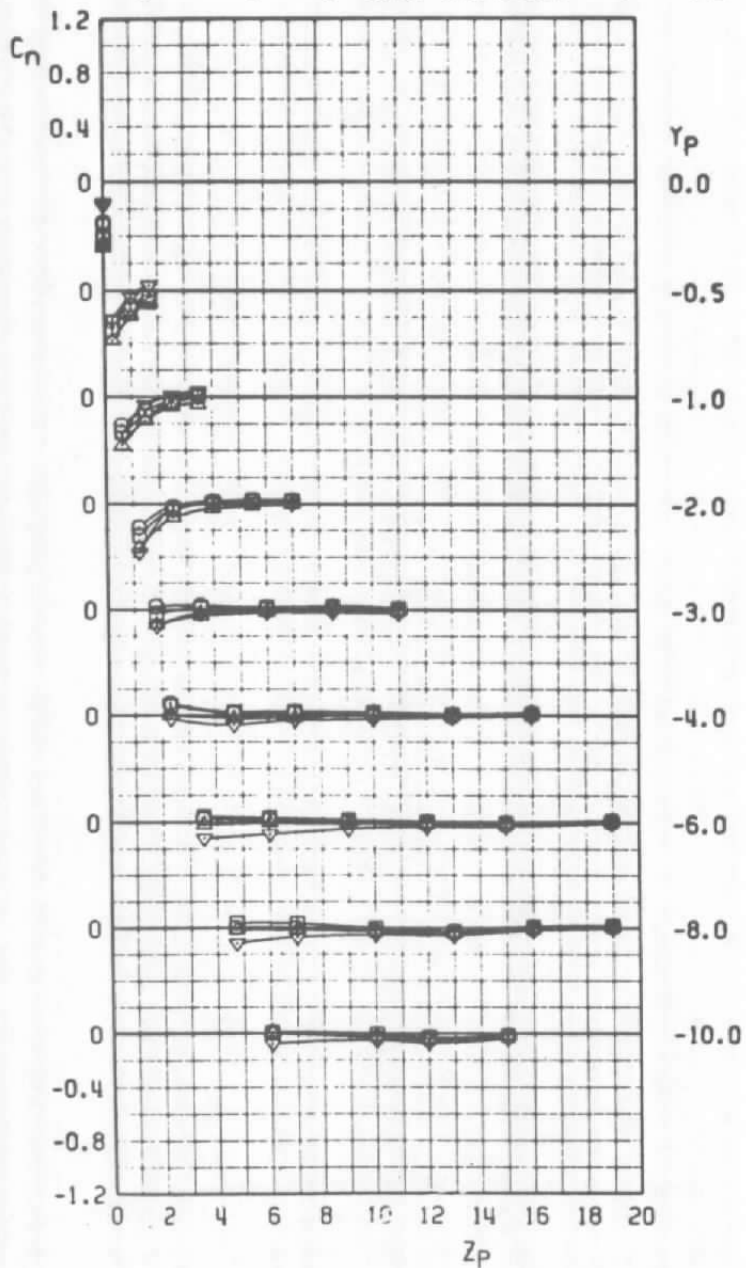
SYMBOL	CONFIG	α	M_∞	STORE	PYLON	RACK
○	1	2	0.60	BLU-27B/B	7	T-2
□	1	2	0.80	BLU-27B/B	7	T-2
△	1	2	0.90	BLU-27B/B	7	T-2
▽	1	2	0.95	BLU-27B/B	7	T-2



d. Side-force coefficient

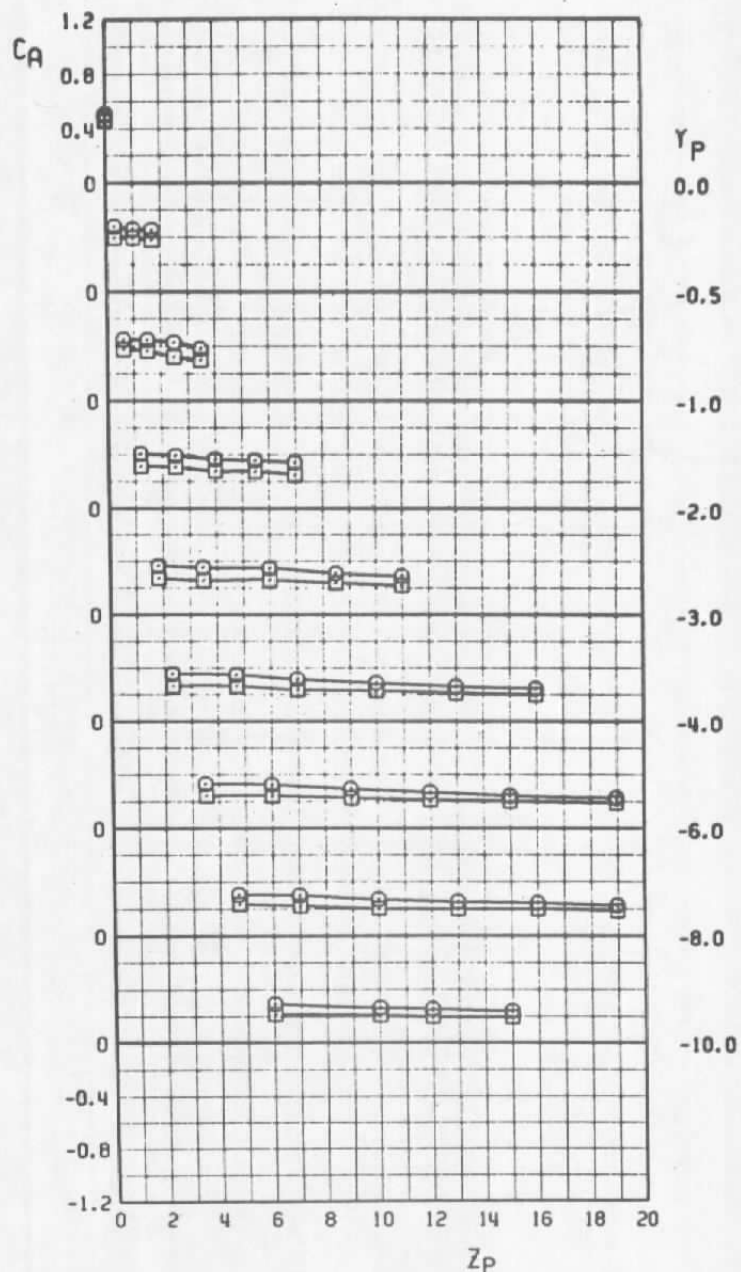
Figure 12. Continued.

SYMBOL	CONFIG	α	M_a	STORE	PYLON	RACK
○	1	2	0.60	BLU-27B/B	7	T-2
□	1	2	0.80	BLU-27B/B	7	T-2
△	1	2	0.90	BLU-27B/B	7	T-2
▽	1	2	0.95	BLU-27B/B	7	T-2



e. Yawing-moment coefficient
Figure 12. Concluded.

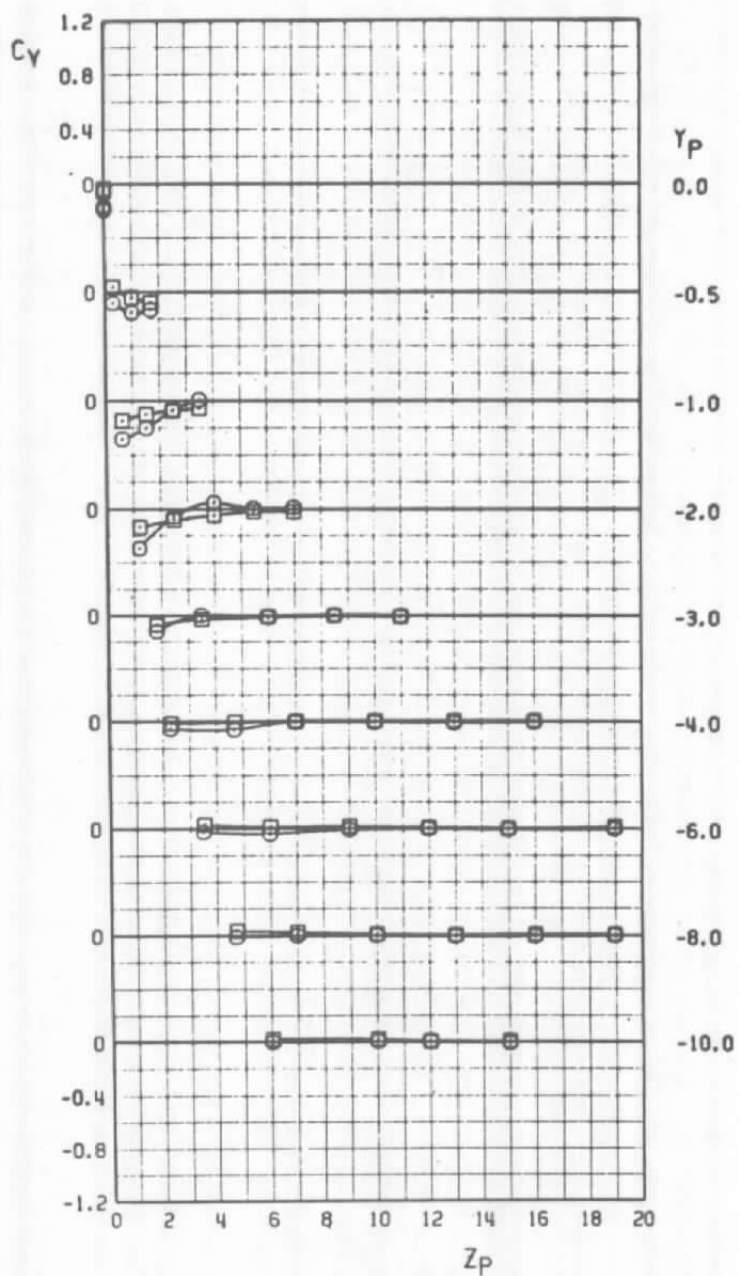
SYMBOL	CONFIG	α	M_∞	STORE	PYLON	RACK
○	1	0	0.95	BLU-27B/B	7	T-2
□	1	2	0.95	BLU-27B/B	7	T-2



a. Axial-force coefficient

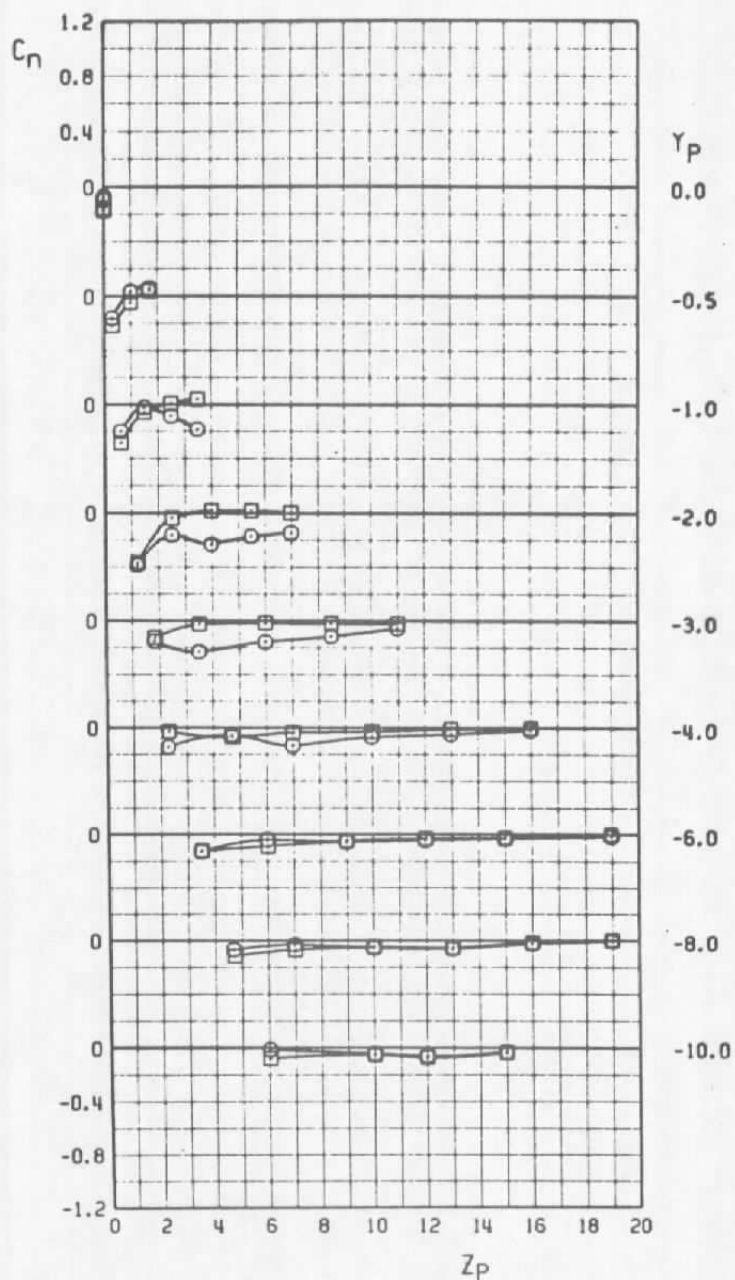
Figure 13. BLU-27B/B coefficient variation with aircraft angle of attack, configuration 1.

SYMBOL	CONFIG	α	M_∞	STORE	PYLON	RACK
○	1	0	0.95	BLU-27B/B	7	T-2
□	1	2	0.95	BLU-27B/B	7	T-2



b. Side-force coefficient
Figure 13. Continued.

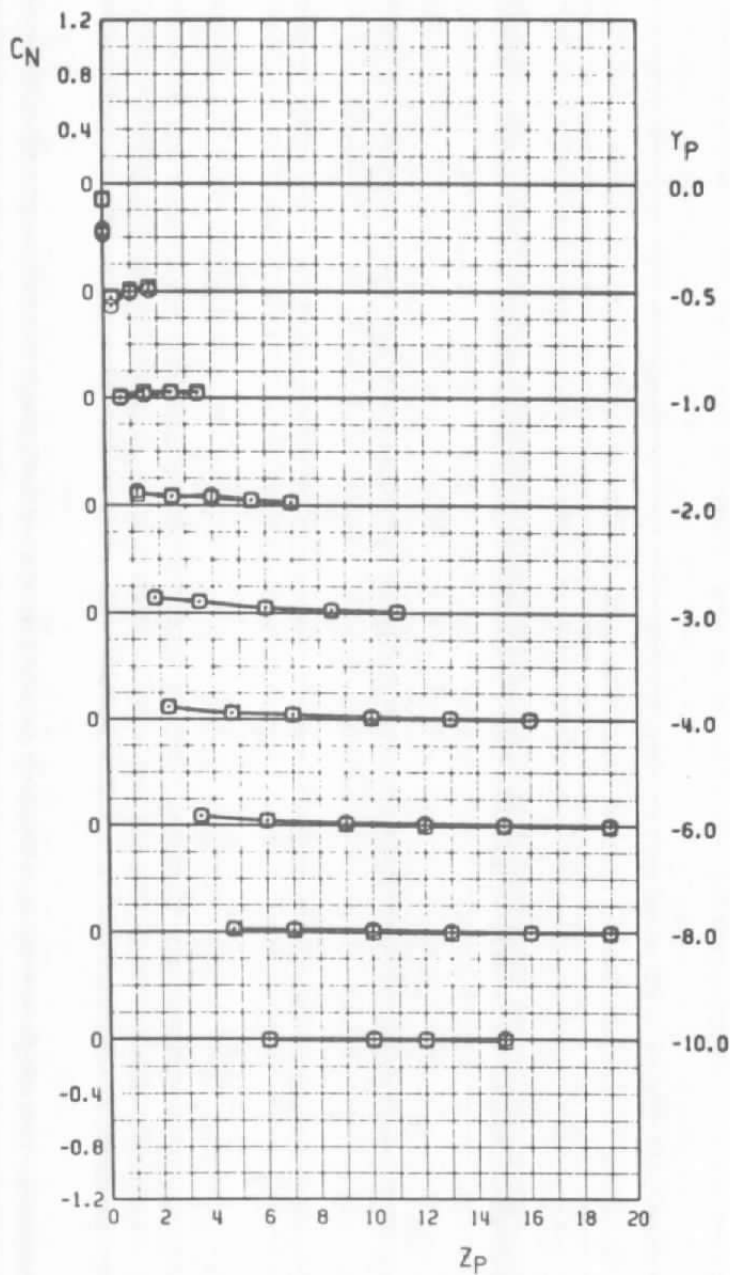
SYMBOL	CONFIG	\in	M_a	STORE	PYLON	RACK
○	1	0	0.95	BLU-27B/B	7	T-2
□	1	2	0.95	BLU-27B/B	7	T-2



c. Yawing-moment coefficient

Figure 13. Concluded.

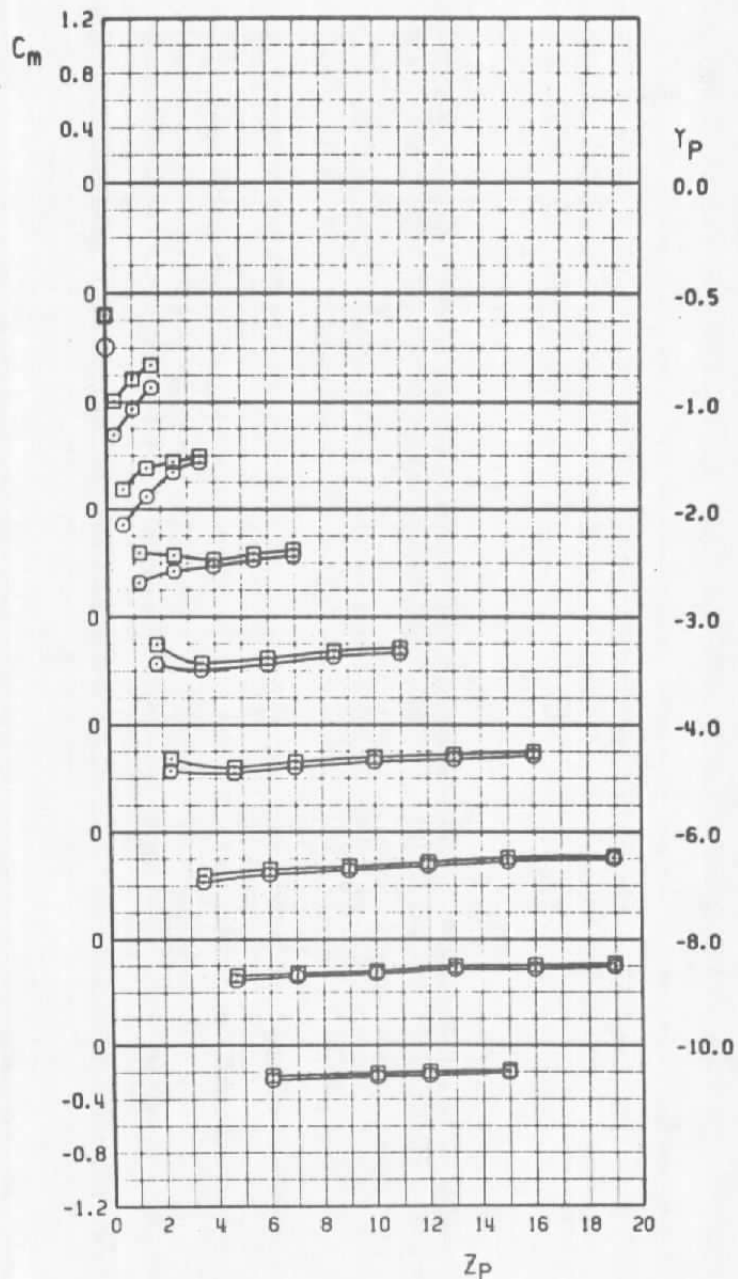
SYMBOL	CONFIG	α	M_∞	STORE	PYLON	RACK
○	1	2	0.95	BLU-27B/B	7	T-2
□	2	2	0.95	BLU-27B/B	7	T-2



a. Normal-force coefficient

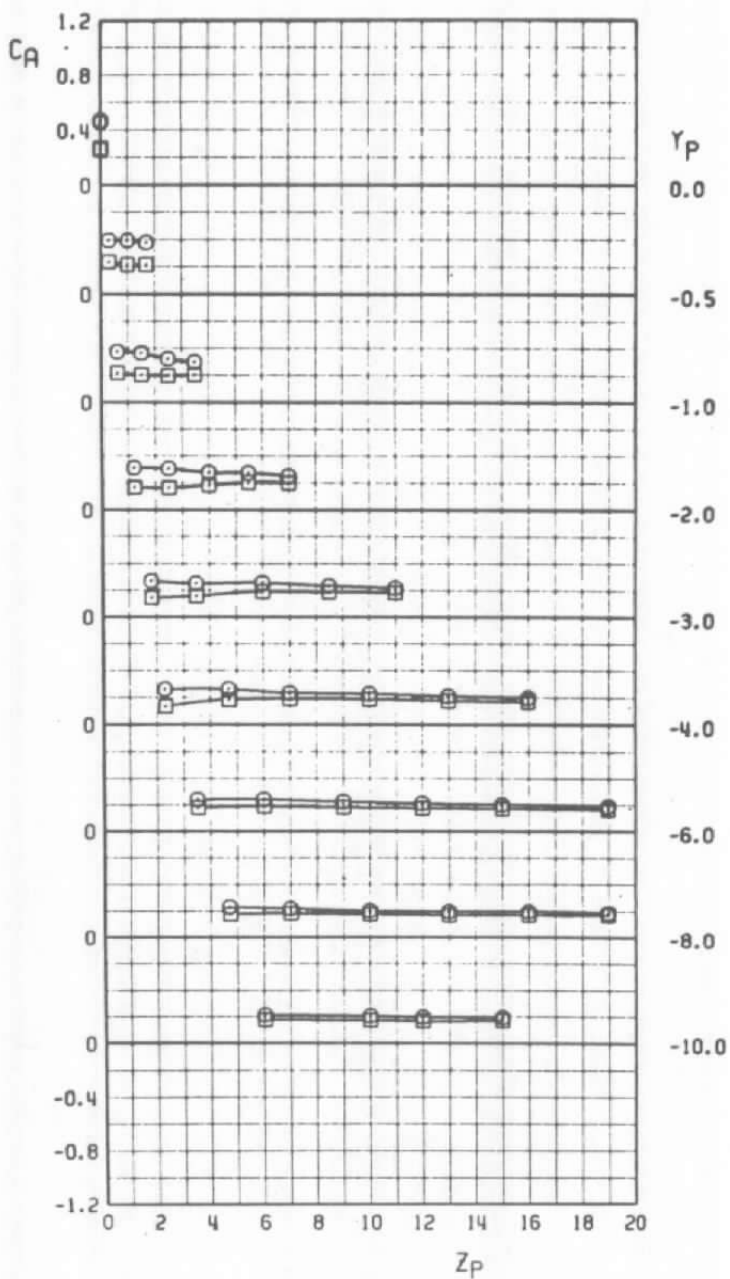
Figure 14. Effect of an adjacent store on the BLU-27B/B, configurations 1 and 2.

SYMBOL	CONFIG	α	M_∞	STORE	PYLON	RACK
○	1	2	0.95	BLU-27B/B	7	T-2
□	2	2	0.95	BLU-27B/B	7	T-2



b. Pitching-moment coefficient
Figure 14. Continued.

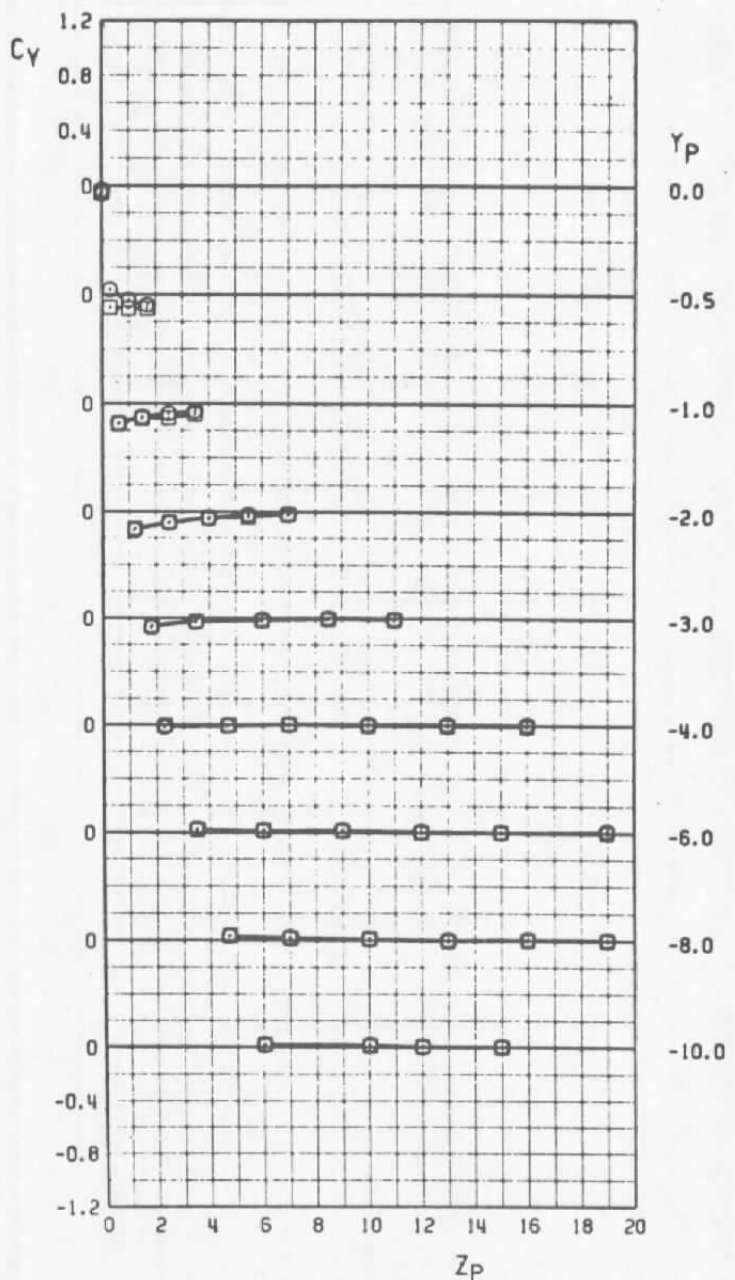
SYMBOL	CONFIG	*	M_∞	STORE	PYLON	RACK
○	1	2	0.95	BLU-278/B	7	T-2
□	2	2	0.95	BLU-278/B	7	T-2



c. Axial-force coefficient

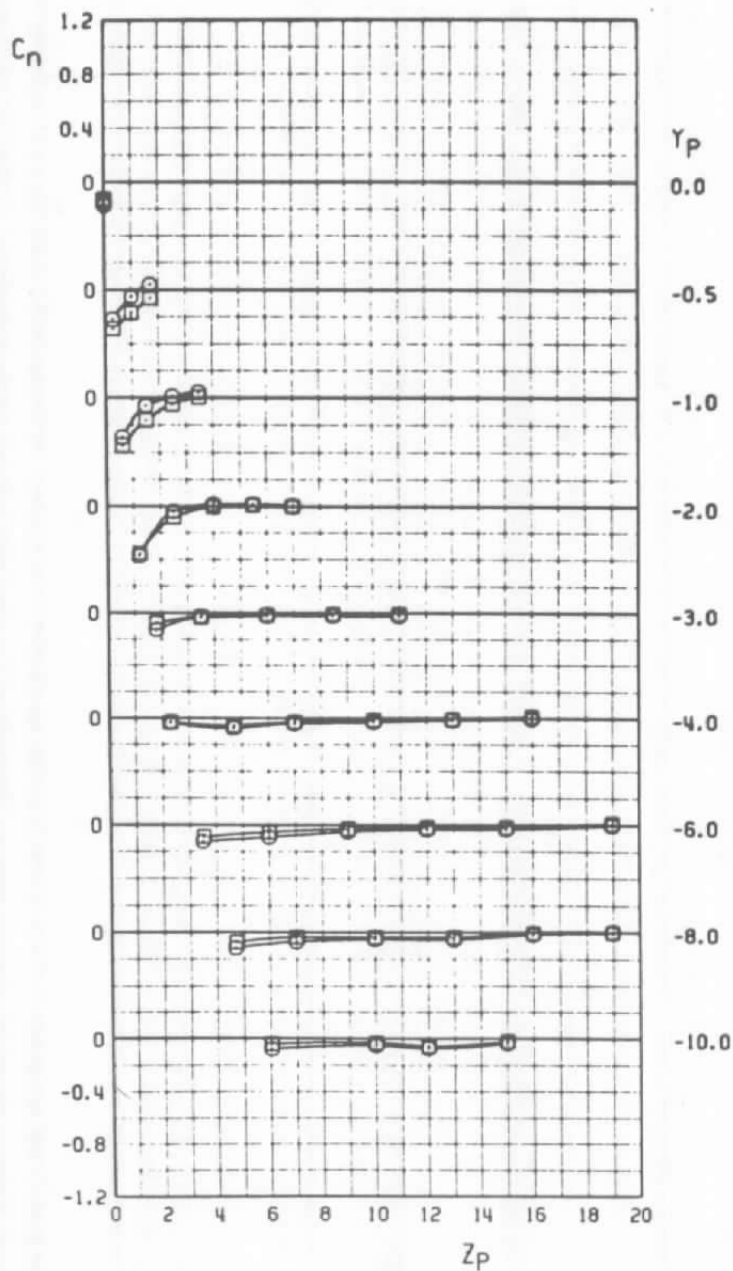
Figure 14. Continued.

SYMBOL	CONFIG	M_∞	STORE	PYLON	RACK	
○	1	2	0.95	BLU-27B/B	7	T-2
□	2	2	0.95	BLU-27B/B	7	T-2



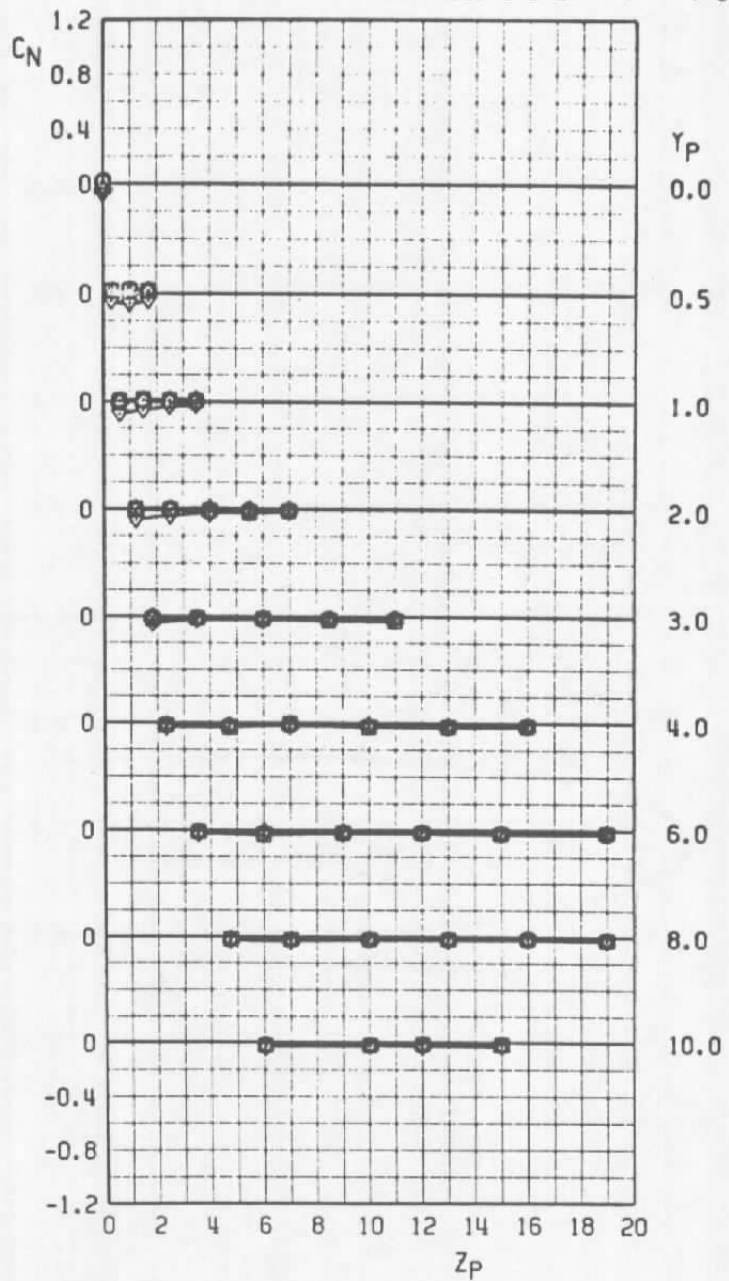
d. Side-force coefficient
Figure 14. Continued.

SYMBOL	CONFIG	α	M_0	STORE	PYLON	RACK
○	1	2	0.95	BLU-27B/B	7	T-2
□	2	2	0.95	BLU-27B/B	7	T-2



e. Yawing-moment coefficient
Figure 14. Concluded.

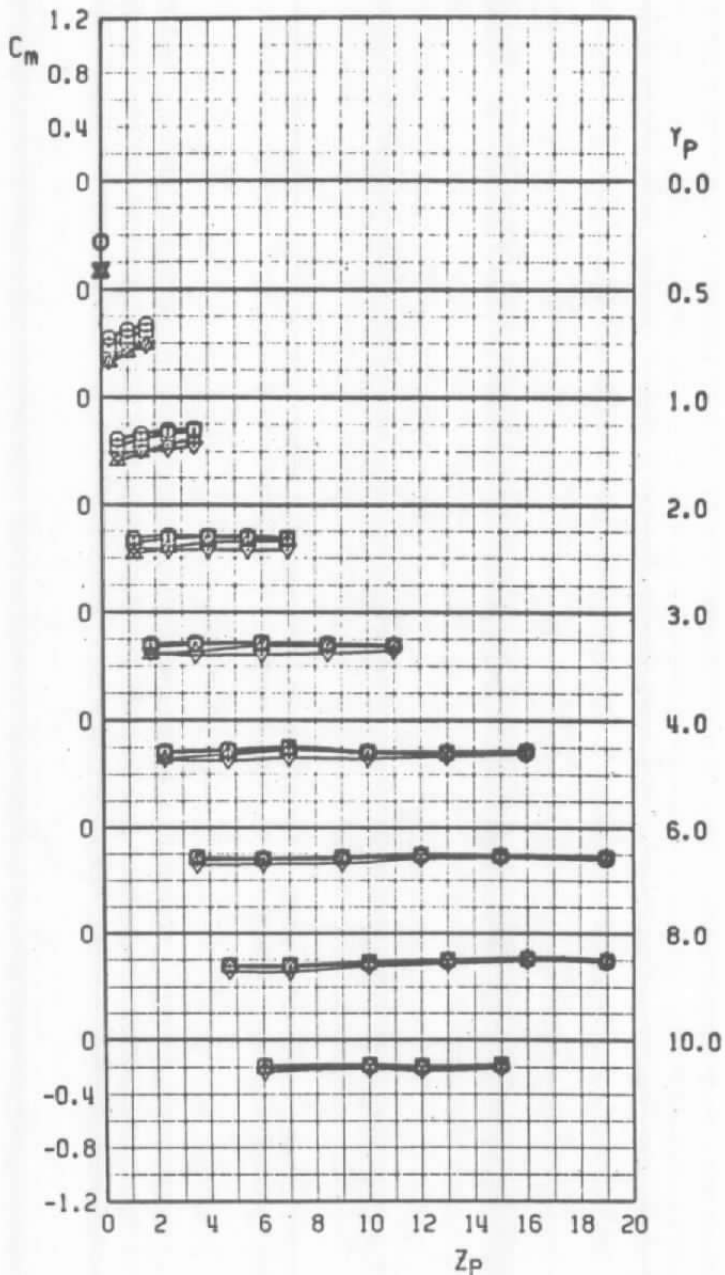
SYMBOL	CONFIG	α	M_∞	STORE	PYLON	RACK
○	3	2	0.60	BLU-27B/B	7	T-3
□	3	2	0.80	BLU-27B/B	7	T-3
△	3	2	0.90	BLU-27B/B	7	T-3
▽	3	2	0.95	BLU-27B/B	7	T-3



a. Normal-force coefficient

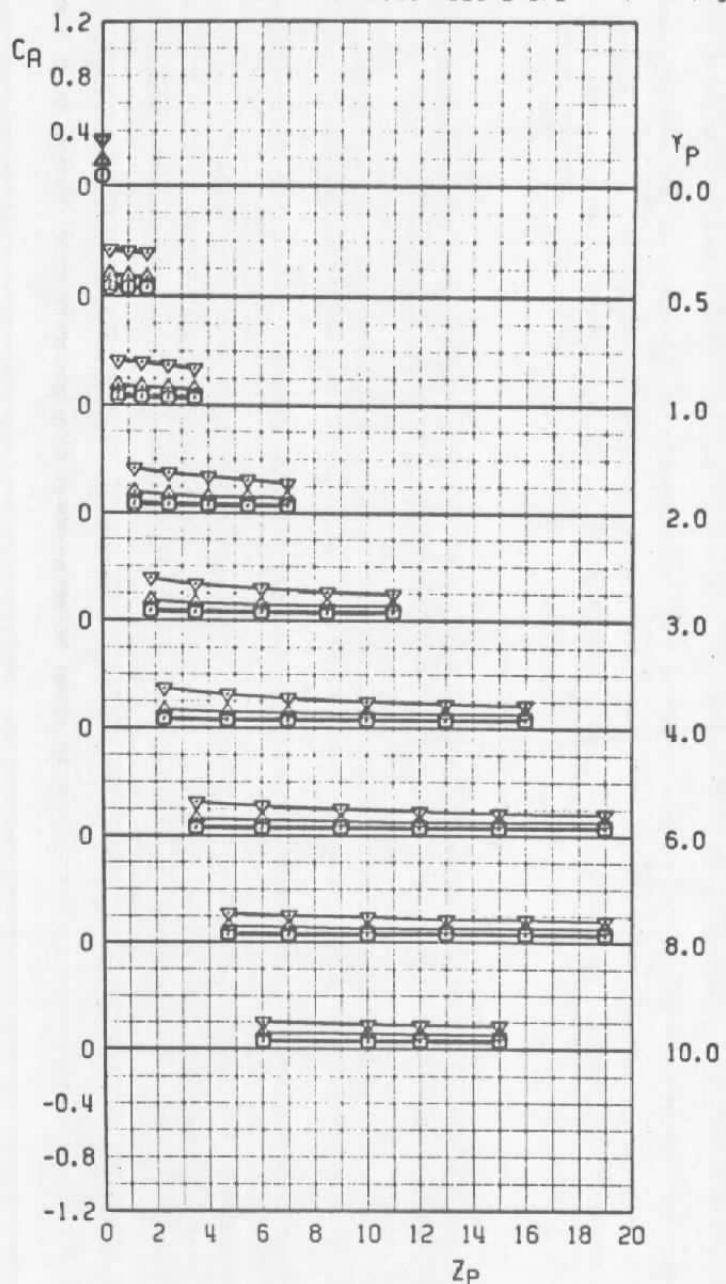
Figure 15. Aerodynamic characteristics of the BLU-27B/B, configuration 3.

SYMBOL	CONFIG	α	M_∞	STORE	PYLON	RACK
○	3	2	0.60	BLU-27B/B	7	T-3
□	3	2	0.80	BLU-27B/B	7	T-3
△	3	2	0.90	BLU-27B/B	7	T-3
▽	3	2	0.95	BLU-27B/B	7	T-3

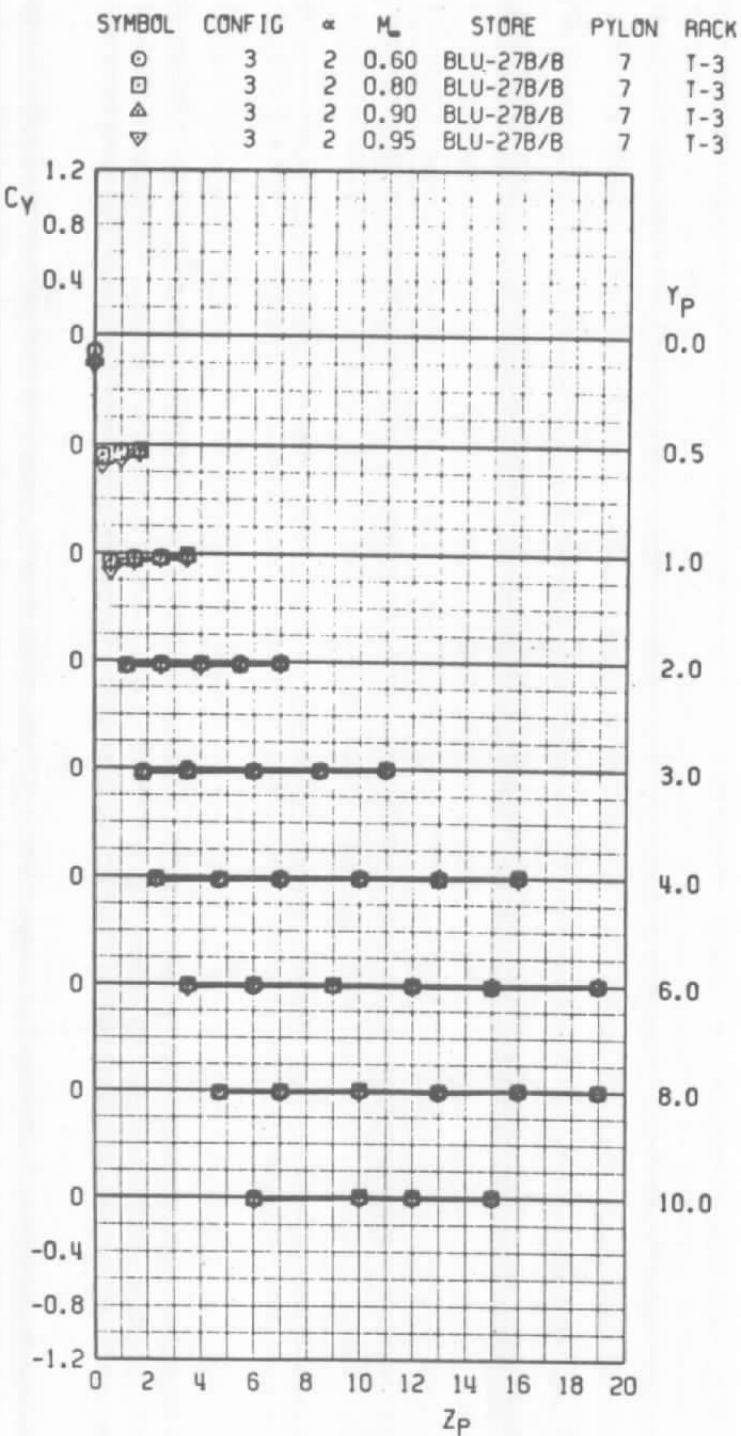


b. Pitching-moment coefficient
Figure 15. Continued.

SYMBOL	CONFIG	α	M_∞	STORE	PYLON	RACK
○	3	2	0.60	BLU-27B/B	7	T-3
□	3	2	0.80	BLU-27B/B	7	T-3
△	3	2	0.90	BLU-27B/B	7	T-3
▽	3	2	0.95	BLU-27B/B	7	T-3

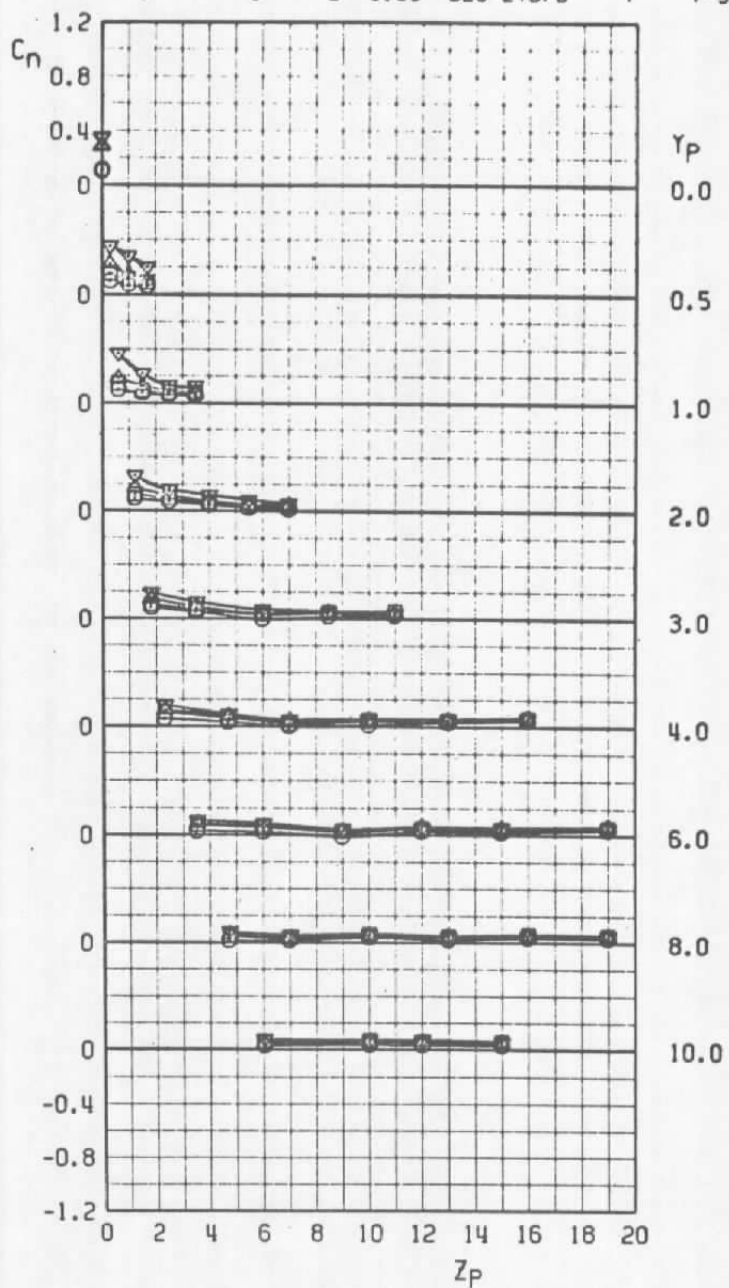


c. Axial-force coefficient
Figure 15. Continued.



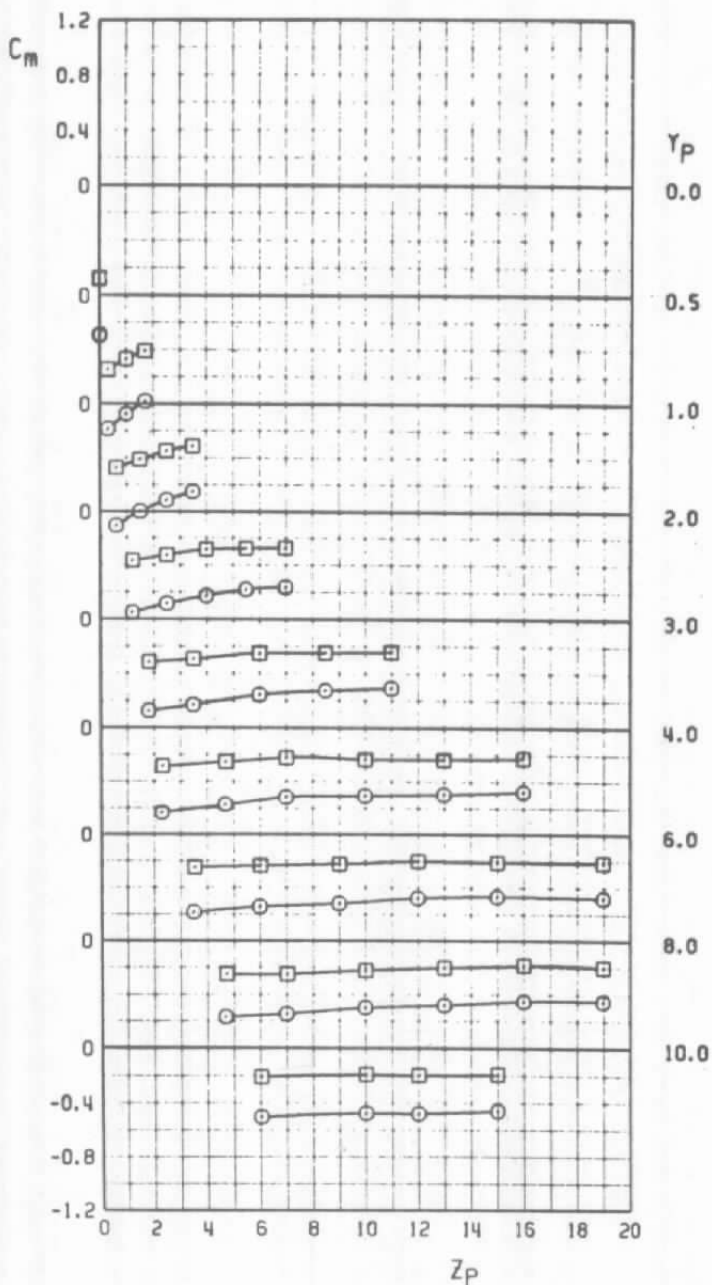
d. Side-force coefficient
Figure 15. Continued.

SYMBOL	CONFIG	α	M_∞	STORE	PYLON	RACK
○	3	2	0.60	BLU-27B/B	7	T-3
□	3	2	0.80	BLU-27B/B	7	T-3
△	3	2	0.90	BLU-27B/B	7	T-3
▽	3	2	0.95	BLU-27B/B	7	T-3



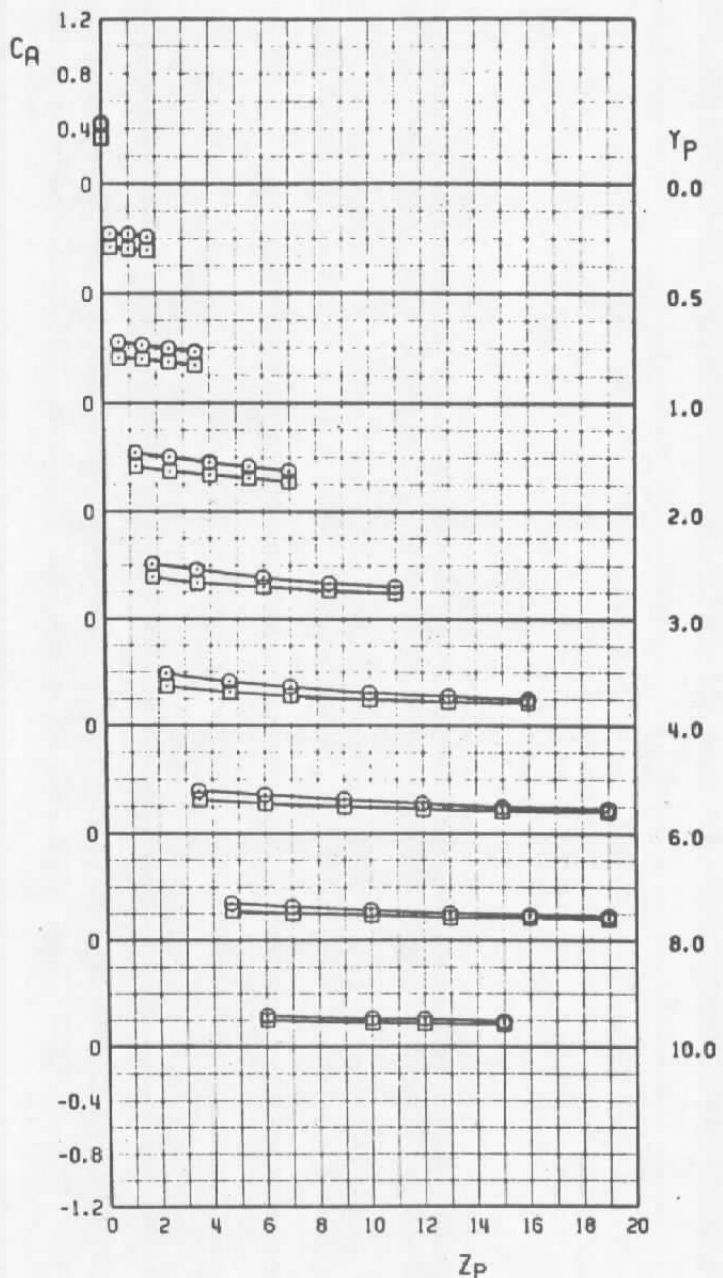
e. Yawing-moment coefficient
Figure 15. Concluded.

SYMBOL	CONFIG	α	M_∞	STORE	PYLON	RACK
○	3	0	0.90	BLU-27B/B	7	T-3
□	3	2	0.90	BLU-27B/B	7	T-3



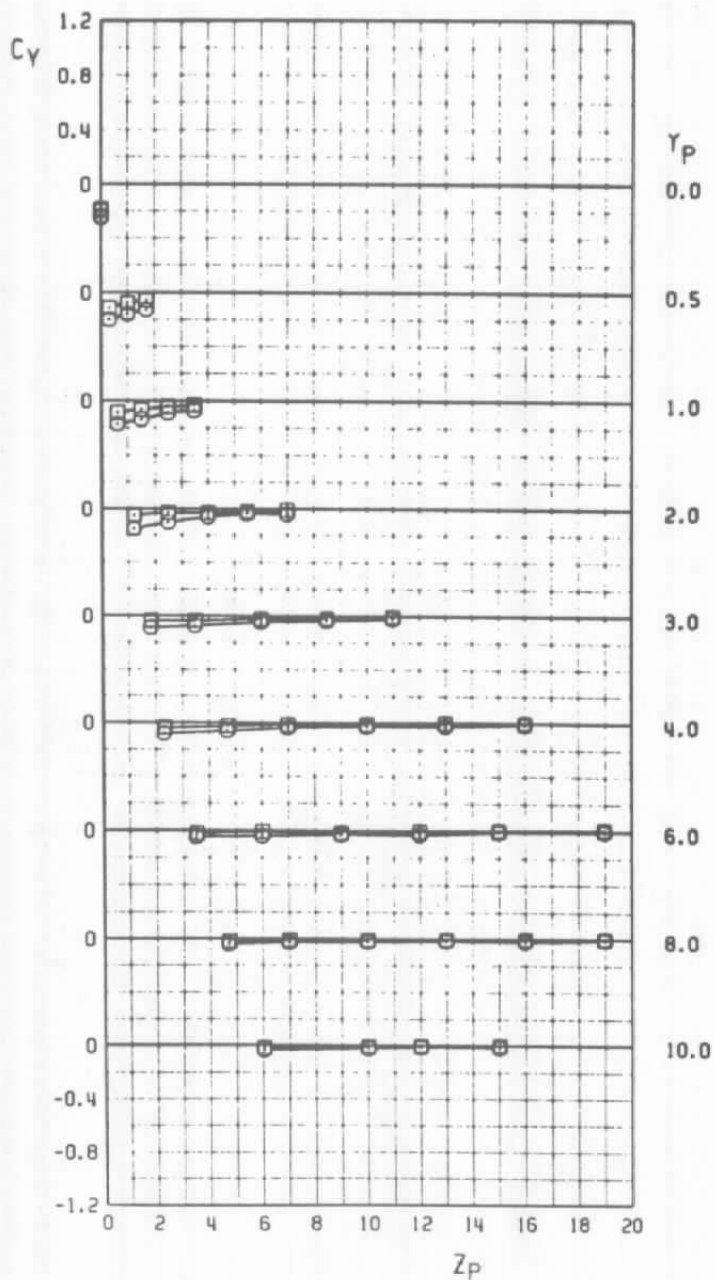
a. Pitching-moment coefficient, $M_\infty = 0.9$
Figure 16. BLU-27B/B coefficient variation with aircraft angle of attack, configuration 3.

SYMBOL	CONFIG	α	M_∞	STORE	PYLON	RACK
○	3	0	0.95	BLU-27B/B	7	T-3
□	3	2	0.95	BLU-27B/B	7	T-3



b. Axial-force coefficient, $M_\infty = 0.95$
Figure 16. Continued.

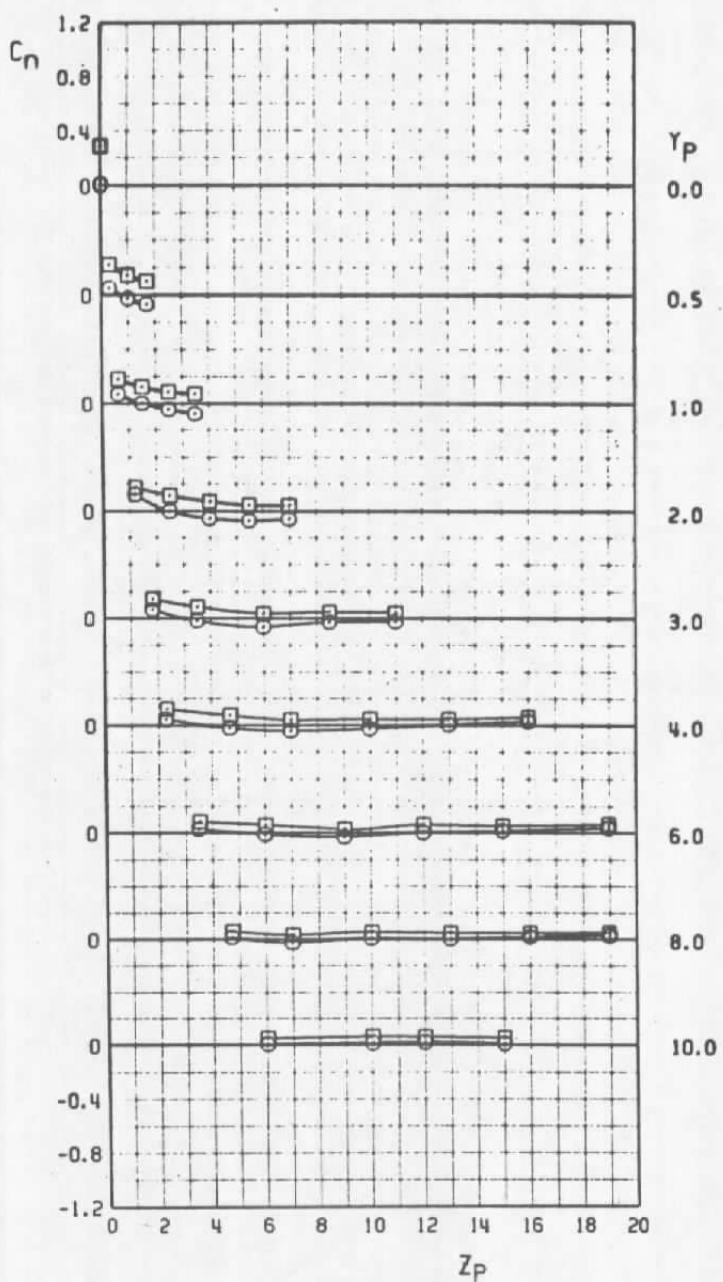
SYMBOL	CONFIG	α	M_∞	STORE	PYLON	RACK
○	3	0	0.90	BLU-27B/B	7	T-3
□	3	2	0.90	BLU-27B/B	7	T-3



c. Side-force coefficient

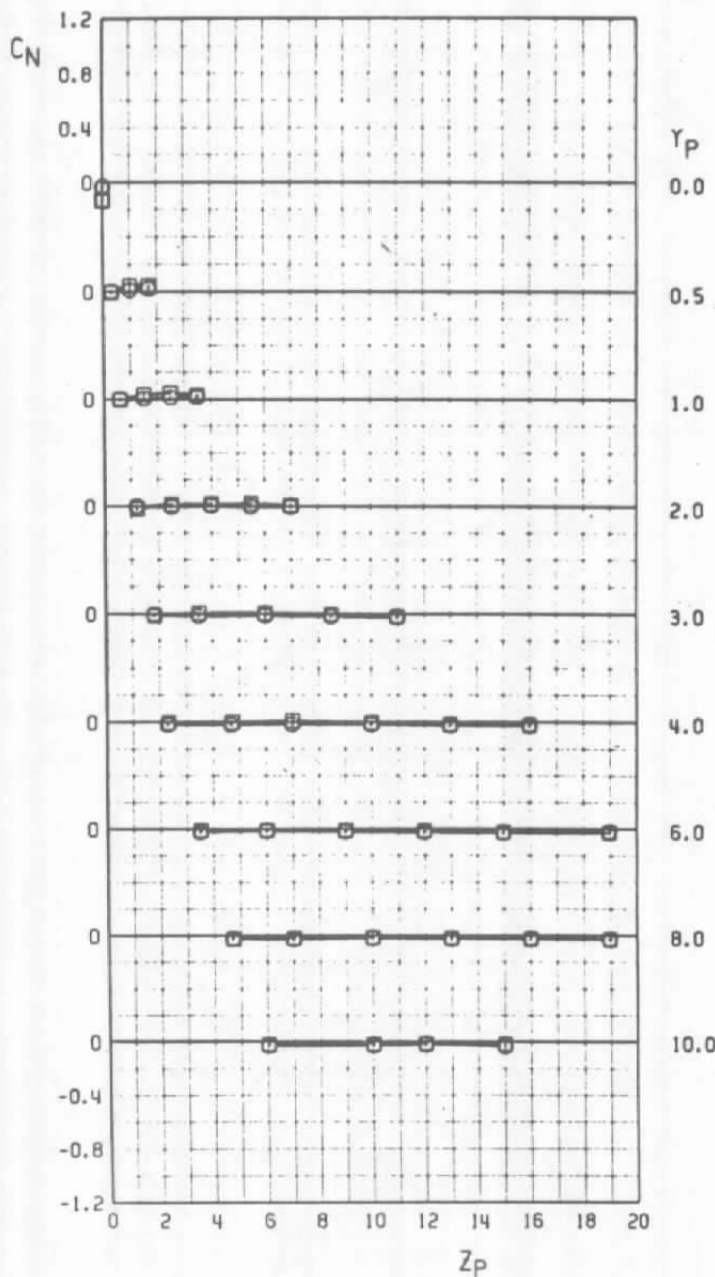
Figure 16. Continued.

SYMBOL	CONFIG	α	M_∞	STORE	PYLON	RACK
○	3	0	0.90	BLU-27B/B	7	T-3
□	3	2	0.90	BLU-27B/B	7	T-3



d. Yawing-moment coefficient
 Figure 16. Concluded.

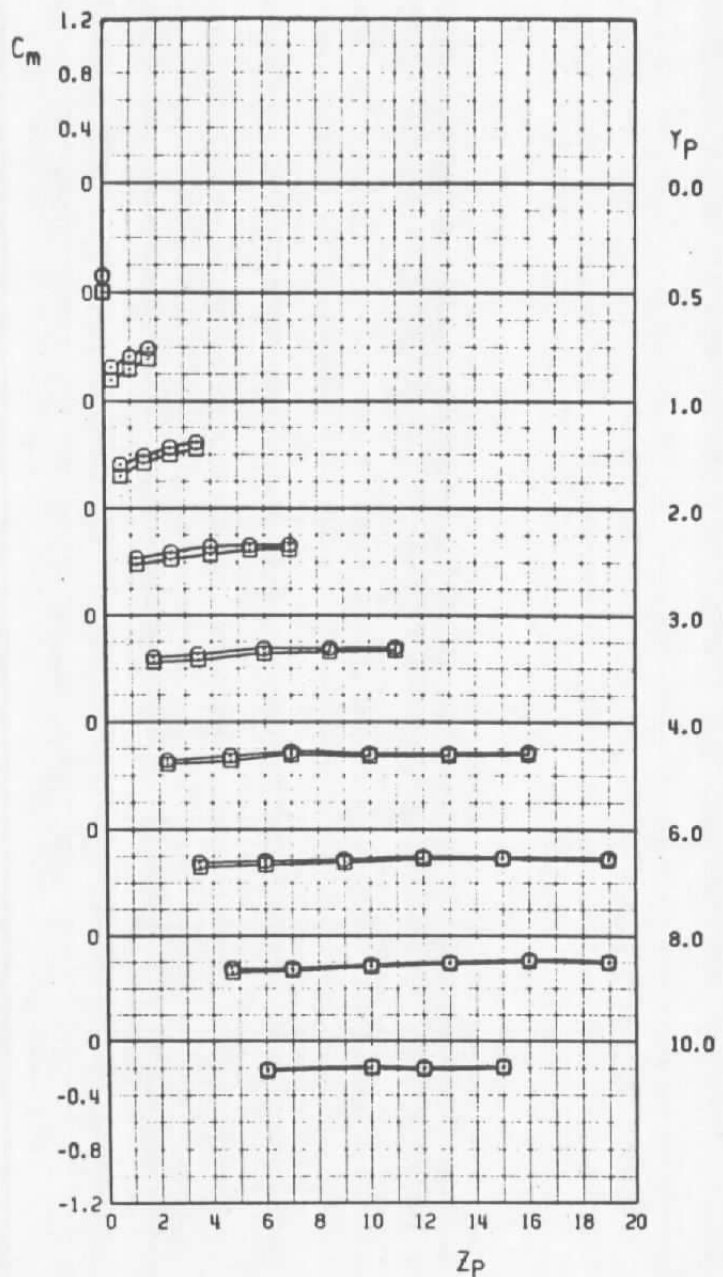
SYMBOL	CONFIG	α	M_∞	STORE	PYLON	RACK
○	3	2	0.90	BLU-27B/B	7	T-3
□	4	2	0.90	BLU-27B/B	7	T-3



a. Normal-force coefficient, $M_\infty = 0.9$

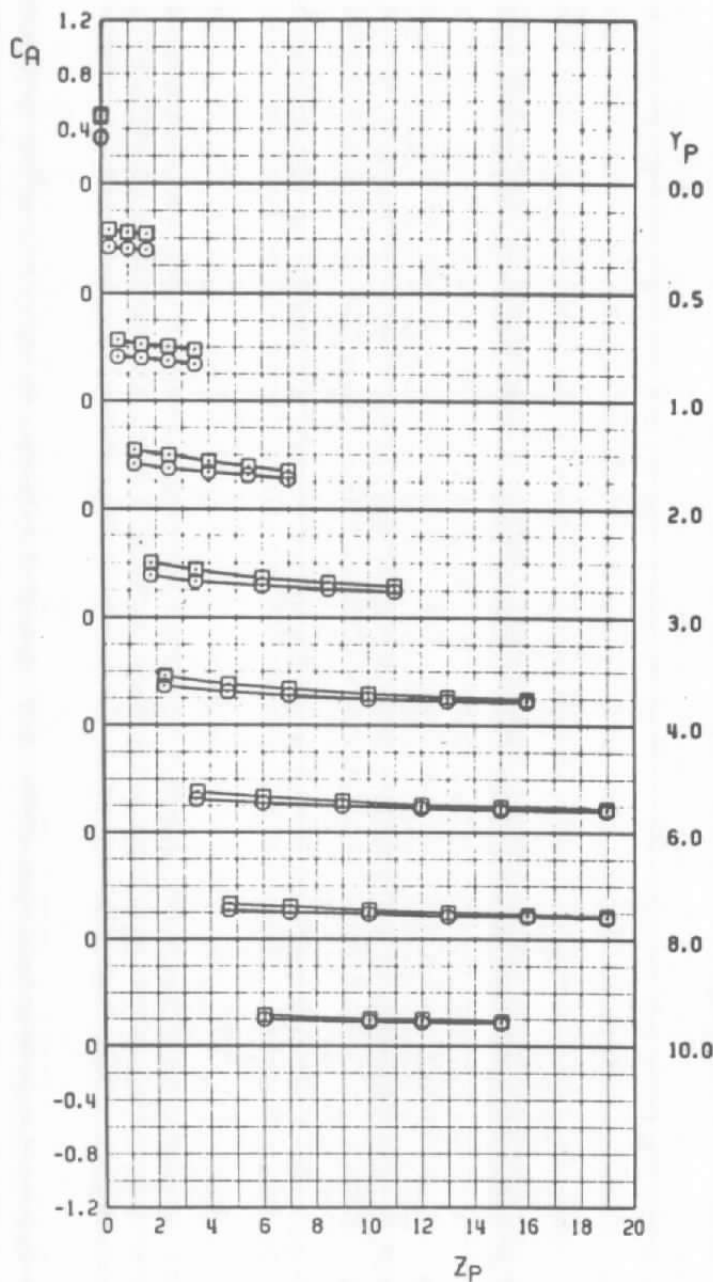
Figure 17. Effect of an adjacent store on the BLU-27B/B, configurations 3 and 4.

SYMBOL	CONFIG	α	M_∞	STORE	PYLON	RACK
○	3	2	0.90	BLU-27B/B	7	T-3
□	4	2	0.90	BLU-27B/B	7	T-3



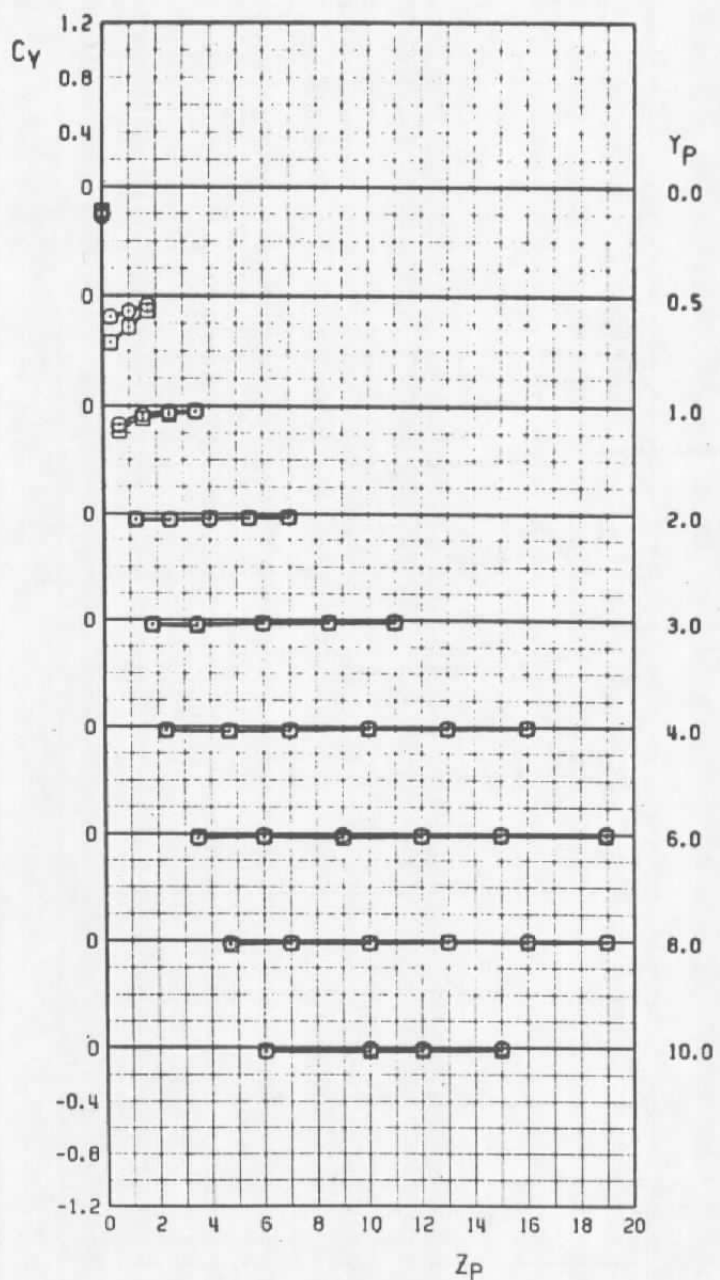
b. Pitching-moment coefficient, $M_\infty = 0.9$
Figure 17. Continued.

SYMBOL	CONFIG	α	M_∞	STORE	PYLON	RACK
○	3	2	0.95	BLU-27B/B	7	T-3
□	4	2	0.95	BLU-27B/B	7	T-3



c. Axial-force coefficient, $M_\infty = 0.95$
Figure 17. Continued.

SYMBOL	CONFIG	α	M_∞	STORE	PYLON	RACK
○	3	2	0.95	BLU-27B/B	7	T-3
□	4	2	0.95	BLU-27B/B	7	T-3



d. Side-force coefficient, $M_\infty = 0.95$

Figure 17. Continued.

SYMBOL	CONFIG	α	M_∞	STORE	PYLON	RACK
○	3	2	0.95	BLU-27B/B	7	1-3
□	4	2	0.95	BLU-27B/B	7	1-3

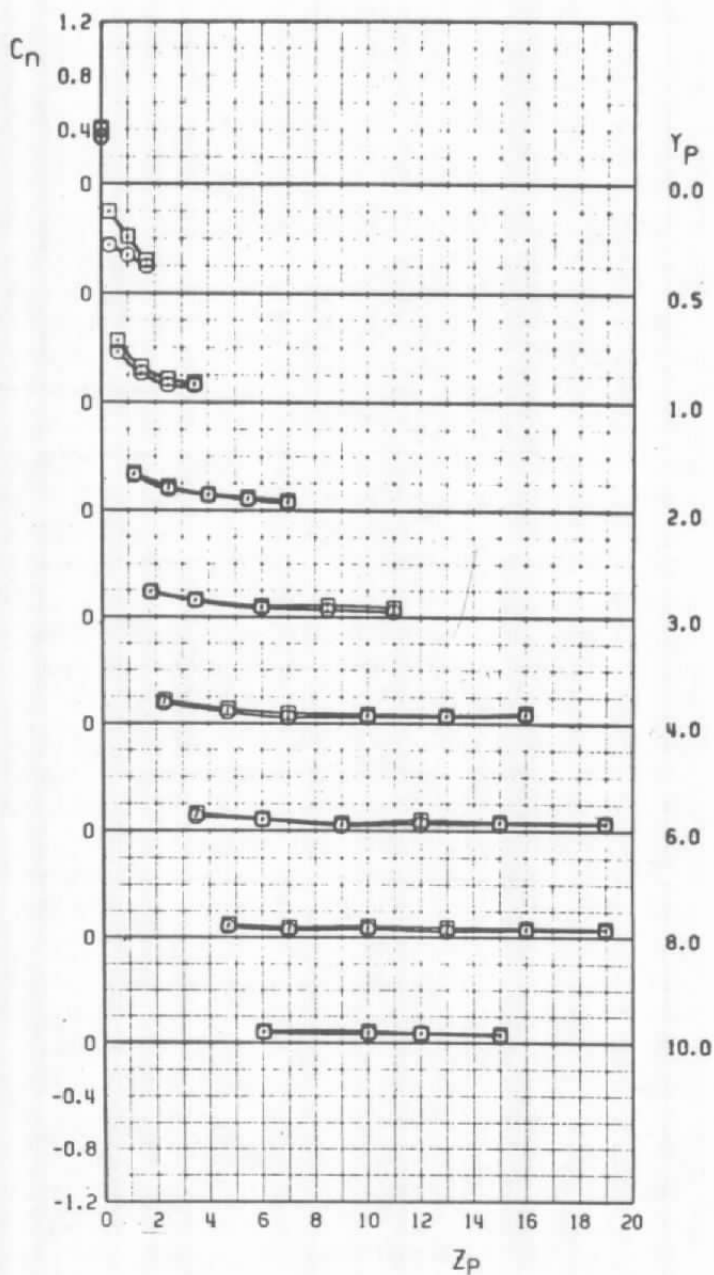
e. Yawing-moment coefficient, $M_\infty = 0.95$

Figure 17. Concluded.

SYMBOL	CONFIG	α	M_∞	STORE	PYLON
○	5	2	0.60	BLU-27B/B	7
□	5	2	0.80	BLU-27B/B	7
△	5	2	0.90	BLU-27B/B	7
▽	5	2	0.95	BLU-27B/B	7

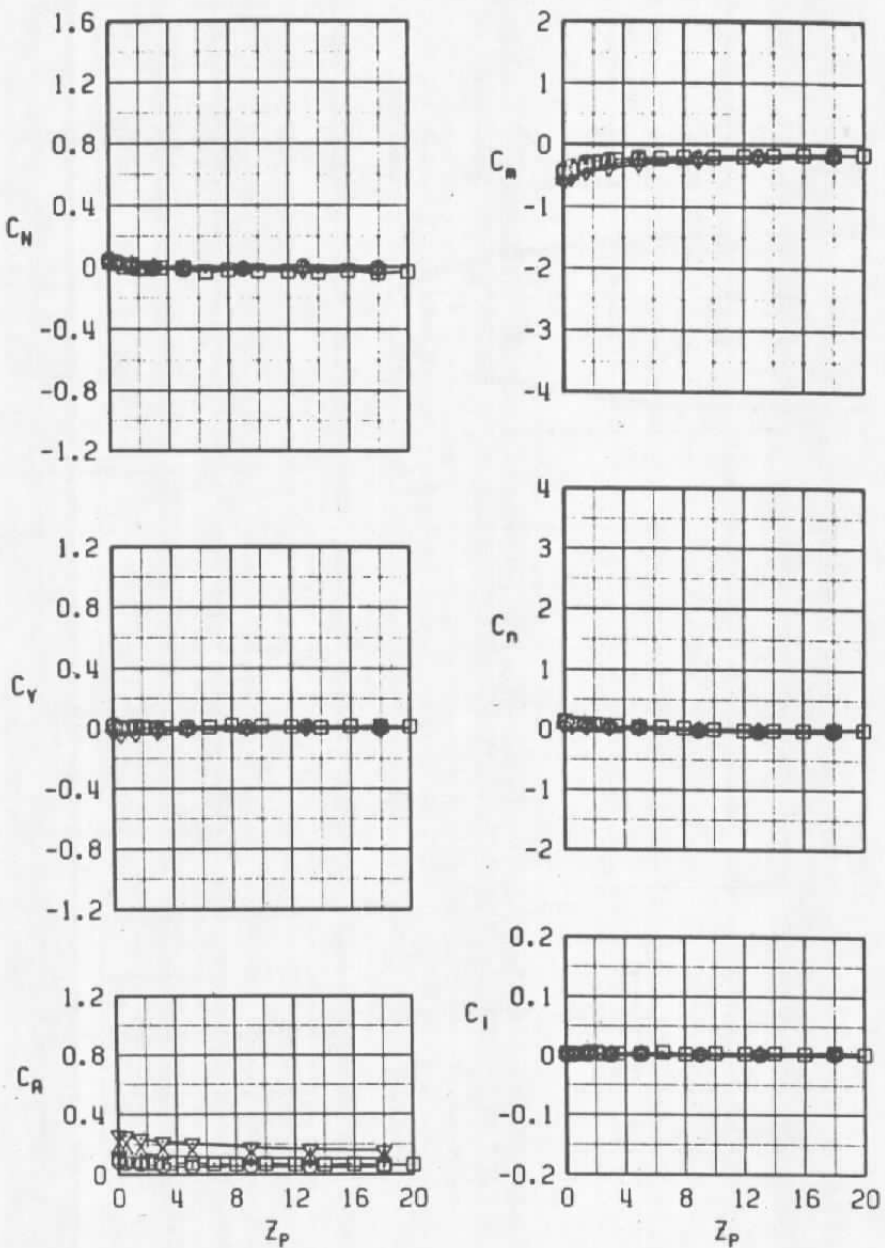


Figure 18. Aerodynamic characteristics of the BLU-27B/B, configuration 5.

SYMBOL	CONFIG	α	M_∞	STORE	PYLON
○	6	2	0.60	BLU-27B/8	6
□	6	2	0.80	BLU-27B/8	6
△	6	2	0.90	BLU-27B/8	6
▽	6	2	0.95	BLU-27B/8	6

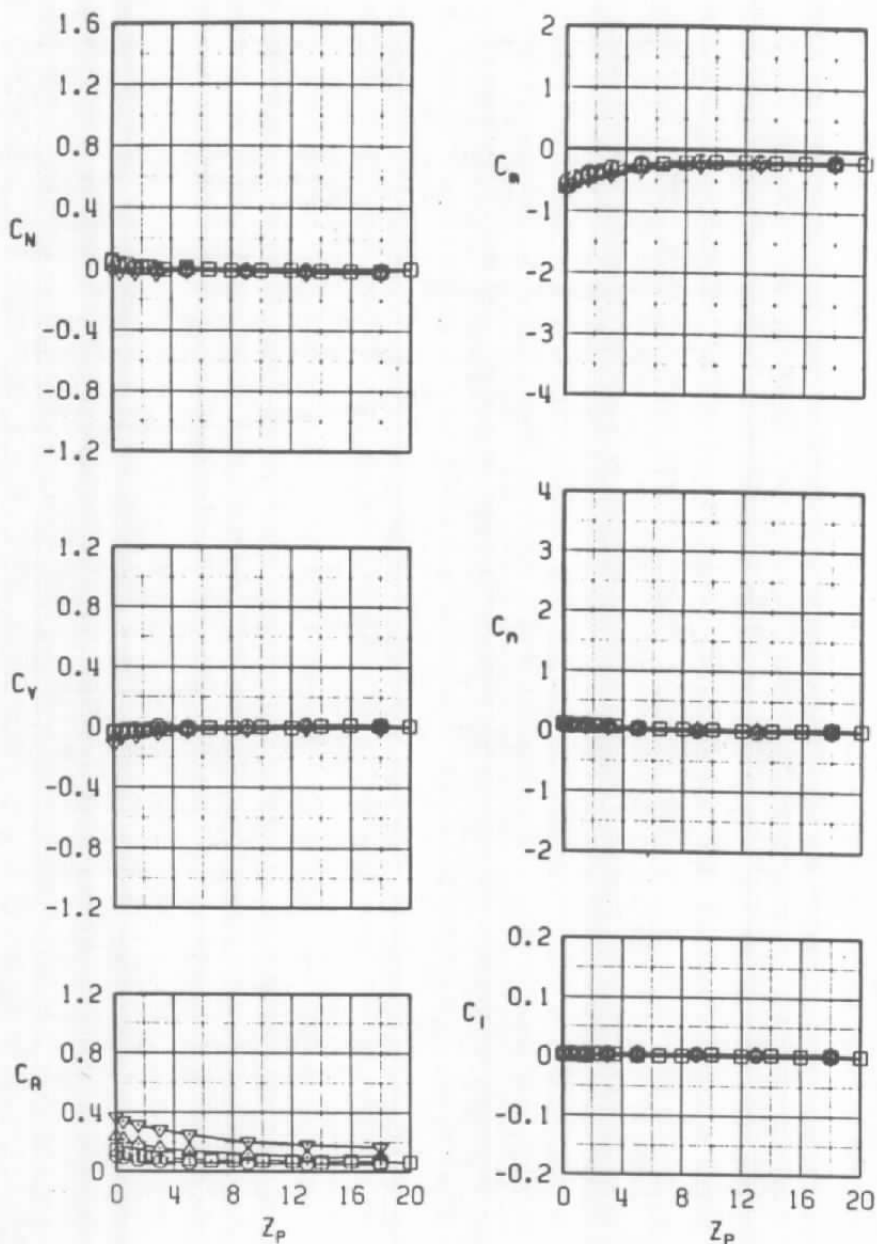


Figure 19. Aerodynamic characteristics of the BLU-27B/B, configuration 6.

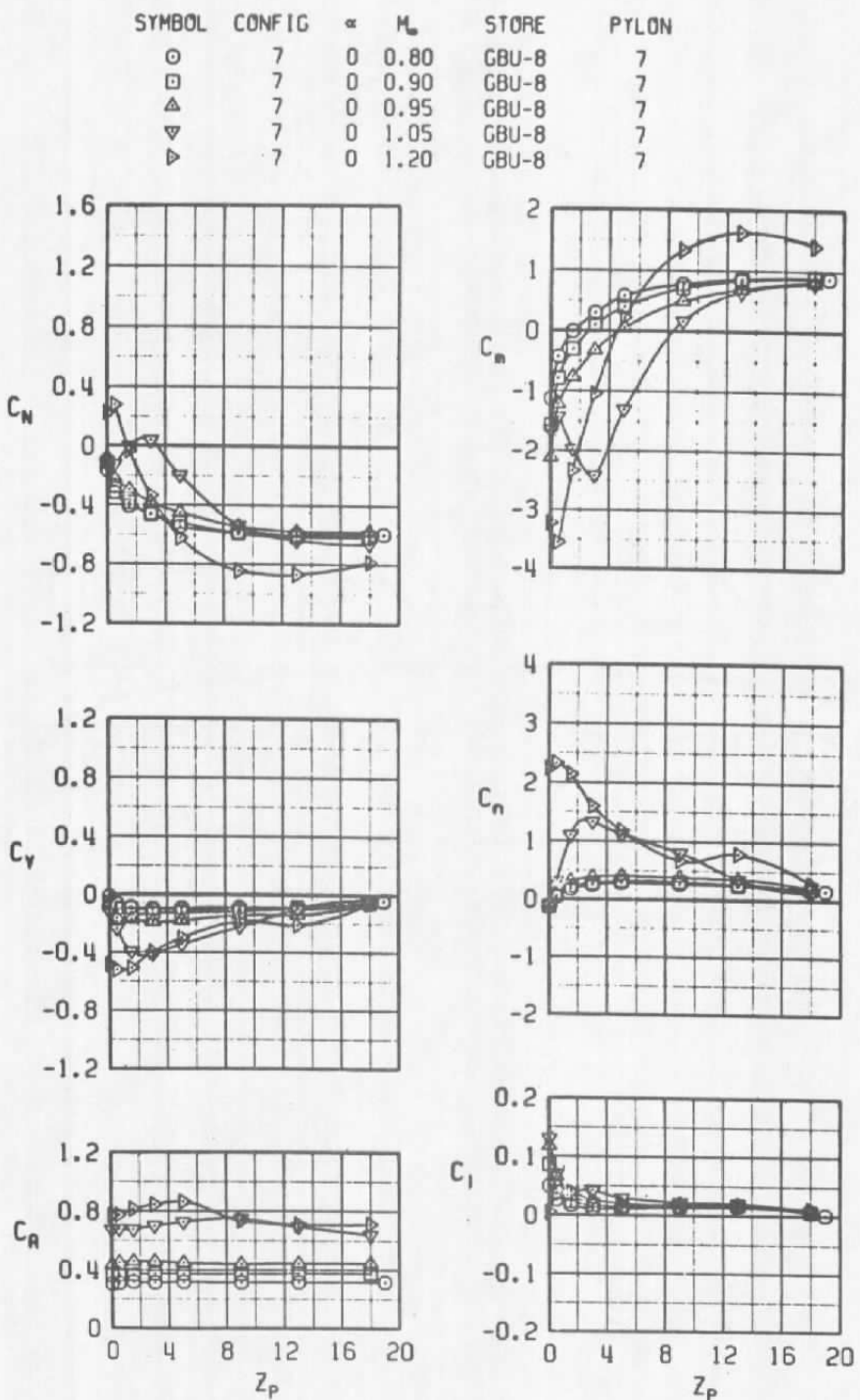


Figure 20. Aerodynamic characteristics of the GBU-8,
configuration 7.

SYMBOL	CONFIG	α	M_∞	STORE	PYLON
○	7	0	0.80	GBU-8	7
□	7	2	0.80	GBU-8	7
△	7	4	0.80	GBU-8	7

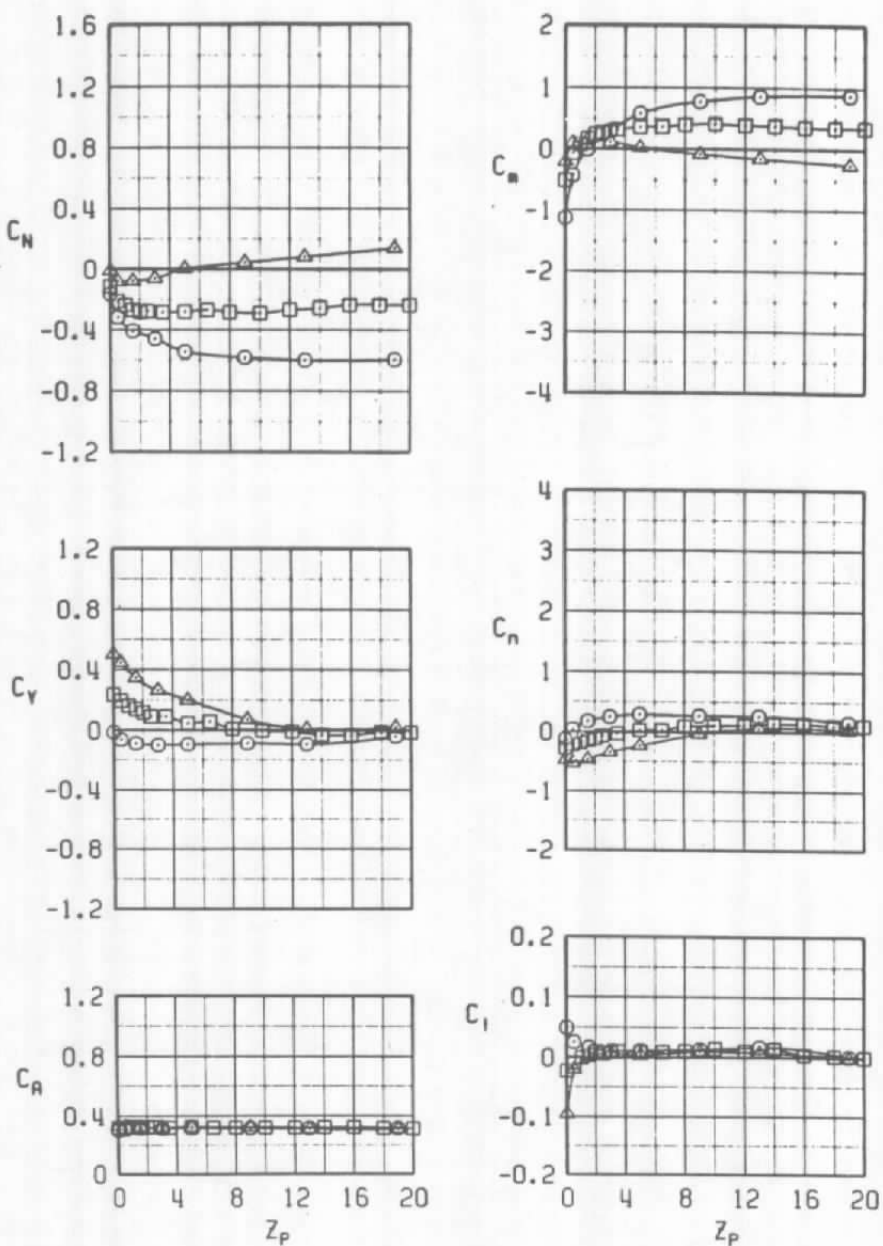


Figure 21. GBU-8 coefficient variation with aircraft angle of attack, configuration 7.

SYMBOL	CONFIG	α	M_∞	STORE	PYLON
○	7	0	1.20	GBU-8	7
□	9	0	1.20	GBU-8	7

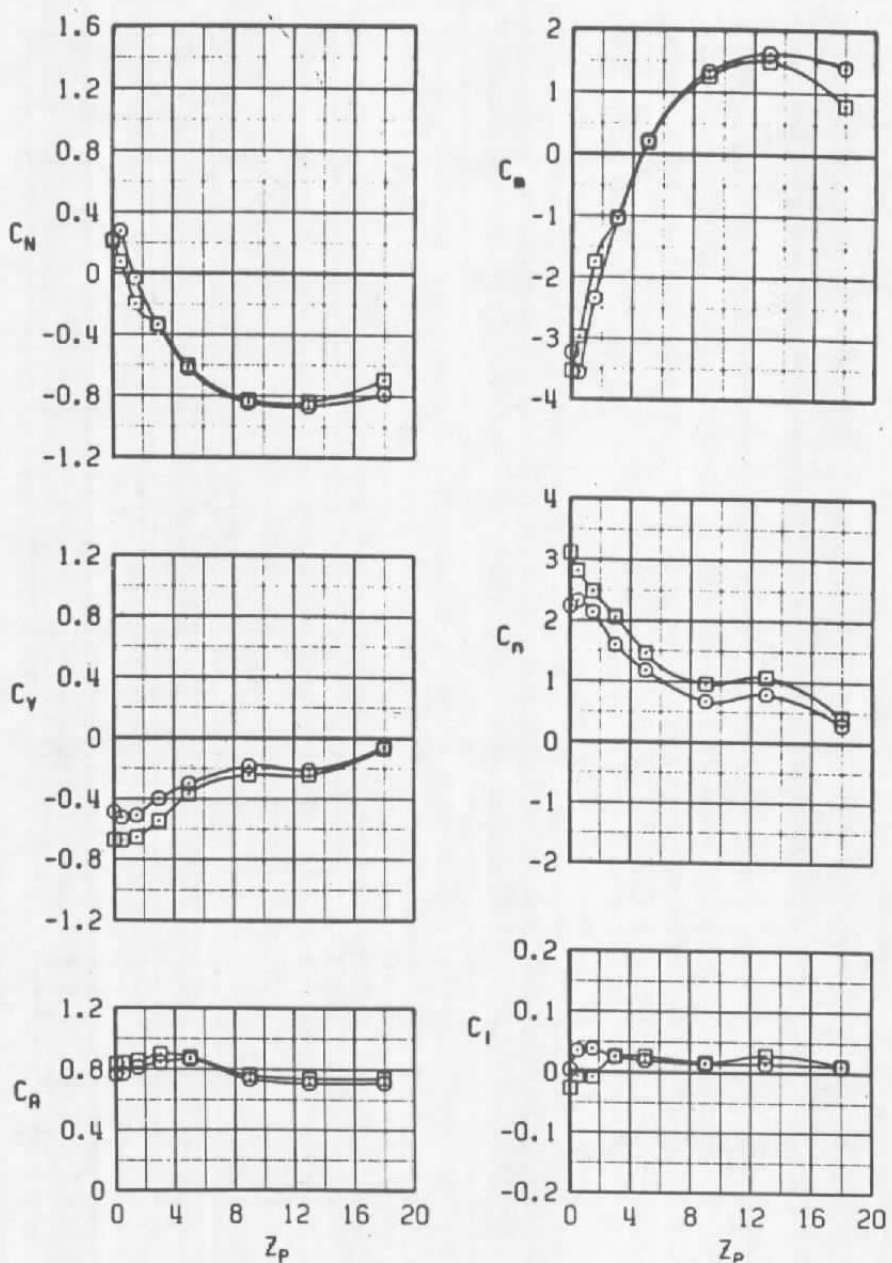


Figure 22. Effect of the addition of an inboard 370-gal fuel tank on the GBU-8, configurations 7 and 9.

SYMBOL	CONFIG	α	M_∞	STORE	PYLON
○	8	0	0.80	CBU-8	6
□	8	0	0.90	CBU-8	6
△	8	0	0.95	CBU-8	6
▽	8	0	1.05	CBU-8	6
▷	8	0	1.20	CBU-8	6

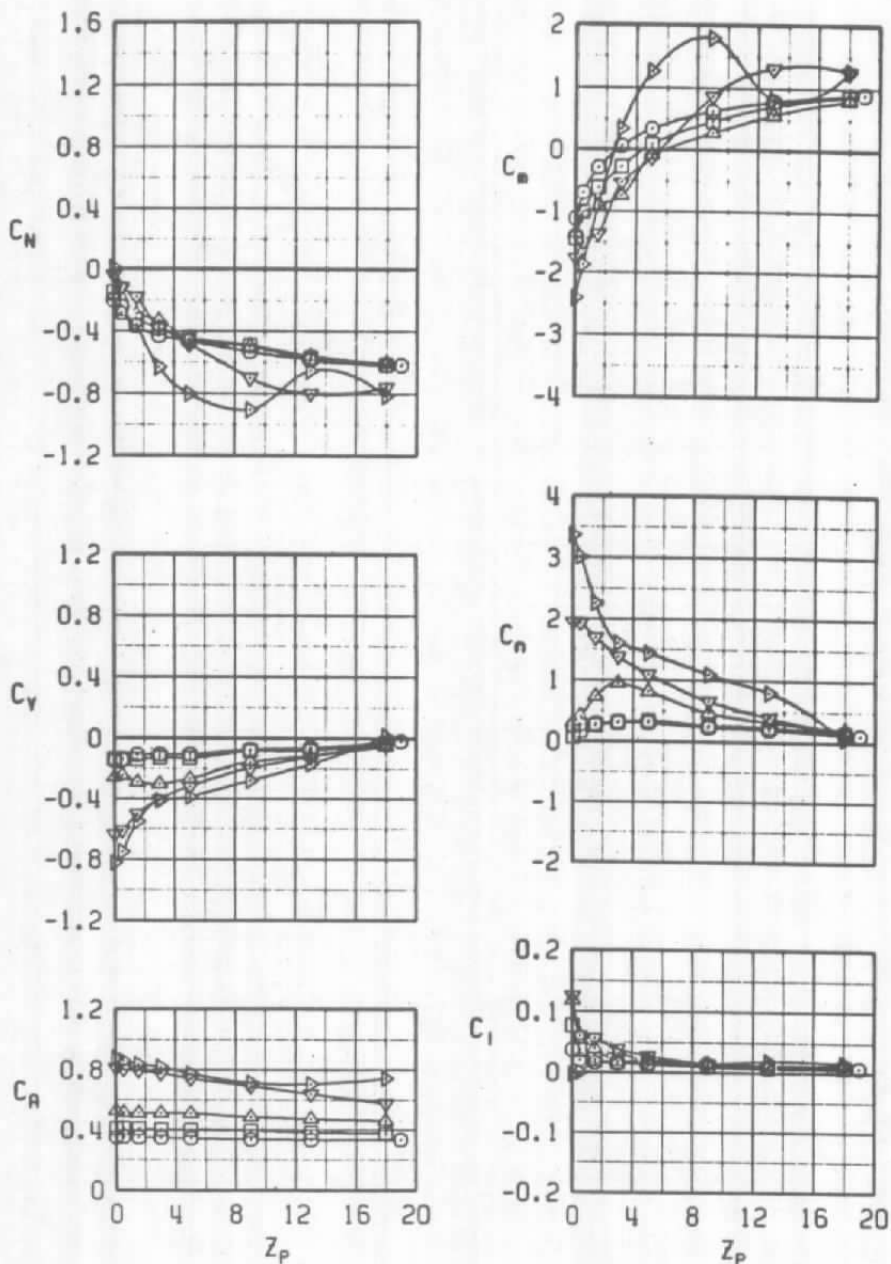


Figure 23. Aerodynamic characteristics of the GBU-8, configuration 8.

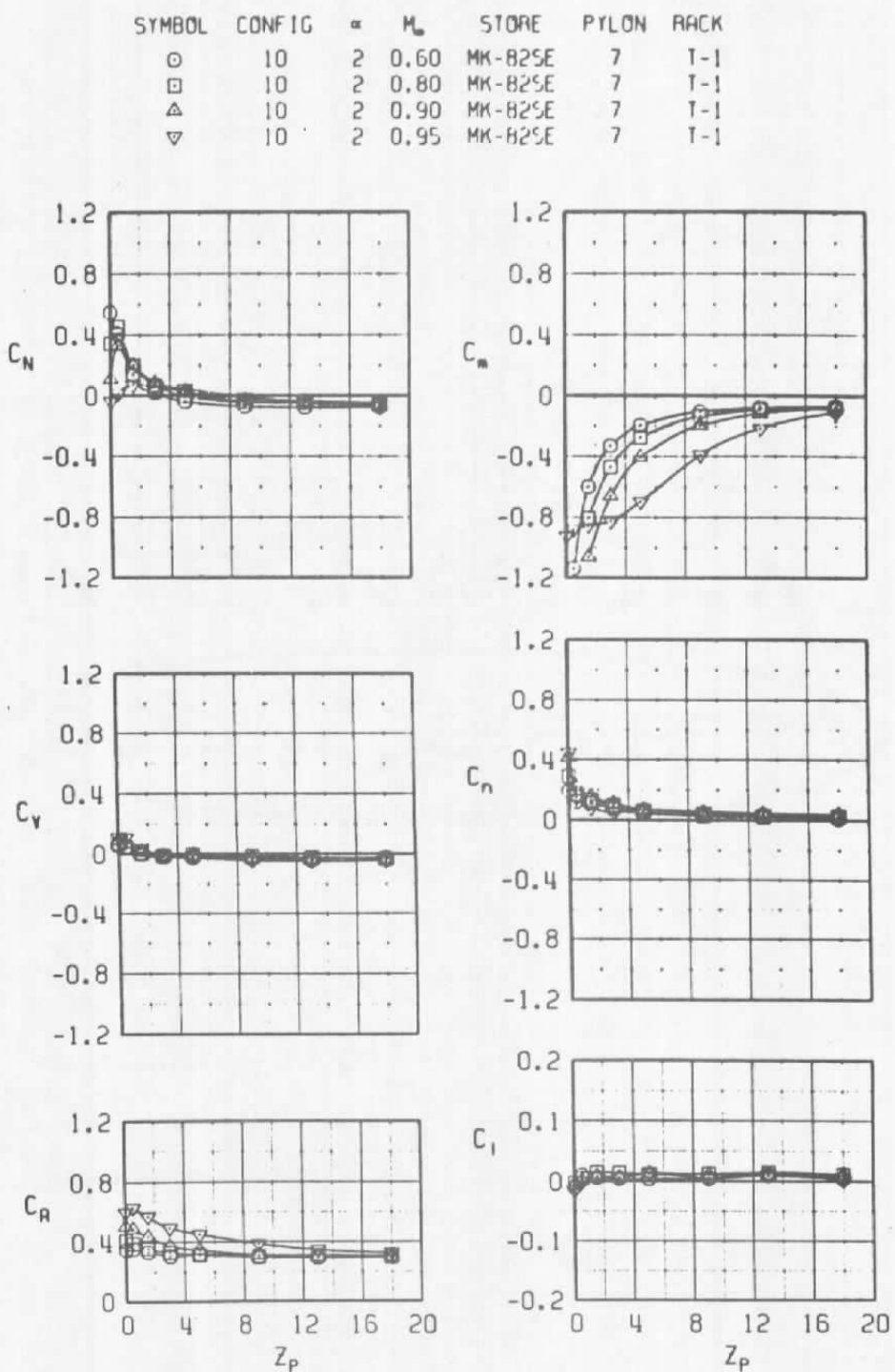


Figure 24. Aerodynamic characteristics of the MK-82SE, configuration 10.

SYMBOL	CONFIG	α	M_∞	STORE	PYLON	RACK
○	10	2	0.60	MK-82SE	7	T-1
□	10	4	0.60	MK-82SE	7	T-1
△	10	6	0.60	MK-82SE	7	T-1
▽	10	10	0.60	MK-82SE	7	T-1

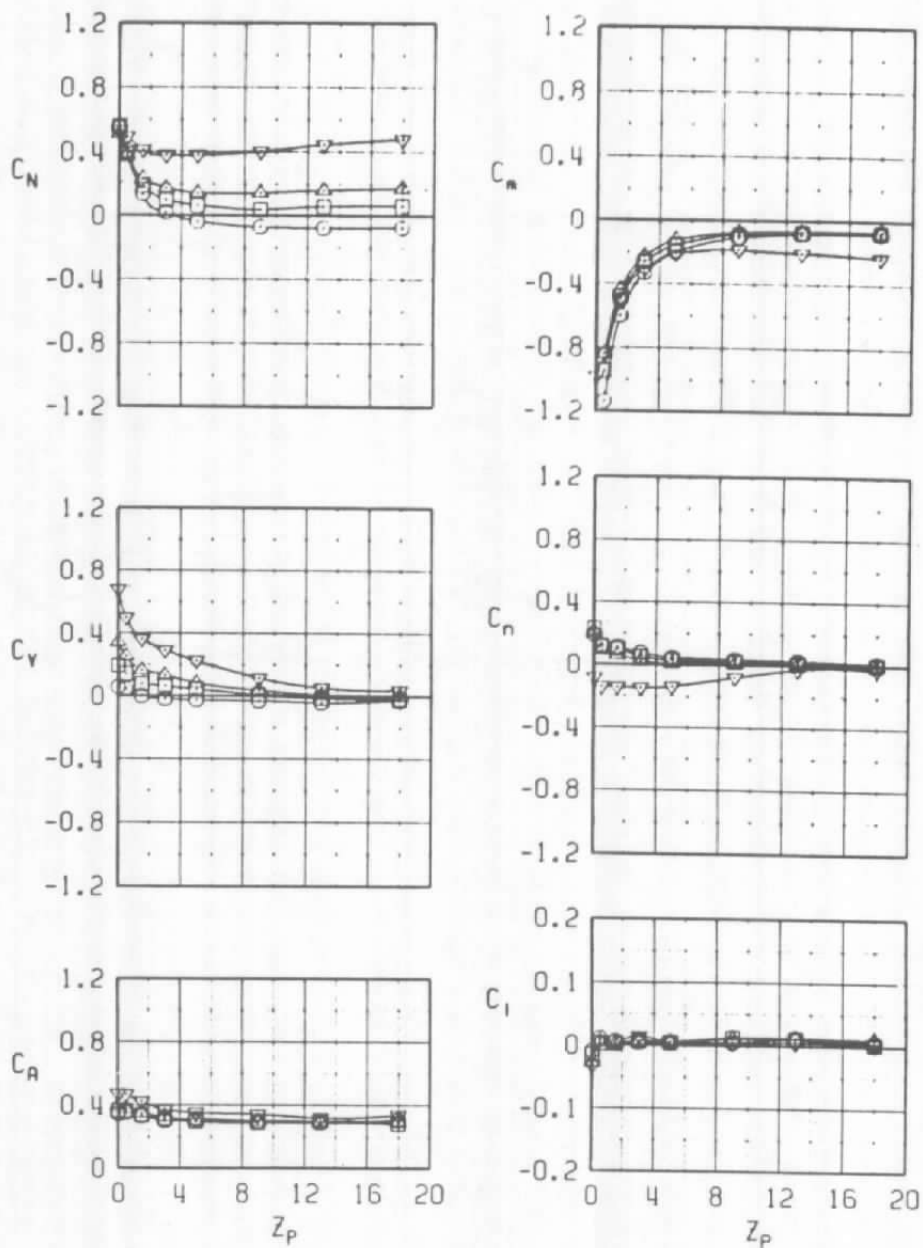
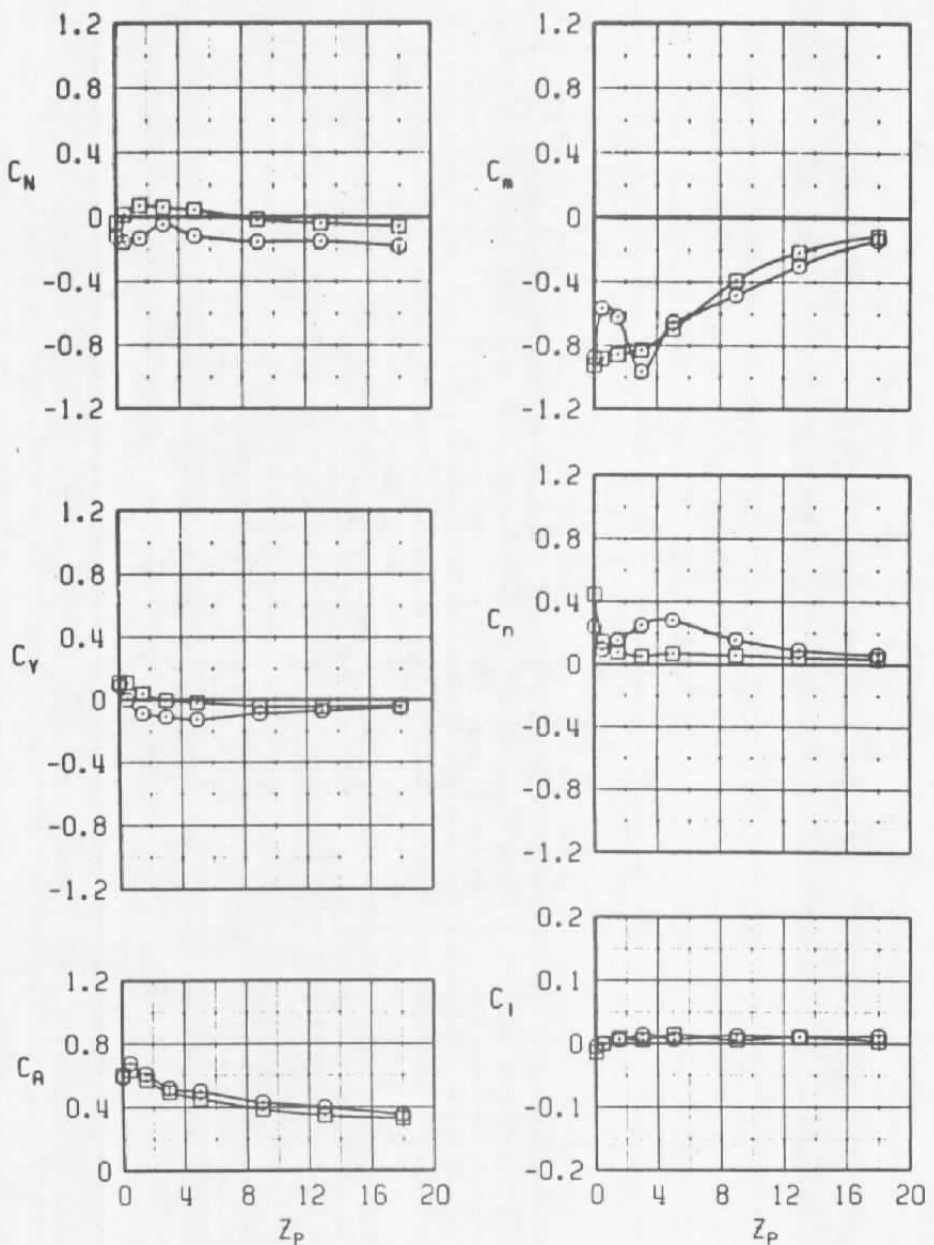
a. $M_\infty = 0.6$

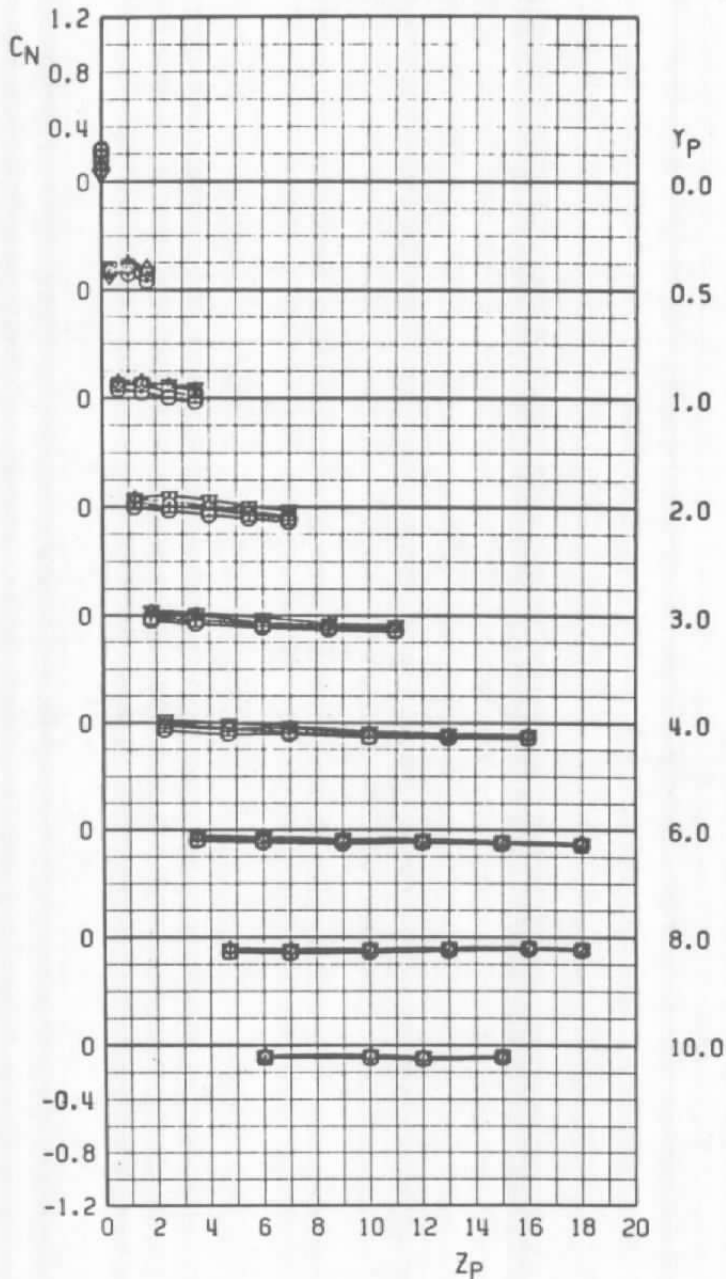
Figure 25. MK-82SE coefficient variation with aircraft angle of attack, configuration 10.

SYMBOL	CONFIG	α	M_∞	STORE	PYLON	RACK
○	10	0	0.95	MK-B2SE	7	T-1
□	10	2	0.95	MK-B2SE	7	T-1



b. $M_\infty = 0.95$
Figure 25. Concluded.

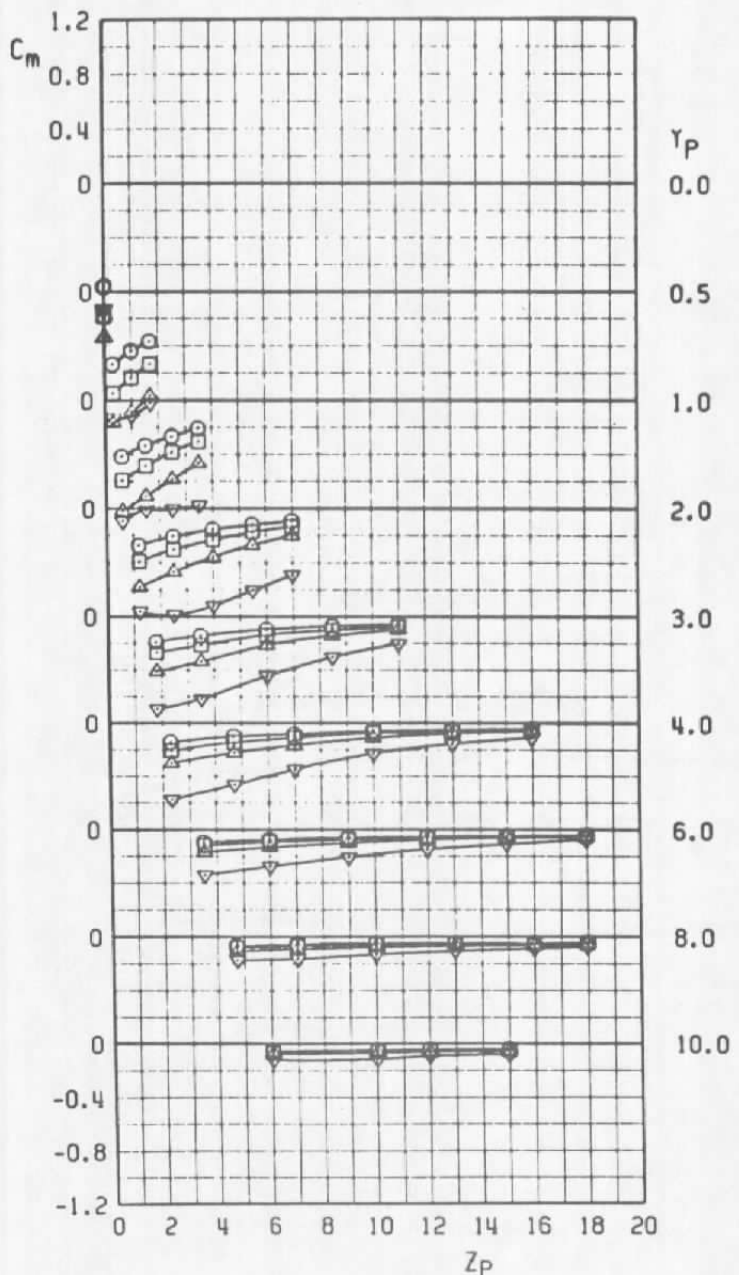
SYMBOL	CONFIG	α	M_∞	STORE	PYLON	RACK
○	11	2	0.60	MK-82SE	7	T-3
□	11	2	0.80	MK-82SE	7	T-3
△	11	2	0.90	MK-82SE	7	T-3
▽	11	2	0.95	MK-82SE	7	T-3



a. Normal-force coefficient

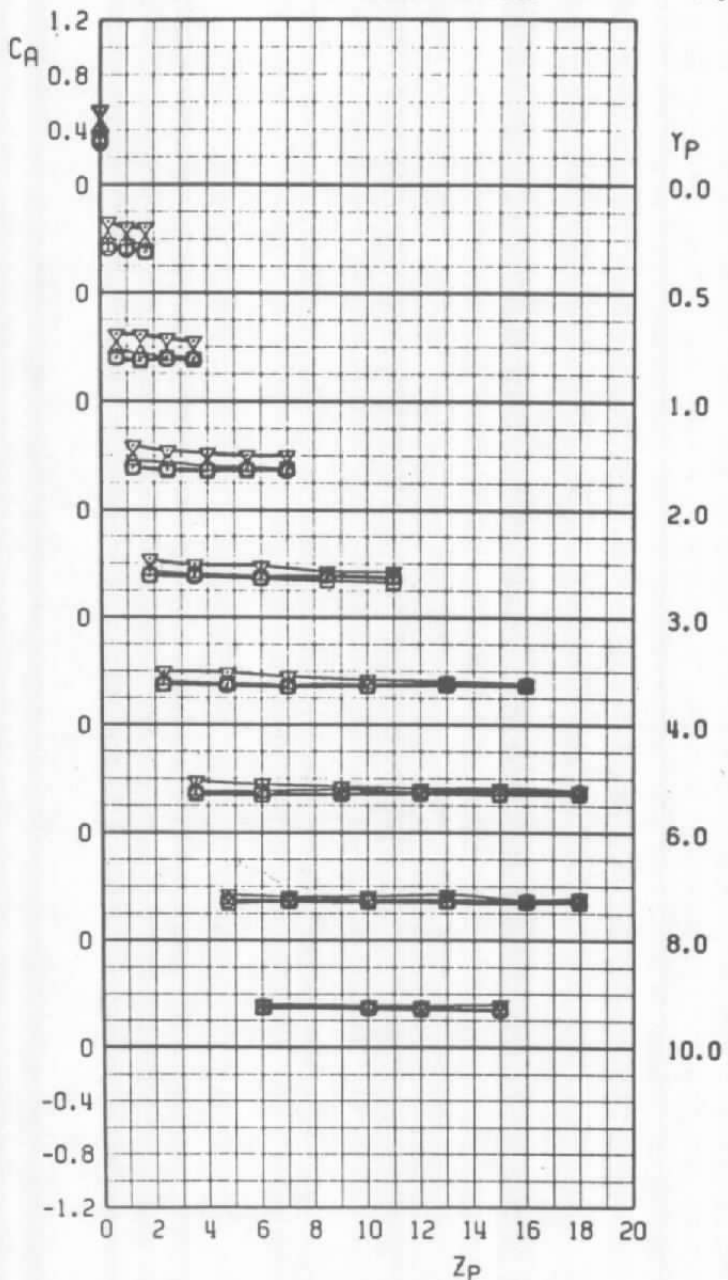
Figure 26. Aerodynamic characteristics of the MK-82SE, configuration 11.

SYMBOL	CONFIG	α	M_∞	STORE	PYLON	RACK
○	11	2	0.60	MK-82SE	7	T-3
□	11	2	0.80	MK-82SE	7	T-3
△	11	2	0.90	MK-82SE	7	T-3
▽	11	2	0.95	MK-82SE	7	T-3



b. Pitching-moment coefficient
Figure 26. Continued.

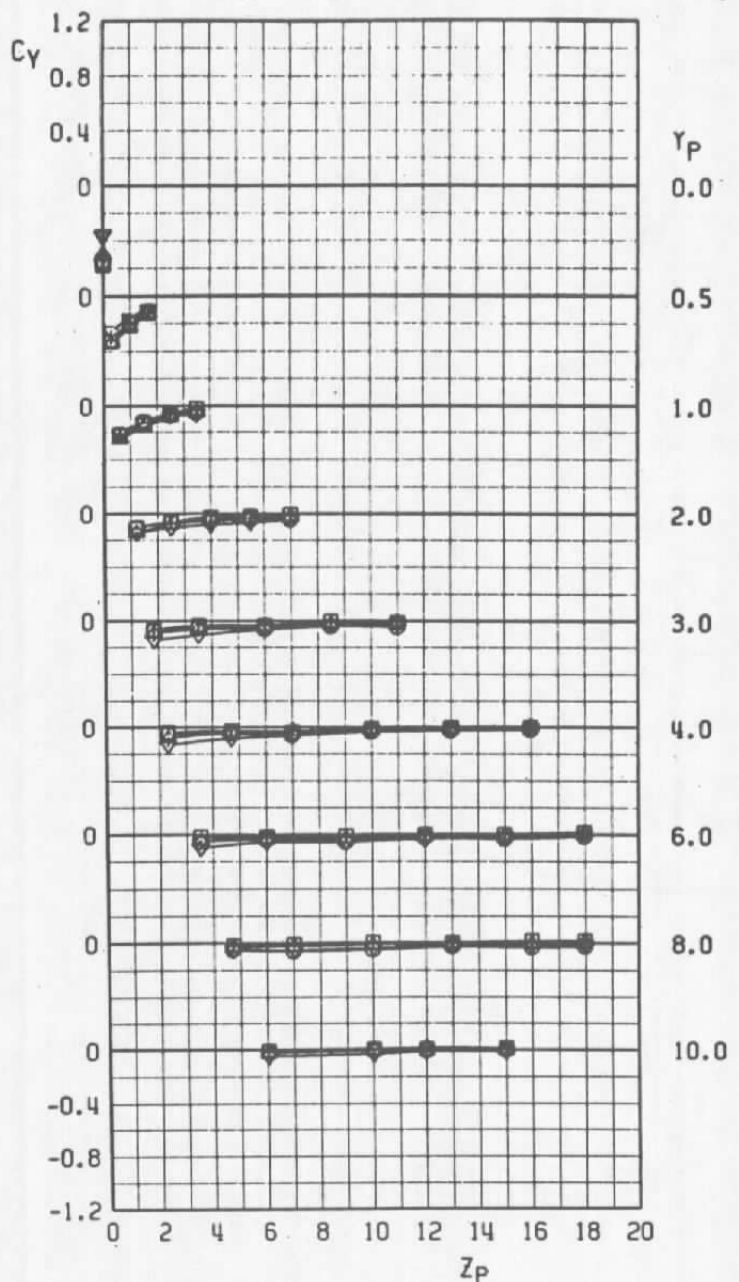
SYMBOL	CONFIG	α	M_∞	STORE	PYLON	RACK
○	II	2	0.60	MK-82SE	7	T-3
□	II	2	0.80	MK-82SE	7	T-3
△	II	2	0.90	MK-82SE	7	T-3
▽	II	2	0.95	MK-82SE	7	T-3



c. Axial-force coefficient

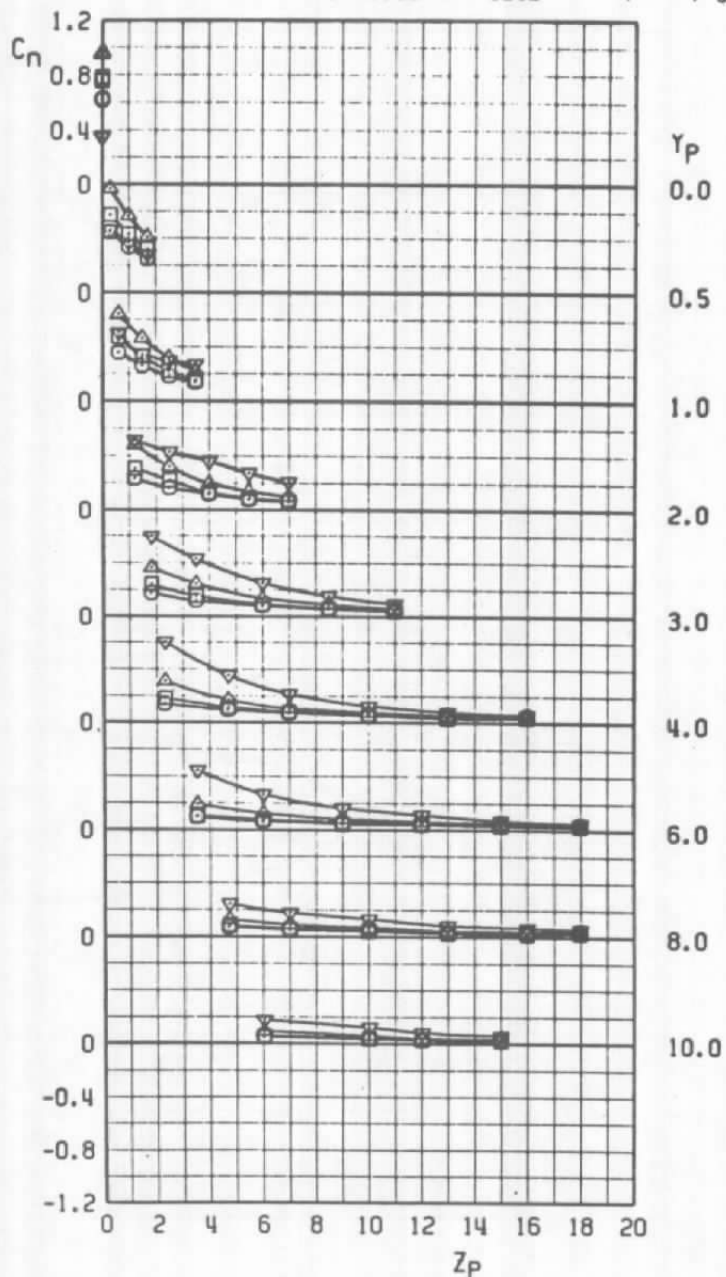
Figure 26. Continued.

SYMBOL	CONFIG	α	M_∞	STORE	PYLON	RACK
○	II	2	0.60	MK-82SE	7	T-3
□	II	2	0.80	MK-82SE	7	T-3
△	II	2	0.90	MK-82SE	7	T-3
▽	II	2	0.95	MK-82SE	7	T-3



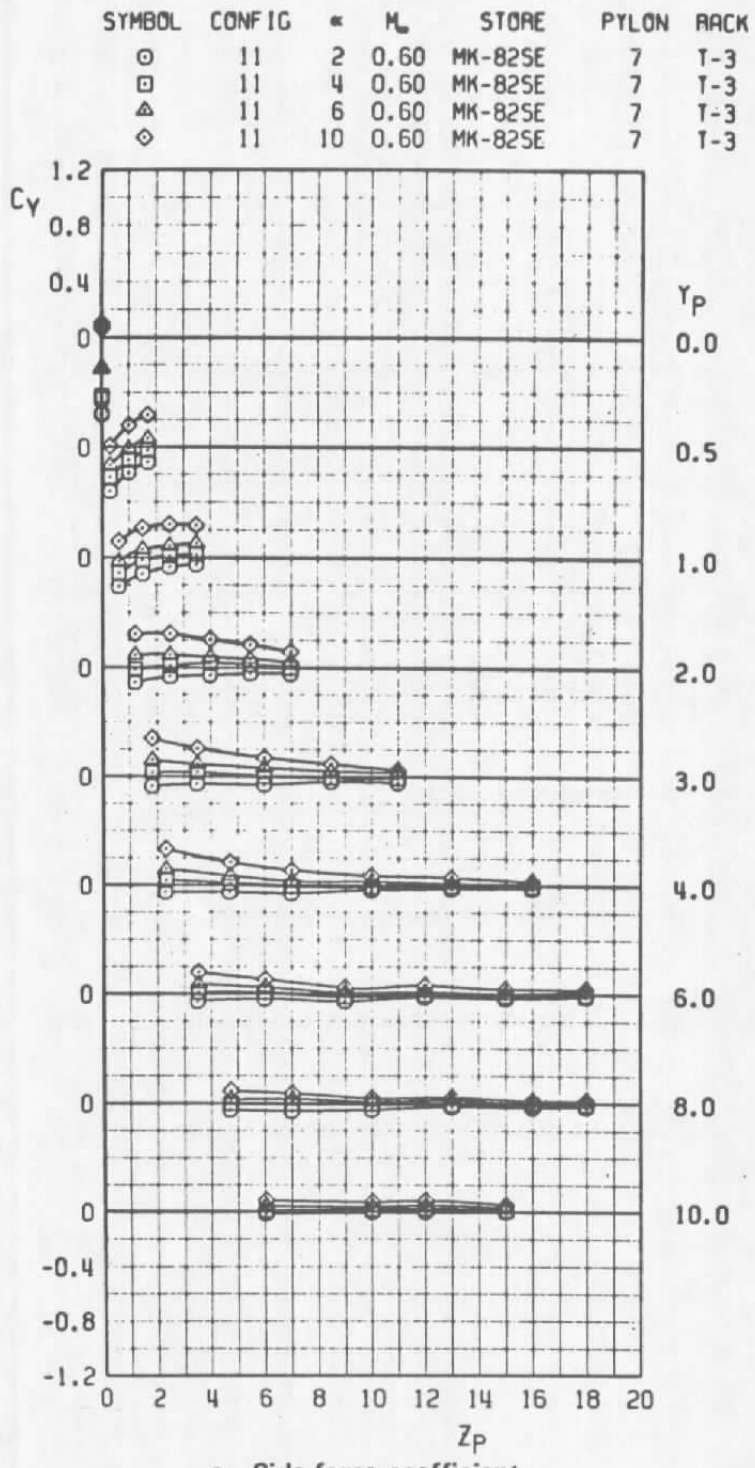
d. Side-force coefficient
Figure 26. Continued.

SYMBOL	CONFIG	α	M_a	STORE	PYLON	RACK
○	11	2	0.60	MK-82SE	7	T-3
□	11	2	0.80	MK-82SE	7	T-3
△	11	2	0.90	MK-82SE	7	T-3
▽	11	2	0.95	MK-82SE	7	T-3



e. Yawing-moment coefficient

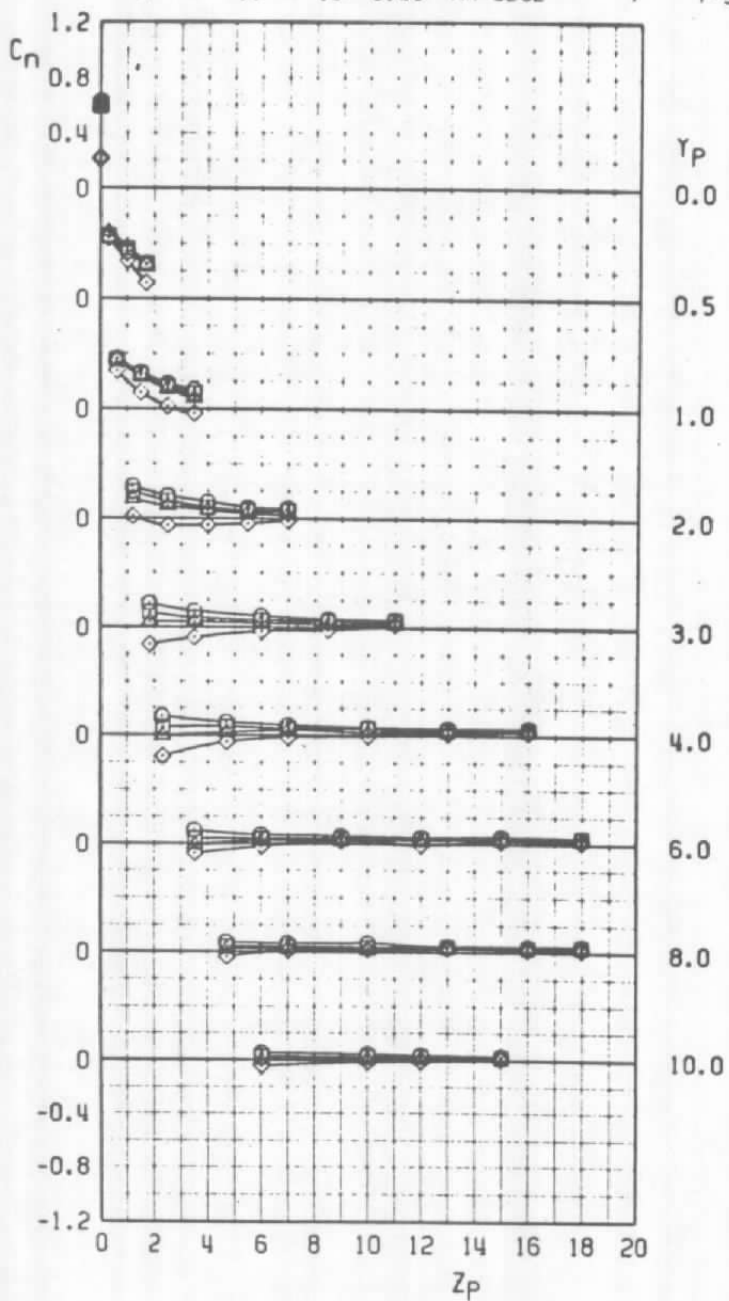
Figure 26. Concluded.



a. Side-force coefficient

Figure 27. MK-82SE coefficient variation with aircraft angle of attack, configuration 11.

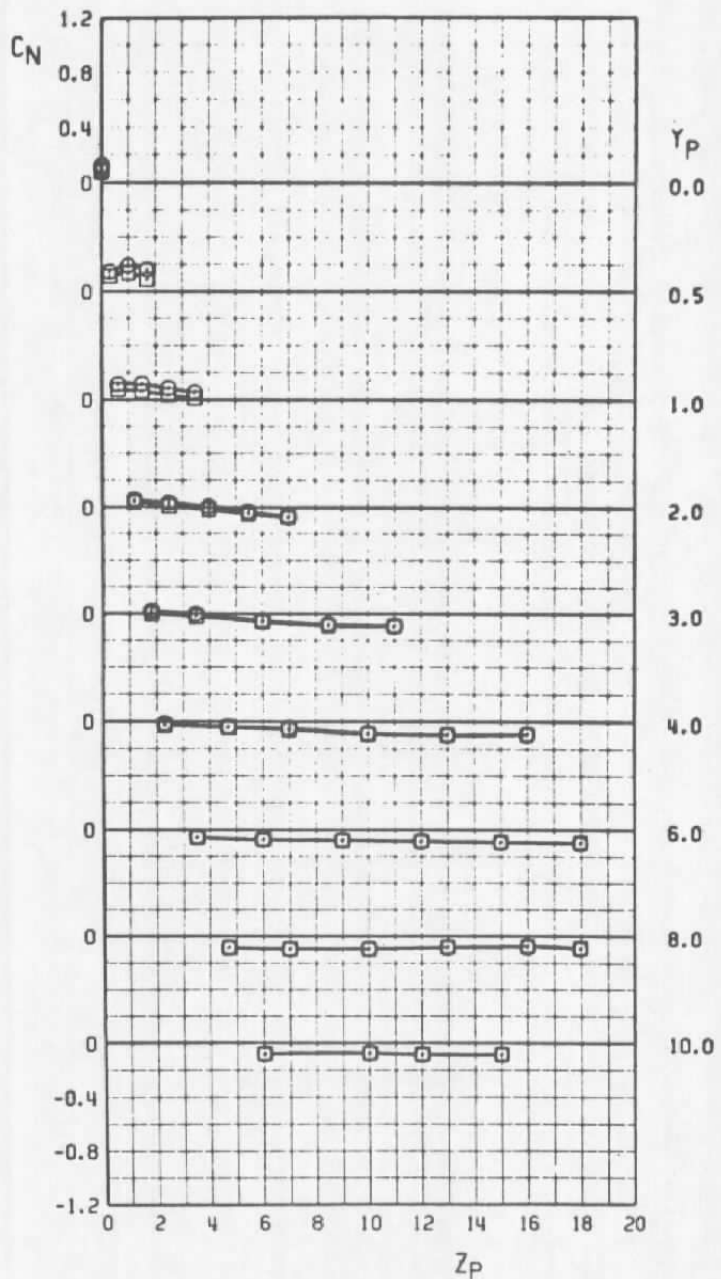
SYMBOL	CONFIG	α	M_e	STORE	PYLON	RACK
○	II	2	0.60	MK-82SE	7	T-3
□	II	4	0.60	MK-82SE	7	T-3
△	II	6	0.60	MK-82SE	7	T-3
◊	II	10	0.60	MK-82SE	7	T-3



b. Yawing-moment coefficient

Figure 27. Concluded.

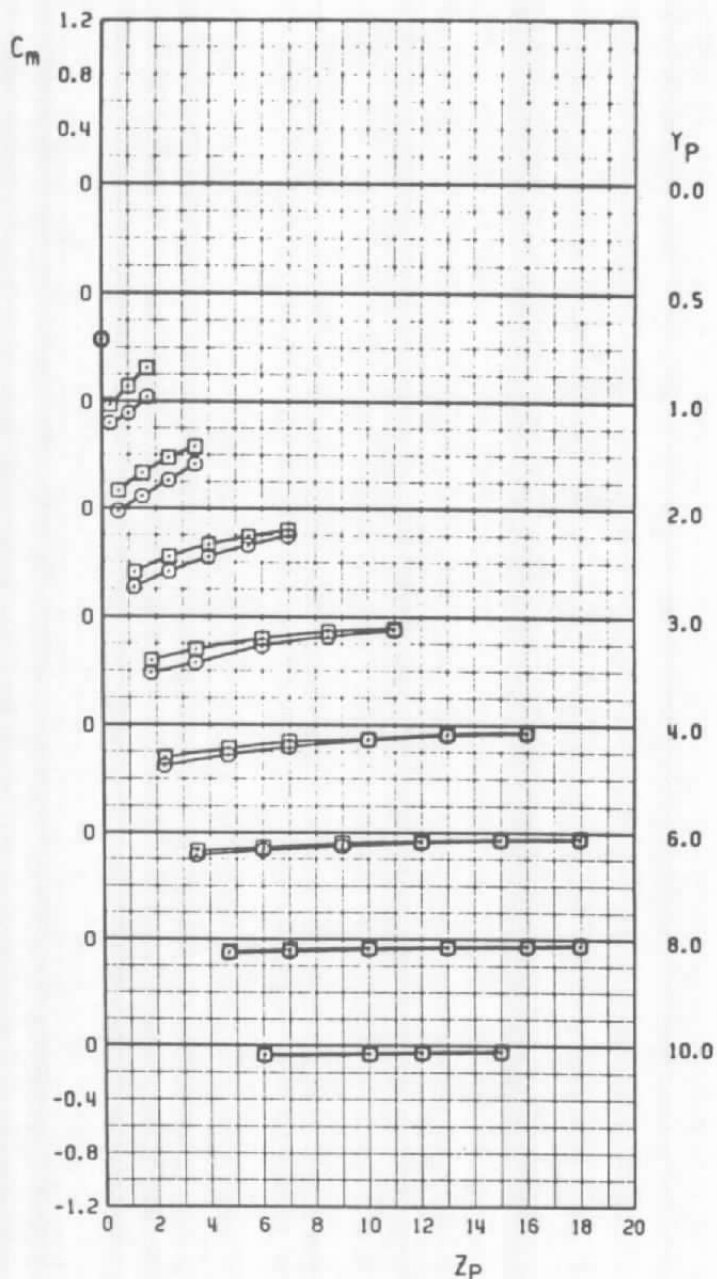
SYMBOL	CONFIG	∞	M_∞	STORE	PYLON	RACK
○	11	2	0.90	MK-82SE	7	T-3
□	13	2	0.90	MK-82SE	7	T-3



a. Normal-force coefficient, $M_\infty = 0.9$

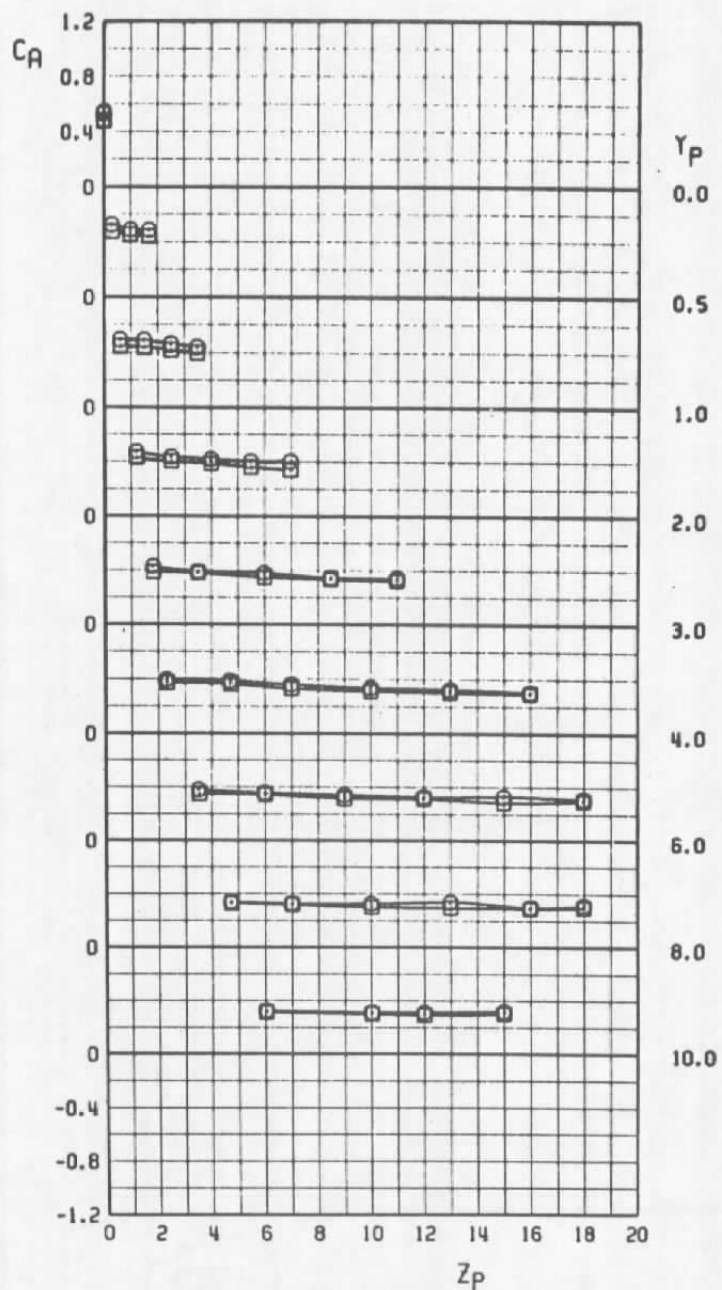
Figure 28. Effect of an adjacent store on the MK-82SE, configurations 11 and 13.

SYMBOL	CONFIG	α	M_∞	STORE	PYLON	RACK
○	11	2	0.90	MK-82SE	7	T-3
□	13	2	0.90	MK-82SE	7	T-3



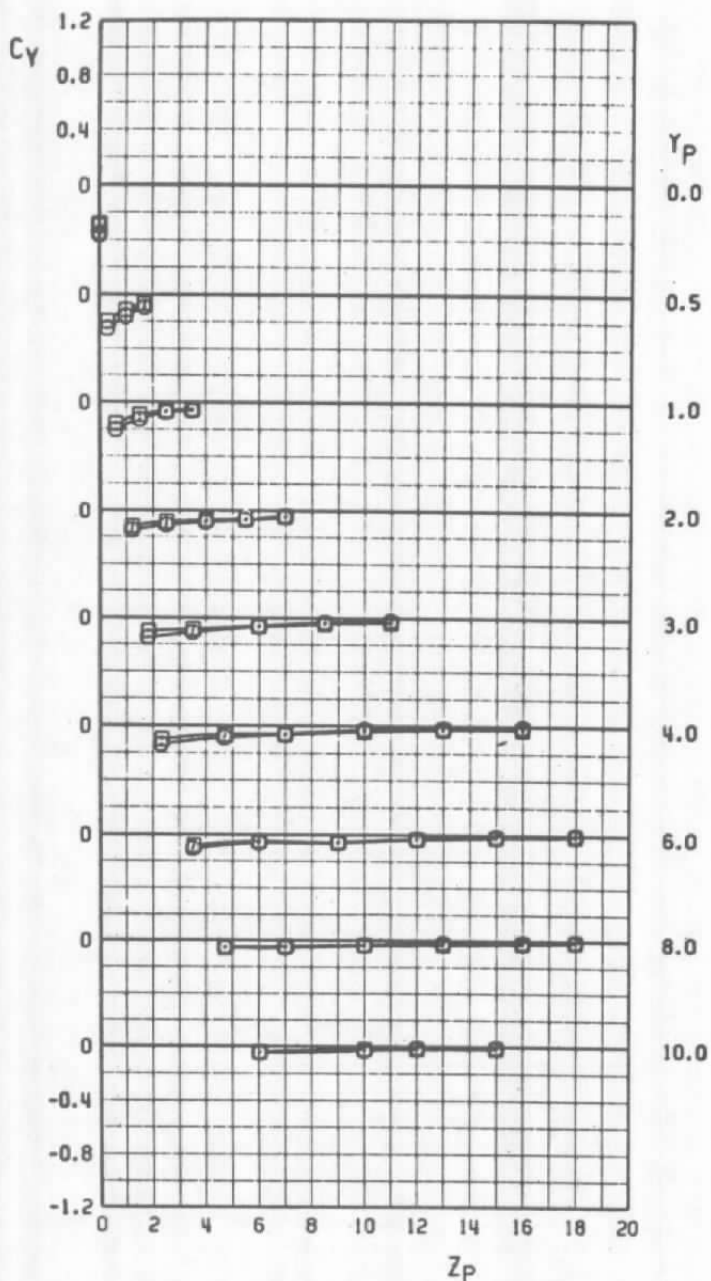
b. Pitching-moment coefficient, $M_\infty = 0.9$
Figure 28. Continued.

SYMBOL	CONFIG	α	M_∞	STORE	PYLON	RACK
○	11	2	0.95	MK-82SE	7	T-3
□	13	2	0.95	MK-82SE	7	T-3



c. Axial-force coefficient, $M_\infty = 0.95$
Figure 28. Continued.

SYMBOL	CONFIG	α	M_∞	STORE	PYLON	RACK
○	11	2	0.95	MK-82SE	7	T-3
□	13	2	0.95	MK-82SE	7	T-3



d. Side-force coefficient, $M_\infty = 0.95$
Figure 28. Continued.

SYMBOL	CONFIG	α	M_∞	STORE	PYLON	RACK
○	11	2	0.95	MK-82SE	7	T-3
□	13	2	0.95	MK-82SE	7	T-3

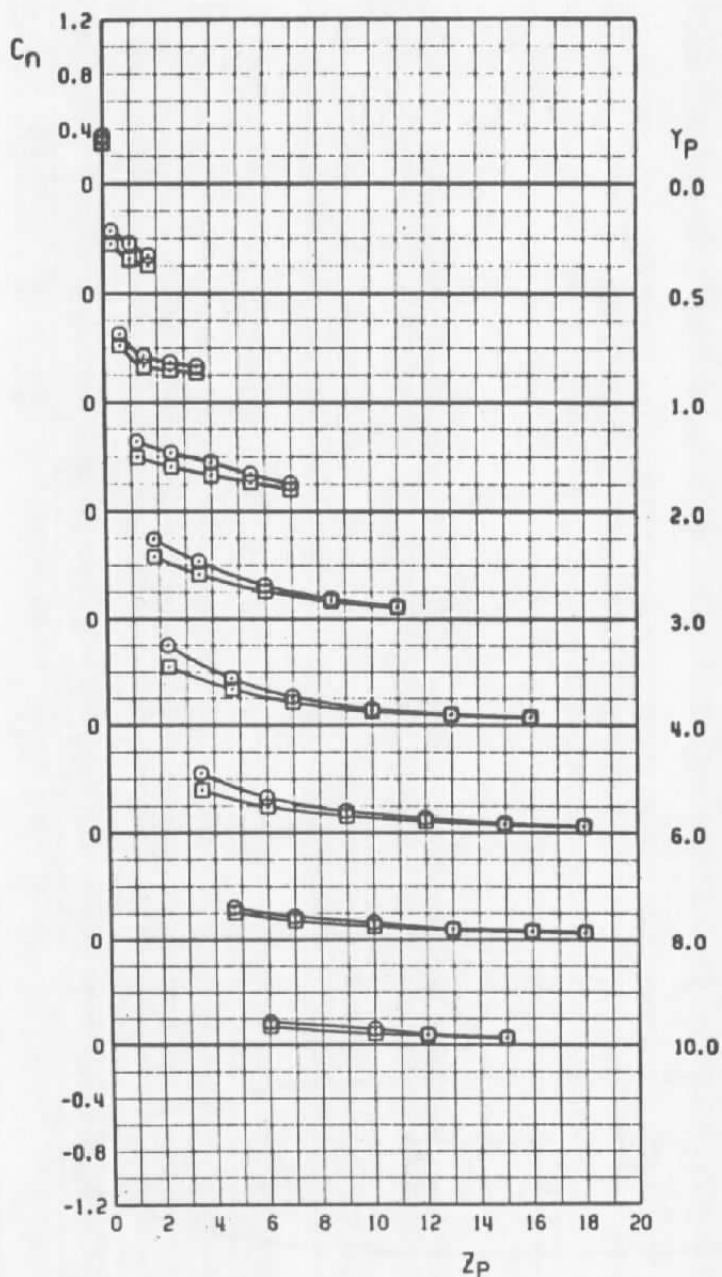
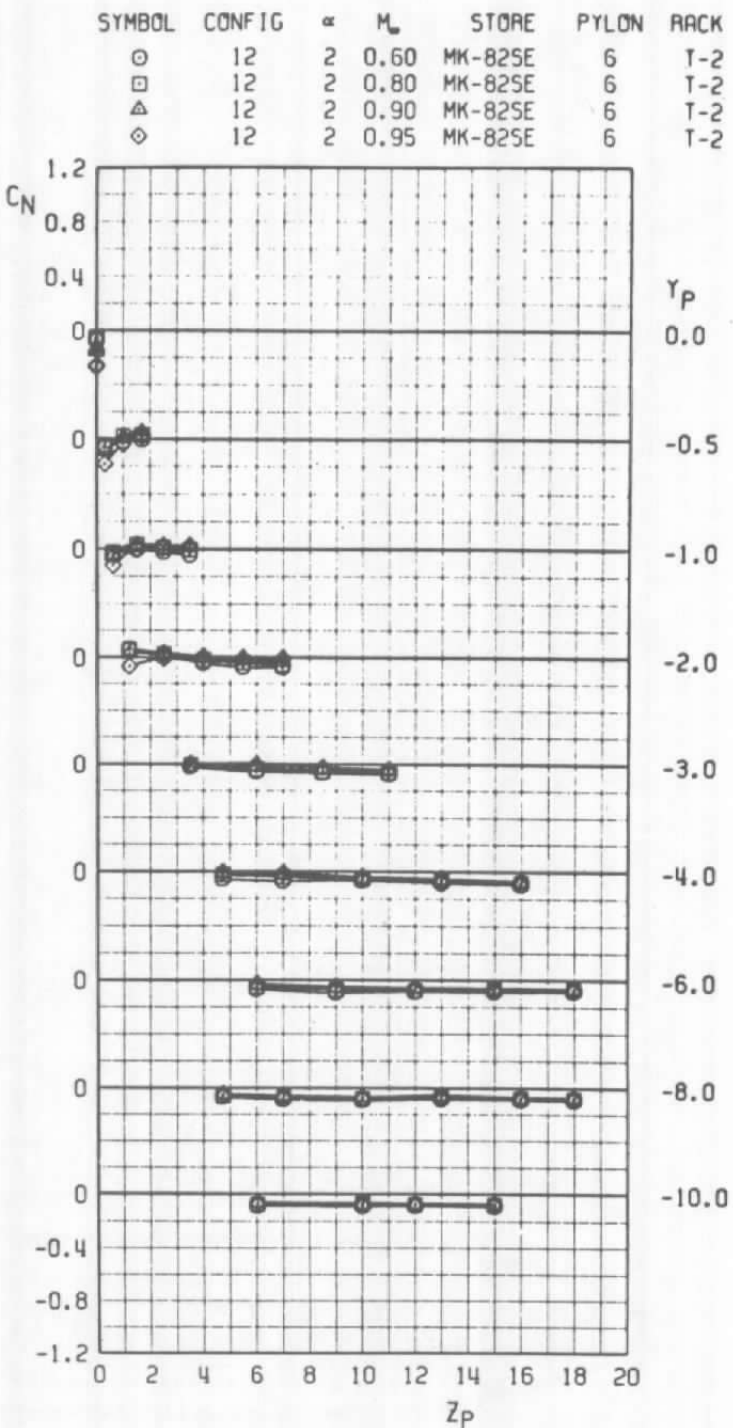
e. Yawing-moment coefficient, $M_\infty = 0.95$

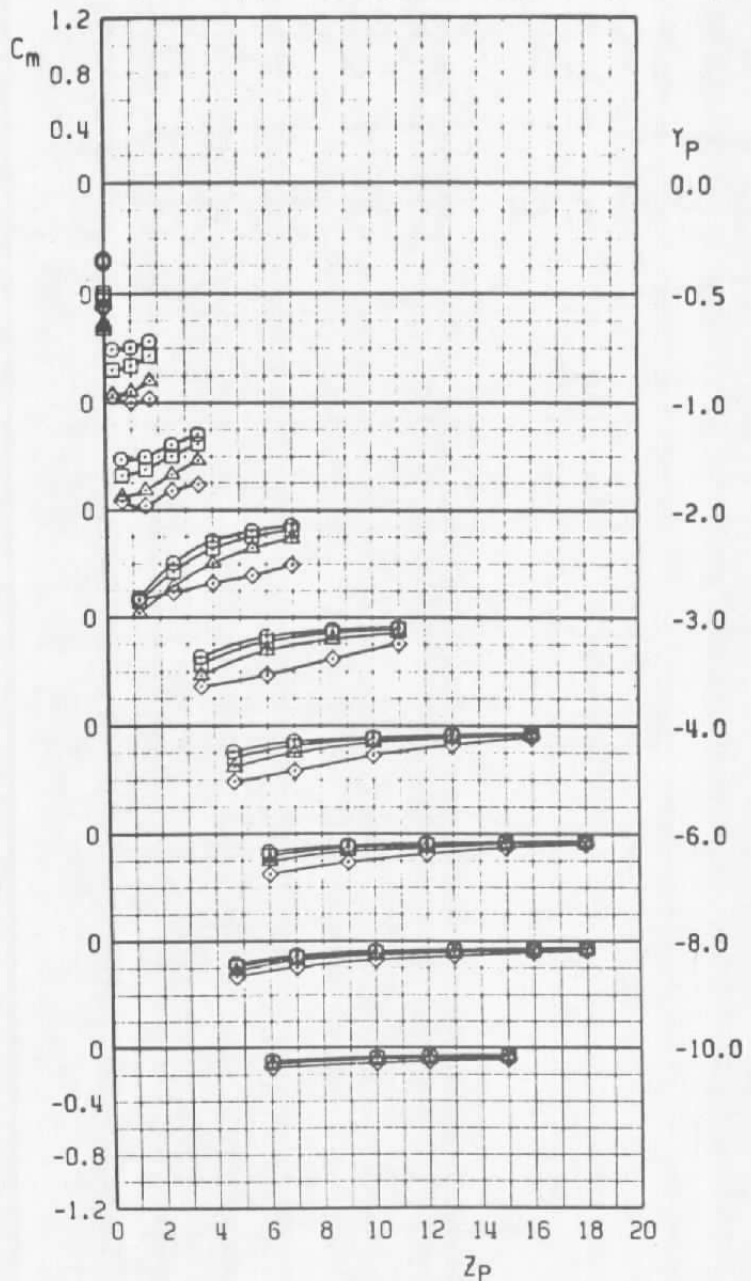
Figure 28. Concluded.



a. Normal-force coefficient

Figure 29. Aerodynamic characteristics of the MK-82SE,
configuration 12.

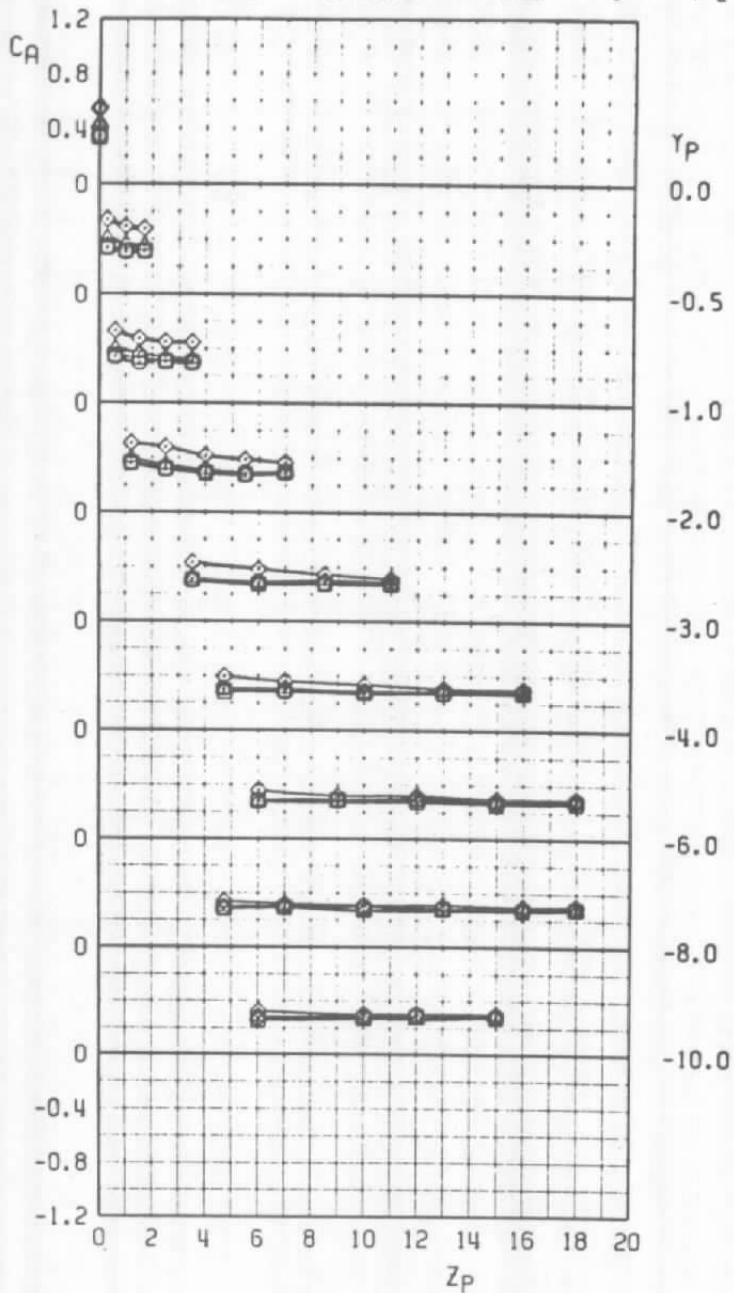
SYMBOL	CONFIG	α	M_∞	STORE	PYLON	RACK
○	12	2	0.60	MK-82SE	6	T-2
□	12	2	0.80	MK-82SE	6	T-2
△	12	2	0.90	MK-82SE	6	T-2
◊	12	2	0.95	MK-82SE	6	T-2



b. Pitching-moment coefficient

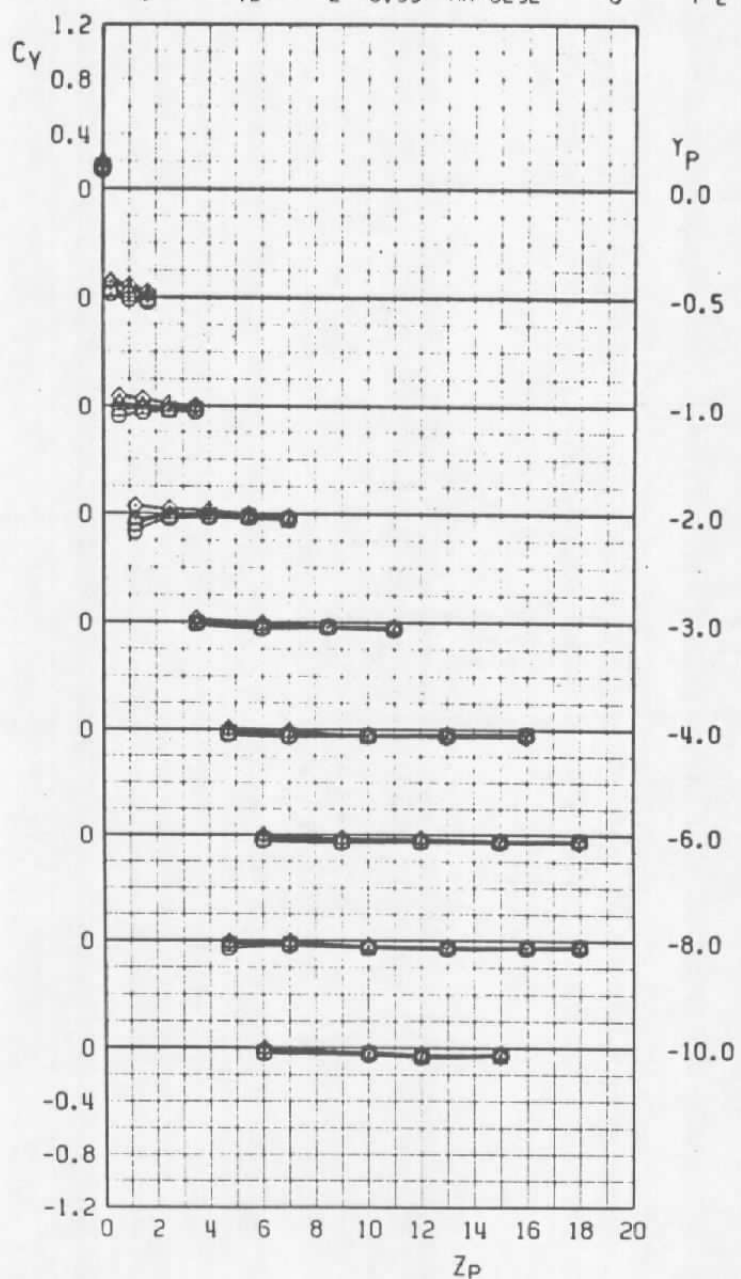
Figure 29. Continued.

SYMBOL	CONFIG	α	M_∞	STORE	PYLON	RACK
○	12	2	0.60	MK-82SE	6	T-2
□	12	2	0.80	MK-82SE	6	T-2
△	12	2	0.90	MK-82SE	6	T-2
◊	12	2	0.95	MK-82SE	6	T-2



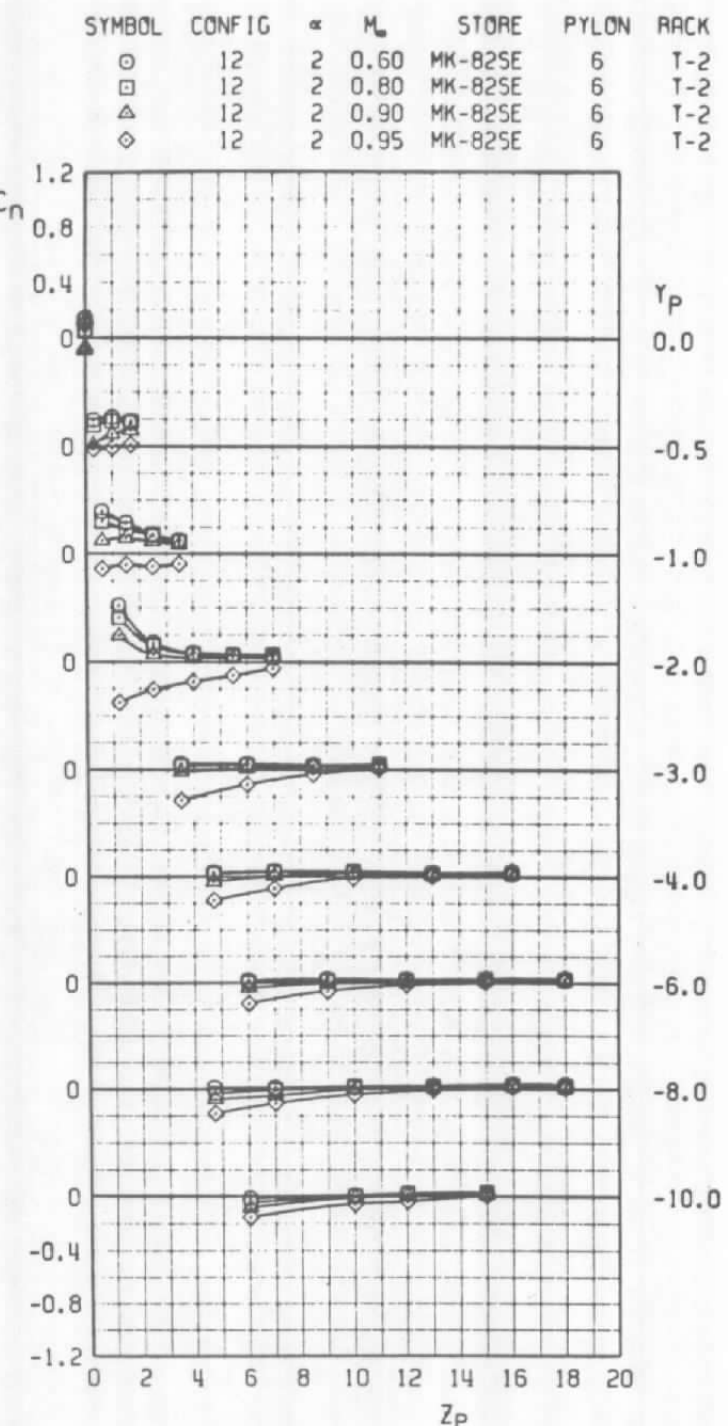
c. Axial-force coefficient
Figure 29. Continued.

SYMBOL	CONFIG	α	M_∞	STORE	PYLON	RACK
○	12	2	0.60	MK-82SE	6	T-2
□	12	2	0.80	MK-82SE	6	T-2
△	12	2	0.90	MK-82SE	6	T-2
◊	12	2	0.95	MK-82SE	6	T-2



d. Side-force coefficient

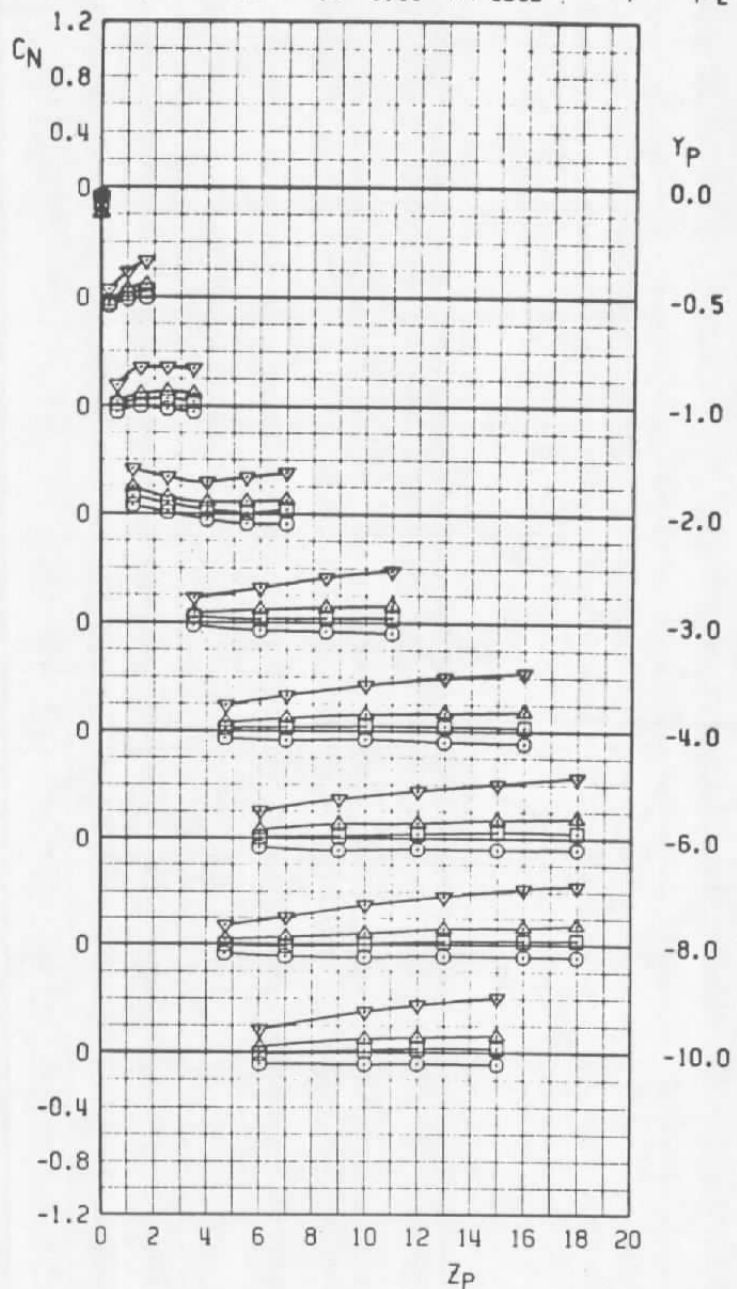
Figure 29. Continued.



e. Yawing-moment coefficient

Figure 29. Concluded.

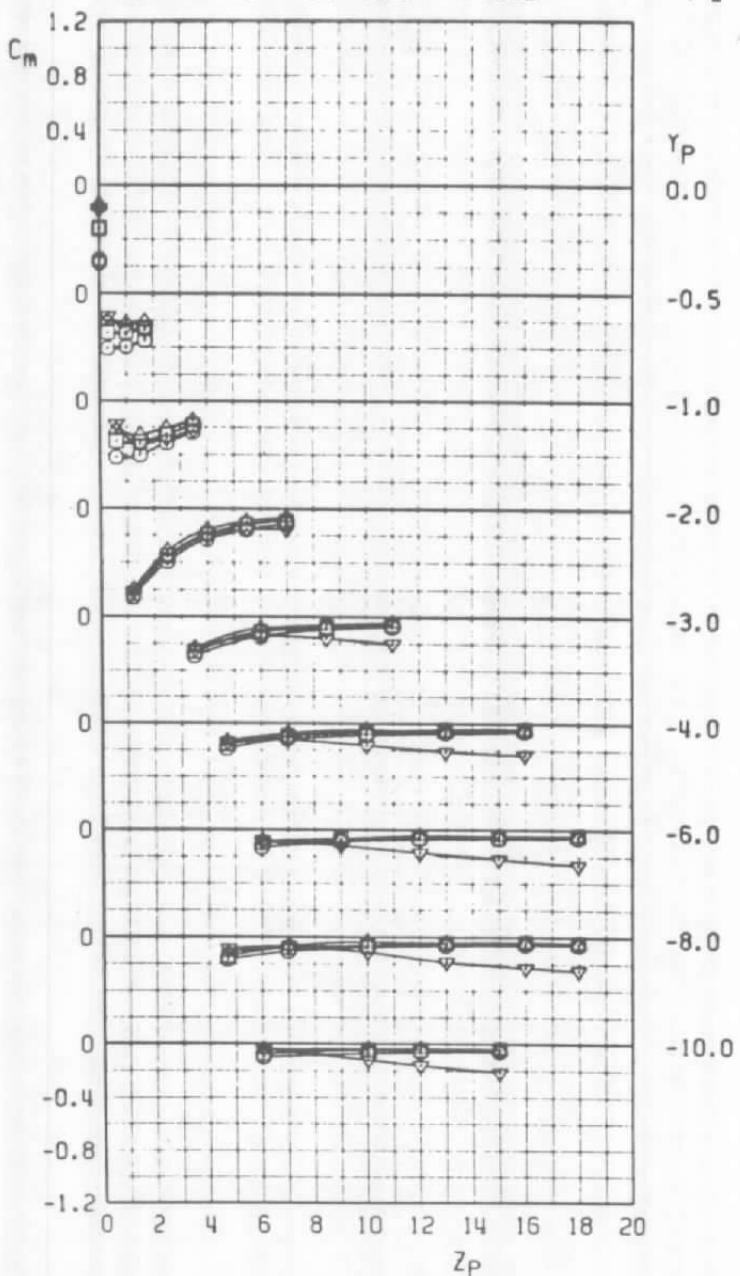
SYMBOL	CONFIG	α	M_∞	STORE	PYLON	RACK
○	12	2	0.60	MK-82SE	7	T-2
□	12	4	0.60	MK-82SE	7	T-2
△	12	6	0.60	MK-82SE	7	T-2
▽	12	10	0.60	MK-82SE	7	T-2



a. Normal-force coefficient

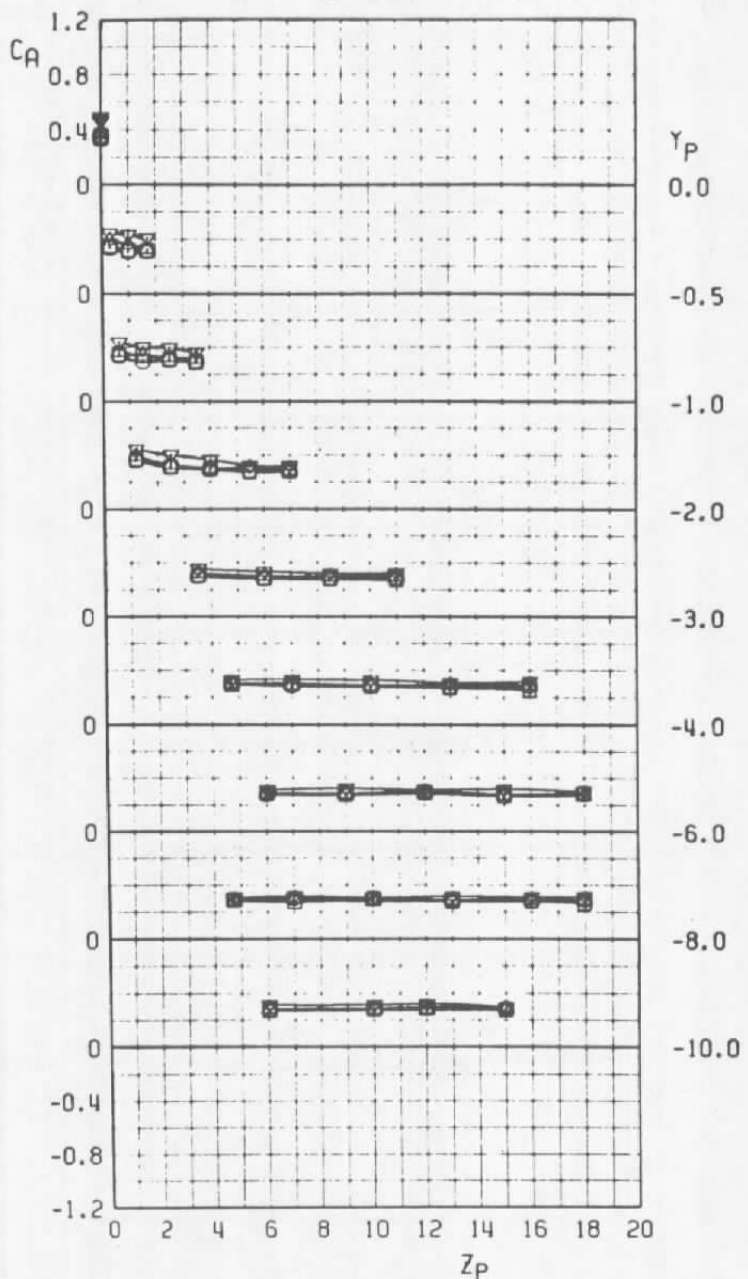
Figure 30. MK-82SE coefficient variation with aircraft angle of attack, configuration 12.

SYMBOL	CONFIG	α	M_∞	STORE	PYLON	RACK
○	12	2	0.60	MK-82SE	7	T-2
□	12	4	0.60	MK-82SE	7	T-2
△	12	6	0.60	MK-82SE	7	T-2
▽	12	10	0.60	MK-82SE	7	T-2



b. Pitching-moment coefficient
Figure 30. Continued.

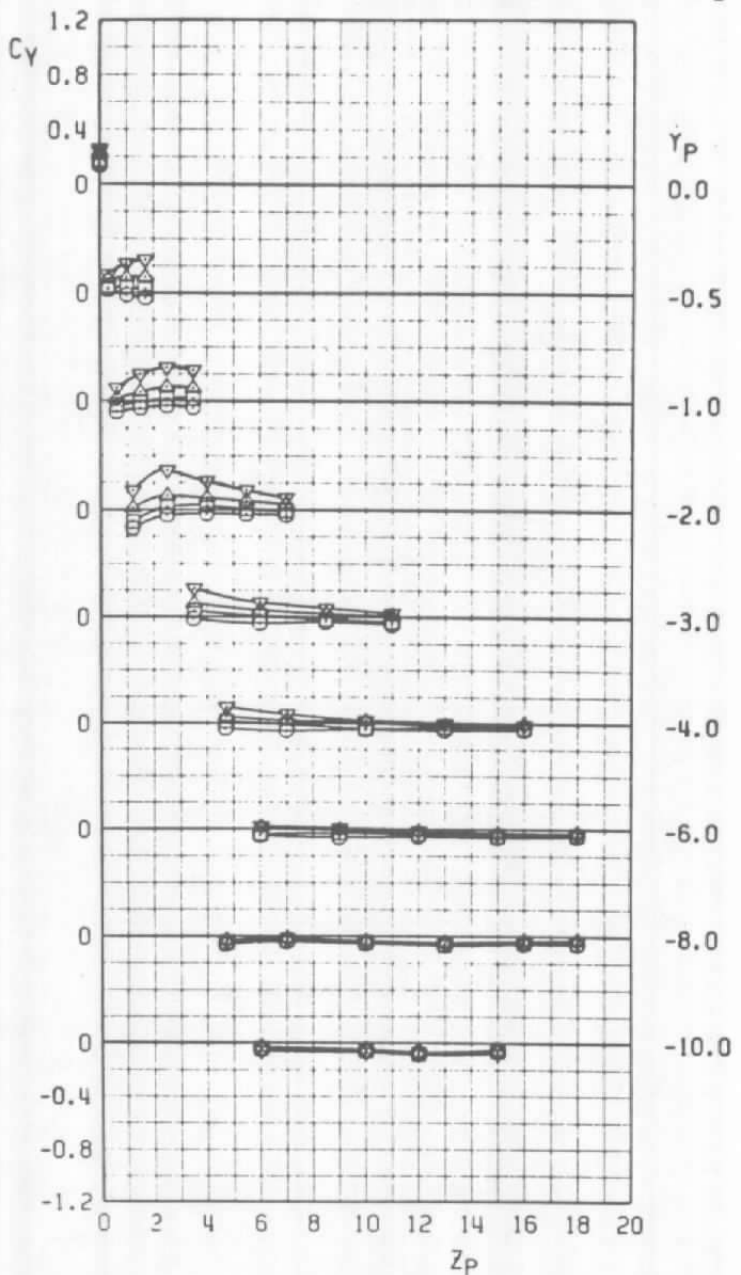
SYMBOL	CONFIG	\in	M_∞	STORE	PYLON	RACK
○	12	2	0.60	MK-82SE	7	T-2
□	12	4	0.60	MK-82SE	7	T-2
△	12	6	0.60	MK-82SE	7	T-2
▽	12	10	0.60	MK-82SE	7	T-2



c. Axial-force coefficient

Figure 30. Continued.

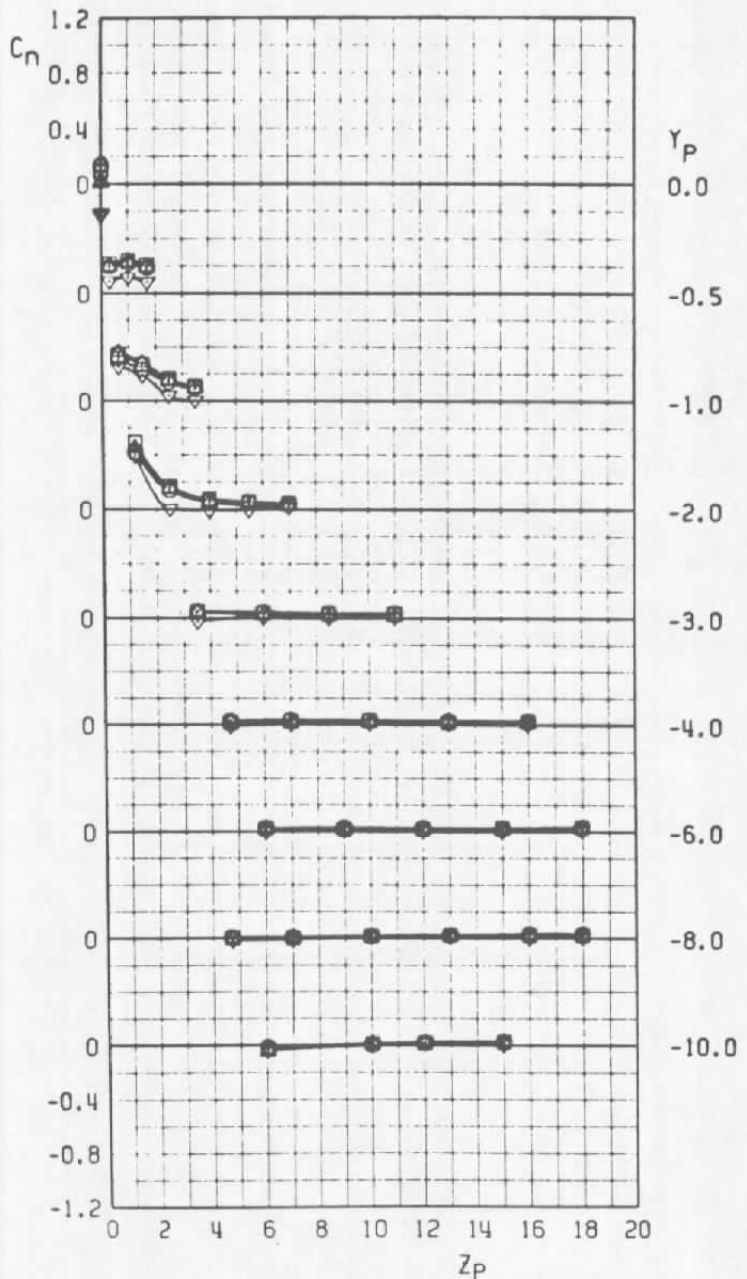
SYMBOL	CONFIG	α	M_∞	STORE	PYLON	RACK
○	12	2	0.60	MK-82SE	7	T-2
□	12	4	0.60	MK-82SE	7	T-2
△	12	6	0.60	MK-82SE	7	T-2
▽	12	10	0.60	MK-82SE	7	T-2



d. Side-force coefficient

Figure 30. Continued.

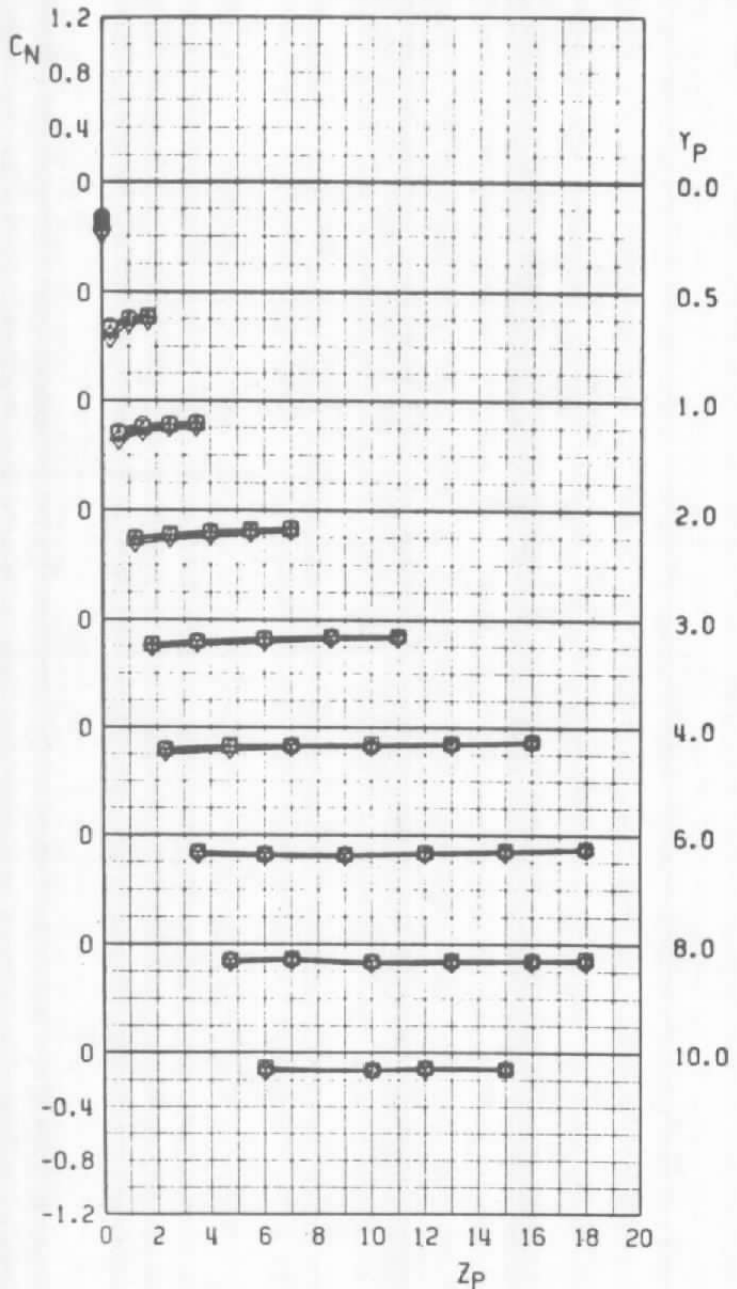
SYMBOL	CONFIG	α	M_{∞}	STORE	PYLON	RACK
○	I2	2	0.60	MK-82SE	7	T-2
□	I2	4	0.60	MK-82SE	7	T-2
△	I2	6	0.60	MK-82SE	7	T-2
▽	I2	10	0.60	MK-82SE	7	T-2



e. Yawing-moment coefficient

Figure 30. Concluded.

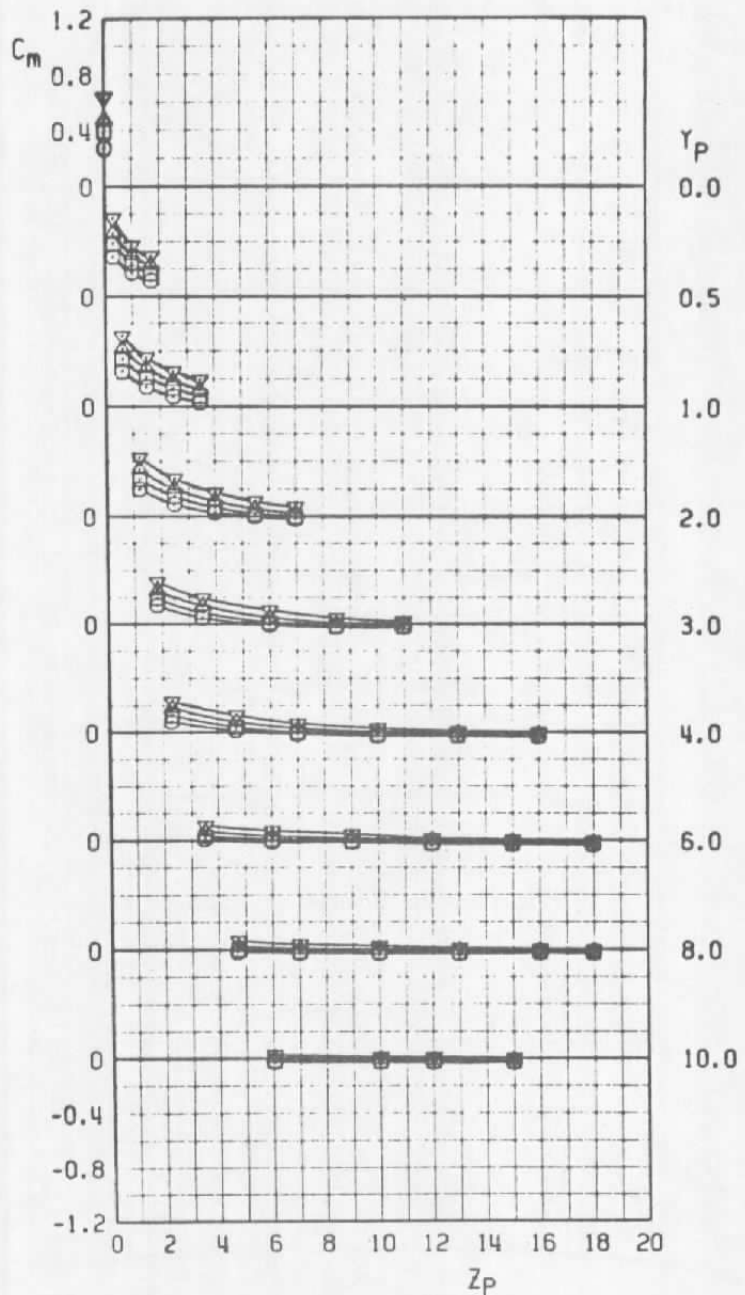
SYMBOL	CONFIG	∞	M_∞	STORE	PYLON	RACK
○	14	2	0.60	MK-82SE	6	M-6
□	14	2	0.80	MK-82SE	6	M-6
△	14	2	0.90	MK-82SE	6	M-6
▽	14	2	0.95	MK-82SE	6	M-6



a. Normal-force coefficient

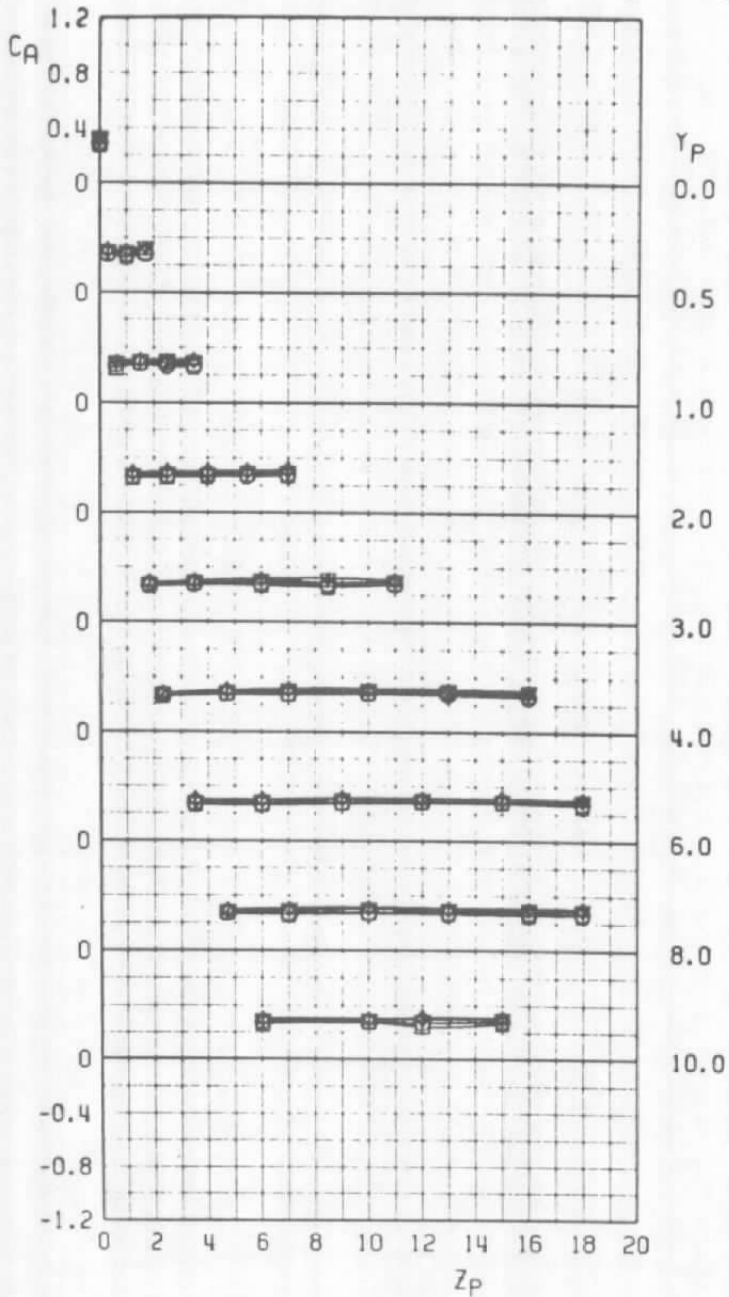
Figure 31. Aerodynamic characteristics of the MK-82SE, configuration 14.

SYMBOL	CONFIG	α	M_∞	STORE	PYLON	RACK
○	14	2	0.60	MK-82SE	6	M-6
□	14	2	0.80	MK-82SE	6	M-6
△	14	2	0.90	MK-82SE	6	M-6
▽	14	2	0.95	MK-82SE	6	M-6



b. Pitching-moment coefficient
Figure 31. Continued.

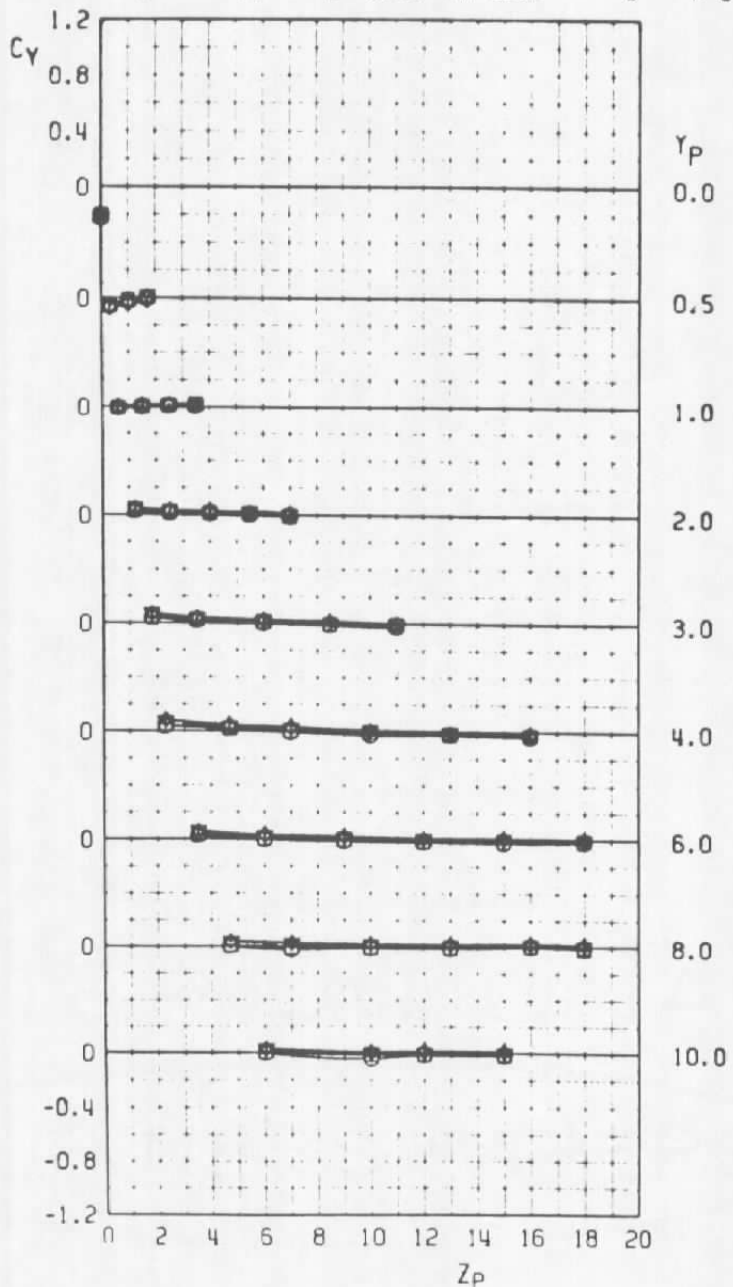
SYMBOL	CONFIG	α	M_∞	STORE	PYLON	RACK
○	14	2	0.60	MK-82SE	6	M-6
□	14	2	0.80	MK-82SE	6	M-6
△	14	2	0.90	MK-82SE	6	M-6
▽	14	2	0.95	MK-82SE	6	M-6



c. Axial-force coefficient

Figure 31. Continued.

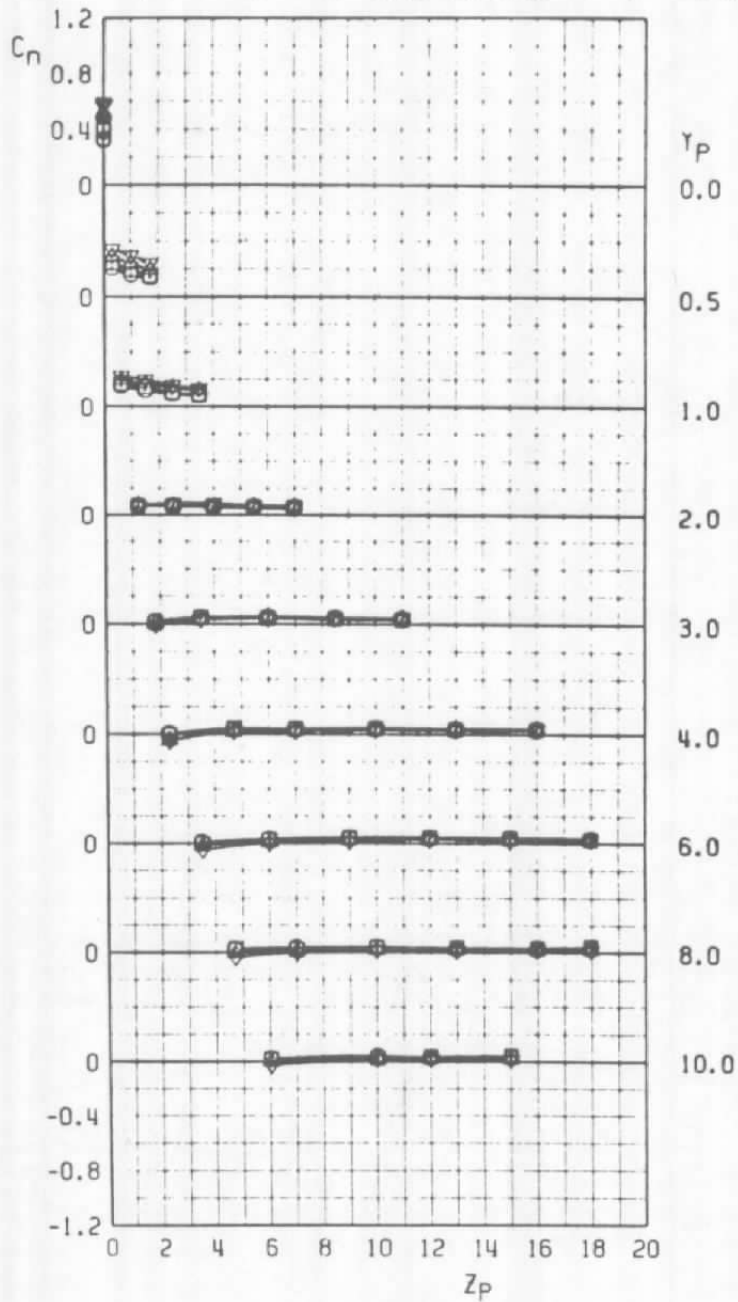
SYMBOL	CONFIG	α	M_∞	STORE	PYLON	RACK
○	14	2	0.60	MK-82SE	6	M-6
□	14	2	0.80	MK-82SE	6	M-6
△	14	2	0.90	MK-82SE	6	M-6
▽	14	2	0.95	MK-82SE	6	M-6



d. Side-force coefficient

Figure 31. Continued.

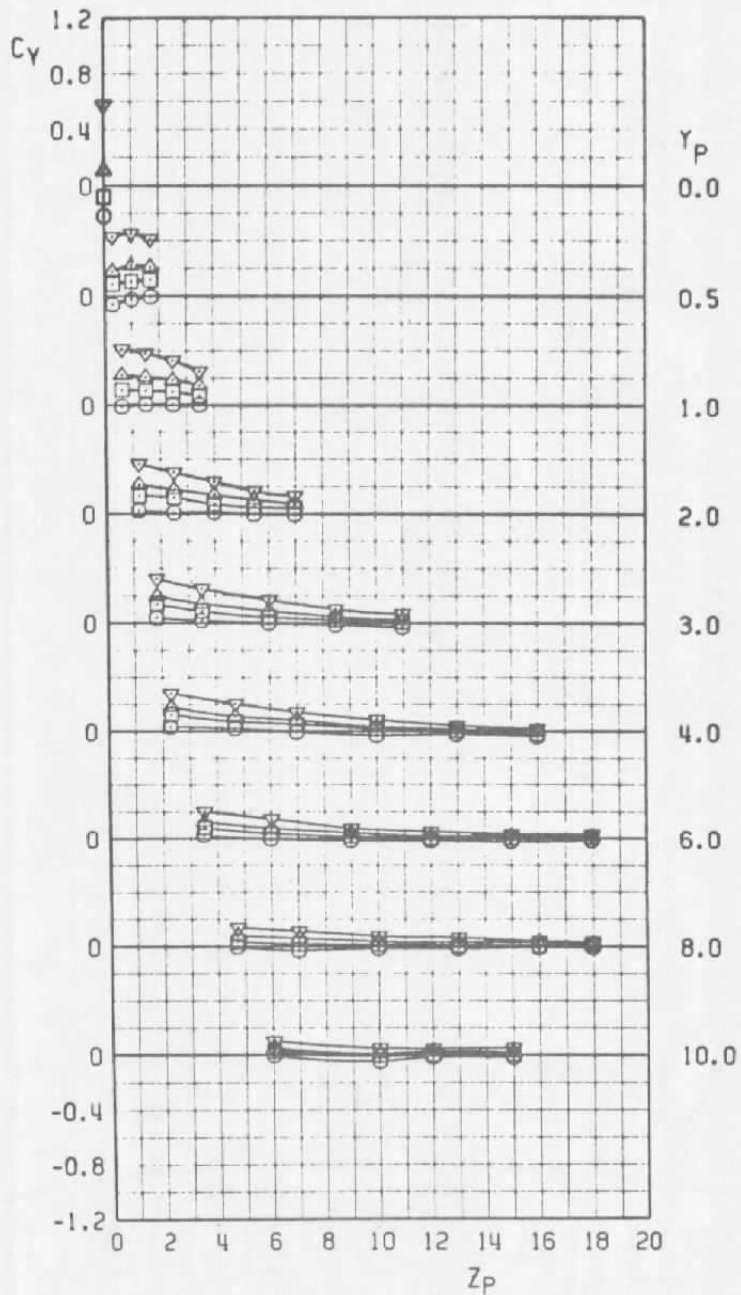
SYMBOL	CONFIG	α	M_c	STORE	PYLON	RACK
○	14	2	0.60	MK-82SE	6	M-6
□	14	2	0.80	MK-82SE	6	M-6
△	14	2	0.90	MK-82SE	6	M-6
▽	14	2	0.95	MK-82SE	6	M-6



e. Yawing-moment coefficient

Figure 31. Concluded.

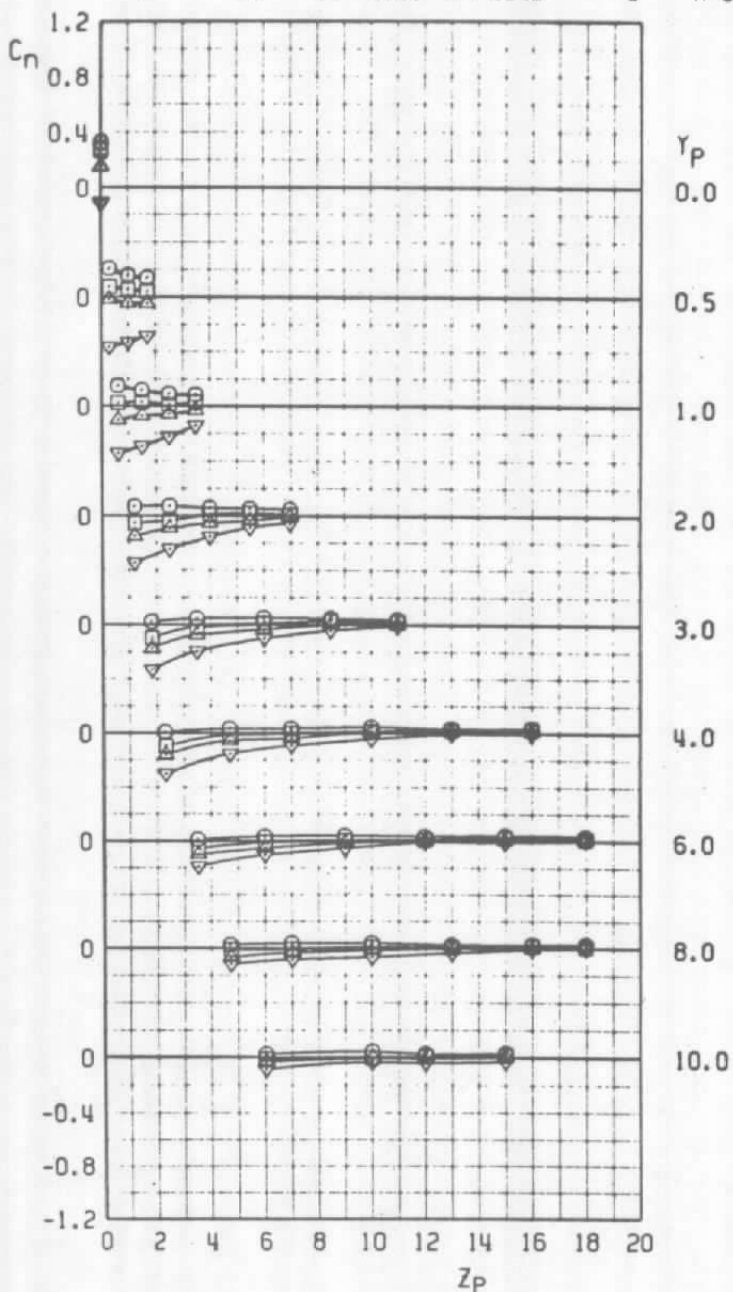
SYMBOL	CONFIG	α	M_∞	STORE	PYLON	RACK
○	14	2	0.60	MK-82SE	6	M-6
□	14	4	0.60	MK-82SE	6	M-6
△	14	6	0.60	MK-82SE	6	M-6
▽	14	10	0.60	MK-82SE	6	M-6



a. Side-force coefficient

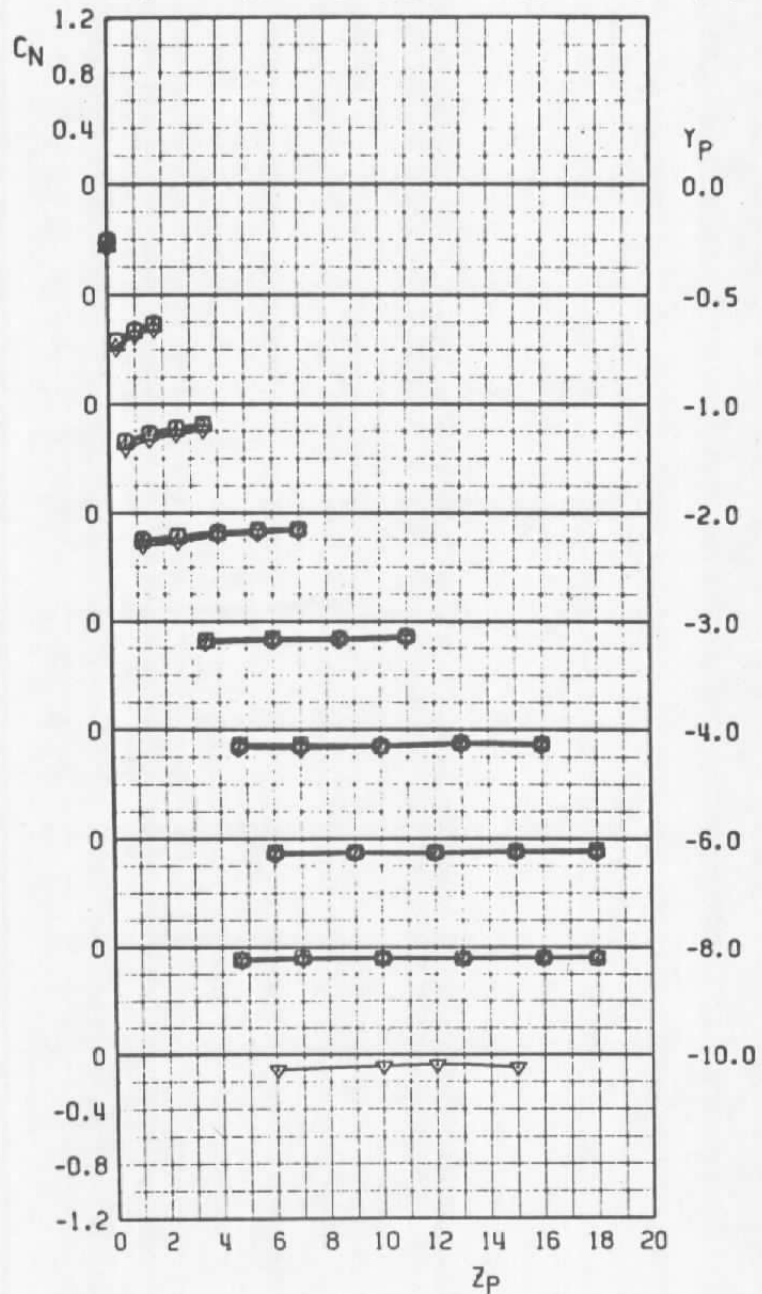
Figure 32. MK-82SE coefficient variation with aircraft angle of attack, configuration 14.

SYMBOL	CONFIG	α	M_c	STORE	PYLON	RACK
○	14	2	0.60	MK-82SE	6	M-6
□	14	4	0.60	MK-82SE	6	M-6
△	14	6	0.60	MK-82SE	6	M-6
▽	14	10	0.60	MK-82SE	6	M-6



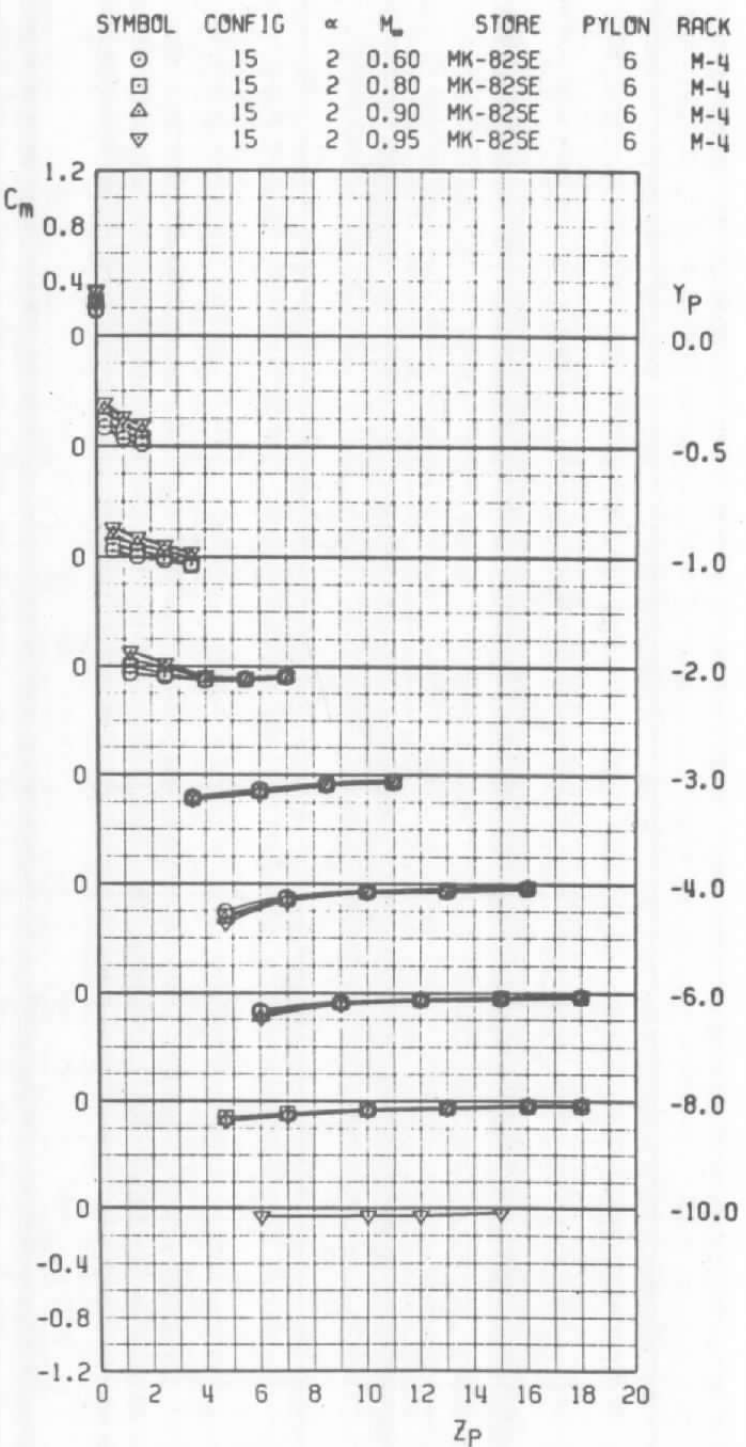
b. Yawing-moment coefficient
Figure 32. Concluded.

SYMBOL	CONFIG	α	M _∞	STORE	PYLON	RACK
○	15	2	0.60	MK-82SE	6	M-4
□	15	2	0.80	MK-82SE	6	M-4
△	15	2	0.90	MK-82SE	6	M-4
▽	15	2	0.95	MK-82SE	6	M-4



a. Normal-force coefficient

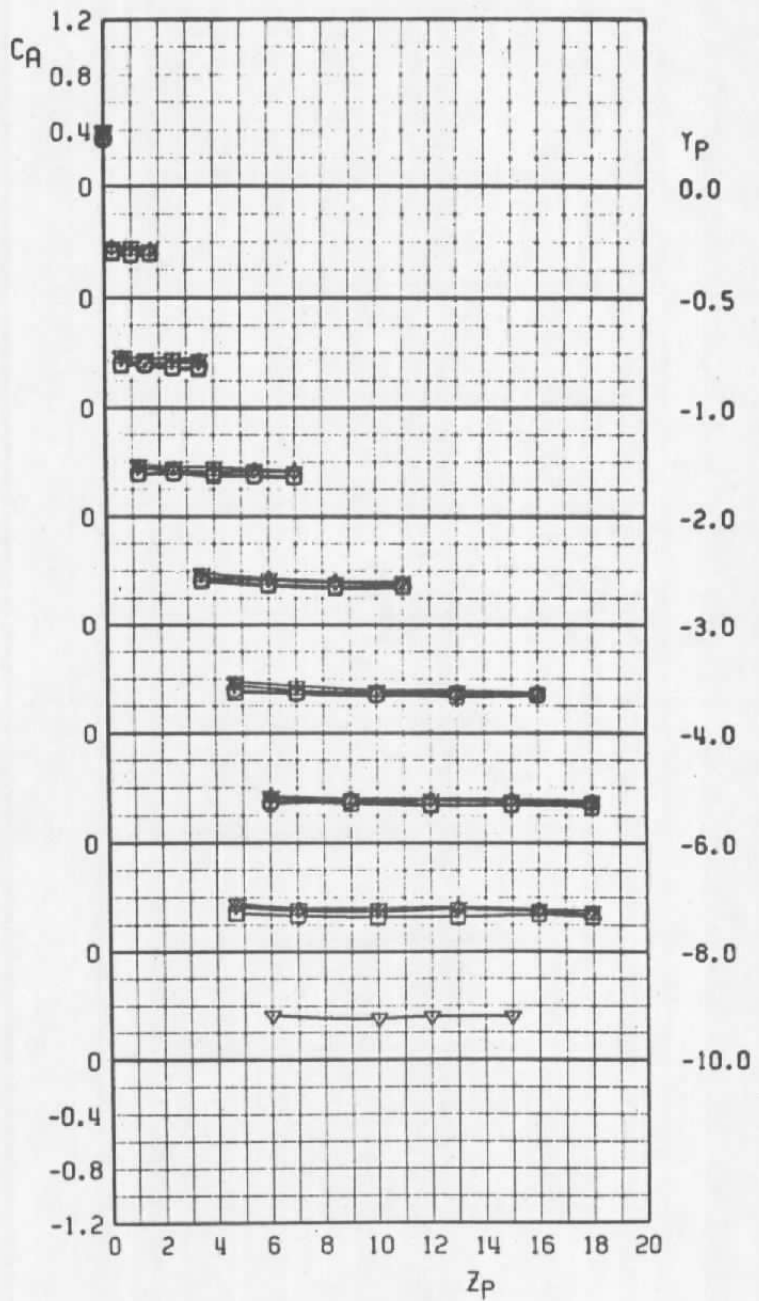
Figure 33. Aerodynamic characteristics of the MK-82SE,
configuration 15.



b. Pitching-moment coefficient

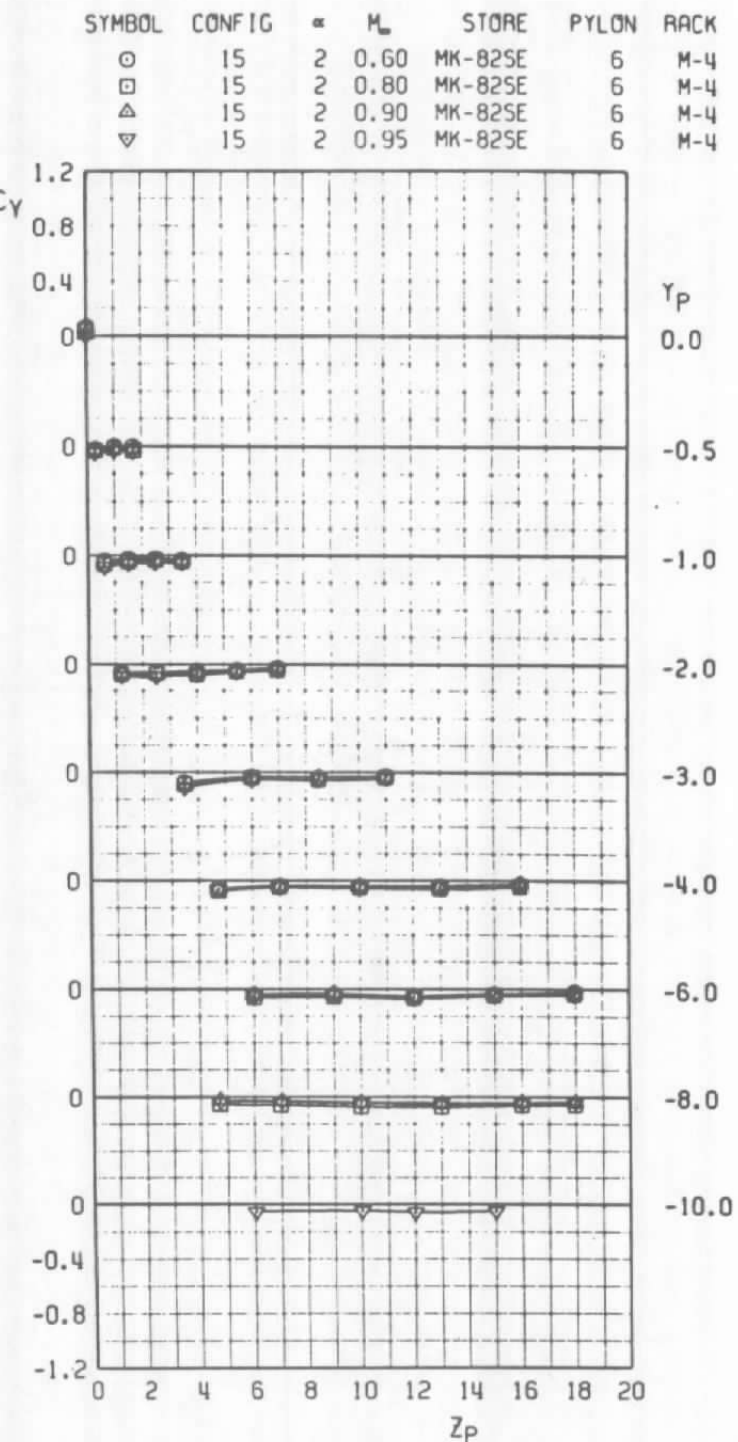
Figure 33. Continued.

SYMBOL	CONFIG	α	M_∞	STORE	PYLON	RACK
○	15	2	0.60	MK-82SE	6	M-4
□	15	2	0.80	MK-82SE	6	M-4
△	15	2	0.90	MK-82SE	6	M-4
▽	15	2	0.95	MK-82SE	6	M-4



c. Axial-force coefficient

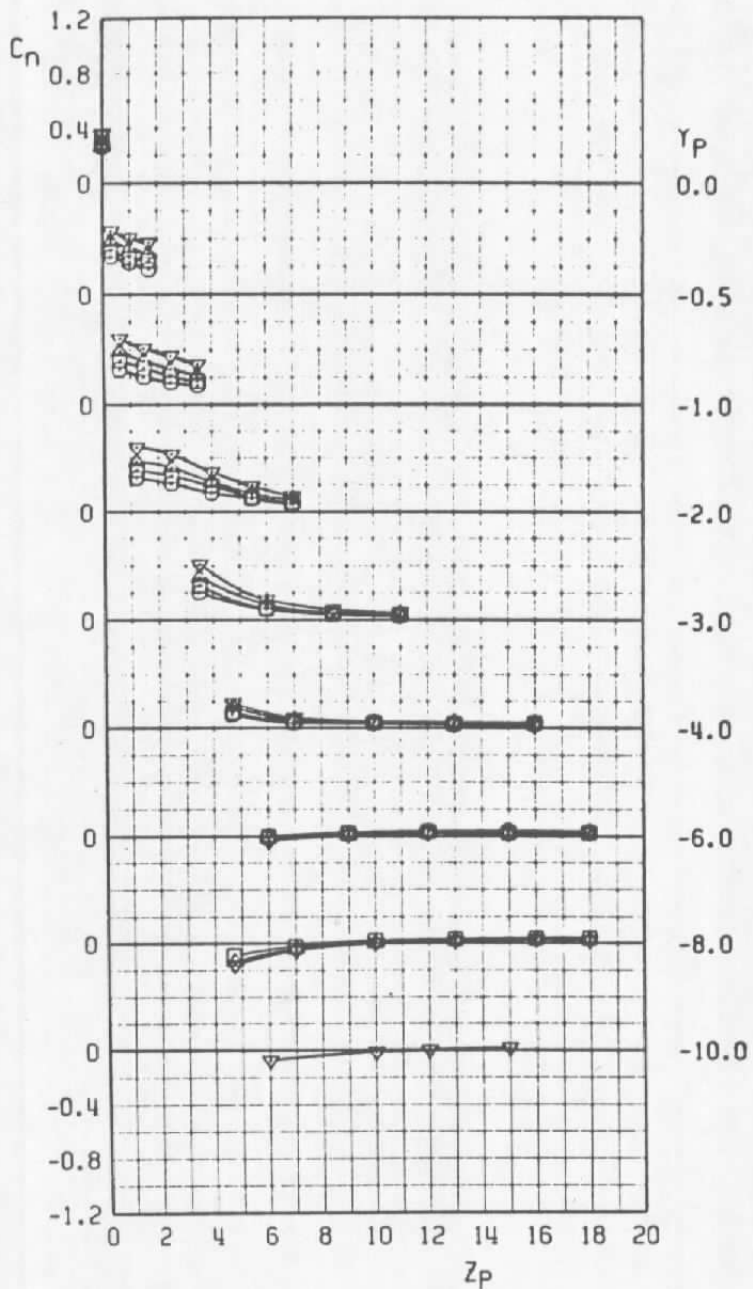
Figure 33. Continued.



d. Side-force coefficient

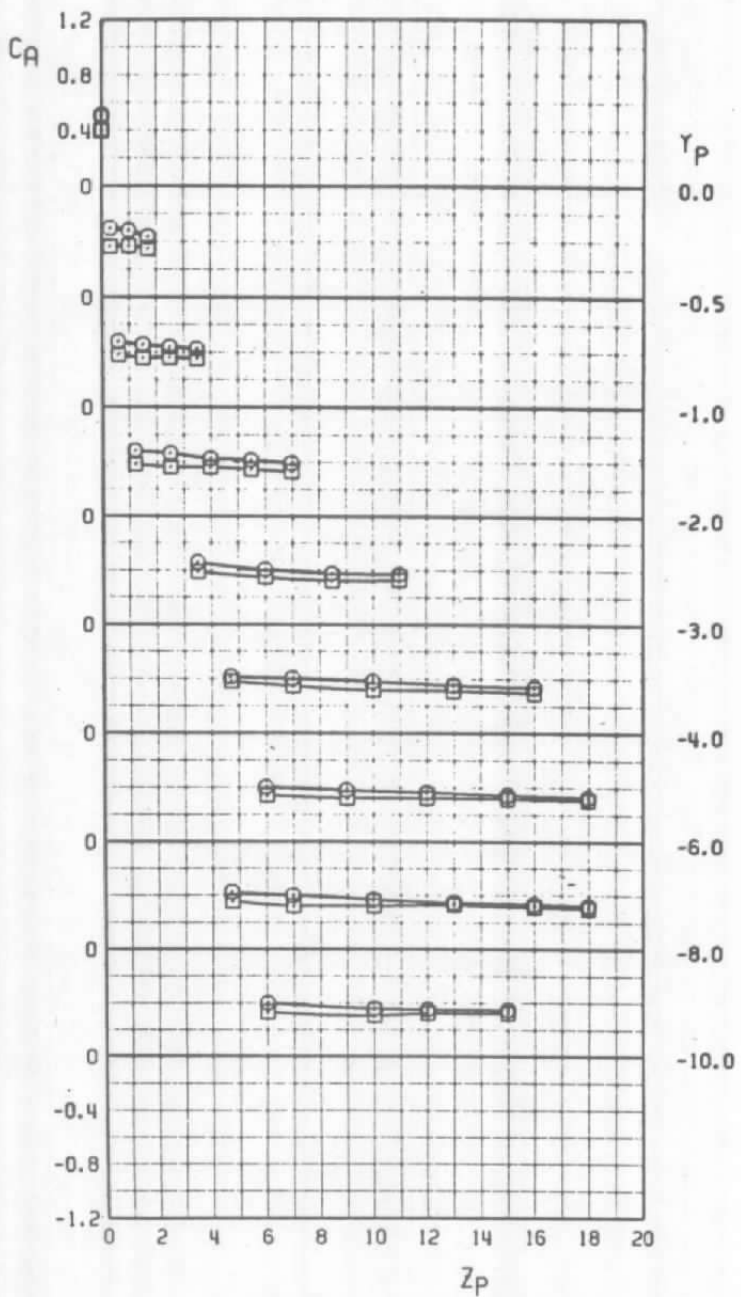
Figure 33. Continued.

SYMBOL	CONFIG	α	M_∞	STORE	PYLON	RACK
○	15	2	0.60	MK-82SE	6	M-4
□	15	2	0.80	MK-82SE	6	M-4
△	15	2	0.90	MK-82SE	6	M-4
▽	15	2	0.95	MK-82SE	6	M-4



e. Yawing-moment coefficient
Figure 33. Concluded.

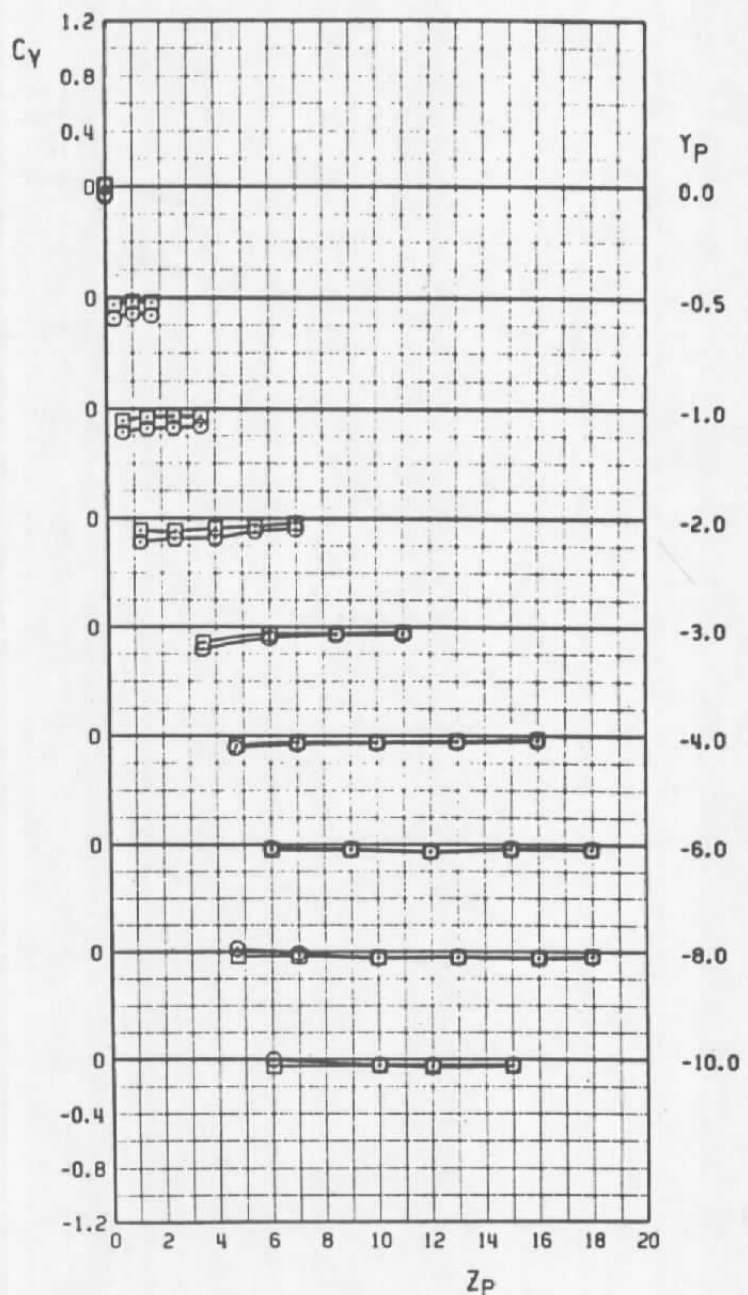
SYMBOL	CONFIG	α	M_∞	STORE	PYLON	RACK
○	15	0	0.95	MK-82SE	6	M-4
□	15	2	0.95	MK-82SE	6	M-4



a. Axial-force coefficient

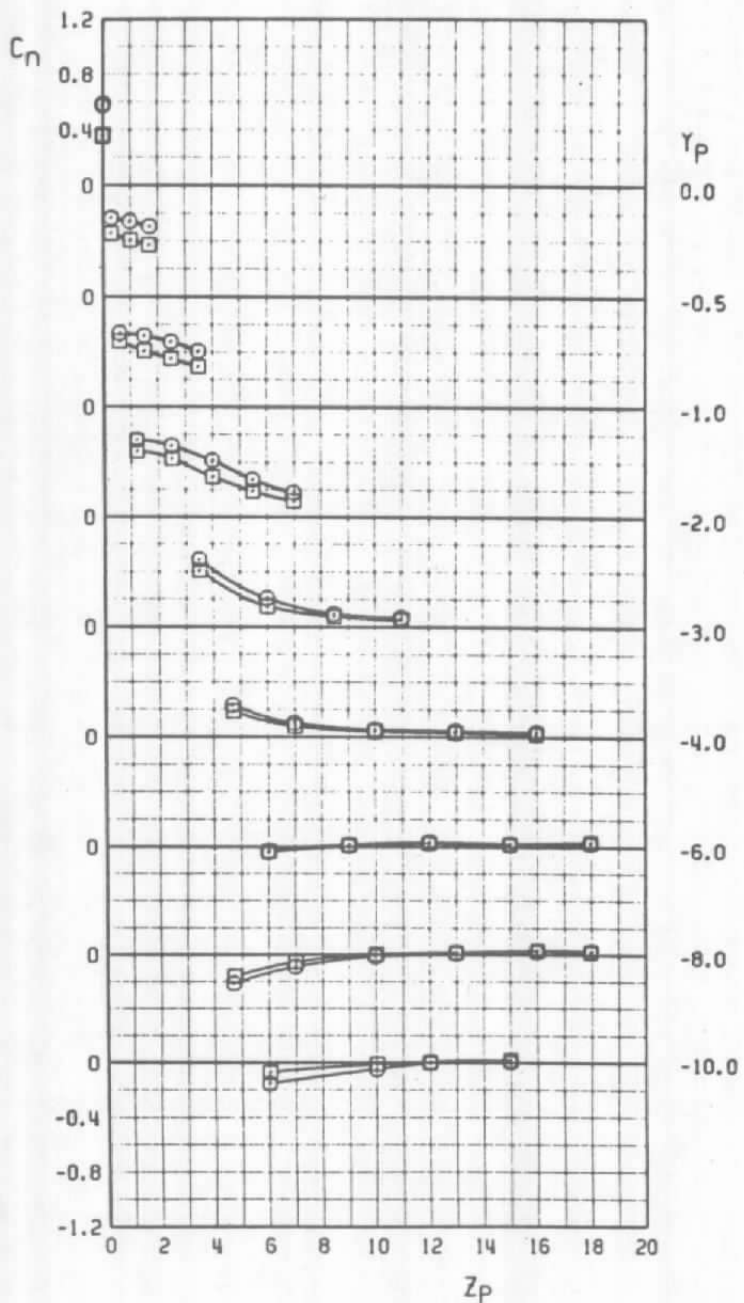
Figure 34. MK-82SE coefficient variation with aircraft angle of attack, configuration 15.

SYMBOL	CONFIG	α	M _∞	STORE	PYLON	RACK
○	15	0	0.95	MK-82SE	6	M-4
□	15	2	0.95	MK-82SE	6	M-4



b. Side-force coefficient
Figure 34. Continued.

SYMBOL	CONFIG	α	M_∞	STORE	PYLON	RACK
○	15	0	0.95	MK-82SE	6	M-4
□	15	2	0.95	MK-82SE	6	M-4



c. Yawing-force coefficient
Figure 34. Concluded.

SYMBOL	CONFIG	α	M_∞	STORE	PYLON
○	16	2	0.60	MK-82SE	7
□	16	2	0.80	MK-82SE	7
△	16	2	0.90	MK-82SE	7
▽	16	2	0.95	MK-82SE	7

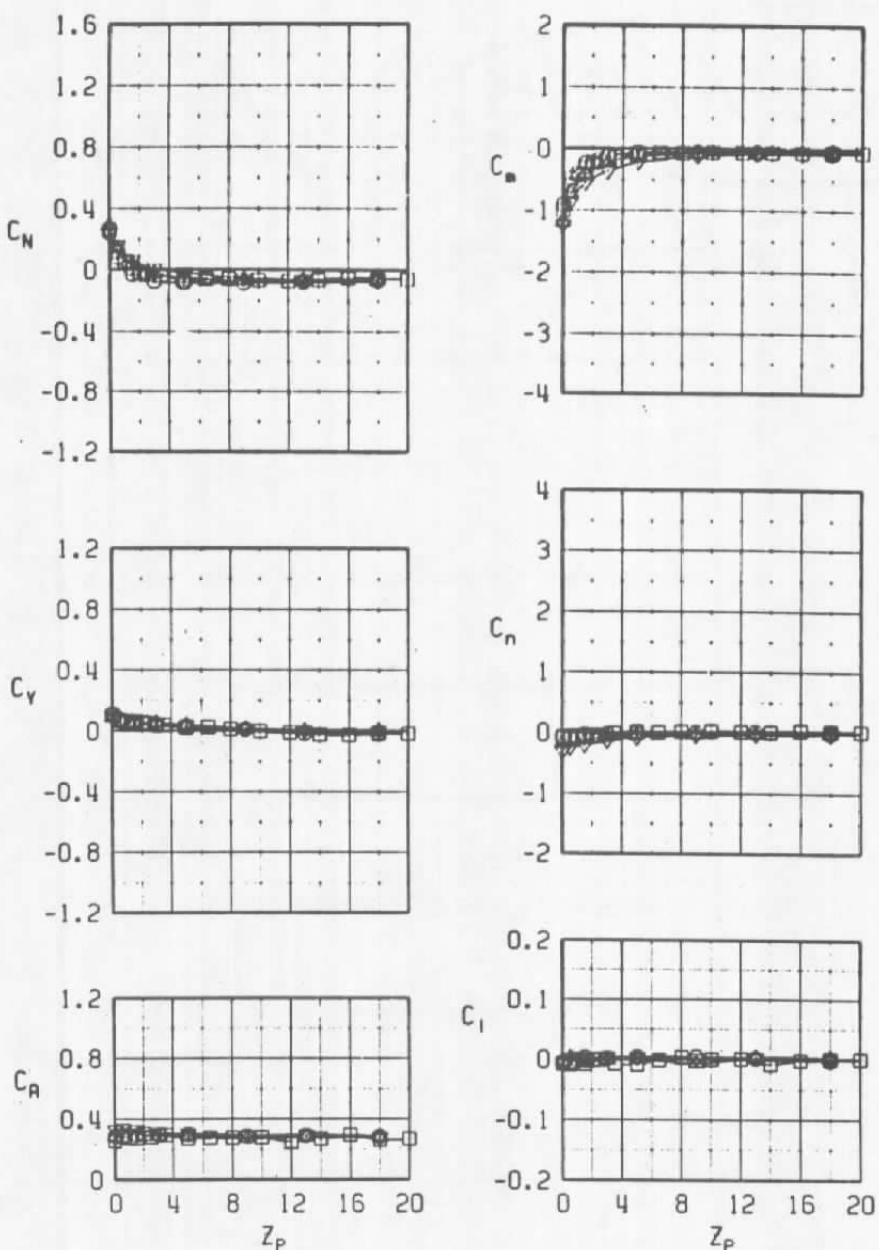


Figure 35. Aerodynamic characteristics of the MK-82SE, configuration 16.

SYMBOL	CONFIG	α	M_∞	STORE	PYLON
○	16	2	0.60	MK-82SE	7
□	16	4	0.60	MK-82SE	7
△	16	6	0.60	MK-82SE	7
▽	16	10	0.60	MK-82SE	7

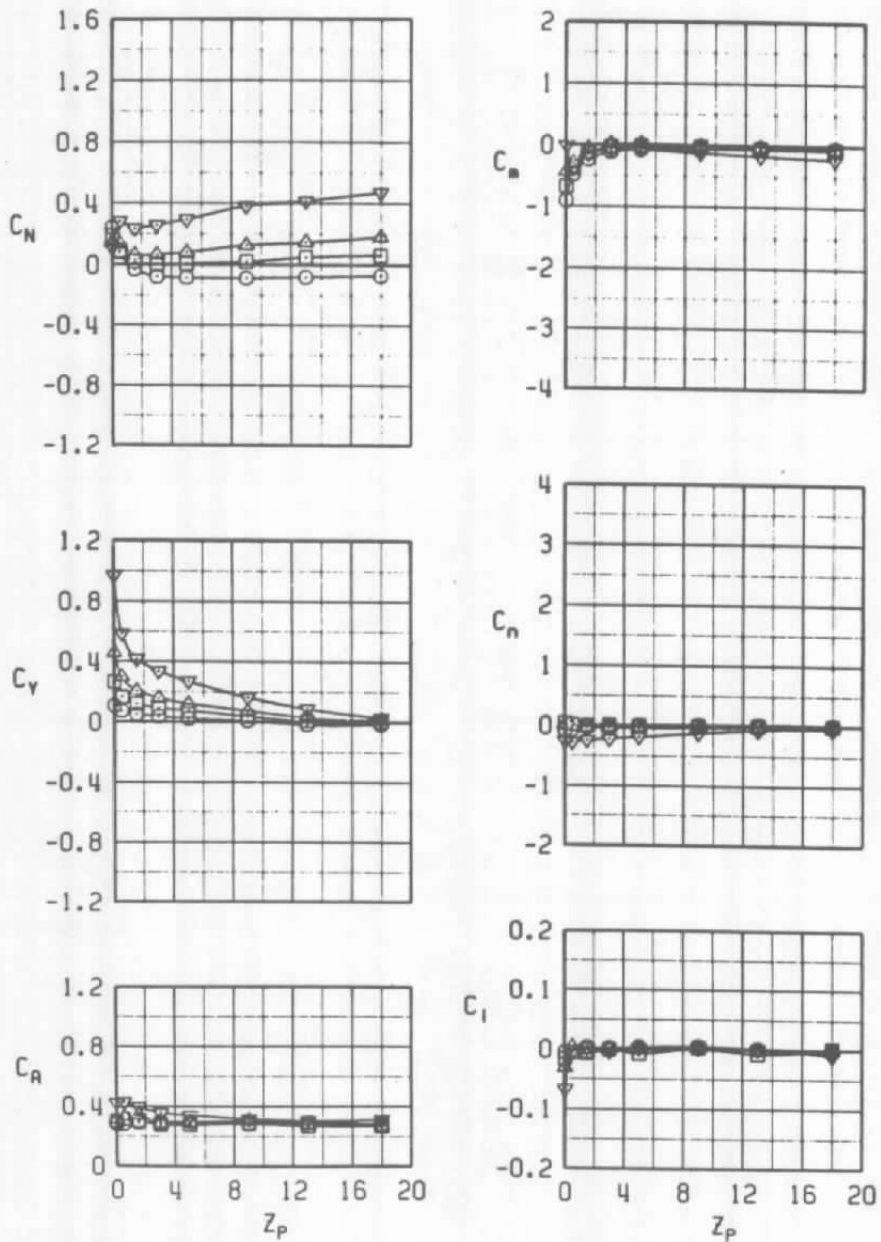


Figure 36. MK-82SE coefficient variation with aircraft angle of attack, configuration 16.

SYMBOL	CONFIG	α	M_∞	STORE	PYLON
○	17	2	0.60	MK-82SE	6
□	17	2	0.80	MK-82SE	6
△	17	2	0.90	MK-82SE	6
▽	17	2	0.95	MK-82SE	6

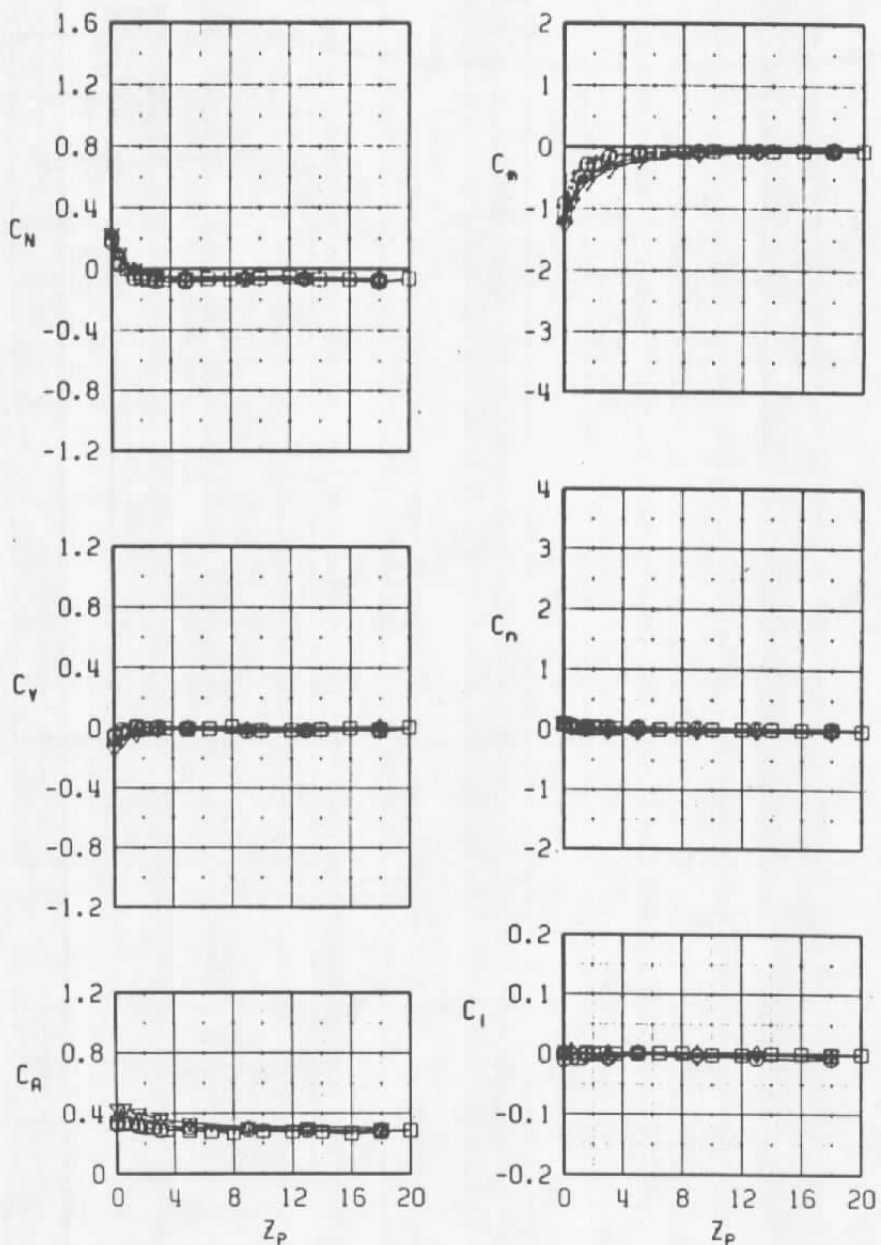


Figure 37. Aerodynamic characteristics of the MK-82SE, configuration 17.

SYMBOL	CONFIG	α	M_∞	STORE	PYLON
○	17	2	0.60	MK-82SE	6
□	17	4	0.60	MK-82SE	6
△	17	6	0.60	MK-82SE	6
▽	17	10	0.60	MK-82SE	6

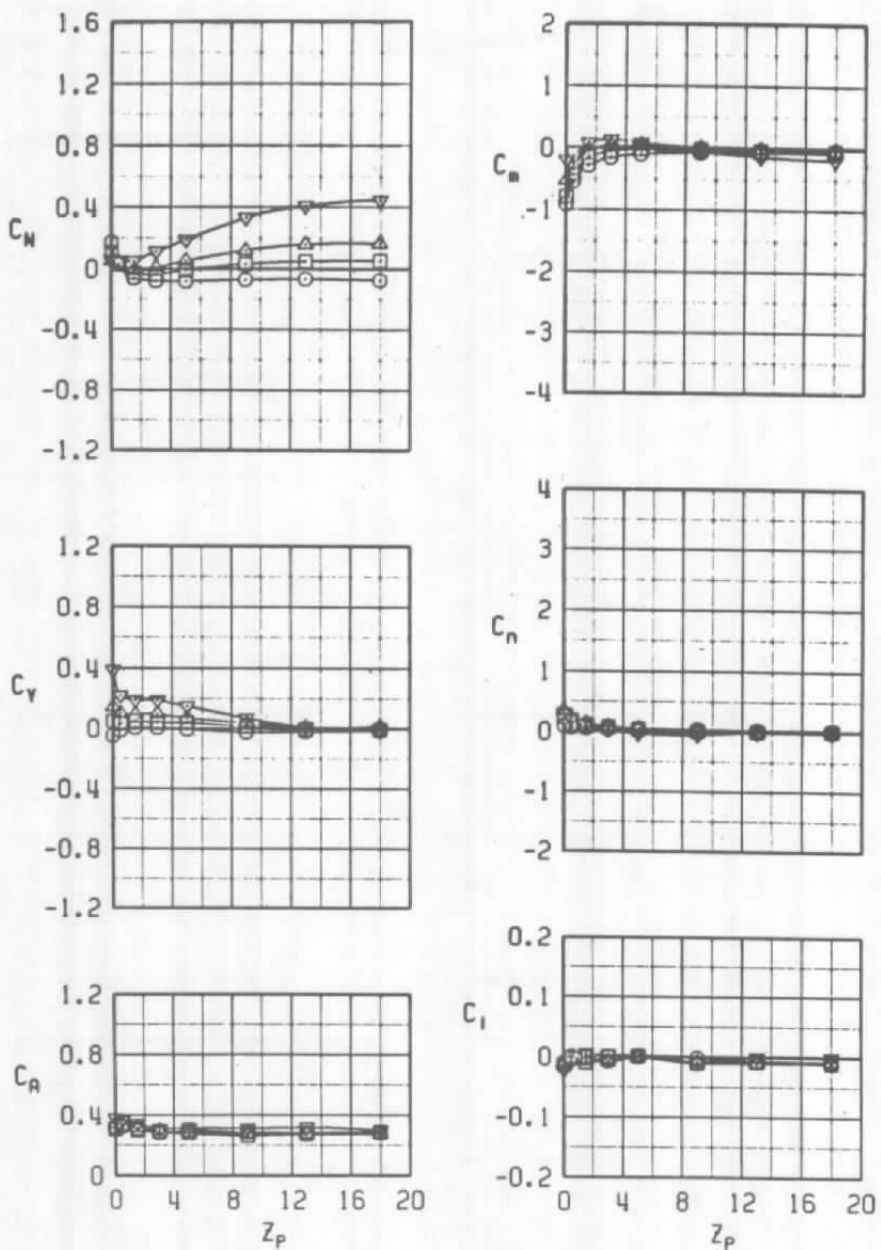


Figure 38. MK-82SE coefficient variation with aircraft angle of attack, configuration 17.

SYMBOL	CONFIG	α	M_∞	STORE	PYLON	RACK	δ_{LE}
○	10	10	0.60	MK-82SE	7	T-1	0
□	10	10	0.60	MK-82SE	7	T-1	15

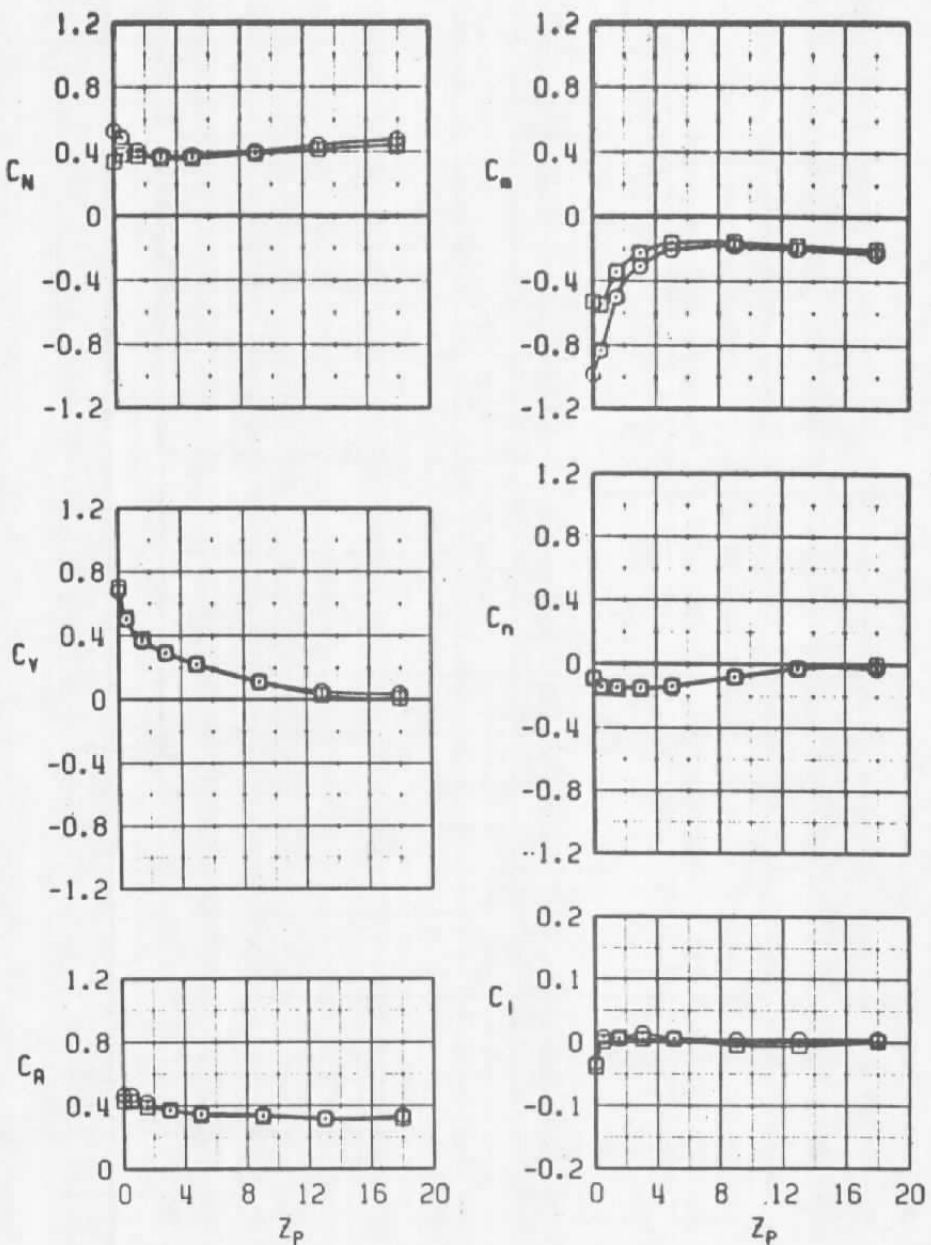
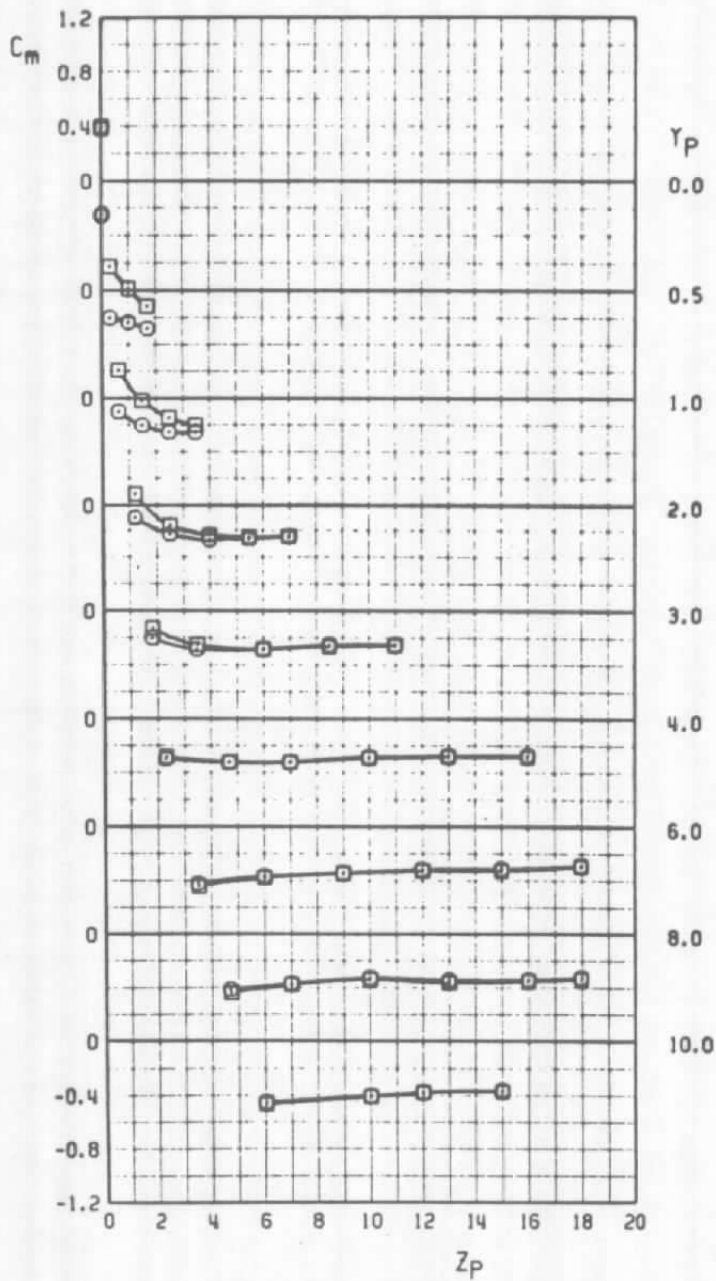


Figure 39. Coefficient with wing leading-edge-flap deflection, configuration 10.

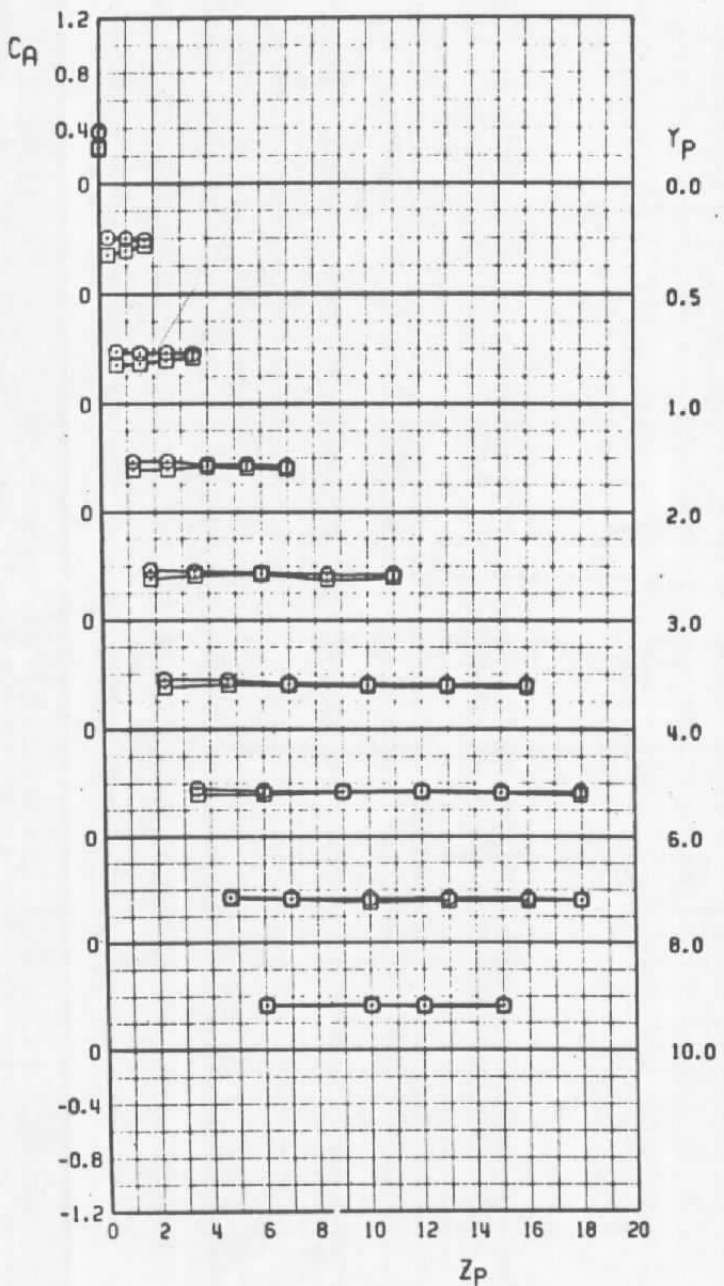
SYMBOL	CONFIG	α	M_∞	STORE	PYLON	RACK	δ_{LE}
○	11	10	0.60	MM-82SE	7	T-3	0
□	11	10	0.60	MM-82SE	7	T-3	15



a. Pitching-moment coefficient

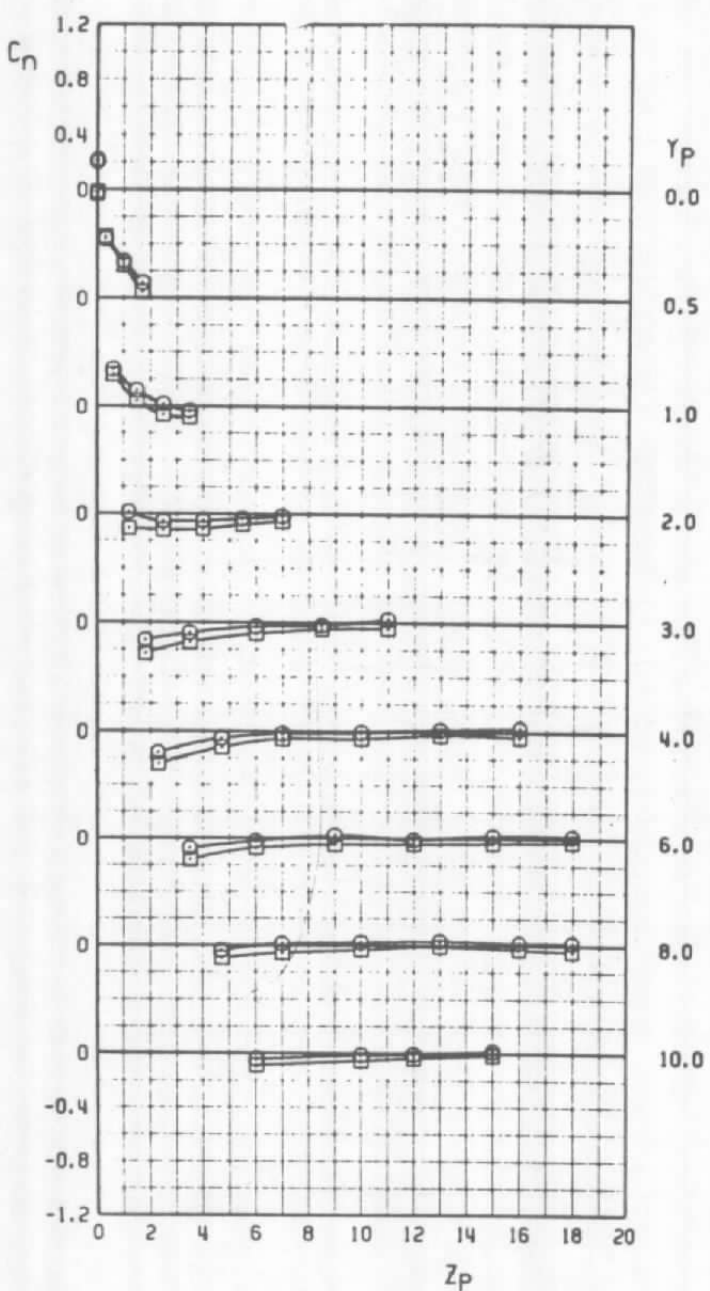
Figure 40. Coefficient variation with wing leading-edge-flap deflection, configuration 11.

SYMBOL	CONFIG	α	M_∞	STORE	PYLON	RACK	δ_{LE}
○	II	10	0.60	MK-82SE	7	T-3	0
□	II	10	0.60	MK-82SE	7	T-3	15



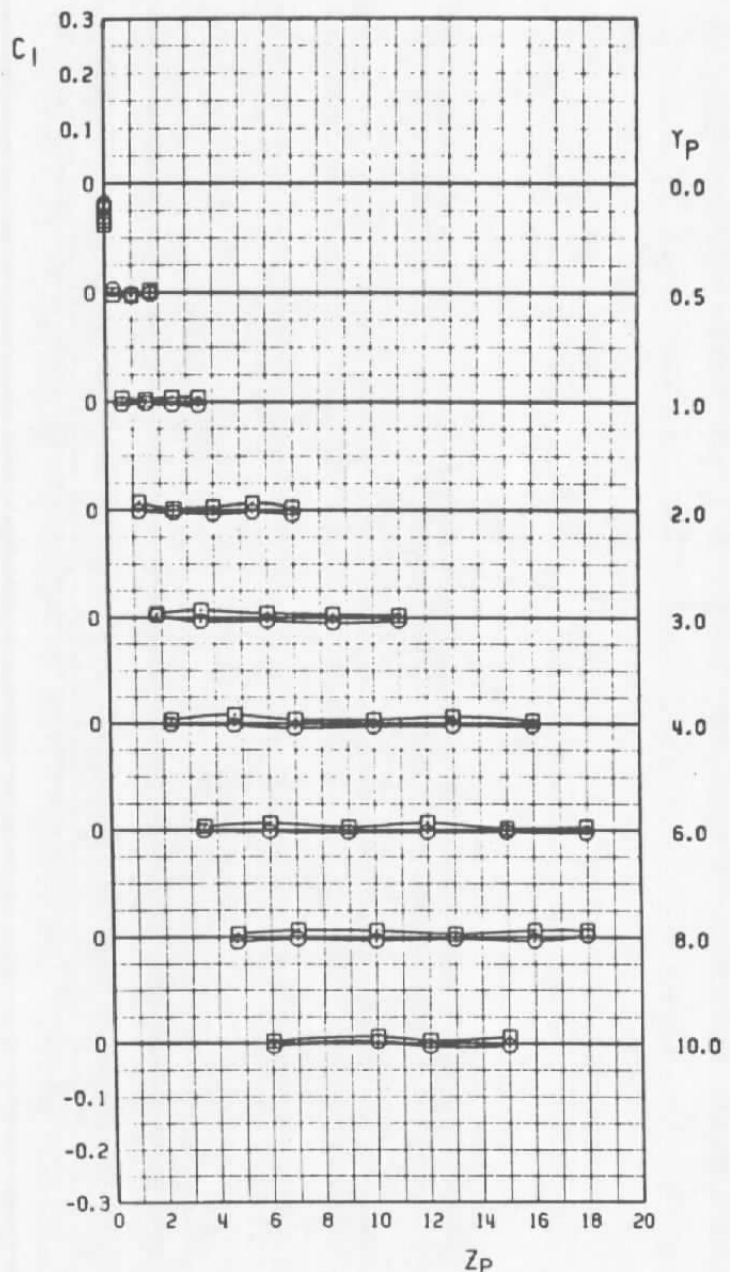
b. Axial-force coefficient
Figure 40. Continued.

SYMBOL	CONFIG	α	M_∞	STORE	PYLON	RACK	δ_{LE}
○	II	10	0.60	MK-82SE	7	T-3	0
□	II	10	0.60	MK-82SE	7	T-3	15



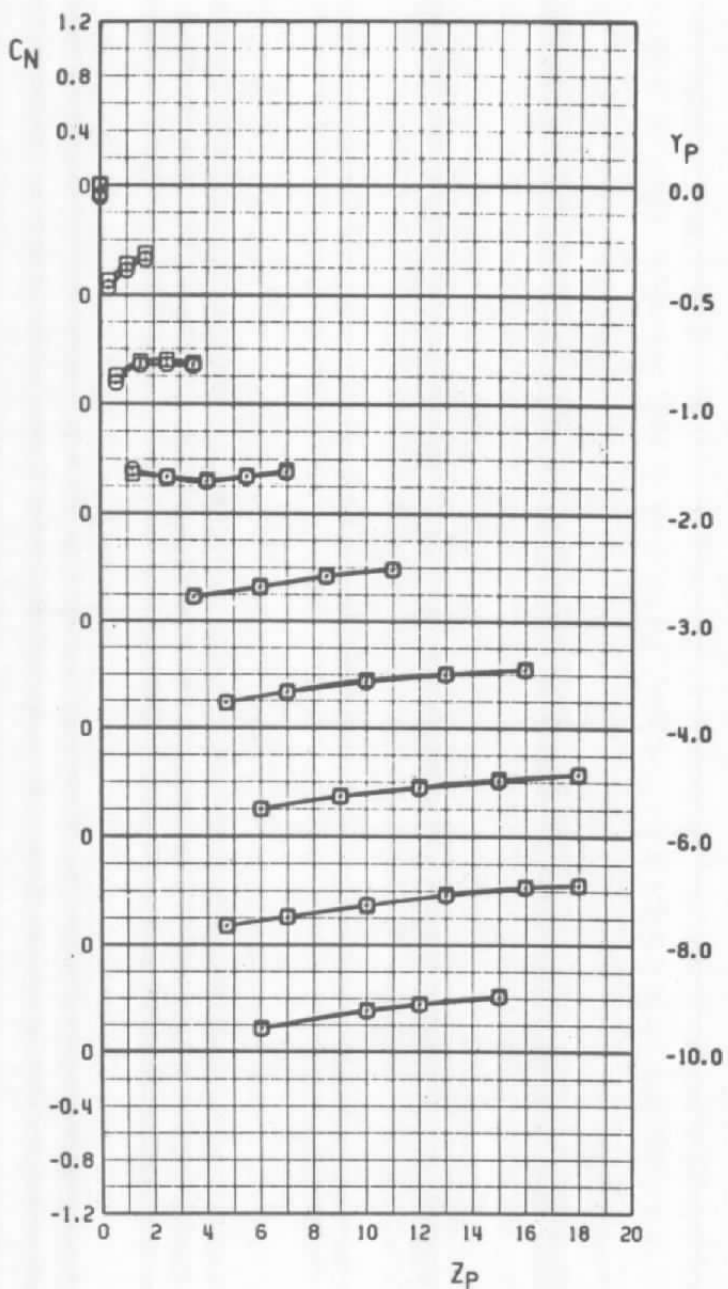
c. Yawing-moment coefficient
Figure 40. Continued.

SYMBOL	CONFIG	α	M_a	STORE	PYLON	RACK	b_{LE}
○	II	10	0.60	MK-82SE	7	T-3	0
□	II	10	0.60	MK-82SE	7	T-3	15



d. Rolling-moment coefficient
Figure 40. Concluded.

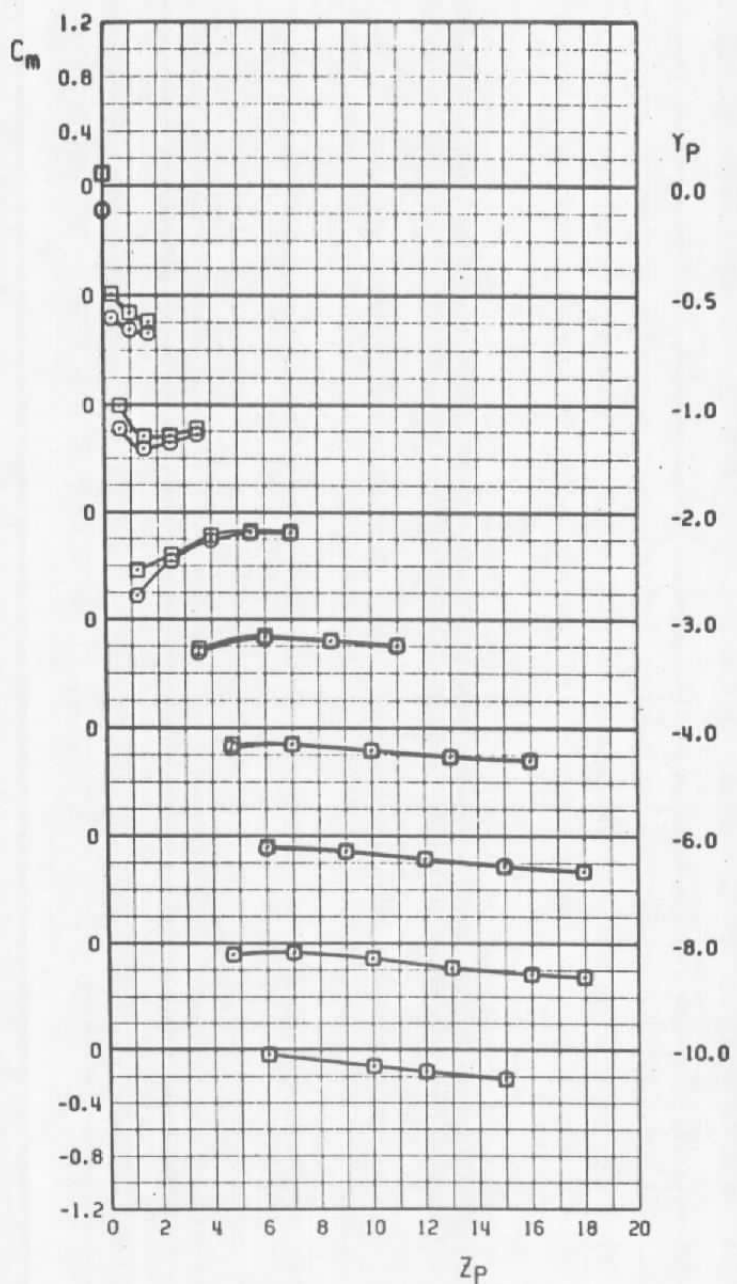
SYMBOL	CONFIG	α	M_∞	STORE	PYLON	RACK	δ_{LE}
○	12	10	0.60	MK-82SE	7	T-2	0
□	12	10	0.60	MK-82SE	7	T-2	15



a. Normal-force coefficient

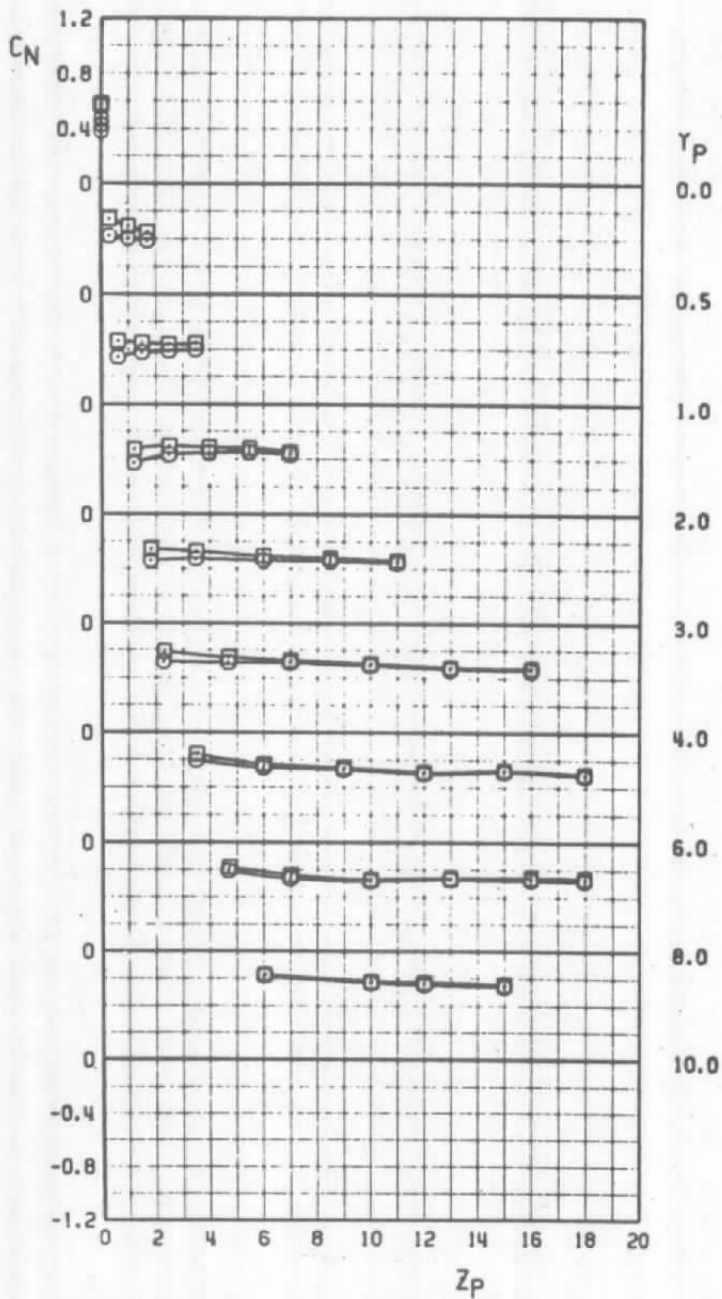
Figure 41. Coefficient variation with wing leading-edge-flap deflection, configuration 12.

SYMBOL	CONFIG	α	M_∞	STORE	PYLON	RACK	δ_{LE}
○	12	10	0.60	MK-82SE	7	T-2	0
□	12	10	0.60	MK-82SE	7	T-2	15



b. Pitching-moment coefficient
Figure 41. Concluded.

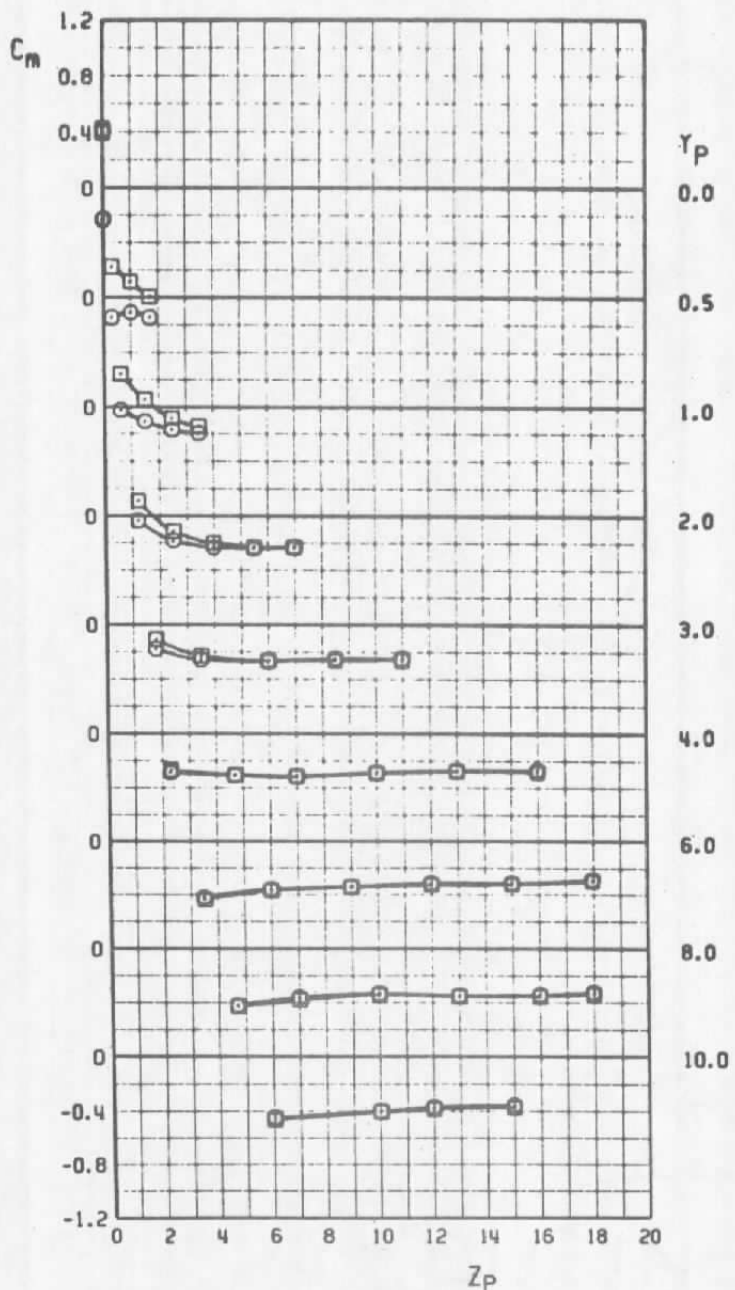
SYMBOL	CONFIG	M_∞	STORE	PYLON	RACK	δ_{LE}	
○	13	10	0.60	MK-82SE	7	1-3	0
□	13	10	0.60	MK-82SE	7	1-3	15



a. Normal-force coefficient

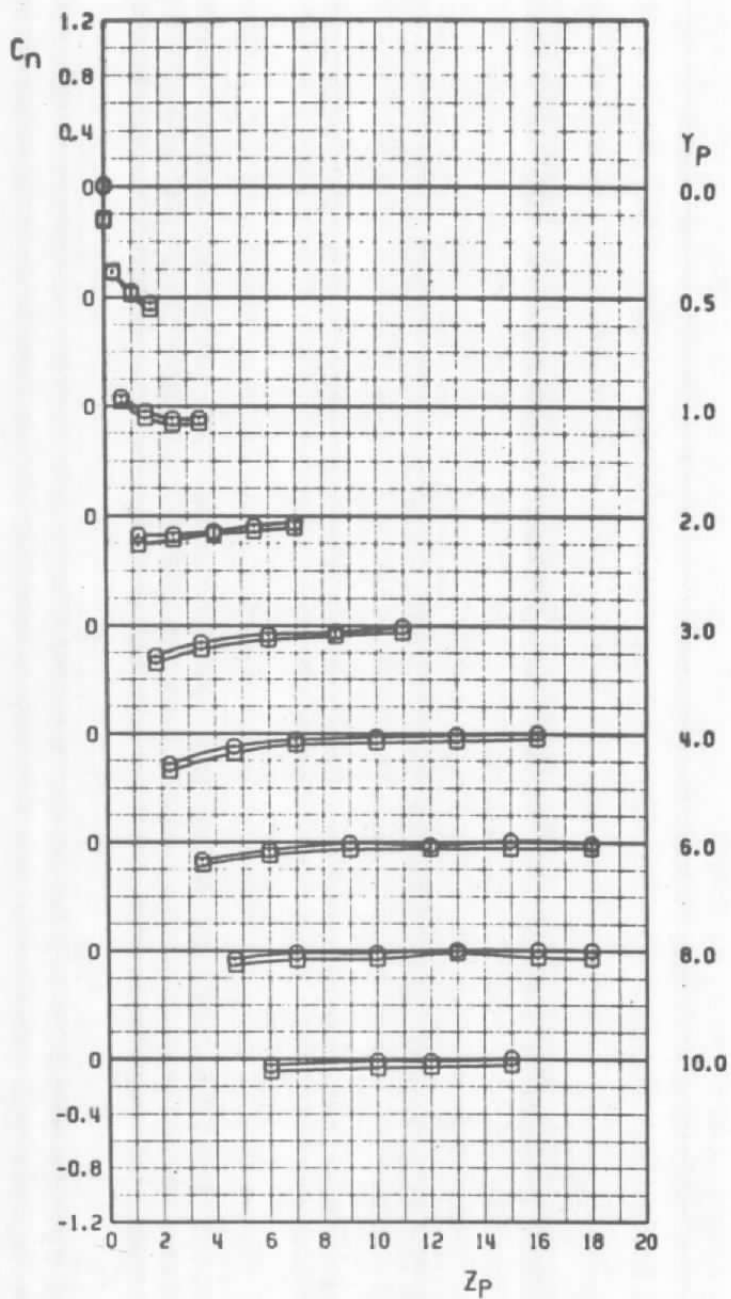
Figure 42. Coefficient variation with wing leading-edge-flap deflection, configuration 13.

SYMBOL	CONFIG	α	M_∞	STORE	PYLON	RACK	δ_{LE}
○	13	10	0.60	MK-82SE	7	T-3	0
□	13	10	0.60	MK-82SE	7	T-3	15



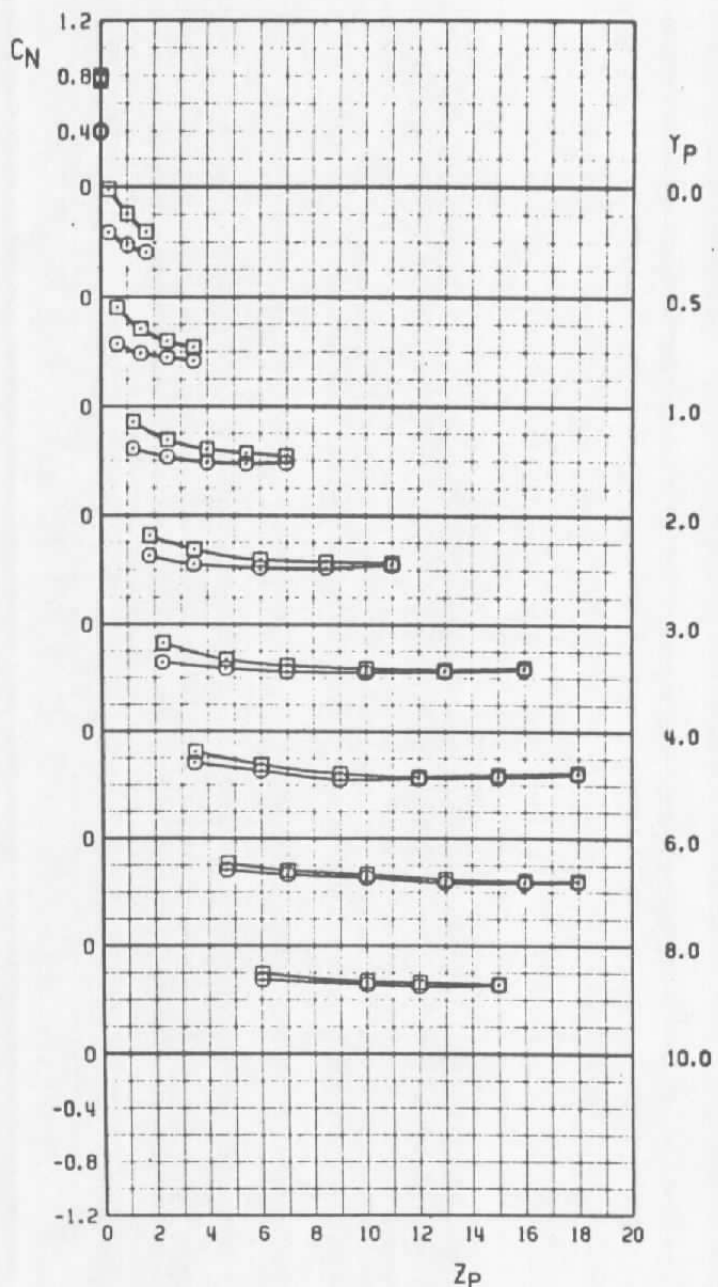
b. Pitching-moment coefficient
Figure 42. Continued.

SYMBOL	CONFIG	M_0	STORE	PYLON	RACK	δ_{LE}	
○	13	10	0.60	MK-82SE	7	T-3	0
□	13	10	0.60	MK-82SE	7	T-3	15



c. Yawing-moment coefficient
Figure 42. Concluded.

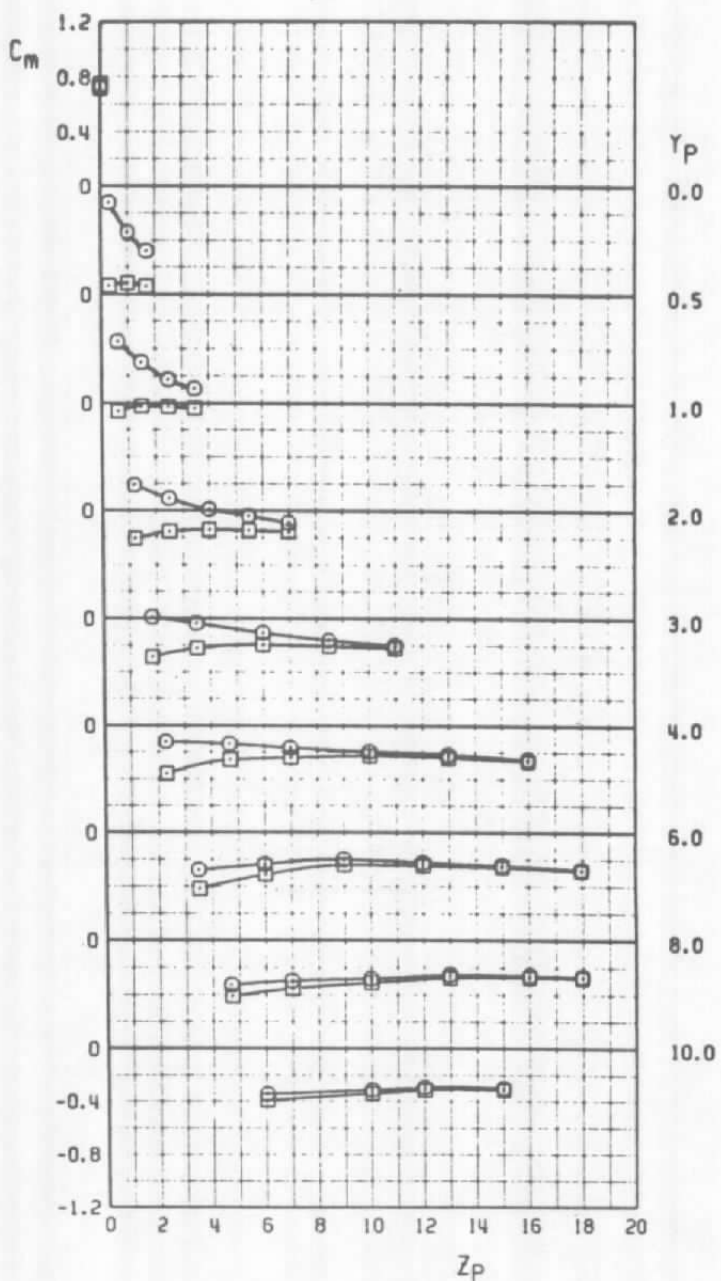
SYMBOL	CONFIG	α	M_∞	STORE	PYLON	RACK	b_{LE}
○	14	10	0.60	MK-82SE	6	M-6	0
□	14	10	0.60	MK-82SE	6	M-6	15



a. Normal-force coefficient

Figure 43. Coefficient variation with wing leading-edge-flap deflection, configuration 14.

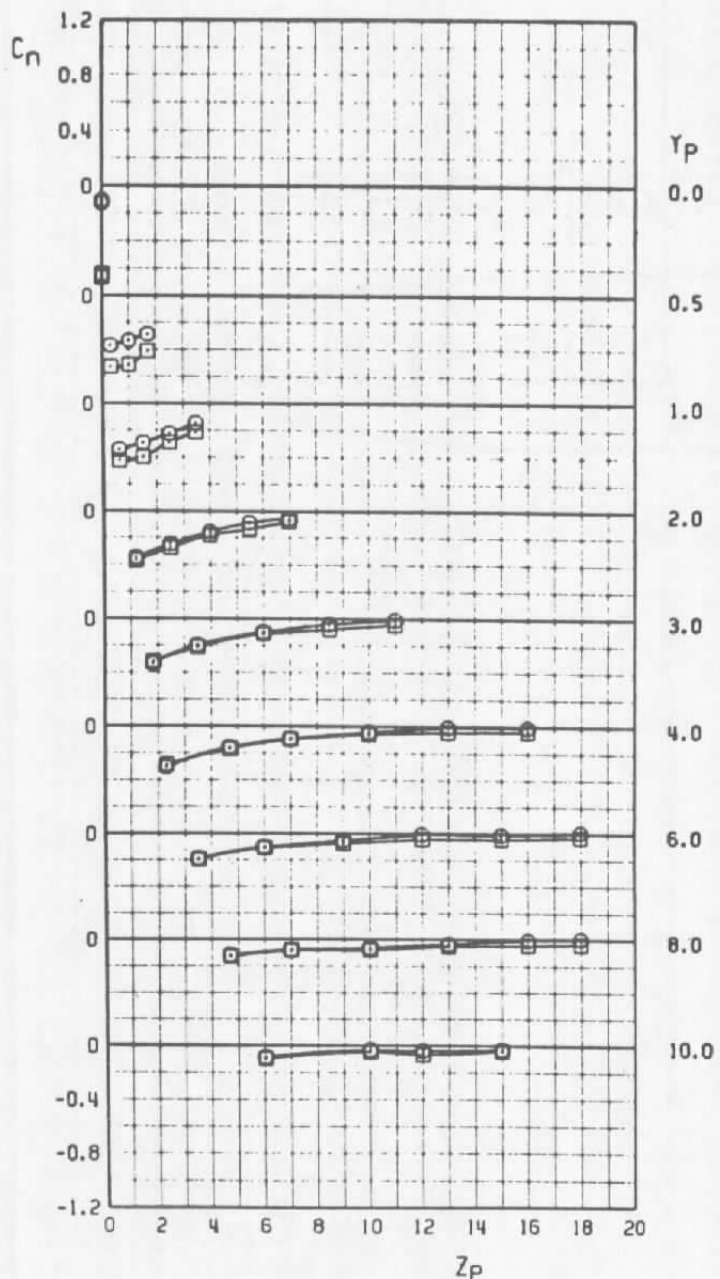
SYMBOL	CONFIG	α	M_∞	STORE	PYLON	RACK	s_{LE}
○	14	10	0.60	MK-82SE	G	M-6	0
□	14	10	0.60	MK-82SE	G	M-6	15



b. Pitching-moment coefficient

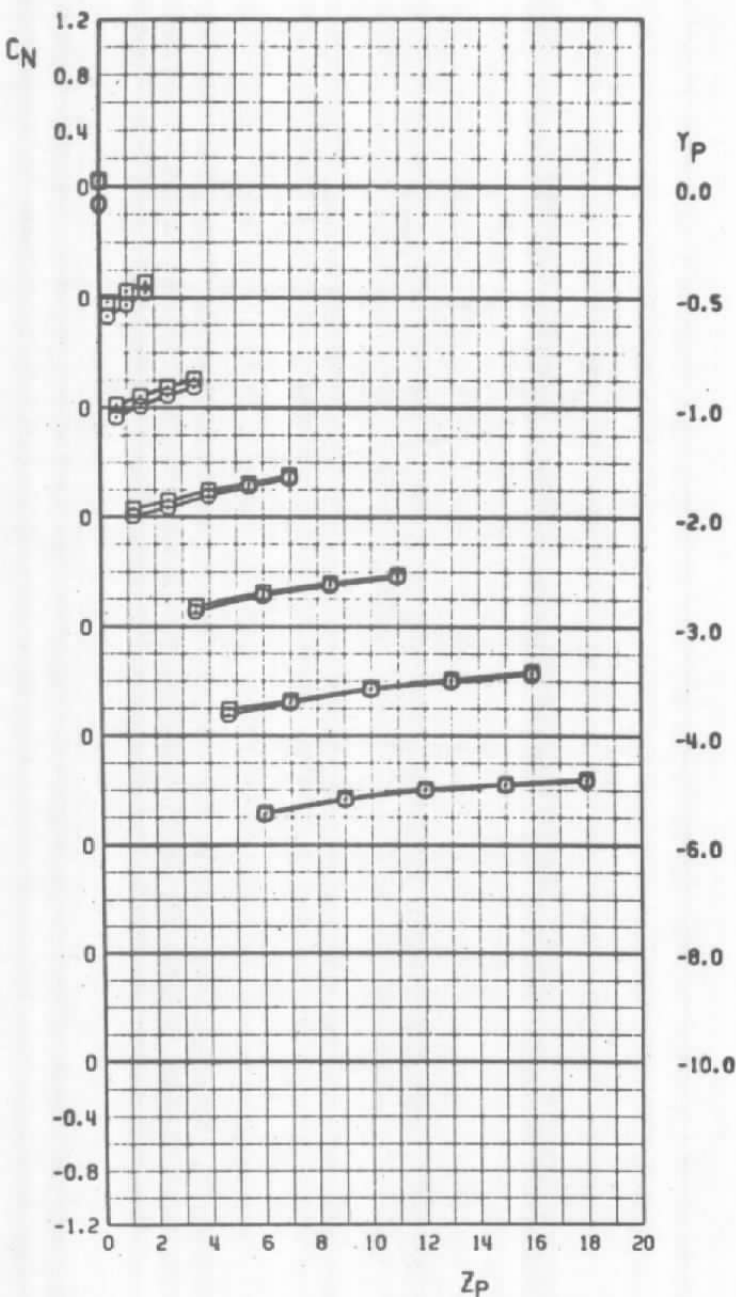
Figure 43. Continued.

SYMBOL	CONFIG	α	M_a	STORE	PYLON	RACK	δ_{LE}
○	14	10	0.60	MK-82SE	6	M-6	0
□	14	10	0.60	MK-82SE	6	M-6	15



c. Yawing-moment coefficient
Figure 43. Concluded.

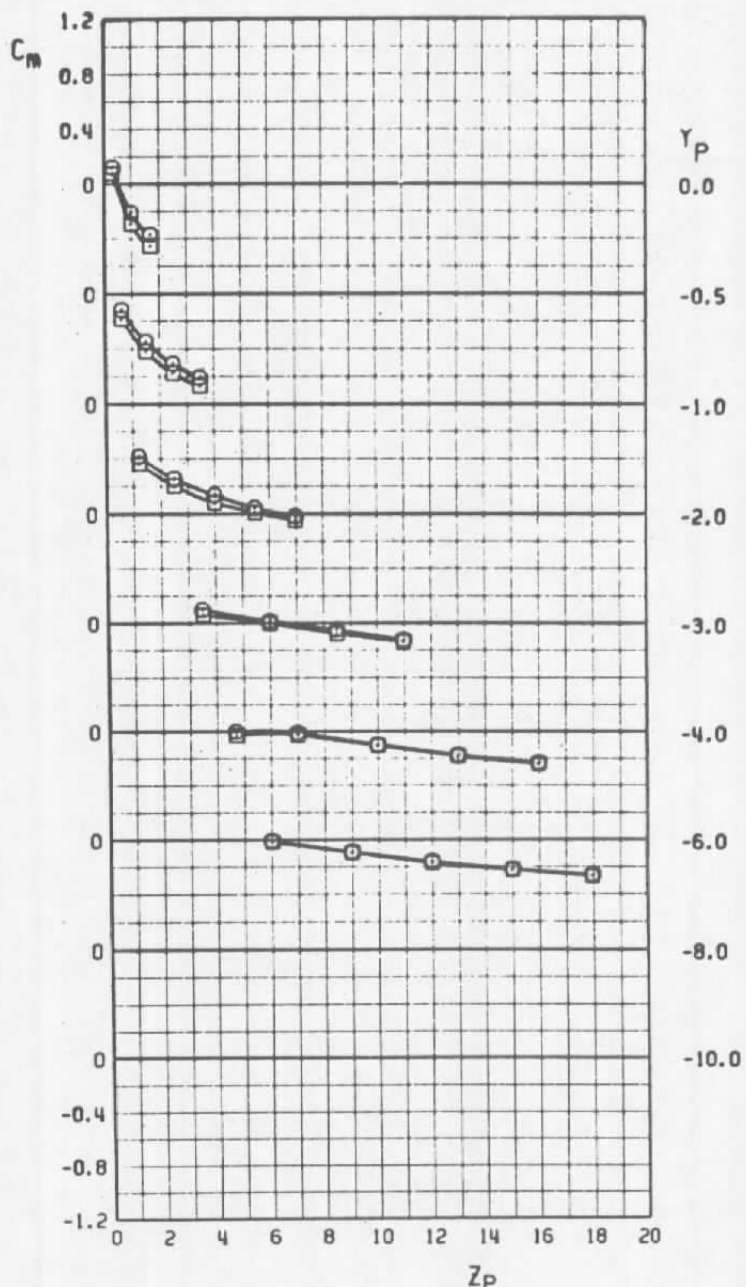
SYMBOL	CONFIG	α	M_∞	STORE	PYLON	RACK	δ_{LE}
○	15	10	0.60	MK-82SE	6	M-4	0
□	15	10	0.60	MK-82SE	6	M-4	15



a. Normal-force coefficient

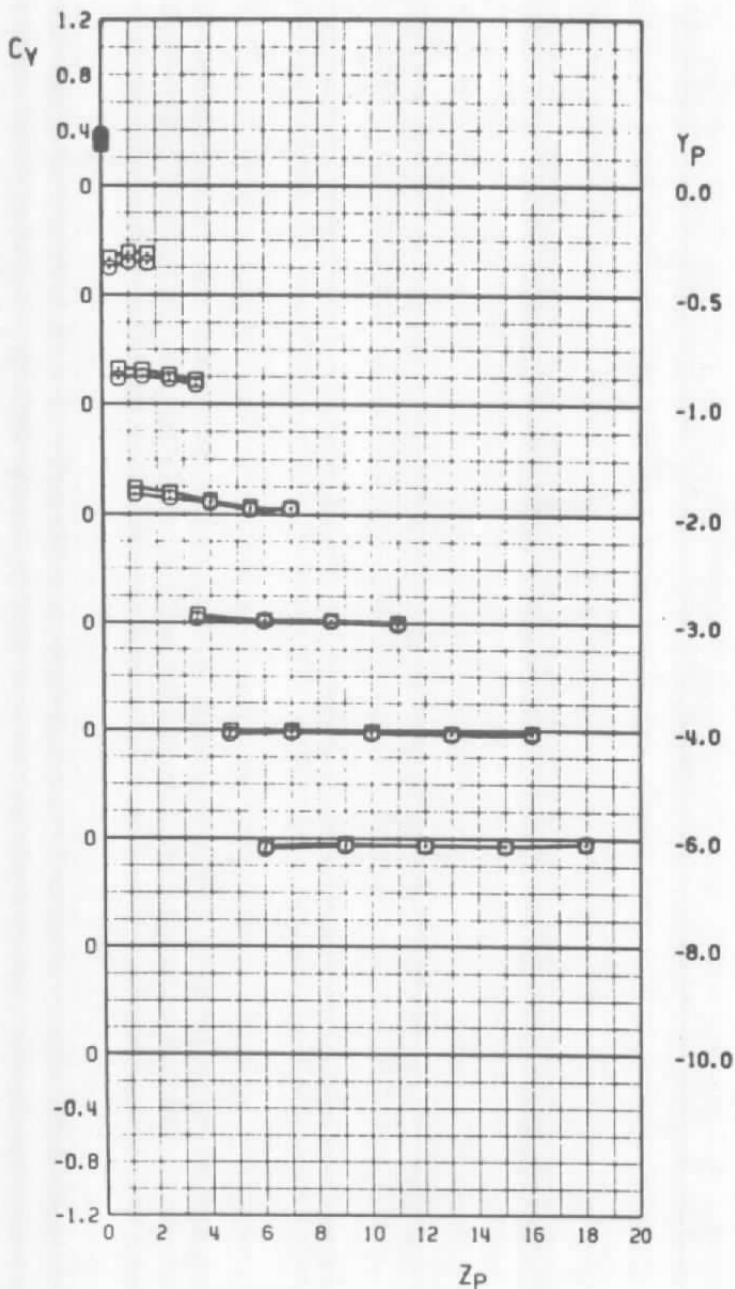
Figure 44. Coefficient variation with wing leading-edge-flap deflection, configuration 15.

SYMBOL	CONFIG	α	M_∞	STORE	PYLON	RACK	δ_{LE}
○	15	10	0.60	MK-82SE	6	M-4	0
□	15	10	0.60	MK-82SE	6	M-4	15



b. Pitching-moment coefficient
Figure 44. Continued.

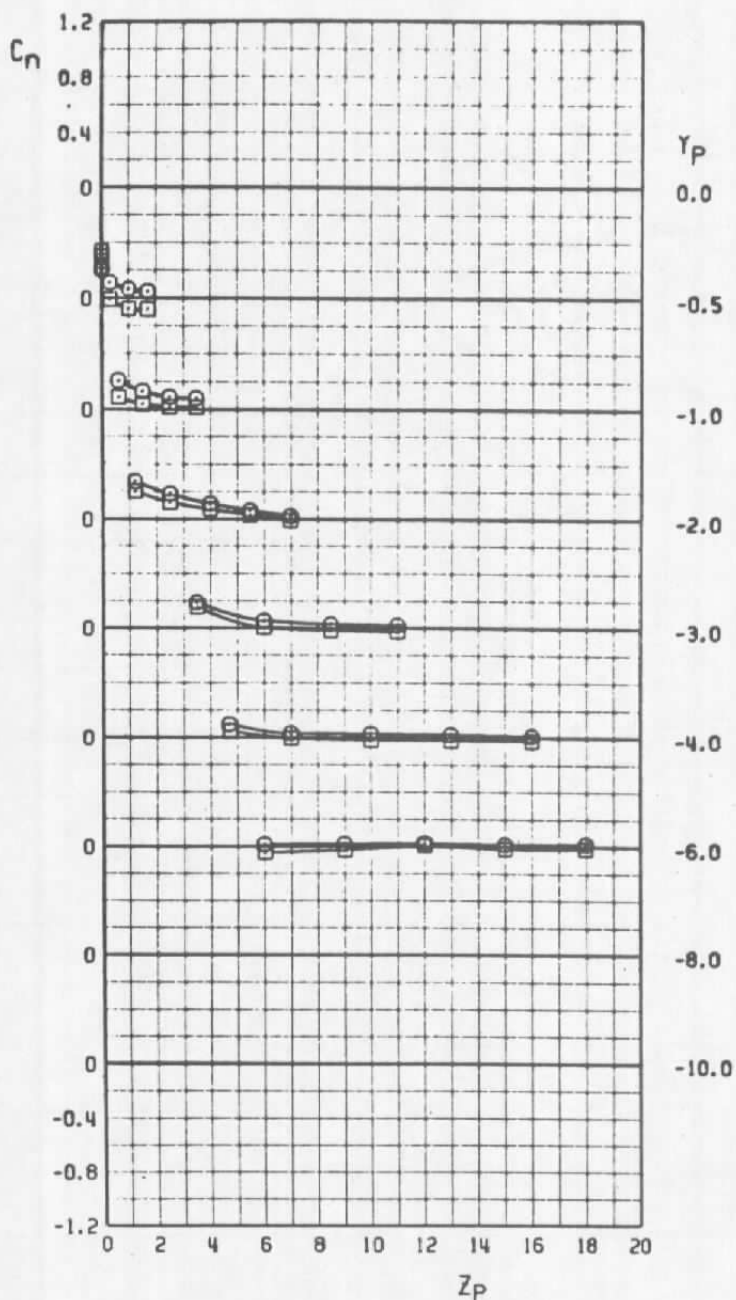
SYMBOL	CONFIG	α	M_∞	STORE	PYLON	RACK	δ_{LE}
○	15	10	0.60	MK-82SE	6	M-4	0
□	15	10	0.60	MK-82SE	6	M-4	15



c. Side-force coefficient

Figure 44. Continued.

SYMBOL	CONFIG	α	M_a	STORE	PYLON	RACK	$C_{L\alpha}$
○	15	10	0.60	MK-82SE	6	M-4	0
□	15	10	0.60	MK-82SE	6	M-4	15



d. Yawing-moment coefficient
Figure 44. Concluded.

SYMBOL	CONFIG	α	M_∞	STORE	PYLON	RACK	δ_{LE}
○	16	10	0.60	MM-82SE	7	NA	0
□	16	10	0.60	MM-82SE	7	NA	15

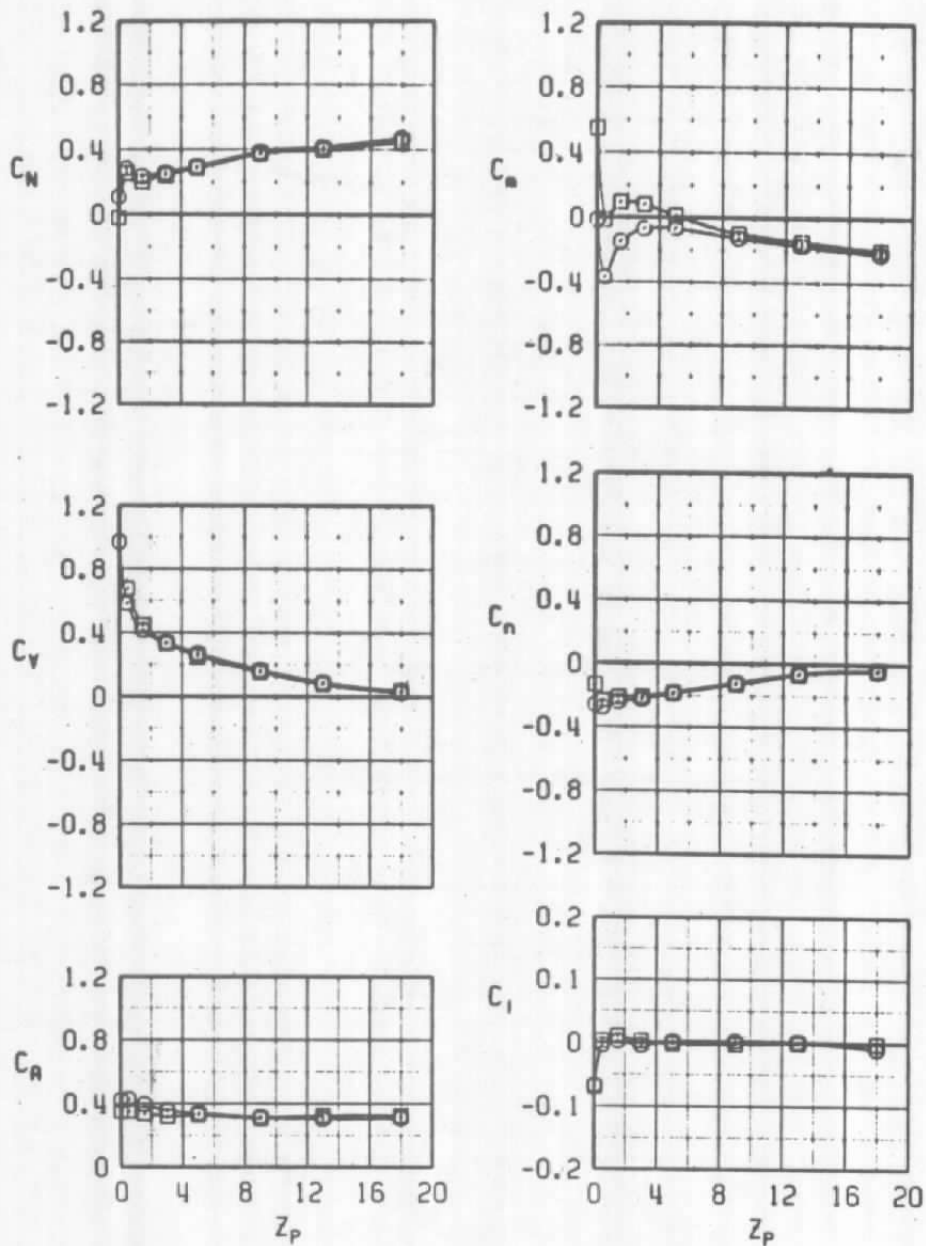


Figure 45. Coefficient variation with wing leading-edge-flap deflection, configuration 16.

SYMBOL	CONFIG	α	M_∞	STORE	PYLON	RACK	δ_{LE}
○	17	10	0.60	MK-82SE	6	NA	0
□	17	10	0.60	MK-82SE	6	NA	15

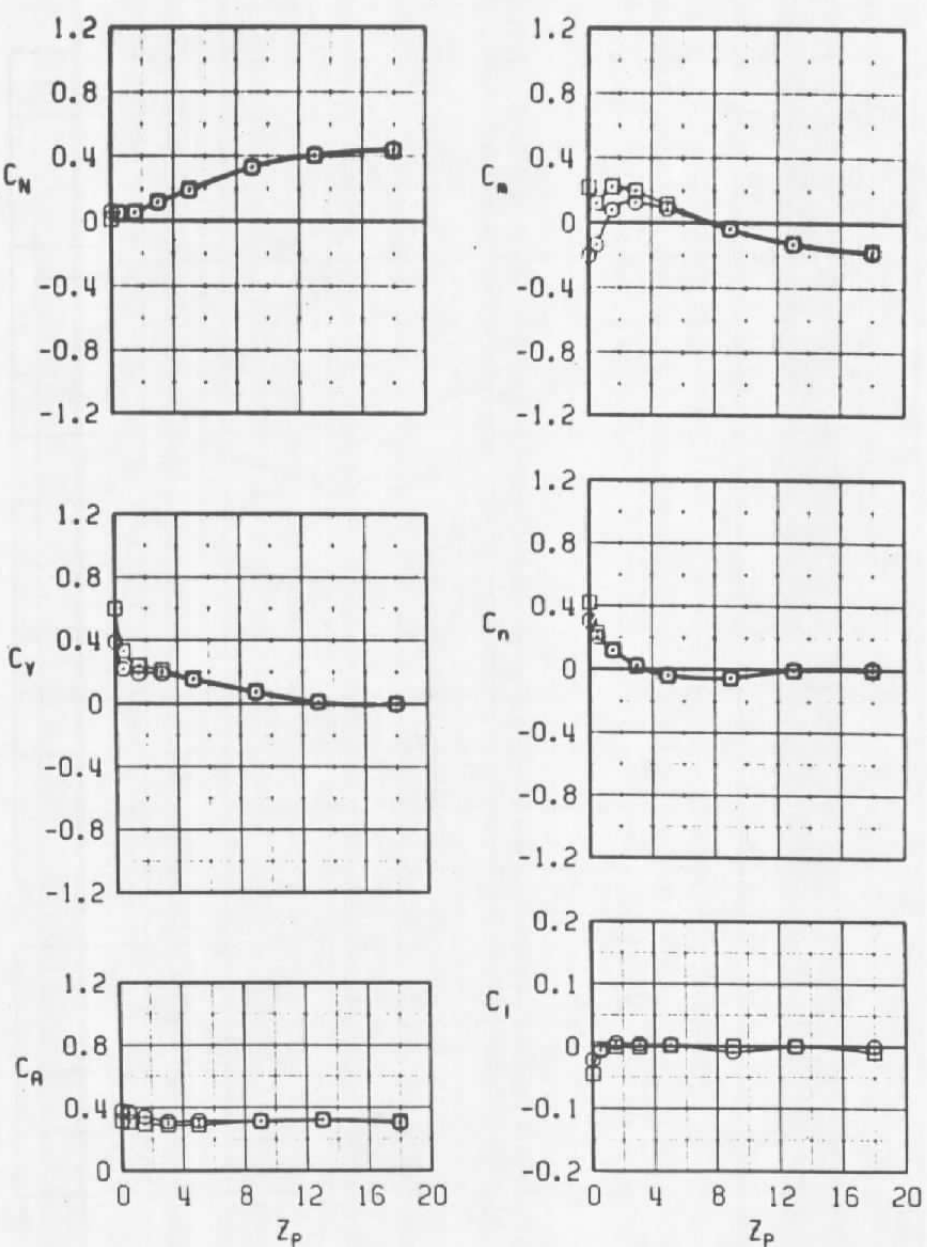


Figure 46. Coefficient variation with wing leading-edge-flap deflection, configuration 17.

Table 1. Metric Model Parameters

	BLU-27 B/B	GBU-8	MK-82SE
b	1. 563	1. 5	0. 896
C_{ℓ_p}	NA	-18. 048	-5. 0
C_{m_q}	NA	-180. 48	-53. 0
C_{n_r}	NA	-180. 48	-53. 0
F_{z₁}	NA	2030. 0 1680. 0 1113. 0*	
F_{z₂}	NA	1780. 0 1333. 3 1900. 0*	
h	NA	5,000	5,000
I_{xx}	NA	24. 7	2. 1
I_{yy}	NA	524. 2	53. 0
I_{zz}	NA	524. 2	53. 0
\bar{m}	NA	70. 243	17. 1
S	1. 917	1. 767	0. 630
X_{cg}	5. 358	6. 608	3. 375
X_{L₁}	NA	0. 817	1. 000
X_{L₂}	NA	-0. 850	-0. 667
Z_E	NA	0. 343	0. 343

*Selected Runs

Table 2. Run Compendium

Conf	M _∞	Store	Pylon	Rack	Station	δLF			α				
						0	4	15	0	2	4	6	10
1	0.6	BLU-27	7	TFR	2	x				x	x	x	x
	0.8						x		x	x	x		
	0.9						x		x	x			
	0.95						x		x	x			
2	0.6					x				x	x	x	x
	0.8					x			x	x	x		
	0.9					x			x	x			
	0.95					x		-	x	x			
3	0.6				3	x			x	x	x	x	x
	0.8					x			x	x	x		
	0.9					x			x	x			
	0.95					x			x	x			
4	0.6					x			x	x	x	x	x
	0.8					x			x	x	x		
	0.9					x			x	x			
	0.95					x		-	x	x			
5	0.6			NA	NA	x			x	x	x	x	x
	0.8					x			x	x	x		
	0.9					x			x	x			
	0.95					x			x	x			
6	0.6		6			x			x	x	x	x	x
	0.8					x			x	x	x		
	0.9					x			x	x			
	0.95					x		-	x	x			
7	0.6	GBU-8	7	NA	NA	x			x	x	x	x	x
	0.8					x			x	x	x		
	0.9					x			x	x			
	0.95					x			x	x			
	1.05					x			x				
8	1.2					x			x				
	0.6		6			x			x	x	x	x	x
	0.8					x			x	x	x		
9	0.9					x			x	x			

Table 2. Continued

Conf	M_∞	Store	Pylon	Rack	Station	δ_{LE}			α				
						0	1	15	0	2	4	6	10
8	0.95	GBU-8	6	NA	NA	x			x	x			
(Cont'd)	1.05						x			x			
	1.2						x		x				
9	0.60		7			x				x	x	x	x
	0.8					x			x	x	x		
	0.9					x			x	x			
	0.95					x			x	x			
	1.05					x			x				
	1.20		↓	↓	↓	x			x				
10	0.4	Mk 82SF	7	TER	1	x				x			
	0.6						x			x	x	x	x
	0.8						x			x	x	x	x
	0.9					x			x	x			
	0.95				↓	x			x	x			
11	0.4			3	x					x			
	0.6						x			x	x	x	x
	0.8						x			x			x
	0.9					x			x	x			
	0.95				↓	x			x	x			
12	0.4			2	x					x			
	0.6						x			x	x	x	x
	0.8						x			x	x	x	x
	0.9						x			x	x		
	0.95		↓	↓	↓	↓			x	x			

Table 2. Continued

Conf	M_∞	Store	Pylon	Rack	Station	δ_{LP}			α				
						0	4	15	0	2	4	6	10
13	0.4	MK-82SE	7	TER	3		x				x		
								x				x	
	0.6						x			x	x	x	x
							x		x		x		
	0.8					x			x	x	x		
	0.9					x			x	x			
14	0.4		6	MER	6	x				x			
							x					x	
	0.6					x				x	x	x	x
						x			x		x		
	0.8					x				x	x	x	
	0.9					x			x	x			
15	0.4		4		4	x				x			
							x					x	
	0.6					x				x	x	x	x
						x			x		x		
	0.8					x			x	x	x		
	0.9					x			x	x			
16	0.4		7	NA	NA	x				x			
							x			x	x	x	x
	0.6						x			x		x	
							x		x		x		
	0.8					x			x	x	x		
	0.9					x			x	x			
	0.95					x			x	x			

Table 2. Continued

Conf	M _∞	Store	Pylon	Rack	Station	δ _{LF}			α				
						0	4	15	0	2	4	6	10
17	0.4	MK-82SF	6	NA	NA	x			x				
	0.6						x				x		
	0.8					x			x	x	x	x	
	0.9						x			x	x		
	0.95						x			x	x		

Conf	M _∞	Trajectory Summary							
		0	4	15	0	2	4	6	10
7	0.6	GBL-5	7	NA	NA	x		x	
	0.8					x		x	
	0.9					x		x	
	0.95					x		x	
	1.05					x		x	
	1.2					x		x	
8	0.6		6			x		x	
	0.8					x		x	
	0.9					x		x	
	0.95					x		x	
	1.05					x		x	
	1.2					x		x	
16	0.6	MK-82SE	7	NA	NA	x		x	
	0.8					x		x	
	0.9					x		x	
	0.95					x		x	
17	0.6		6			x		x	
	0.8					x		x	
	0.9					x		x	
	0.95					x		x	

Table 2. Concluded

Freestream Summary		
Store	M_∞	α_S
BLU-27	0.6	Schedule D
	0.8	
	0.9	
	0.95	
GBU-8	0.6	Schedule B
	0.8	Schedule C
	0.9	Schedule C
	0.95	Schedule B
	1.05	Schedule A
	1.20	Schedule A
MK-82SE	0.4	Schedule D
	0.6	
	0.8	
	0.9	
	0.95	
	1.05	
	1.2	Schedule C

Schedule A: $\alpha_S = -4, -2, 0, 2, 4, 6, 8, 10, 12, 16, 20$

Schedule B: $\alpha_S = -4, -2, 0, 2, 4, 6, 8, 10, 12, 16, 20, 24$

Schedule C: $\alpha_S = -4, -2, 0, 2, 4, 6, 8, 10, 12, 16, 20, 24, 28$

Schedule D: $\alpha_S = -4, -2, 0, 2, 4, 6, 8, 10, 12, 16, 20, 24, 28, 32$

Table 3. Typical Data Uncertainties

Trajectory Data								
Store	M_∞	Δt	ΔX	ΔY	ΔZ	$\Delta \theta$	$\Delta \psi$	$\Delta \phi$
MK-82SE	0.6	0.21	0.008	0.007	0.007	0.12	0.12	NA
MK-82SE	0.95	0.21	0.019	0.015	0.015	0.28	0.28	NA
GBU-8	0.6	0.31	0.004	0.005	0.006	0.02	0.08	1.2
GBU-8	1.2	0.31	0.012	0.017	0.018	0.07	0.25	3.7

Aerodynamic Loads Data									
Store	M_∞	ΔC_N	ΔC_Y	ΔC_A	ΔC_f	ΔC_m	ΔC_M	ΔM_∞	Δq_∞
BLU-27	0.6	0.010	0.009	0.007	0.003	0.013	0.008	0.005	4.6
	0.8	0.011	0.010	0.007	0.003	0.013	0.010	0.005	2.8
	0.95	0.009	0.009	0.006	0.003	0.011	0.007	0.005	2.4
GBU-8	0.6	0.014	0.010	0.007	0.004	0.026	0.020	0.005	4.6
	0.9	0.012	0.010	0.007	0.003	0.024	0.019	0.005	2.8
	1.2	0.009	0.008	0.007	0.003	0.018	0.015	0.010	2.4
MK-82SE	0.4	0.030	0.030	0.034	0.033	0.047	0.047	0.005	5.4
	0.8	0.020	0.020	0.025	0.023	0.032	0.032	0.005	2.8
	0.95	0.017	0.017	0.021	0.019	0.027	0.027	0.005	2.4

NOMENCLATURE

BL	Aircraft buttock line from plane of symmetry, in., model scale
b	Store reference dimension, ft, full scale
C_A	Store measured axial-force coefficient, axial force/ $q_\infty S$
C_λ	Store rolling-moment coefficient, rolling moment/ $q_\infty Sb$
C_{λ_p}	Store roll-damping derivative, $dC_\lambda/d(pb/2V_\infty)$
C_m	Store pitching-moment coefficient, referenced to the store cg, pitching moment/ $q_\infty Sb$
C_{m_q}	Store pitch-damping derivative, $dC_m/d(qb/2V_\infty)$
C_N	Store normal-force coefficient, normal force/ $q_\infty S$
C_n	Store yawing-moment coefficient, referenced to the store cg, yawing moment/ $q_\infty Sb$
C_{n_r}	Store yaw-damping derivative, $dC_n/d(rb/2V_\infty)$
C_Y	Store side-force coefficient, side force/ $q_\infty S$
FS	Aircraft fuselage station, in., model scale
F_{z_1}	Forward ejector force, lb
F_{z_2}	Aft ejector force, lb
h	Simulated pressure altitude, ft

I_{xx}	Full-scale moment of inertia about the store X_B axis, slug-ft ²
I_{yy}	Full-scale moment of inertia about the store Y_B axis slug-ft ²
I_{zz}	Full-scale moment of inertia about the store Z_B axis, slug-ft ²
M_∞	Free-stream Mach number
\bar{m}	Full-scale store mass, slugs
p_t	Free-stream total pressure, psfa
p_∞	Free-stream static pressure, psfa
q_∞	Free-stream dynamic pressure, psf
S	Store reference area, ft ² , full scale
t	Real trajectory time from initiation of trajectory, sec
V_∞	Free-stream velocity, ft/sec
WL	Aircraft waterline from reference horizontal plane, in., model scale
X	Separation distance of the store cg parallel to the flight axis system X_F direction, ft, full scale measured from the prelaunch position
X_{cg}	Full-scale cg location, ft, from nose of store

x_{L_1}	Forward ejector location relative to the store cg, positive forward to store cg, ft, full scale
x_{L_2}	Aft ejector piston location relative to the store cg, positive forward of store cg, ft, full scale
x_p	Separation distance of the store cg parallel to the pylon axis system x_p direction, ft, full scale measured from the prelaunch position
y_p	Separation distance of the store cg parallel to the flight axis system y_p direction, ft, full scale measured from the prelaunch position
z_p	Separation distance of the store cg parallel to the flight axis system z_p direction, ft, full scale measured from the prelaunch position
z_E	Ejector piston stroke length, ft, full scale
z_p	Separation distance of the store cg parallel to the pylon axis system z_p direction, ft, full scale measured from the prelaunch position
α	Aircraft model angle of attack relative to the free-stream wind vector, deg
α_s	Store model angle of attack relative to the free-stream wind vector, deg

- θ Angle between the store longitudinal axis and its projection in the $X_F - Y_F$ plane, deg
- φ Angle between the projection of the store lateral axis in the $Y_F - Z_F$ plane and the Y_F axis, deg
- ψ Angle between the projection of the store longitudinal axis in the $X_F - Y_F$ plane and the X_F axis, deg

FLIGHT-AXIS SYSTEM COORDINATES

Directions

- X_F Parallel to the free-stream wind vector, positive direction is forward as seen by the pilot
- Y_F Perpendicular to the X_F and Z_F directions, positive direction is to the right as seen by the pilot
- Z_F In the aircraft plane of symmetry, perpendicular to the free-stream wind vector, positive direction is downward

The flight-axis system origin is coincident with the aircraft cg and remains fixed with respect to the parent aircraft during store separation. The X_F , Y_F , and Z_F coordinate axes do not rotate with respect to the initial flight direction and attitude.

STORE BODY-AXIS SYSTEM COORDINATES

Directions

- X_B Parallel to the store longitudinal axis, positive direction is upstream in the prelaunch position

- y_B Perpendicular to the store longitudinal axis, and parallel to the flight-axis system X_F-Y_F plane when the store is at zero roll angle, positive direction is to the right looking upstream when the store is at zero yaw and roll angles
- z_B Perpendicular to both the x_B and y_B axes, positive direction is downward as seen by the pilot when the store is at zero pitch and roll angles

The store body-axis system origin is coincident with the store cg and moves with the store during separation from the parent airplane. The x_B , y_B , and z_B coordinate axes rotate with the store in pitch, yaw, and roll so that mass moments of inertia about the three axes are not time-varying quantities.

PYLON-AXIS SYSTEM COORDINATES

Directions

- x_p Parallel to the aircraft longitudinal axis, positive direction is forward as seen by the pilot
- y_p Perpendicular to the x_p axis and parallel to the flight-axis system X_F-Y_F plane, positive direction is to the right as seen by the pilot
- z_p Perpendicular to both the x_p and y_p axes, positive direction is downward

The pylon-axis system origin is coincident with the store cg in the prelaunch carriage position. The axes are rotated with respect to the flight-axis system by the pitch angles of the aircraft. Both the origin and the direction of the coordinate axes remain fixed with respect to the flight-axis system throughout the trajectory.